












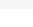


Davies Dong Eu Min Van Wagenen Corry DelPriore Dryden Lee Park Coleman Abernathy Bartholomeusz Doyle King Dunn DeVries Wang Elliott 1973

View Arrange By Action Share Edit Tags

Name	^	Date Modified	Size	Kind
 Davies 2000 presentation Creatine Creatinine biosensors2000 Van Wagenen Eu Min		Nov 14, 2018, 7:03 PM	719 KB	PDF D
 Davies 2002 ICBC Lactate Assay Corry.pdf		Aug 14, 2006, 8:48 PM	801 KB	PDF D
 Davies 2003 Diabetes Analytes abernathy Poster.pdf		Oct 31, 2017, 10:26 AM	1.3 MB	PDF D
 Davies 2003 IEEE Personal Sensors bartholomeusz.pdf		Apr 2, 2003, 12:35 PM	2.2 MB	PDF D
 Davies R 2001 Luciferase Stabilization An...i-Luminescence Van Wagenen ICBC 2000		Jan 5, 2018, 10:25 AM	587 KB	PDF D
 DelPriore 1982 Ag Silver SERS Doyle.pdf		Aug 14, 2006, 8:32 PM	1.1 MB	PDF D
 Dong 1987 LDL Lipoprotein Adsorption Coleman.pdf		Nov 11, 2018, 9:30 PM	4.1 MB	PDF D
 Dong 1987 Lipoprotein Adsorption coleman.pdf		Aug 12, 2006, 8:18 PM	3.7 MB	PDF D
 Dryden 1988 Wilhelmy Dynamics lee park bk.pdf		Aug 12, 2006, 8:31 PM	2.5 MB	PDF D
 Dunn 1973 Polyester Tendon king de vries.pdf		Aug 11, 2006, 6:05 PM	4.1 MB	PDF D
 Elliott 1983 doyle XPS Photoelectron Spectroscopy Sensitivity Factors HP5950B.pdf		Aug 12, 2006, 8:41 PM	1.8 MB	PDF D
 Eu 1998 Galactose Galactosuria Assay Anal Biochem Wang.pdf		Apr 1, 2006, 1:01 PM	542 KB	PDF D
 Eu 1998 ISBC Galactokinase Activity.pdf		Aug 12, 2006, 7:08 PM	1.1 MB	PDF D
 Eu 2001 Luciferase Immobilization Biotin BCCP.pdf		Sep 14, 2001, 11:25 PM	552 KB	PDF D

Bioluminescence Assays for Creatine and Creatinine for Biosensor Applications: A Preliminary Study

Rupert Davies*, Rick Van Wagenen†, Ji-yang Eu‡, Dong Min*, and Joseph Andrade*

*Department of Bioengineering and ‡Department of Materials Science and Engineering, University of Utah, Salt Lake City, Utah, 84112

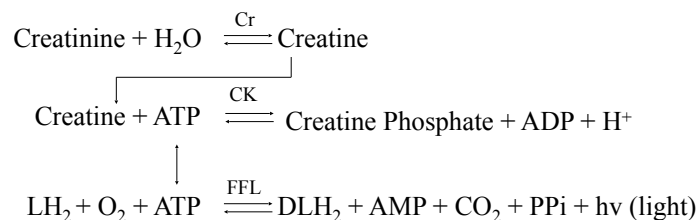
†Protein Solutions, Inc., Salt Lake City, 84108

Introduction

The development of a low-cost, home-care biosensor for kidney function would be valuable for out-patient treatment of kidney transplant patients. Serum creatinine concentration is a widely used marker of kidney function (or an estimate of the Glomerular Filtration Rate[GFR]). In normal patients, serum creatinine concentrations are $74 \pm 9 \mu\text{M}$ [1,2]. Since creatinine is an end product of muscle metabolism, circulating creatinine concentrations depend on total muscle mass. In kidney transplant patients, creatinine concentrations are generally higher at $129 \pm 31 \mu\text{M}$ [3]. Serum creatinine concentrations provide an excellent marker for acute events such as tubular necrosis, cyclosporine nephrotoxicity, and rejection [3]. Additionally, serum creatinine can be used to follow chronic rejection. In kidney transplant patients, an increase in serum creatinine concentrations of approximately 20% above baseline is considered significant and generally prompts additional investigations into possible kidney damage or rejection.

Several biosensor formats have been previously developed to measure serum creatinine concentrations including: amperometric, spectrometric, colorimetric, and immuno-based, and bioluminescence.

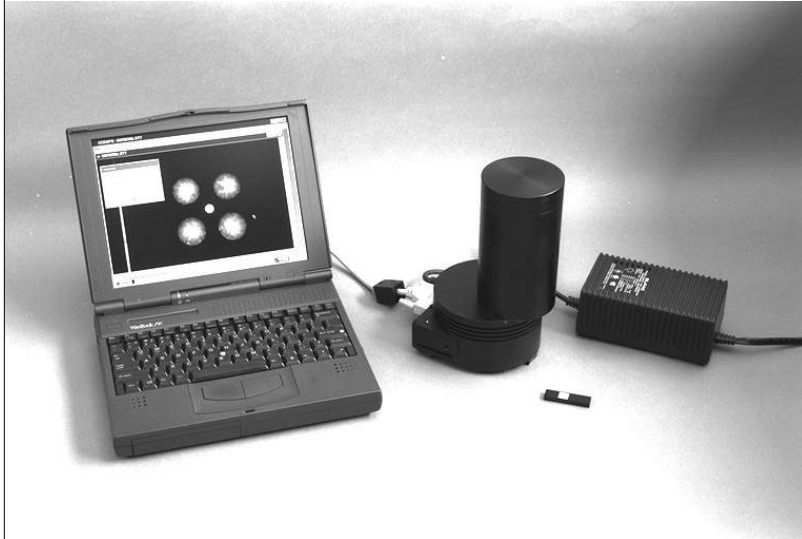
Bioluminescence was chosen based on high sensitivity, which leads to smaller blood sample sizes, and the possibility of measuring a number of other pertinent physiological markers at the same time with a bioluminescence format. A prototype CCD camera device for measuring bioluminescence was developed by Protein Solutions, Inc. in parallel with these assays. The homogeneous creatinine and creatine enzymatic assays would be based on the following reactions.



Since serum creatine concentrations are within the same range as creatinine concentrations, a functional creatinine biosensor based on these reactions would require the measurement of creatine as well as creatinine. The measurement of creatine may be important for the monitoring of several pathologies or treatments.

The firefly luciferase (FFL) reaction produces light in proportion to adenosine triphosphate (ATP) concentrations. The light (yellow-green [562 nm]) produced by the firefly luciferase reaction can be observed by a luminometer, CCD camera, and even the naked eye. The creatinine and creatine assays were studied with a luminometer and the Protein Solutions, Inc., prototype device (shown in Figure 1).

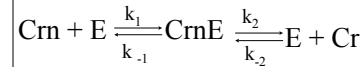
Figure 1 - Protein Solutions, Inc. CCD Prototype Device



Modeling Reactions

The following reaction schemes for the creatininase and creatine kinase reactions were used to derive the equations 1 and 3 with typical enzyme kinetic assumptions. Using the Michaelis-Menten definitions for the maximum velocity and the Michaelis-Menten Constants, equation 1 was converted to equation 2.

Creatininase Reaction Scheme



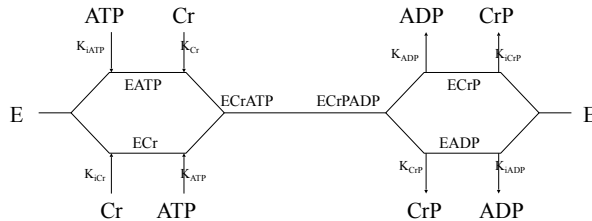
Equation 1

$$v = \frac{\frac{k_2 k_1 [\text{Crn}][\text{E}]}{k_2 - k_{-1}} - \frac{k_{-2} k_{-1} [\text{Cr}][\text{E}]}{k_2 - k_{-1}}}{1 + \frac{k_1 [\text{Crn}]}{k_2 - k_{-1}} + \frac{k_{-1} [\text{Cr}]}{k_2 - k_{-1}}}$$

Equation 2

$$v = \frac{V_f \frac{[\text{Crn}]}{K_{\text{Crn}}} - V_r \frac{[\text{Cr}]}{K_{\text{Cr}}}}{1 + \frac{[\text{Crn}]}{K_{\text{Crn}}} + \frac{[\text{Cr}]}{K_{\text{Cr}}}} \quad \begin{matrix} V_f = k_2 [\text{E}] \\ V_r = k_{-1} [\text{E}] \end{matrix} \quad \begin{matrix} K_{\text{Crn}} = \frac{k_2 - k_{-1}}{k_1} \\ K_{\text{Cr}} = \frac{k_2 - k_{-1}}{k_{-2}} \end{matrix}$$

Creatine Kinase Reaction Scheme



Equation 3

$$v = \frac{V_f [\text{Cr}][\text{ATP}] - V_r \frac{[\text{CrP}][\text{ADP}] K_{\text{Cr}} K_{\text{ATP}}}{K_{\text{ADP}} K_{\text{ICr}}}}{K_{\text{Cr}} K_{\text{ATP}} + K_{\text{ATP}} [\text{Cr}] + K_{\text{Cr}} [\text{ATP}] + [\text{Cr}][\text{ATP}] + \frac{K_{\text{CrP}} K_{\text{ADP}}}{K_{\text{ADP}} K_{\text{ICr}}} + \frac{K_{\text{Cr}} K_{\text{ATP}} [\text{ATP}][\text{CrP}]}{K_{\text{CrP}} K_{\text{IADP}}} + \frac{K_{\text{Cr}} K_{\text{ATP}} [\text{ADP}]}{K_{\text{ADP}}} + \frac{K_{\text{Cr}} K_{\text{ATP}} [\text{CrP}]}{K_{\text{CrP}}} + \frac{K_{\text{Cr}} K_{\text{ATP}} [\text{CrP}][\text{ADP}]}{K_{\text{CrP}} K_{\text{ADP}}}}$$

Equations 2 and 3 can be combined by using mass balance equations. The creatininase and creatine kinase equations can be solved numerically. Based on the assumption that the firefly luciferase Reaction is much slower than the creatinase and creatine kinase

reactions, the firefly luciferase reaction was modeled by converting the ATP concentration into light output with an empirical factor. The maximum velocity and Michaelis-Menten constants used in the model for creatininase and creatine kinase were previously determined by K. Rikitake et al., and J.F. Morrison et al., respectively [4,5].

Figure 2 depicts time course of light production for several different creatinine concentrations. The model and associated assumptions seem appropriate, based on the similarity of the model results to the experimental results shown on Figure 7. Figure 3 depicts a creatinine calibration curve based on the model.

Figure 2 - Time Course of Light Production for Creatinine Biosensor

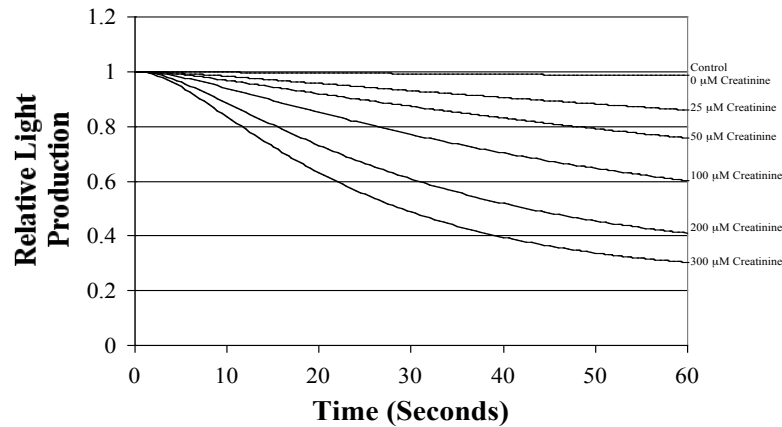
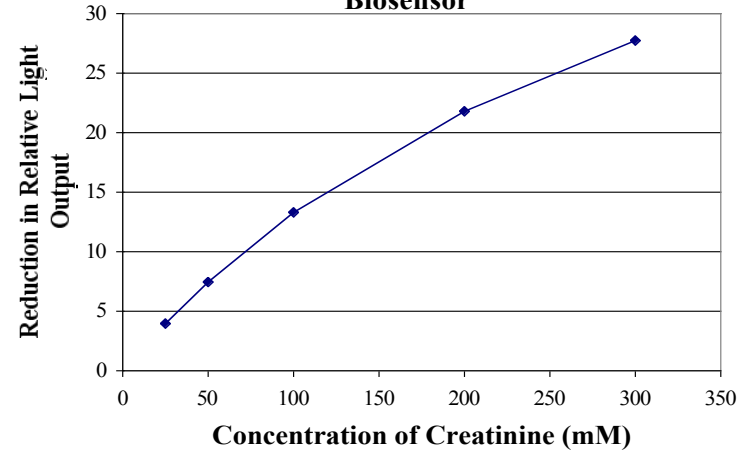
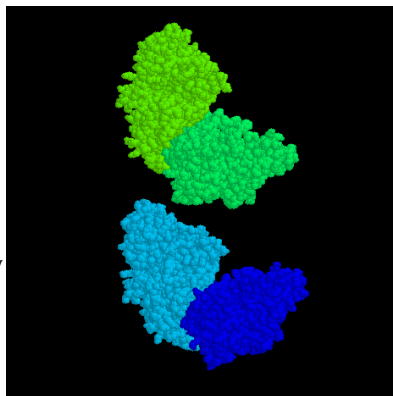


Figure 3 - Calibration Curve for Creatinine Biosensor



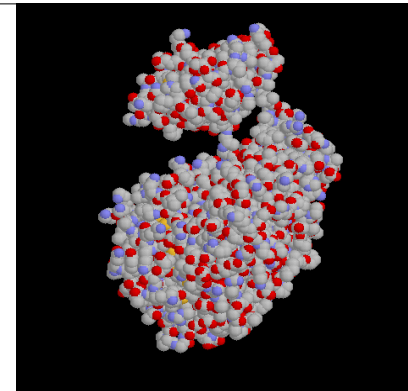
Methods and Materials

Homogeneous assays for creatinine and creatine were performed with creatininase, creatine kinase, and firefly luciferase. Creatininase forms both octamers and hexamers (175 kD for the octamer composed of 23kD subunits). A zinc (or Mn, Co, Mg, Fe, or Ni) ion is necessary for creatininase's functionality. Creatininase is robust especially in regards to heat. The muscle and brain creatine kinase isozymes



Crystal Structure of Creatine Kinase (Chicken Brain) [6]

generally form dimers (80 kD as a dimer and 40 kD as a subunit), while the mitochondrial isozymes form dimers, hexamers and octamers (340 kD as a octamer and 42 kD as a subunit). Creatine kinase is relatively labile. Firefly luciferase is approximately 62 kD in size. Firefly luciferase is naturally found in fireflies; however, the firefly luciferase used in these experiments was recombinant (with hexahistidine tag for purification).



Crystal Structure of Firefly Luciferase

Results and Discussion

The interference between the three reactions was found to be insignificant in the range of substrate and enzyme concentration ranges used in these assays. Figure 4 depicts the results from a pH optimum experiment ($n=3$, $CV=5\%$) for the creatine assay recorded by a TD 20/20 luminometer. Based on these results, the pH optimum of the creatine and creatinine assays appeared to be dominated by the pH optimum for the firefly luciferase reaction, which has a pH optimum at approximately 7.6.

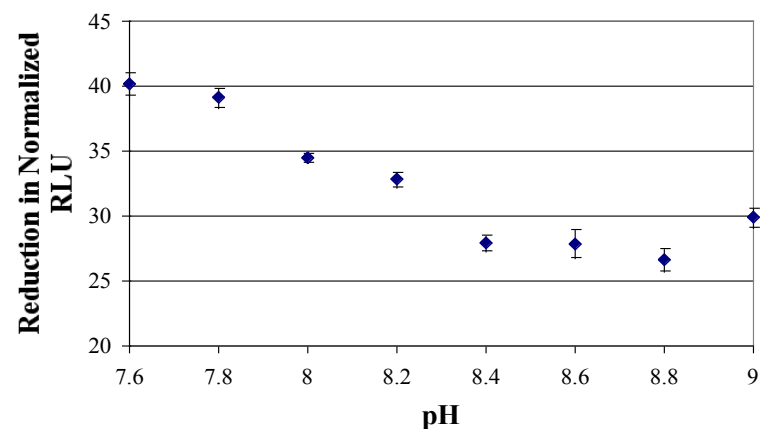
Based on manipulations of the creatinine assay model, the optimum calibration curve was found at the maximum concentration of creatine kinase, which is limited by its solubility (approximately 5 mg/mL). This result was confirmed with creatine assay experiments. Figure 5 shows the effect of enzyme ratio between creatine kinase and luciferase on the calibration curve for the creatine assay recorded with a TD 20/20 luminometer ($n=3$, $CV=6\%$). The creatine and creatinine assays were found to be relatively insensitive to firefly luciferase concentrations.

The creatine and creatinine homogeneous assays were plagued with highly variable peak heights of the bioluminescence signal. Based on modeling experiments, the bioluminescence peak height should be constant with different creatinine and creatine concentrations. Therefore, bioluminescence signal measured by the TD 20/20 luminometer was normalized to peak height. However, the Protein Solutions, Inc. CCD prototype can only measure the integration of the bioluminescence signal, not the time course necessary to capture the peak height.

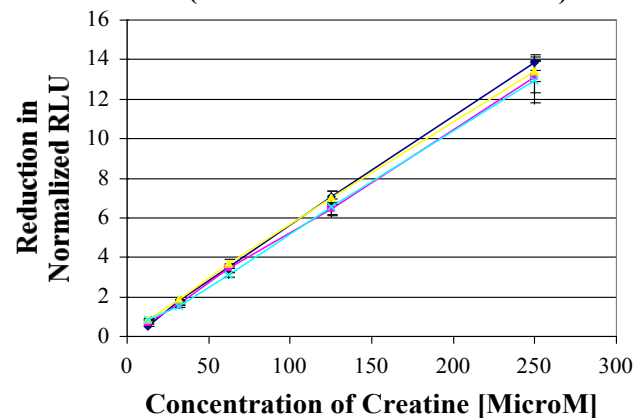
This limitation leads to large coefficients of variations (CVs [approximately 20%]) in the calibration curves measured with the prototype. Several additives including EDTA and DTT were used in attempts to decrease CVs associated with the prototype. Other than decreasing the magnesium concentration (below the optimum for the firefly luciferase reaction), which is shown in Figure 6 to have mild effect, the addition of these additives did not decrease the CVs. Due to these difficulties, interferences from serum constituents and proteins and comparisons with conventional assays were not performed.

Figures 7 and 8 show the results from creatinine assay ($n=3$, $CV=5.5\%$) and the corresponding creatinine calibration curve. The calibration curve of creatinine assays was shown to improve with increased assay time (from 60 to 180 seconds).

Figure 4 - Creatine Assay (pH Optimum)



**Figure 5 - Enzyme Ratio
(Creatine kinase to Luciferase)**



**Figure 6 - Creatine Assay with CCD Prototype
Biosensor**

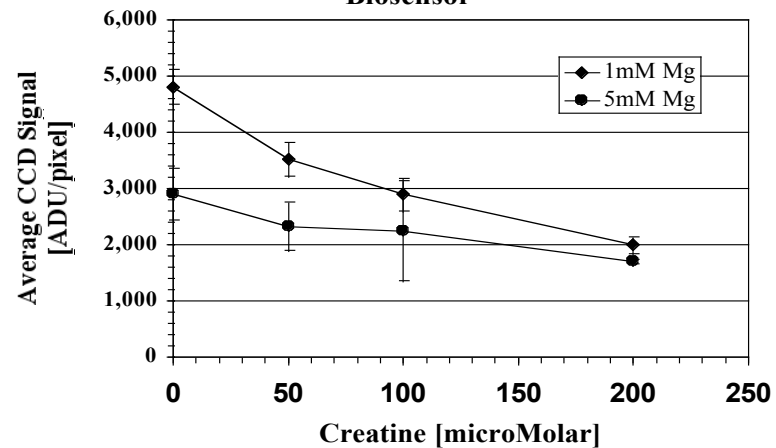


Figure 7 - Creatinine Assay

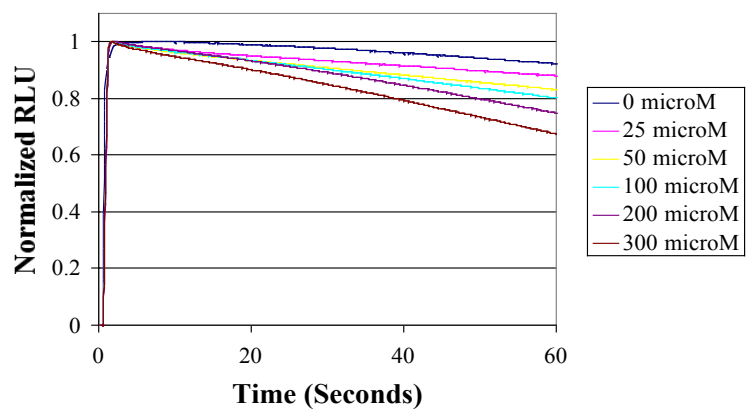
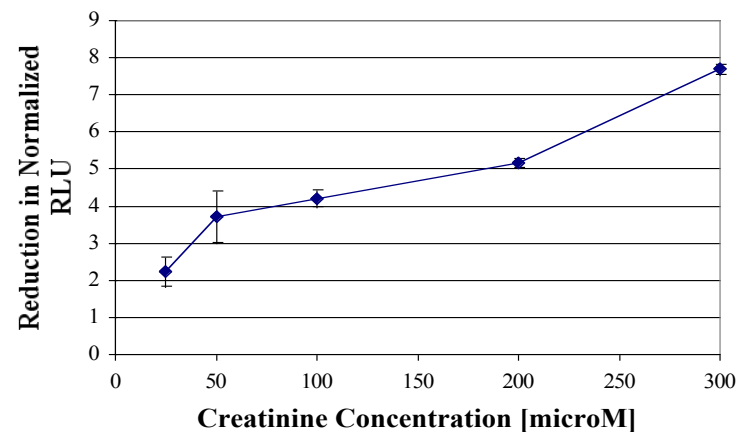


Figure 8 - Calibration Curve for Creatinine



Conclusions

Although the homogeneous assays for creatinine and creatine recorded by the TD 20/20 luminometer and normalized to peak heights had appropriate coefficient of variations (CVs) for a functional biosensor, the CVs associated with the Protein Solutions, Inc., CCD prototype need to be improved for a functional biosensor for creatinine and creatine. The decreased amplification by coenzyme A of the bioluminescence signal with decreasing ATP concentrations will be studied as a method to improve the resolution of the assays.

Acknowledgements

Special thanks to Protein Solutions, Inc., and Dr. Russell Stewart for laboratory space and Dr. John Holman, Jr. for helpful discussions. This work has been partially supported by the Whitaker Foundation (a grant in the Cost Reducing Health Care Technologies program- a joint program with the National Science Foundation) and NIH SBIR Phase I grant (1R43DK55426-1)

References

Normal Reference Values for Creatine, Creatinine, and Carnitine are Lower in Vegatarians, Joris Delanghe et al., Clinical Chemistry, 1989, Vol. 35, No. 8, p. 1802-1803

Biological variation of serum and urine creatinine and creatinine clearance: ramifications for interpretation of results and patient care, Elizabeth M.S. Gowans et al., Annals of Clinical Biochemistry, 1988, Vol. 25, p. 259-263

Predicting Glomerular Filtration Rate After Kidney Transplantation, Brian J. Nankivell et al., 1995, Vol. 59, p. 1683-1689

Creatinine Amidohydrolase (Creatininase) from *Pseudomonas putida*, K. Rikitake et al., 1979, J. Biochem., Vol. 86, p. 1109-1117

The Mechanism of the Reaction Catalysed by Adenosine Triphosphate-Creatine

Phosphotransferase, J.F. Morrison et al.,
1965, Biochem. J., Vol. 97, p. 37-52

Crystal structure of brain-type creatine
kinase at 1.41 Å resolution, Michael Eder
et al., Protein Science, 1999, Vol. 8 p.
2258-2269

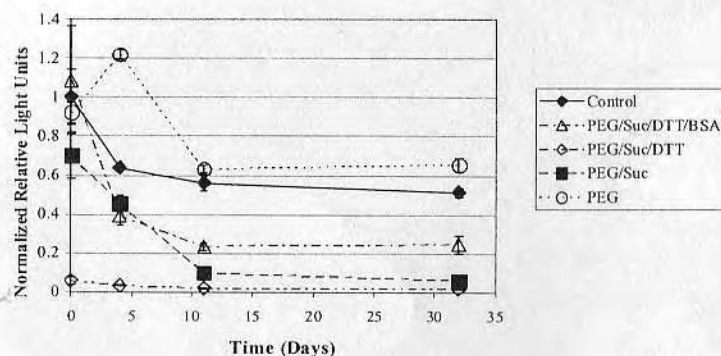


Figure 3. Decreased lactate assay activity with storage time after lyophilization. The light intensity is normalized to the control (no excipients) before lyophilization.

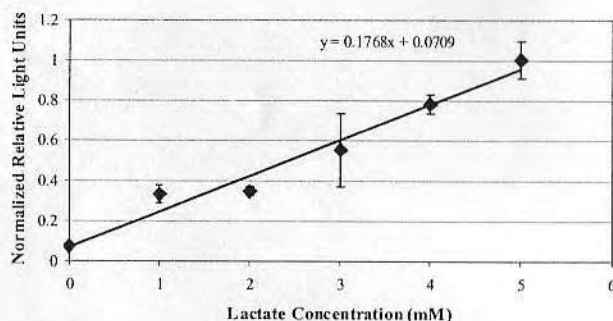


Figure 4. Calibration curve for lactate observed in the miniaturization experiment. The light intensity is normalized to the highest average light intensity measurement.

REFERENCES

1. Min D, Andrade J. Preliminary study of the optimum conditions for lactate sensor based on bacterial bioluminescence. In: Hastings JW, Kricka LJ, Stanley PE. editors. *Bioluminescence and Chemiluminescence*. Chichester: John Wiley & Sons, 1997: 275-8.
2. Davies RH. Thesis in progress
3. Girotti S, Grigolo B, Ferri E, Ghini S, Carrea G, Bovara R, Roda A, Motto R, Petilino R. Bioluminescent flow sensor for the determination of L-(+)-lactate. *Analyst* 1990; 115: 889-94.

LACTATE ASSAY BASED ON BACTERIAL BIOLUMINESCENCE: ENHANCEMENT, DRY REAGENT DEVELOPMENT, AND MINIATURIZATION

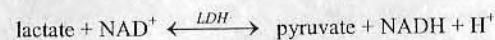
RH DAVIES, JW CORRY, JD ANDRADE

Dept of Bioengineering, University of Utah, Salt Lake City, 84112, USA

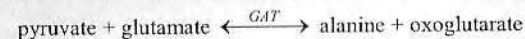
Email: rupert.davies@m.cc.utah.edu

INTRODUCTION

Bacterial bioluminescence can be used as an enzymatic sensor to measure reduced nicotinamide adenine dinucleotide (NADH) as well as analytes that can be coupled to NADH. Lactate can be measured using lactate dehydrogenase (LDH) coupled to the bacterial bioluminescence system of flavin mononucleotide (FMN): NADH oxidoreductase (OR) and bacterial luciferase (BL):



Lactate sensors are useful for clinical analyses, food and beverage analyses, and in sports medicine. Lactate concentrations in blood (normal without exercise), tears, and sweat are approximately 0.5 mmol/L, 2.5 mmol/L, and 12 mmol/L, respectively. Some advantages of a bioluminescent lactate assay are sensitivity and small sample volumes. A previously reported aqueous homogeneous lactate assay¹ was enhanced with the additional of glutamic-alanine transaminase (GAT), which consumes pyruvate, thereby increasing NADH production by LDH.



Since a biosensor for lactate would be stored a room temperature, the aqueous assay was converted to a dry reagent assay with the addition of several common excipients, including sucrose (Suc), polyethylene glycol (PEG), dithiothreitol (DTT), bovine serum albumin (BSA), and ethylenediaminetetraacetic acid (EDTA). Formulations were tested before and after lyophilization as well as after weeks and months of storage. Aqueous and dry reagent lactate assays are being miniaturized for the development of a multi-analyte biosensor.²

METHODS

Instrumentation

Bioluminescence was measured in relative light units with a photon multiplier tube (PMT)-based luminometer (Turner Designs TD 20/20).

Reagents (from Sigma unless noted otherwise)

All assays were performed in a solution of 0.05 M Tris buffer at pH 7.6 and at room temperature. The final concentrations for the enhancement experiment were 1 mM NAD^+ ; 1, 3, and 5 mM lactate; 0.055 mg/mL LDH; 0.02 mM FMN; 0.07 mM dodecyl aldehyde (Aldrich); 17.5 nM OR; and 20 nM BL with/without 5 mM glutamate and 0.014 mg/mL GAT. The final concentration for the inhibition and lyophilization experiments were 1 mM NAD^+ ; 5 mM lactate, 0.15 mg/mL LDH, 0.02 mM FMN, 0.07 mM dodecyl aldehyde, 100 nM OR, 20 nM BL, 5 mM glutamate and 0.085 mg/mL GAT with 0.5 M sucrose (Pfanstiehl), 0.2 mg/mL PEG (8kD), 10 mg/mL BSA, 0.1 mM EDTA and 100 mM DTT. The final concentrations for the miniaturization experiment were 1 mM NAD^+ ; 1, 2, 3, 4, and 5 mM lactate, 0.5 mg/mL LDH, 0.125 mM FMN, 0.07 mM dodecyl aldehyde, 100 nM OR, 20 nM BL, 2 mM glutamate and 0.1 mg/mL GAT.

Procedures

The enhancement, inhibition and lyophilization experiments were performed by injecting 50 μL of lactate solutions into the 250 μL of reagent mixtures in 12mm (diameter) x 50mm luminometer tubes (Turner Designs). The miniaturization experiment was performed by injecting 5 μL of lactate solution into 25 μL of reagent mixtures in 12mm x 50mm luminometer tubes. Lyophilization was performed in two stages with a Virtis 12EL Lyophilizer. The lyophilized mixture was reconstituted with 250 μL of reagent-grade water and BL/OR mixture immediately, 1 week, and 1 month after lyophilization. The storage conditions were room temperature and in the dark.

RESULTS AND DISCUSSION

Note that several different ranges of lactate concentration were used, corresponding to the different physiological samples of interest. The addition of GAT to the lactate assay increased the light intensity by approximately 20%, Fig. 1, which is considerably less than the 117 to 183% previously reported.³

The results of the inhibition study, Fig. 2, show that none of the excipients used in the lyophilization experiment greatly inhibited the lactate assay with GAT. Although EDTA did not significantly inhibit the lactate assay, EDTA was removed as an excipient because prior lyophilization experiments (results not shown) indicated greatly decreased activity of the lactate assay immediately after lyophilization with EDTA. The activity of lactate assay with the exception of OR and BL was measured with room temperature storage time, Fig. 3. The excipients that appear to preserve the most activity of the lactate assay after 30 days of room temperature storage were PEG alone and the addition of BSA to the PEG/Suc/DTT mixture, Fig. 3. Note that the 0 and 3 day points correspond to pre- and post-lyophilization and that little to no additional activity was lost from one week to one month.

The miniaturization experiment shows that even though the volume of the assay and sample have been reduced an order of magnitude the calibration curves for lactate changed very little between Fig. 1 and Fig. 4.

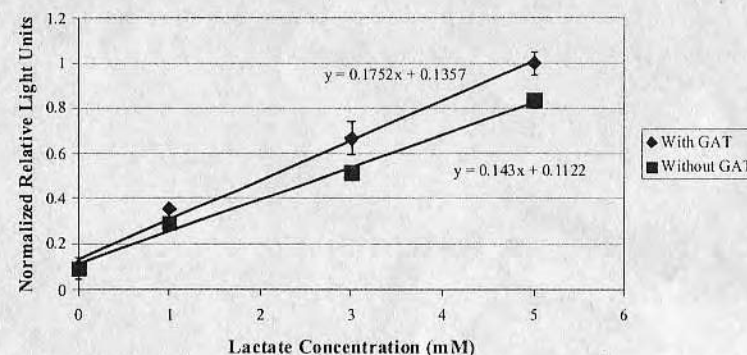


Figure 1. Large volume (300 μL) lactate assay enhanced by GAT. All points represent the average of five integrated over 90 seconds light intensity measurements. The light intensity is normalized to the highest average light intensity measurement. All error bars indicate one standard deviation.

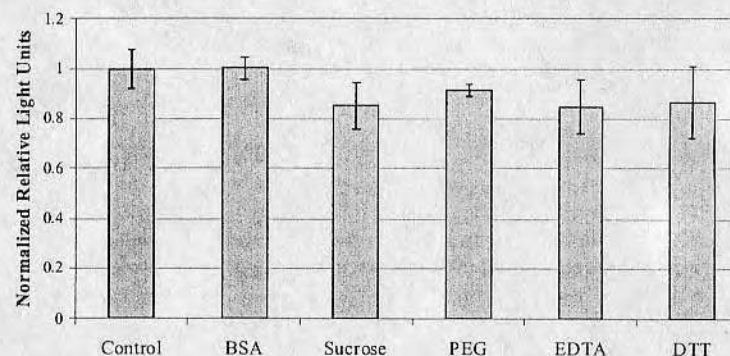
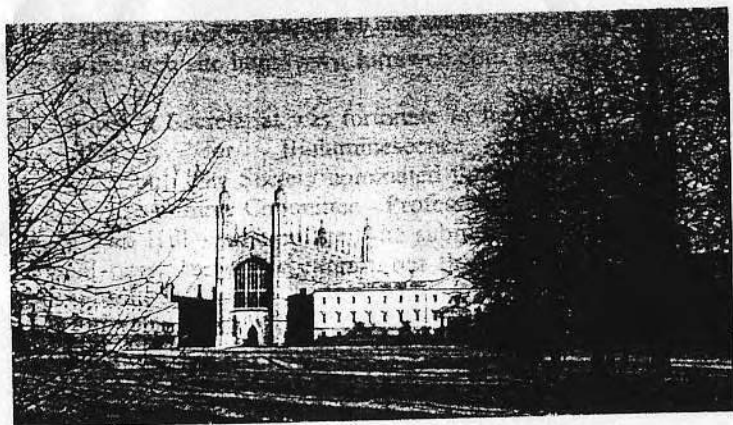


Figure 2. Excipient inhibition of potential lactate assay. The light intensity is normalized to the average control light intensity measurement.

BIOLUMINESCENCE & CHEMILUMINESCENCE

Progress & Current Applications



editors

Philip E. Stanley

Cambridge Research & Technology Transfer Ltd., England

Larry J. Kricka

*Department of Pathology & Laboratory Medicine
University of Pennsylvania School of Medicine, USA*

World Scientific
New Jersey • London • Singapore • Hong Kong

Published by

World Scientific Publishing Co. Pte. Ltd.

P O Box 128, Farrer Road, Singapore 912805

USA office: Suite 1B, 1060 Main Street, River Edge, NJ 07661

UK office: 57 Shelton Street, Covent Garden, London WC2H 9HE

British Library Cataloguing-in-Publication Data

A catalogue record for this book is available from the British Library.

BIOLUMINESCENCE & CHEMILUMINESCENCE: PROGRESS & CURRENT APPLICATIONS

Copyright © 2002 by World Scientific Publishing Co. Pte. Ltd.

All rights reserved. This book, or parts thereof, may not be reproduced in any form or by any means, electronic or mechanical, including photocopying, recording or any information storage and retrieval system now known or to be invented, without written permission from the Publisher.

For photocopying of material in this volume, please pay a copying fee through the Copyright Clearance Center, Inc., 222 Rosewood Drive, Danvers, MA 01923, USA. In this case permission to photocopy is not required from the publisher.

ISBN 981-238-156-2

This book is printed on acid-free paper.

Printed in Singapore by Uto-Print

Diabetes-Related Luminescent Assays for Multi-Analyte Measurement

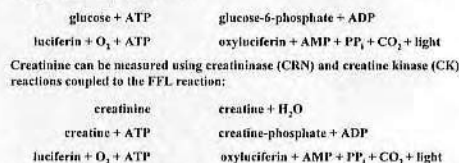
Rupert Davies, Jeremy Abernathy, Joseph Andrade
Dept of Bioengineering, University of Utah, Salt Lake City, 84112, USA
Email: rupert.davies@mc.utah.edu

INTRODUCTION

Luminescence-based analysis can potentially measure a wide range of metabolites with the same device. Most metabolites of interest can be coupled to a luminescence detection system. Luminescence-based analysis is particularly useful for multi-analyte devices. Some advantages of luminescent assays are sensitivity and small sample volumes. We are currently developing a variety of luminescence-based analytical assays that will ultimately be combined onto a multi-analyte hand-held device. Our goal is to develop quantitative analytical systems for the measurement of up to 50 analytes in 50 microliters or smaller volumes of physiologic fluids, such as blood and urine. Ultimately, if the potential of luminescence-based assays is realized, nearly all biochemicals could be quantitatively and specifically measured in small volume samples via relatively inexpensive, reliable instruments in point-of-care environments.

Glucose and creatinine are important in the diagnosis, management and treatment of diabetic patients. Creatinine has been included because diabetes is the number one cause of kidney disease and a third of all diabetics may ultimately develop a form of kidney disease. Glucose and creatinine are both measured by coupling enzymatic reactions (glucokinase; creatinase and creatine kinase; respectively) to the bioluminescent firefly luciferase reaction. In both cases the light measured is proportional to the concentration of the analyte in the sample. The glucose and creatinine assays need only small sample volumes and have been lyophilized to increase storage stability and ease of application.

Firefly as well as bacterial bioluminescence and chemiluminescence can be used as an enzymatic sensor to measure adenosine triphosphate (ATP), reduced nicotinamide adenine dinucleotide (NADH), and hydrogen peroxide (H_2O_2), respectively, as well as analytes that can be coupled to ATP, NADH, and H_2O_2 . Many bioluminescence assays have been previously developed.¹ For instance, glucose can be measured by coupling the glucokinase (GK) reaction to the firefly luciferase (FFL) reaction:



Glucose is frequently measured for the management of diabetes. Glucose concentrations in blood can range from 3 to 6 mM in normal patients and 5 to 20 mM in diabetics. Glucose concentrations in tears and saliva are approximately 1/20 and 1/30 of blood concentrations,^{2,3} respectively. Creatinine sensors are useful for assessing renal condition. Creatinine concentrations in tears and blood are approximately 75 μM ⁴ and approximately 1/10 in saliva.⁵

Since a bioluminescence-based biosensor will be stored at room temperature, aqueous assays were converted to dry reagent assays with the addition of several common excipients, including sucrose (Suc), dithiothreitol (DTT), polyethylene glycol (PEG), dextran (Dex), bovine serum albumin (BSA), trehalose (Tre) and mannitol (Man). Dry reagent assays are being reduced in volume for the development of a multi-analyte biosensor.⁶

METHODS

Instrumentation

Bioluminescence was measured in relative light units with a photon multiplier tube (PMT)-based luminometer (Turner Designs TD 20/20). Bioluminescent images were collected with a thermally cooled, charge-coupled device (CCD) camera (Santa Barbara Instrument Group ST-7).

Reagents (from Sigma unless noted otherwise)

All glucose experiments were performed in a buffer solution of 0.1M tricine at pH 8.5 while all creatinine and ATP assay experiments were performed in a buffer solution of 0.5 M glycine-glycine at pH 7.8 and at room temperature.

The final concentrations for the glucose inhibition and lyophilization experiments were: 1 mM luciferin (Biosynth); 1 μM FFL (Promega); 5 μM ATP/ Mg^{2+} ; 1 μM and 10 μM glucokinase for inhibition and lyophilization experiments, respectively; 0.5 M sucrose (Pfanstiehl); 0.5 M trehalose (Pfanstiehl); 0.5 M mannitol (Pfanstiehl); 6 mg/mL PEG (8kD); 2.5 mg/mL BSA; 5 mg/mL Dextran (Pharmacia 40kD); and 10 mM DTT. The final glucose concentration for the inhibition experiments was 10 μM .

Reagents (cont.)

The final concentrations for the creatinine experiments were: 0.2 mM luciferin (Biosynth); 100 μM FFL (Promega); 1 μM ATP/ Mg^{2+} ; 350 nM creatinase; and 40 μM creatine kinase.

The final concentrations for the ATP chip experiment were: 1 mM luciferin (Biosynth); 500 nM FFL (Promega); 1 μM ATP/ Mg^{2+} ; 0.5 M sucrose (Pfanstiehl); 2.5 mg/mL BSA; and 5 mg/mL Dextran (Pharmacia 40kD).

Procedures

The glucose and creatinine experiments were performed by injecting 2 μL of glucose solution or 5 μL of creatinine solution into 8 μL and 25 μL of reagent mixture in 12 mm (diameter) x 50 mm luminometer tubes (Turner Designs), respectively. Lyophilization was performed in two stages with a Virtis 12EL Lyophilizer in Kimble culture tubes. The glucose lyophilized mixture was reconstituted with 8 μL of reagent-grade water immediately, 1 week (7 days), and 1 month (30 days) after lyophilization. The ATP chips were reconstituted with a gel equilibrated in a ATP standard solution after 20 days of storage. The storage conditions were at room temperature in the dark for the ATP chips and the glucose lyophilized assay was additionally stored in a desiccated vacuum chamber.

RESULTS AND DISCUSSION

Note that several different ranges of concentration were used, corresponding to the different physiological samples of interest. The results of the glucokinase inhibition study, Figure 1, show that none of the excipients tested exhibited significant inhibition; with the exception of sucrose and trehalose. Since previous studies showed that the combination of sucrose, DTT, BSA, and dextran most effectively preserved firefly luciferase activity,⁶ mannitol was used to replace the sugar, sucrose.

The activity of glucokinase and firefly luciferase was measured as a function of storage time, Figures 2 and 3, respectively. Note that the -4 and 0 day points correspond to an aqueous experiment prior to lyophilization and reconstituted experiment immediate post-lyophilization, respectively. Little additional activity was observed to be lost from one week to one month, with the exception of the control (no excipients). The excipient combination that appears to preserve the most activity of the firefly luciferase and glucokinase after 30 days of room temperature storage was mannitol, BSA, and DTT. The majority of the activity loss in glucose assay appears to be due to the instability of firefly luciferase. Figure 4 shows the light intensity time course for the lyophilized glucose assay after 30 days of storage. Figure 5 shows the glucose assay calibration curve after 30 days of storage. Even though the firefly luciferase lost over 90% of its original activity after 30 days of storage, a useful glucose assay could still be obtained. Note that the dynamic range of the glucose assay can be adjusted to the millimolar range by decreasing the concentration of glucokinase (results not shown).

The light intensity time course for the creatinine assay is shown in Figure 6. Figure 7 shows the creatinine assay calibration curve. Lyophilization studies of the creatinine assay as well as lyophilization studies of the glucose assay in a chip format are in progress.

The results of the ATP chip experiment, Figure 8, show that 1 μM ATP can be detected in 1 μL of sample (1 picomole of ATP) even after 20 days of room temperature storage.⁸ Note that heterogeneity of the light intensity in the well of the chip may be due to the shape of the gel used to reconstitute the ATP chip.

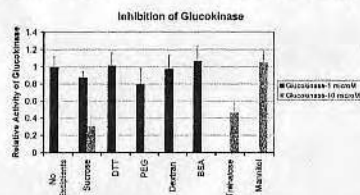


Figure 1. Excipient inhibition of glucokinase. The light intensity is normalized to the peak light intensity measurement for each replicate. All columns represent the average of five light intensity measurements collected over 120 seconds. All error bars indicate one standard deviation.

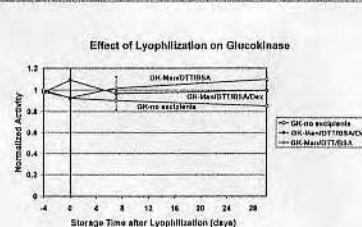


Figure 2. Glucokinase activity with storage time after lyophilization. The light intensity is normalized to the control (no excipients) before lyophilization. All point represent the average of five light intensity measurements collected over 85 seconds. Glucokinase activity was measured by the reduction of light intensity.

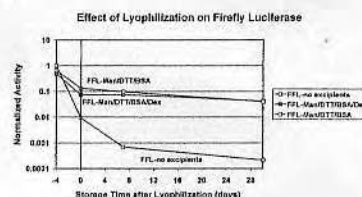


Figure 3. Firefly luciferase activity with storage time after lyophilization. The light intensity is normalized to the control (no excipients) before lyophilization. All point represent the average of five light intensity measurements collected over 85 seconds. Firefly luciferase activity is measured by peak light intensity.

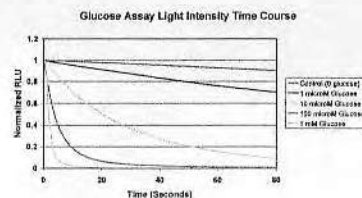


Figure 4. Light intensity time course for lyophilized glucose assay. Each curve represents the average of five replicates.

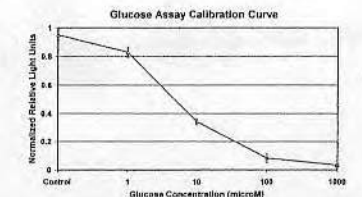


Figure 5. Calibration curve for glucose observed in the lyophilization experiment after 30 days of storage at room temperature in a desiccated vacuum chamber. All points represent the average of five light intensity measurements collected over 85 seconds.

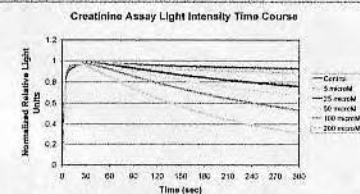


Figure 6. Light intensity time course for creatinine assay. Each curve represents the average of five replicates.

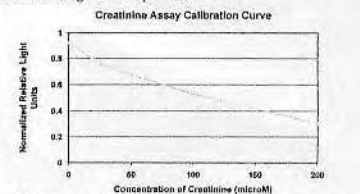


Figure 7. Calibration curve for creatinine assay. All points represent the average of five light intensity measurements collected over the last 10 seconds of the time course.



Figure 8. CCD image of 1 μM ATP sample in 0.4 μL wells. The image is after 20 days of room temperature storage. This figure demonstrates that we are currently developing multi-channel, multi-analyte arrays.

CONCLUSIONS

- None of the excipients tested significantly inhibited glucokinase, with the exception of sucrose and trehalose.
- The excipient combination of mannitol, DTT, and BSA appeared to most effectively protect glucokinase and firefly luciferase from room temperature storage.
- Even though the firefly luciferase loss over 90% of its original activity after 30 days of storage, a useful glucose assay could still be obtained.
- Creatinine can be effectively measured with the bioluminescence-based assay.
- Even after 20 days of storage, 1 μM ATP can be detected in 0.4 μL of sample (0.4 picomole of ATP).

ACKNOWLEDGEMENTS

We would like to acknowledge the support of NIH RFA-PAR-01-057, Project RR17329, Technology Development for Biomedical Applications Grant and our industrial partners.

REFERENCES

- Brudin S, Wettermark G. Bioluminescence Analysis 1992: VCH.
- Kung J, Fulop G, Friedman AH. Tear urea nitrogen and creatinine levels in renal patients. *Arch Ophthalmol*, 1988, Vol 66, PP 407-12.
- Forhal JN, Collins RE, Skalkell GK, Simonsen PI. Glucose concentrations in parol fluid and venous blood of patients attending a diabetic clinic. *J R Soc Med*, 1981, Vol 74, PP 725-8.
- Gowan EM, Fraser CG. Biological variation of serum and urine creatinine and creatinine clearance: ramifications for interpretation of results and patient care. *Ann Clin Biochem*, 1988, Vol 25, PP 259-63.
- Lloyd JE, Broughton A, Selby C. Salivary creatinine assays as a potential screen for renal disease. *Ann Clin Biochem*, 1996, Vol 33, PP 428-31.
- Davies RH. University of Utah thesis in progress.
- Davies RH, Van Wageningen RA, and Andrade JD. Stabilization of firefly luciferase with antioxidants: a preliminary study. 11th International Symposium on Bioluminescence and Chemiluminescence 2000, Monterey, California: John Wiley & Sons.
- Davies RH, Burkholtz DA, Andrade JD. Personal Sensors for the Diagnosis and Management of Metabolic Disorders. *IEEE Eng Med Biol Mag*, in press.



©MASTERSERIES, ©EYEWIRE

Personal Sensors for the Diagnosis and Management of Metabolic Disorders

Luminescence-Based Analysis that Facilitates the Measurement of Multiple Metabolites from Small Sample Volumes for Use in Point-of-Care or In-Home Environments

RUPERT DAVIES,
DANIEL A. BARTHOLOMEUSZ,
AND JOSEPH ANDRADE

The management of metabolic disorders could be greatly enhanced by patients and physicians if they had the ability to measure and track their disorder just as a diabetic does with a glucometer. To address this, we are developing a disposable, dipstick-type, and quantitative analytical device for the measurement of multiple analytes in small sample volumes. Such a device could be used for the prediction, diagnosis, and management of various diseases or clinical conditions at the point-of-care (POC) and eventually in-home environments. Since nearly all analytes of interest can be coupled to luminescence reactions, luminescence-based analysis can potentially measure a wide range of analytes with the same device [1]. These luminescence-based assays can be inexpensively packaged in a stable form within an array of analytical wells. A photodetector array incorporated into a handheld device can measure the various analyte concentrations by the proportional light intensities from the array of luminescent assays. The highly sensitive nature of luminescence-based analyses means that more analytes can be measured from smaller sample volumes. Furthermore, simple, rapid and inexpensive acquisition and presentation of a patient's multiple biochemical conditions would lead to patient/provider empowerment and improved disease management.

Background

Many diseases and clinical conditions have biochemical origins, consequences, or markers that can be used to predict, diagnose, or manage these pathologies. Effective management of some pathologies require regular, routine clinical chemistry measurements of various analytes. A well-known example is glucose and glycosylated hemoglobin measurements necessary for the management of diabetes [2]. Other diseases such as the inborn metabolic diseases phenylketonuria (PKU) [3] and galactosemia [4] also need regular monitoring of relevant analytes.

Although clinical chemistry and analytical laboratories can routinely assay carbohydrates, amino acids, vitamins, and other low molecular weight biochemicals important to metabolism, in practice most of the major metabolites are rarely determined. Indeed, the direction in clinical medicine has been toward ordering less chemical tests rather than more, because of the interest in minimizing healthcare costs and thus in reducing "unnecessary tests." The expense of

most tests lies in the cost of central or commercial reference laboratories. These laboratories have expensive and sophisticated detection methods. Given the current expense of laboratory testing, cost-benefit analyses argue against more comprehensive biochemical analyses, except in high-risk or related situations. However, if the cost of clinical chemistry tests were significantly decreased, the cost-benefit analyses would be different, likely leading to recommendations for more rather than fewer tests.

Advanced biosensors can significantly reduce the cost of analyses by bringing the analytical testing to the POC. Designed properly, POC biosensors can rapidly measure multiple analytes from small sample volumes. This would provide the clinician with rapid chemical analyses, resulting in shorter patient visits and stays while also improving patient comfort [5]. Many POC biosensors measure key analytes (cholesterol, lactate, glucose) that usually exist in the millimolar concentration range. These biosensors are generally not sensitive enough for analyzing other important metabolites that exist in the micro to sub-microMolar range. Current POC biosensors utilize enzymatic, electrochemical, and optical (fluorescence and absorbance) methods to detect various analytes.

Luminescence-based analysis has the advantage that it is generally 100 to 1,000 times more sensitive than common spectroscopic/colorimetric methods [6], [7]. Chemiluminescence is light produced by compounds undergoing specific oxidation reactions, while bioluminescence is when these reactions are catalyzed by enzymes [7]. The most well-known example of bioluminescence is the firefly; however, other organisms employ similar reactions to produce light; e.g., bacteria, fish, and fungi. All bioluminescent reactions employ an enzyme called "luciferase," which facilitates the oxidation of an energetic substrate, called "luciferin," into an excited state, where it emits a photon. There are many different luciferases and luciferins with at least 30 different known bioluminescent reactions in nature.

The most common chemiluminescence reaction involves the oxidation of luminol, which produces blue (450 nm) luminescence. This reaction can be used to measure hydrogen peroxide (H_2O_2) and can be catalyzed by transition metals or horseradish peroxidase. The yellow-green (580 nm) bioluminescence of fireflies is based on the enzyme-catalyzed oxi-

dation of firefly luciferin utilizing adenosine triphosphate (ATP) as a highly specific co-reactant. The blue (490 nm) bioluminescence of marine bacteria is closely coupled to a reduced nicotinamide adenine dinucleotide (phosphate) [NAD(P)H]-dependent enzyme reaction. Thus, Mother Nature has literally given us two unique, ultrasensitive, and highly specific reactions for the measurement and monitoring of ATP and of NAD(P)H, while luminol chemiluminescence can be used to measure H_2O_2 . When analytes are coupled to ATP, NAD(P)H, or H_2O_2 via metabolic reactions, the intensity of luminescence is proportional to the concentration of the specific biochemical of interest in the sample. The reactions are sensitive to ATP or NAD(P)H over five orders of magnitude in concentration [6] without dilution or modification of the sample fluid. Since most of biochemistry depends on ATP and/or NAD(P)H or can be linked to H_2O_2 , practically all metabolic reactions or metabolites can be monitored or measured by luminescence via one or more enzyme-linked reactions (see a biochemical or metabolic pathways chart [8] or www.expasy.ch/cgi-bin/search-biochem-index). There is a large body of literature on the development of sensors for ATP, NAD(P)H, and H_2O_2 -dependent processes, using the firefly luciferase, bacterial luciferase, and luminol chemiluminescence reactions, respectively [6], [7].

Luminescence-based analysis remains underutilized as a commercial diagnostic method for multi-analyte systems. A reaction that produces photons has many advantages: the problems associated with color perception or wavelength separation are eliminated, as in the case of reflectance colorimetry; no light source is needed, as in the case of fluorescence spectroscopy; and no usage of electrodes, which can become contaminated, as in the case of much of analytical electrochemistry. The increased sensitivity due to the high signal-to-noise ratio intrinsic to luminescence measurements means only small sample volumes are required, thus making it possible to simultaneously measure many different metabolites. Measuring 10 to 20 different analytes may be possible within the 10-microliter sample volume now used to measure only glucose with commercial glucometers. With increasing demand for minimally invasive sampling that reduces patient discomfort and inconvenience, available sample volumes will probably decrease. Ultimately, if the potential of luminescence-based assays is realized, many relevant biochemicals could be quantitatively and specifically measured in small volume samples via relatively inexpensive, reliable instruments in point-of-care environments.

Inexpensive and reliable analyses of many biochemicals at the POC would enable clinicians to diagnose and treat even complex diseases and pathologies. Biochemical reactions do not exist or operate in isolation, and every reaction is obviously dependent on many other reactions through the principles of biochemical networks, reaction kinetics, and equilibria [8]. We must have the tools to move beyond mono-parameter chemical paradigms. Most of the papers we read deal only with one chemical parameter—with mono-parameter specific hypotheses or correlations. Biochemistry, medicine, and biology are not that simple. We need devices that can easily and inexpensively measure the many relevant biochemical parameters to provide the information base to more fully understand and effectively treat biochemical diseases in shorter time.

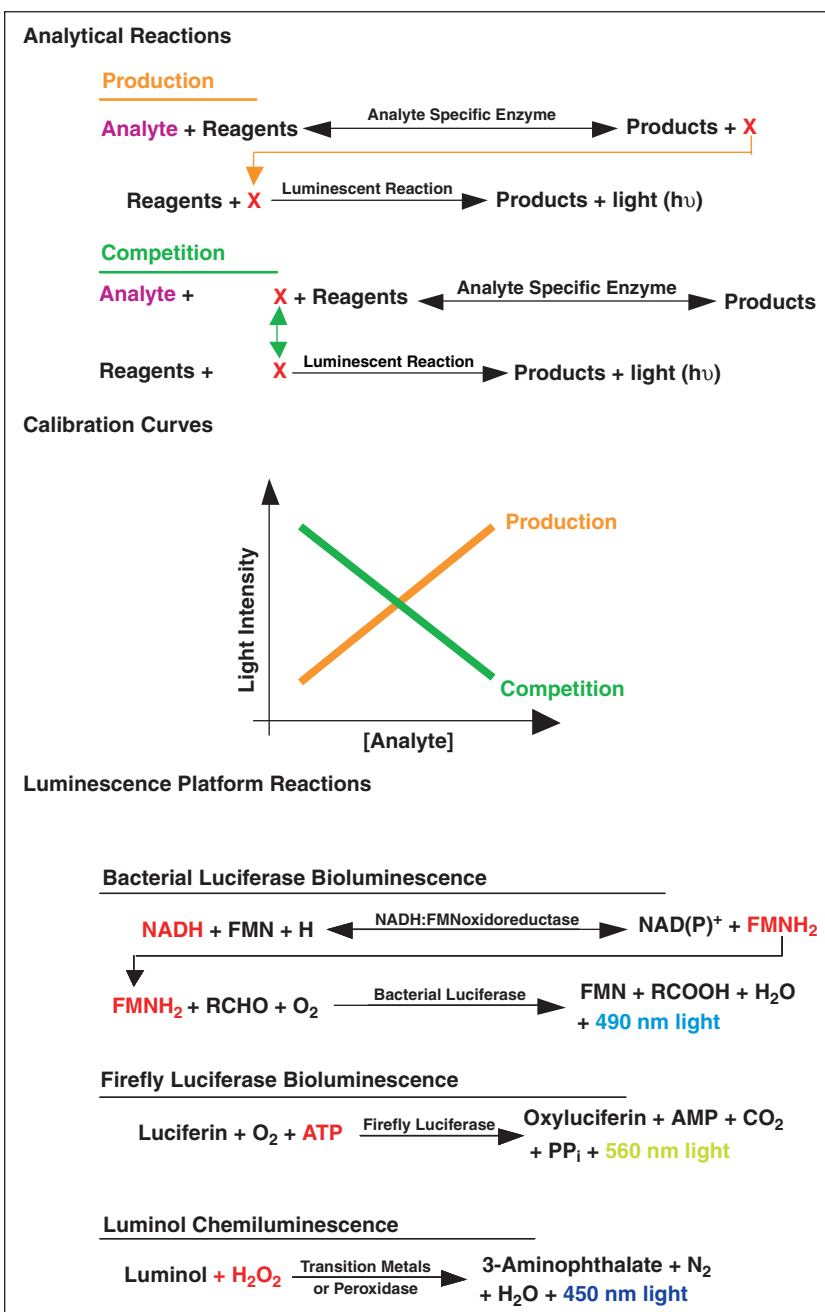


Fig. 1. Analytical reactions coupling analyte to luminescent reactions for assays. Idealized calibration curves for both production and competition assays are shown.

Part of our interest in this project is patient empowerment—getting patients to assume responsibility and control of their own diseases.

Dealing with many different channels of information is difficult. Therefore, we also address what is sometimes called the “cockpit problem”—how does a pilot, for example, deal with the tens and even hundreds of sensors and their outputs in a modern jet cockpit? How does an anesthesiologist, surgeon, or nurse deal with the myriad of monitors and signals in the typical operating room or intensive care suite? In our case, how do physicians, patients, and family members effectively deal with the interactions among many different analytes? Fortunately, advances in data analysis, parameter presentation, and data visualization allow this challenge to be effectively addressed. We are using multiparameter visualization tools, particularly multi-axes radar plots, to produce disease- and condition-specific icon-like patterns, which are easily recognizable.

A physician or patient need not use all the data generated but merely focus on the several channels of immediate clinical need and interest. Generally, many of the analytes needed for one disease are also important and relevant to other diseases, due to the interrelationship and highly interconnected nature of metabolism. Thus, the economic problems associated with developing a home assay for rare conditions such as PKU or galactosemia are minimized by producing one sensor that is useful for many applications and will be invaluable to clinical research.

Part of our interest in this project is patient empowerment—getting patients to assume responsibility and control of their own diseases. If, for example, PKU patients are given their biochemical information, particularly their phenylalanine concentration on a very regular basis, they will, in turn, utilize that information to regulate their own diet, much the way diabetics do by monitoring their glucose levels. We are now using some of the biosensing technologies in a modern, interactive science center (www.utahsciencecenter.org) to educate the general and journalistic public about the importance of informed patient empowerment. By providing the information that patients want, we give them some feedback that can improve their outcomes by allowing appropriate biochemical control of their disease (drugs, diet, etc.). This information empowerment means that patients, through direction from their physician, can monitor and manage their conditions away from the hospital, thus reducing patient visits and overall health management costs.

Approach

Our goal is a ChemChip system that is analogous to the present generation of glucose dipsticks and glucometers in terms of ease of use, quality of data, and low cost. The ChemChip, however, is able to simultaneously measure multiple analytes without increasing sample volume. The ChemChip requires several components to implement luminescence-based analytical chemistry in a POC device and display the relevant information

to the user in a form that is easy to interpret. The ChemChip system is summarized below and depicted in Figure 2.

ChemWare

Since nearly all biochemicals can be measured by luminescence assays, the first step is to select analytes appropriate for the prediction, diagnosis, or management of a particular pathology or clinical condition. The algorithm used to develop assays is depicted in Figure 3.

The algorithm of developing a luminescent assay for a particular analyte starts with finding possible reaction pathways that couple the analyte to ATP, NAD(P)H, or H_2O_2 . In general, any kinase, dehydrogenase, or oxidase could be used to couple an analyte to the ATP, NAD(P)H, or H_2O_2 platforms, respectively. These pathways are ranked based on smallest number of reactions involved, type of luminescent assay (a production assay is generally more sensitive than a competition assay), whether the assay is an homogeneous (single stage) assay rather than heterogeneous (multi-stage) assay, and on enzyme availability and/or cost. The advantage of a homogeneous assay is that all the reactions occur in the same stage, meaning the ChemChip can be quite simple. A heterogeneous assay would require one stage of reactions to be completed before the sample is moved to the next stage. However, since enzymatic reactions may have vastly different pH optimums or other conflicting reaction requirements, the challenge is optimizing the reaction conditions to provide a useful analytical output. However, if such an optimization is not feasible, a heterogeneous assay can still be used to measure the analyte.

The next step includes the simulation of the highest ranked pathways, based on reported kinetic parameters. The proposed assays are assessed by using enzyme kinetic models solved by numerical methods packages such as GEPASI [9]. These simulations have been used to evaluate numerous possible metabolic reactions coupled to the firefly luciferase for ATP [10], the bacterial luciferase system for NAD(P)H [11], or luminol chemiluminescence for H_2O_2 in terms of optimum assay performance.

The best-performing assays from the kinetic simulations are then evaluated in aqueous assay format. The luminescent assays are first developed as traditional aqueous assays, which are then modified to a lyophilized or dry-reagent format. Figure 4 shows glucose as an example. Assay development experiments include assessing buffer type, pH, reagent concentration, enzyme concentration, enzyme ratio, and other appropriate parameters initially assessed by the kinetic model. The optimum enzyme and reagent concentrations are determined with the goal of maximizing light output and resolution of the assay. Furthermore, the enzyme concentration can be adjusted to change the dynamic detection range of the

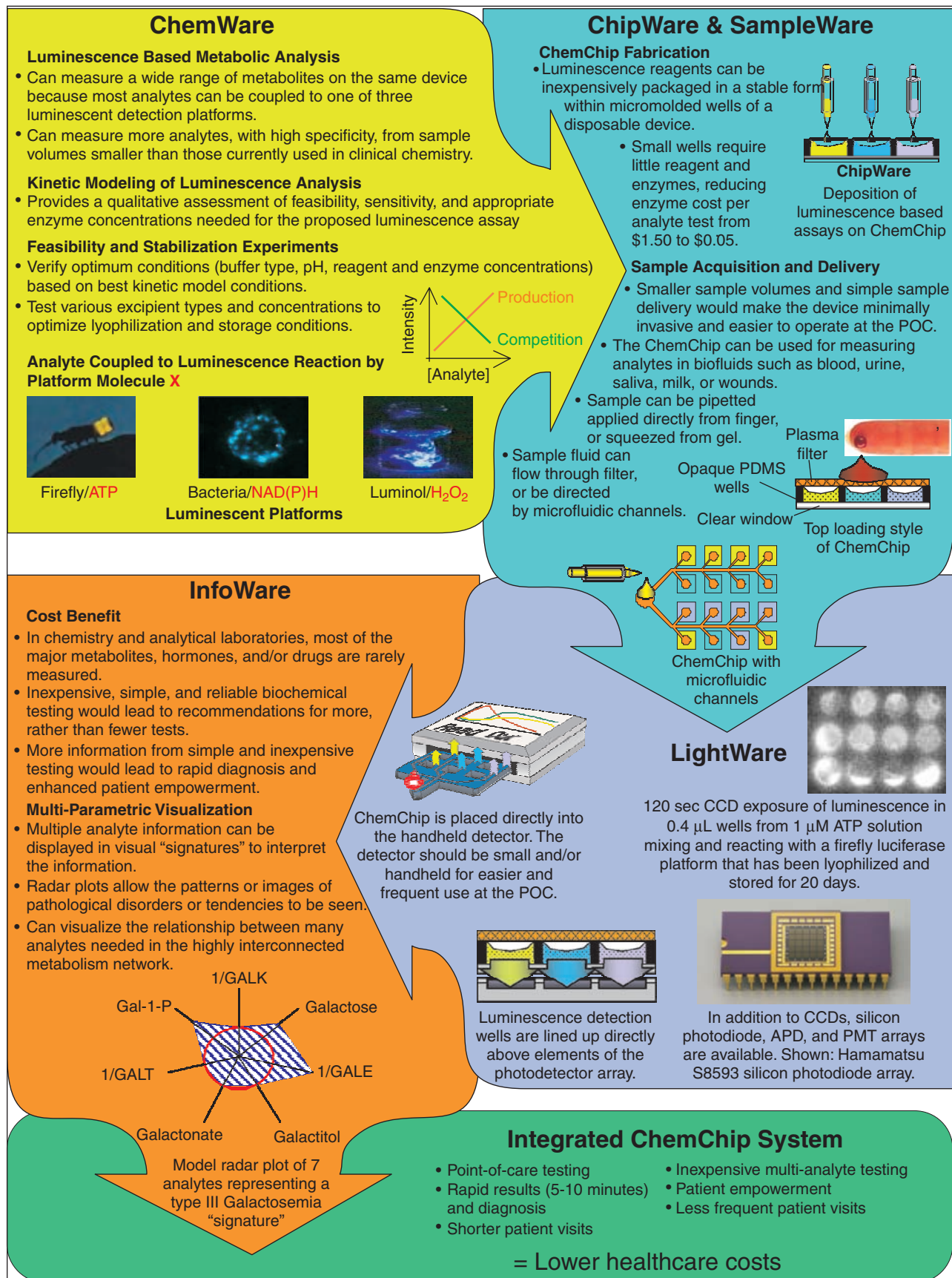


Fig. 2. The development of the ChemChip system.

Our goal is a ChemChip system that is analogous to the present generation of glucose dipsticks and glucometers in terms of ease of use, quality of data, and low cost.

assay. The optimum pH of the assay is determined because different enzymes generally have different optimum pHs for maximum catalytic activity. Additionally, inhibition of each of the reaction constituents on other reactions is assessed. The optimized aqueous assay serves as a starting point for the lyophilized or dry-reagent assay.

Our work to date has focused on establishing the practicality of the ATP and NAD(P)H sensors as well as the feasibility of specific substrate sensors using the ATP and NAD(P)H platforms. We have used galactose as the prototype ATP-dependant analyte (for application to gala-

ctosemia [12]) and phenylalanine as the prototype NAD(P)H sensor, with PKU as the specific application [13]. Additionally, our work to date has resulted in assays and protocols for the analytes listed in Table 1.

With the close collaboration of Dr. R. Stewart, we have engineered and recombinantly (*E. coli*) produced a set of enzymes also listed in Table 1 with which enhanced sensors can be developed. The polyhistidine (polyHis) tag permits simple, one-step purification of the *E. coli*-produced proteins. The biotin carboxyl carrier protein (BCCP) domain permits specific binding of biotin so that protein immobilized to avidin or to

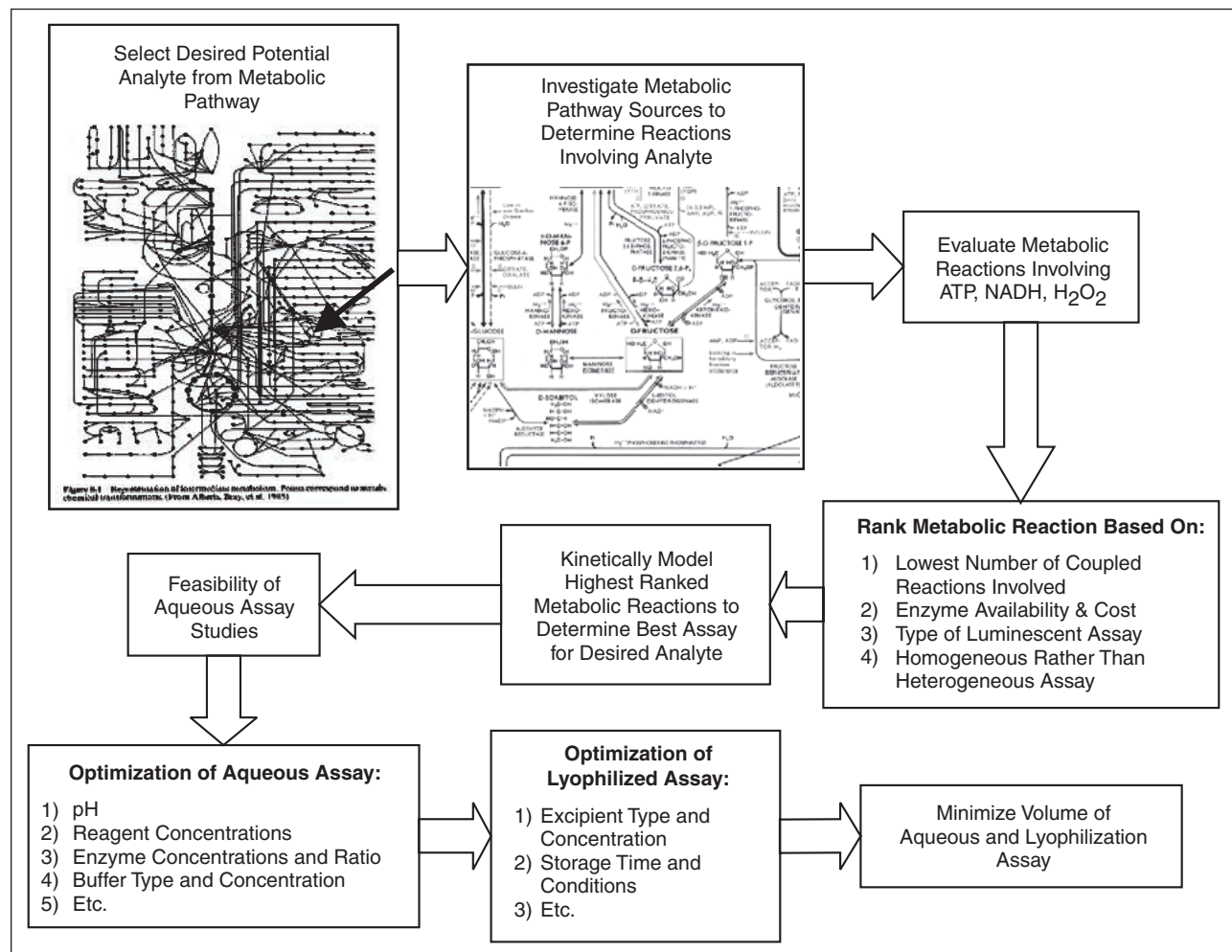


Fig. 3. Flow diagram for new assay development. Possible enzymes are chosen at the second step based on metabolic pathways involving the substrate. Various metabolic pathways are explored for choosing possible routes to producing or depleting ATP, NADH, or H_2O_2 .

streptavidin substrates results in little or no loss in activity. We have also performed DNA shuffling (directed molecular evolution) studies of the Lux (bacterial luciferase) gene, resulting in a bacterial luciferase with significantly enhanced thermal stability (unpublished). The availability of such unique proteins enhances sensor development and application.

Enzyme stability is key to the development of biosensors. Selecting enzymes that are inherently robust is important so that they retain activity after deposition and lyophilization. Lyophilization stabilizes enzymes for long-term storage by reducing both mechanical and chemical degradation. Mechanical or physical degradation includes aggregation or precipitation, while chemical degradation includes oxidation, deamidation, and hydrolysis. Although lyophilization generally increases the long-storage stability of protein, the processes of lyophilization (freezing and drying) can also degrade the enzyme. However, with appropriate stabilizing excipients and preservatives, the degradation during lyophilization long-term storage can be minimized. The enzyme solutions and chemiluminescence cocktails must be stable for long periods, ideally 12 months and longer. We have assessed and adopted various excipient mixtures for maintaining activity after lyophilization [21]. We use disaccharides and neutral, hydrophilic polymers in order to control the glass transition temperature, which must be greater than the final storage temperature of the lyophilized enzyme. The sugar to protein weight ratio should be at least 1 to 1, although stability can be further increased with greater sugar-weight ratios (5 to 1) for some enzymes [21]. Antioxidants such as dithiothreitol and glutathione are used during lyophilization and subsequent storage to prevent oxidation of enzyme and sensitive reagents. Bovine serum albumin (BSA) is used for surface passivation and as a stabilizing agent.

The bioluminescent reagents (ATP, FMN, bacterial and firefly luciferase, oxidoreductase, etc.) are mixed thoroughly with the preservatives and added to each well of the biosensor. The biosensor and reagents are flash frozen with liquid nitrogen followed by a two-stage lyophilization process. The first stage of lyophilization proceeds at -50°C and < 100 mTorr pressure. The second stage of lyophilization proceeds at $+30^{\circ}\text{C}$ and < 100 mTorr pressure. The time for each

stage depends on the sample volume and container (sample well) dimensions.

Our experience to date with firefly luciferase [22], with a glucose assay via firefly luciferase, and with a lactate assay via the bacterial luciferase system [23], indicates preservation of activity for up to eight weeks of storage. Results

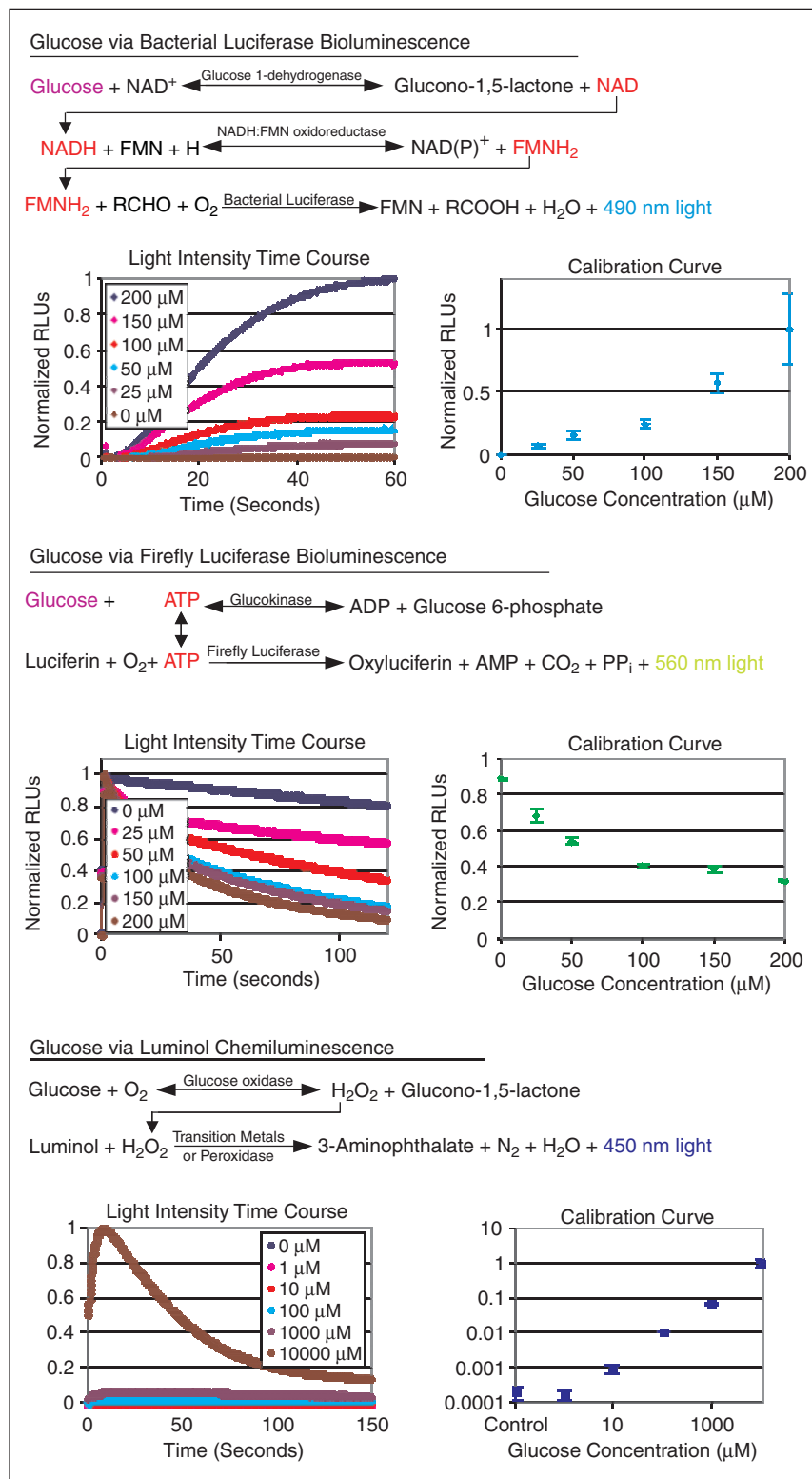


Fig. 4. Glucose assay reaction via luminescence. Light intensity time course and calibration curve for each of the glucose assays (RLU = relative light unit).

TABLE 1. Existing protocols for assays developed for luminescence platforms. Engineered and recombinant enzymes for assay development.

Platform	Firefly Luciferase Bioluminescence Adenosine Triphosphate (ATP)	Bacterial Luciferase Bioluminescence Reduced nicotinamide-adeninedinucleotide (NADH)	Luminol Chemiluminescence Hydrogen Peroxide (H ₂ O ₂)
Existing protocols for assays	ATP (14), Galactose (15), Glucose (14), Creatine (14), Creatinine (14), Urea (14)	NADH (16), Phenylalanine (16), Lactate (17), Galactose (14), Glucose (14), Glutathione (14)	H ₂ O ₂ (14), Glucose (14), Creatine (14), Creatinine (14)
Engineered and recombinant enzymes	Firefly luciferase (<i>Photinus pyralis</i>) (18); Firefly luciferase with a BCCP (biotin—expressing) domain (19) and with a polyhistidine (poly-His) tail (19); Galactokinase with poly-His (15); Galactokinase with BCCP (15)	Bacterial NADH:FMN oxidoreductase (<i>Vibrio fischeri</i>) with the BCCP domain (20); Bacterial luciferase (<i>Vibrio harveyi</i>) with BCCP domain (20); Phenylalanine dehydrogenase with BCCP domain and poly-Histail (16)	—

for the lyophilization of the lactate assay via bacterial luciferase bioluminescence are shown in Figure 5. Additionally, we have been working toward decreasing the reaction volume to less than one microliter.

Ultimately, each individual well of the ChemChip will contain a “cocktail” of reagents specific to the particular analyte and/or specific analyte concentration range. The reagent cocktails will be prepared in a lyophilized form for stability. The assay arrays will be tested with reference blood or urine and validated against standard and available methods.

ChipWare

A major benefit of biosensor chips will be reduced cost. Using the ubiquitous microprocessor as a metaphor, ChemChips could be inexpensively manufactured by the millions, thus greatly reducing the cost per chip. A variety of microfabrication techniques can be used to build arrays of detection wells, where each well has an independent luminescence-based analytical assay. Each unique assay can be deposited and stabilized in small quantities in the detection wells, thus reducing the cost of enzymes. For simple POC operation, the detector should have low power consumption, making it possible to use as a benchtop or handheld device. The smaller and less expensive the device, the easier it would be to implement in home and clinical use.

Fabrication

An initial ChemChip prototype has been made in a silicon wafer by anisotropic etching wells of various sizes and depth [24]. An aqueous firefly luciferase solution was placed in the wells and covered with a glass cover slip, which squeezed out the excess fluid. The wells were coated with silver to enhance light collection by increasing the collection angle of the luminescent signal to a CCD camera (ST6-E, Santa Barbara Instruments Group, Santa Barbara, California) (Figure 6). While a

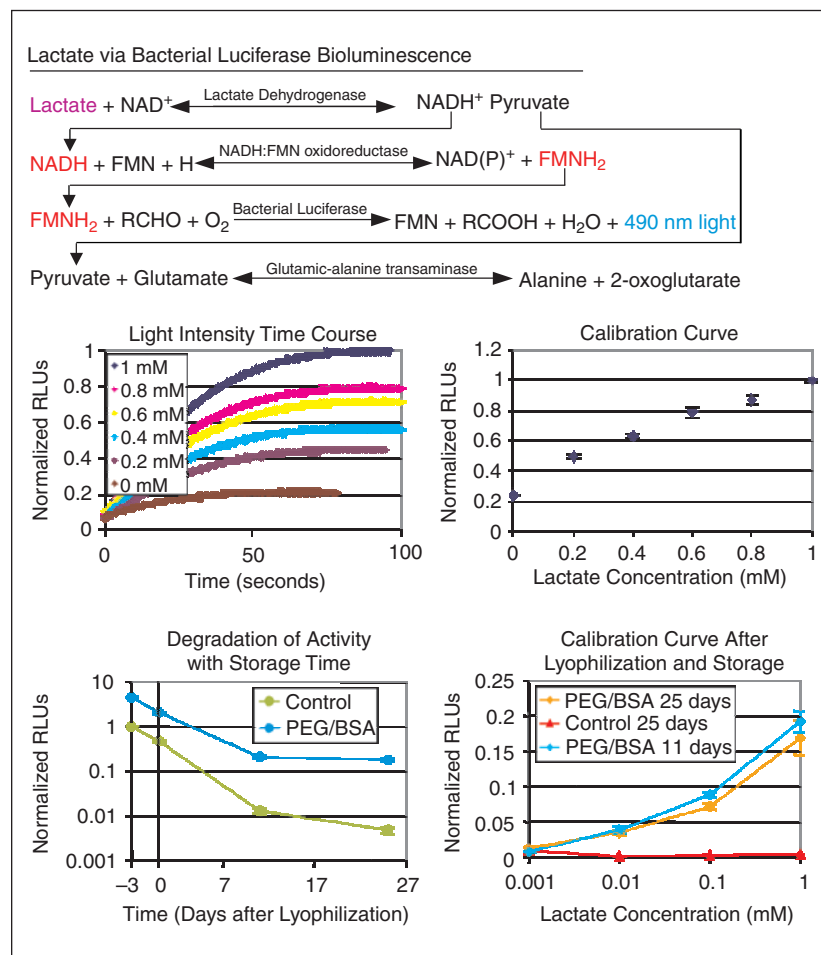


Fig. 5. Lactate assay reaction via bacterial luciferase bioluminescence. Light intensity time course, calibration curve, degradation of activity with storage time, and calibration curve after lyophilization and storage for the lactate assay.

If the potential of the ChemChip is realized, practically all relevant disease markers over a wide range of molecular weights and concentrations could be quantitatively and specifically measured for disease diagnosis and management.

silicon wafer prototype has helped us access detection limits of the CCD, the final device would be too expensive, due to complicated fabrication of microfluidic structures in silicon. It would also be impractical to bond clear windows to the silicon due to high temperature glass bonding, which would destroy lyophilized enzymes deposited in the wells.

Other ChemChip prototypes have been created in poly(dimethylsiloxane) (PDMS) using “soft-lithography” approaches developed by others [25], [26]. This method involves photolithographically patterning high-profile structures in photoresist (SU-8, MicroChem Corp. Newton, MA) on a silicon wafer. An uncured solution of PDMS is then poured on top of the patterned SU-8 and cured. After curing, the PDMS is removed, resulting in a pattern of channels and wells molded into the PDMS that are inverted replicates of the photolithographically patterned SU-8 structures. Clear PDMS, glass, or polystyrene windows can be temporarily or permanently bonded to PDMS forming hermetic seals with the PDMS and enclosing the microfluidic structures [25]. Through-hole features can also be molded in the PDMS. Multiple layers of PDMS with the through hole features can be stacked, creating a multilayered microfluidic device [26].

Currently, few microfabricated biosensors have multiple enzymes packaged in stabilized form [27]. Our current ChemChip development uses soft-lithography because it is ideal for rapid prototyping and for depositing, lyophilizing, and sealing luminescence-based assays in microfluidic structures without high temperatures or caustic chemicals associated with other microfabrication methods [28]. Initial studies used soft lithography to make microchannels in opaque PDMS (Sylgard 184, Dow Corning, Midland, Michigan) and measure ATP/firefly luciferase bioluminescence in channels of various lengths [29]. Another prototype followed the layered PDMS patterning method described by Jo et al. [26]. Here, we patterned a 5×5 array of 1 mm diameter holes in 0.5-mm thick PDMS. The PDMS was then bonded to glass cover slides, turning the holes into clear bottom wells. A 0.5 μL of a luminescent solution (5 mM Luciferin, 500 nM firefly luciferase, 2.5 mg/mL BSA, 0.5 M sucrose, 10 mM DDT, and 2.5 mg/mL dextran in 0.1 M trycine buffer—pH 7.8) was pipetted by hand into each of the wells (see ChipWare in Figure 2). The array was lyophilized according to procedures described above. The lyophilized array was stored at room temperature for 20 days in the dark. A hydrogel equilibrated in 1 μM ATP solution was then placed on the top side of the well to rehydrate the lyophilized reagents and initiate the lu-

minescent reaction. The resultant 120-second uncooled CCD exposure of the luminescent array shows that a minimum of 0.4×10^{-12} moles of ATP can be detected in each well (see the 3×4 array in LightWare of Figure 2). Calibration curves have not been performed for this array as of yet.

Our ongoing experiments involve building smaller volume detection wells and addressing reagent deposition issues associated with it. Smaller analytical wells would further reduce the amount of sample needed for measuring more analytes within the detection limit of the particular assay. Smaller amounts of reagents and enzymes would be used to reduce the cost of the ChemChip. The glucose assay via the ATP/firefly luciferase platform described above would cost about US\$1.50 in enzymes per test for sample volumes of about 10 μL . By reducing the well and sample volume size to about 1 μL , the cost in enzymes would be reduced to about US\$0.05 per test. As the detection wells become smaller, greater precision is required for depositing the right amount of reagent solutions before lyophilization. These reagents can be deposited by ink-jet printing methods down to a volume range of 10 nL to 100 μL .

Sample Ware

We have tested two methods of sample delivery to the ChemChip. A top-loading, through-flow ChemChip has been tested for certain types of samples. Hydrogels equilibrated in

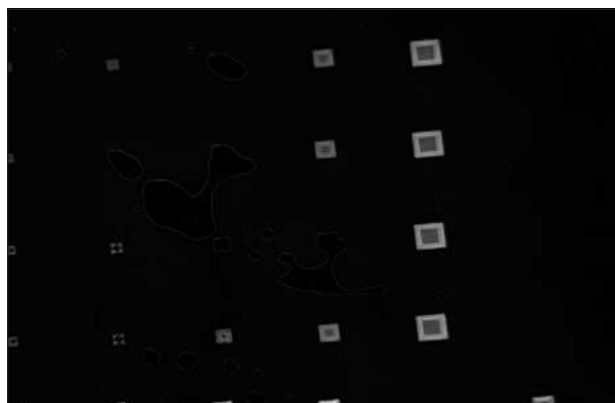


Fig. 6. A 20-sec integration of bioluminescence in anisotropically etched wells of various sizes, 250 μm depth. Note the enhanced light collection from the reflective 54.7° walls compared to the center of the wells. Measurements were taken using a CCD camera (ST6-A, Santa Barbara Instruments Group, Santa Barbara, California).

a sample solution have been placed on top of the ChemChip array of wells containing lyophilized luminescent reagents (see LightWare of Figure 2). We have also tested commercially available plasma separation membranes and filters for sample delivery qualities. These membranes can be bonded to the array of PDMS wells after the reagents are lyophilized [30]. Sample solutions containing the analytes of interest are then flooded onto the filter layer and flow into the wells, activating the bioluminescent detection assays (see the top-loading ChemChip in SampleWare of Figure 2). Initial studies on microfluidic sample delivery in PDMS-molded microchannels show that sample fluid can travel by capillarity to specific reaction wells [26]. These PDMS channels can be modified to minimize protein binding [28] or to be made hydrophilic [31]. These microfluidic channels can also be made as a separate PDMS layer and bonded directly to the PDMS layer containing the luminescent reagents in the wells.

LightWare

Detectors

While CCD cameras have been used in preliminary experiments described above, other detectors, such as silicon photodiode, avalanche photodiode (APD), and photomultiplier tube (PMT) arrays, are available and can improve the detection limits due to their higher normalized detectivity. (See a "Detectors Technical Discussion," published by ThermoOriel Instruments, Stratford, CT, <http://www.oriel.com/homepage/down/pdf/06002.pdf>, for a tutorial on detector sensitivity and normalized detectivity.) Ideally, an array of detector elements with element dimensions approximate to that of the channels and wells would maximize the light collected per detector surface area by reducing or eliminating the inactive spaces between elements. The resolution of standard CCD detectors is not necessary for measuring overall intensities from the channels or wells seen in LightWare of Figure 2. Commercially available silicon photodiodes, APD, and PMT arrays designed for low-light detection are ideal for producing a hand-held detector that can simultaneously measure signals from multiple analytical channels. The wells in the ChemChip array seen in LightWare of Figure 2 were designed to line up with the elements of the low-powered Hamamatsu S8593 silicon photodiode array (Hamamatsu, Bridgewater, New Jersey), also seen in LightWare of Figure 5.

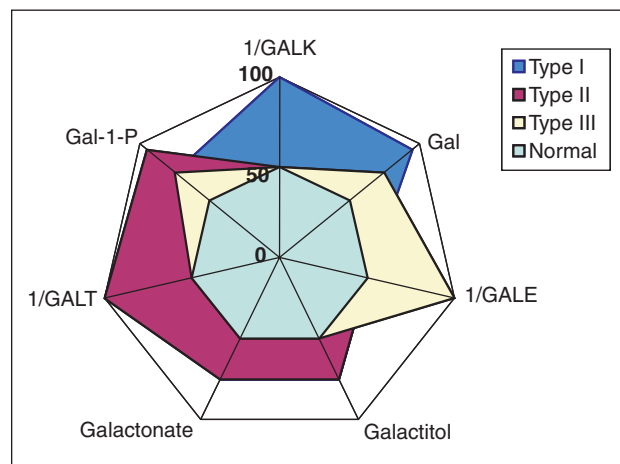


Fig. 7. A preliminary radar plot for galactosemia. Normality is represented by the inner locus, the various galactosemia types by the other three patterns.

Measurement and Calibration

Luminescent measurements are generally reported in relative light units (RLUs), a unit applicable to particular instrument setups. In order to compare the performance of the different detector arrays and bioluminescent assays under different conditions (wet and lyophilized), each detector element can be calibrated to report measurements in units of radiance ($\text{W}/\text{cm}^2/\text{sr}$), which normalizes intensity to the collection angle of the system. Currently, most chemiluminescent and bioluminescent measurement systems are calibrated with luminol standards, which are prone to mixing variation and other errors [32]. We calibrate photodetectors, using a light emitting diode (LED) standard, which accounts for the spectral properties of the sources and detectors [33]. This calibration procedure will determine the variance in sensitivity between detector elements and their sensitivity at different operating conditions such as temperature.

While variation between detector elements may vary, a calibrated photodetector will help establish onboard calibration features within the ChemChip. Reference detection wells for each type of assay would normalize the luminescence of other channels to account for changes in enzyme activity that would occur over time during the storage of the ChemChip [5].

In order to meet FDA approval, each assay must meet the Clinical Laboratory Improvement Amendments of 1988 (CLIA) [5]. The maximum error from each test should not exceed one-third of the analytical quality requirement set forth by CLIA for that test (3.3% of target for many analytes) [5]. For galactose and lactate, the maximum allowable error is 10%, which means the total error of the bias and the coefficient of variation for both these tests should be 3.3% of their corresponding lower target range values (20 and 500 μM , respectively).

InfoWare

How can we deal with 15 different channels of chemical information? How can physicians, patients, and family members effectively deal with the interactions among 15 different metabolites, nutrients, and drugs? Fortunately, advances in data analysis, parameter presentation, and visualization—coupled with appropriate modeling, simulation, and sensitivity analyses—allow this challenge to be effectively addressed. A simple but highly useful approach to multidimensional “visualization” is the use of radar, spider, or star plots (all synonymous) utilizing radial, polar, or even spherical 3-D coordinate systems to present multidimensional data [34].

We have used radar plots in a preliminary way to simplify and to visualize the complexity of protein interfacial reactions [35]. We are now using it as a means to present multiparameter clinical chemistry data so that the visual pattern generated by the locus of points on the spider plot is designed to reflect particular disease states and metabolic conditions [15]. Although such plots are incorporated in some plotting and graphical analysis packages and software, and widely used in certain specific fields such as sensory assessment, they have not been widely applied in most other areas of science. There has been limited use in clinical medicine, which has demonstrated that such approaches have enormous potential. Perhaps the clearest example of an n -dimensional radar plot visualization method applied to clinical medicine and clinical biochemistry is the work of Cerra et al. [36] dealing with the nutritional management of

metabolic stress. Their study of the role of branched chain amino acids in the stress response presented the data in a unique radial or star plot, similar to those that we have used in our protein studies.

The potential of simple methods for the visualization of multiparameter clinical chemistry data can be illustrated with the case of galactosemia [15]. Table 2 shows how four key metabolites and the three enzyme activities are altered in the three different types of galactosemia. With a seven-channel biosensor, we could measure all seven analytes and present the data in a radar plot to enhance recognition and distinction of the three types of galactosemia. This is shown in Figure 7. The challenge in effective multiparameter data presentation with radial plots is to position and scale the axes to produce easily recognizable signatures [34]. Note that the enzyme axes are the reciprocal of enzyme activity. Normality is represented by the inner heptagon (made by connecting the points on each of the seven individual concentration axis). Type II galactosemia “points” to the left, type I to the top, and type III to the right. Sensing channels can be designed to measure enzyme concentration (activity) as well as for substrate or product activity. If we want to measure a particular enzyme’s activity, we produce a channel with an excess of substrate and co-reactants and look for product (via an ATP, NAD(P)H, or H₂O₂ coupled reaction). We have already done this for galactokinase activity [15].

Future Work

Immunoassays

We have recently extended our biosensor interests to include chemiluminescent immunoassays in order to access analytes not readily measurable by enzyme-based reactions. Homogeneous immunoassays require no separation or washing steps (for antibody-bound and unbound components), whereas heterogeneous assays generally require one or more separation steps. Some commonly used homogeneous chemiluminescence immunoassay techniques include Enzyme-Multiplied ImmunoTechnique (EMIT) and Cloned Enzyme-Donor Immunoassay (CEDIA).

EMIT is especially useful in detecting small molecules such as therapeutic drugs and steroid hormones. The basic principle is that the enzymatic activity of enzyme-analyte conjugates is modulated by the binding of specific antibodies. The enzyme activity is decreased when antibodies bind to the analyte-enzyme conjugates, due to binding-induced conformational change and/or steric hindrance of the enzyme active site by the bound antibody. Commonly used marker enzymes in EMIT assays are glucose-6-phosphate dehydrogenase and malate dehydrogenase, both of which involve NAD(P)H and can thus be coupled to the bacterial bioluminescence platform. The resulting luminescence indicates the activity of the marker enzyme, which is proportional to the analyte concentration.

The CEDIA method uses an enzyme acceptor (EA) and an analyte-labeled enzyme donor (ED). The presence of free analyte ties up the drug-specific antibody, allowing ED and

TABLE 2. The concentration (or activity) change of metabolites and enzymes in whole blood for different types of galactosemia.

	Type-I Galactosemia (GALK deficient)	Type-II Galactosemia (GALT deficient)	Type-III Galactosemia (GALE deficient)
GALK	↓↓↓	—	—
GALT	—	↓↓↓ ^a	—
GALE	—	—	↓↓↓
Gal ^b	↑↑↑	↑↑	↑↑
Gal-1-P	↑↑	↑↑↑	↑↑
Galactitol ^b	↑↑↑	↑↑↑	N.A.
Galactonate ^b	↑↑↑	↑↑↑	N.A.

GALK = Galactokinase, GALT = Galactose-1-phosphate uridylyltransferase, GALE = UDP-galactose 4'-epimerase, Gal = Galactose, Gal-1-P = Galactose-1-phosphate, ↑↑↑ = highly increased, ↑↑ = moderately increased, ↓↓↓ = highly decreased, — = unchanged, N.A. = not available. ^a = Variants of Type II galactosemia have higher GALT activity. ^b = Elevated concentrations of these metabolites are also found in urine.

EA to assemble, producing active enzyme. Low or no drug in the sample results in the binding of antibody to the ED-drug conjugate, preventing the assembly of the intact enzyme. In both EMIT and CEDIA methods, the marker enzyme activity increases with increasing analyte concentration. The marker enzymes in the CEDIA assay involve H₂O₂ and can thus be coupled to the luminol chemiluminescent reaction.

Ultimately, if the potential of the ChemChip is realized, practically all relevant disease markers over a wide range of molecular weights and concentrations could be quantitatively and specifically measured for disease diagnosis and management. Multiple analytes (~50) could be measured in small volume physiologic fluid samples (~50 microliters or smaller) via relatively inexpensive, reliable instruments in point-of-care as well as home environments.

Acknowledgments

We acknowledge early support of this work by the NSF/Whitaker Foundation Program on Cost Reducing Health Care Technologies. We also acknowledge early support from Protein Solutions, Inc. (this company no longer exists) and ongoing support from several current corporate partners. The University of Utah provided funds from its Technology Incentives program. We acknowledge NIH grant RFA PAR-01-057, Project RR17329, Technology Development for Biomedical Applications, “Multi-Analyte Micro-Devices for Biomedical Applications” for ongoing support. We further acknowledge discussions with other colleagues and co-workers, including Drs. Ed Clark, John Holman, Rick Van Wagenen, Russel Stewart, Jarmila Janatova, Steve Kern, Norm Waitzman, and Robert Huefner.

Rupert Davies was born in 1973 and received his B.S.E. in environmental and civil engineering from the University of Michigan, Ann Arbor, in 1995. He is currently pursuing his

Ph.D. in bioengineering at the University of Utah. His research interests include bioluminescence, biomaterials, and biomimicry.

Daniel A. Bartholomeusz was born in 1974 and received his B.S. in bioengineering from the University of California-San Diego in 1999. He is currently pursuing his Ph.D. in bioengineering at the University of Utah. His research interests include microfabrication of biosensors and metabolic modeling.

Joseph Andrade received a B.S. degree in materials science from San Jose State University in 1965 and a Ph.D. in metallurgy and materials science from the University of Denver in 1969. He joined the University of Utah in 1969 and is a professor in the Colleges of Engineering and Pharmacy at the University of Utah in Salt Lake City. During his 30-year academic career, he has served as chairman of the Department of Bioengineering and dean of the College of Engineering (1983-1987). He directs the 4M Lab (Lab for the Modeling, Measurement, and Management of the Metabolome). He is internationally recognized for his research on biomaterials and bio-compatibility. Technical honors include the Ebert Prize of the Academy of Pharmaceutical Sciences, the Clemson Award of the Society for Biomaterials, the Outstanding Surface Scientist Award of the Surfaces in Biomaterials Foundation, and a number of local awards, including the Governor's Medal for Science and Technology and the University of Utah's Distinguished Research award. He has published over 100 peer-reviewed technical papers, edited five books, holds five patents (with another pending), and graduated 23 doctoral students and 21 masters students. He also serves as director and chair of the Utah Science Center, a new, modern, interactive science and technology center with a strong bioengineering and energy flavor, scheduled to open in 2004.

Address for Correspondence: Dr. Joseph D. Andrade, 50 S. Central Campus Dr., 2480 MEB, Salt Lake City, UT 84112-9202 USA. Tel: +1 801 581 4379. Fax: +1 801 585 5361. E-mail: joeandrade@uofu.net

References

- [1] J. Andrade, C. Wang, D.-J. Min, C. Eu, R. Van Wagenen, and R. Scheer, "Toward dollar devices for measuring metabolic biochemistry," in *Anti-Microbial, Anti-Infective Materials*, S.P. Sawan and G. Manivannan, Eds. Technomic Publishing, 1999, pp. 317-329.
- [2] D.B. Sacks, D.E. Bruns, D.E. Goldstein, N.K. Maclaren, J.M. McDonald, and M. Parrott, "Guidelines and recommendations for laboratory analysis in the diagnosis and management of diabetes mellitus," *Clin. Chem.*, vol. 48, pp. 436-472, 2002.
- [3] U. Wendel and U. Langenbeck, "Towards self-monitoring and self-treatment in phenylketonuria—A way to better diet compliance," *Eur. J. Pediatr. (Suppl. 1)*, vol. 155, pp. S105-S107, 1996.
- [4] S. Segal and G. Berry, "Disorders of galactose metabolism," in *The Metabolic and Molecular Bases of Inherited Disease*, vol. 1, 7th ed., C. Scriver, Ed. New York: McGraw-Hill, 1995, pp. 967-1000.
- [5] T.H. Grove, "In vitro diagnostics: Bringing testing to the point of care," *Medical Device & Diagnostic Industry*, pp. 78-94, Apr. 2000.
- [6] S. Brolin and G. Wettermark, *Bioluminescence Analysis*. Weinheim, Germany: VCH, 1992.
- [7] A.K. Campbell, *Chemiluminescence*. Chichester, U.K.: VCH, 1985.
- [8] G. Michal, *Biochemical Pathways*. New York: Wiley, 1999, pp. 277.
- [9] P. Mendes, "GEPASI: A software package for modeling the dynamics, steady states and control of biochemical systems," *Comp. Applic. Biol. Sci.*, vol. 9, pp. 563-571, 1993.
- [10] J.W. Smith, R.H. Davies, J.D. Andrade, and R.A. Van Wagenen, "Optimizing biosensor design with computer modeling: A case study involving Creatine," in *Proc. 11th Int. Symp. Bioluminescence & Chemiluminescence*, P.J. Herring, J.F. Case, B.H. Robison, S.H.D. Haddock, L.J. Kricka, and P.E. Stanley, Eds. Singapore: World Scientific, 2001, pp. 309-312.

- [11] Y. Feng, R.H. Davies, and J.D. Andrade, "Enzyme kinetics model of the bacterial luciferase reactions for biosensors applications," presented at the 12th Int. Symp. Bioluminescence & Chemiluminescence, Robinson College, Cambridge, U.K., 2002.
- [12] J.Y. Eu, C.Y. Wang, and J. Andrade, "Homogeneous bioluminescence assay for galactosuria: Interference and kinetic analysis," *Anal. Biochem.*, vol. 271, pp. 168-176, 1999.
- [13] D. Min, R. Stewart, and J. Andrade, "Developing a biosensor for L-phenylalanine based on bacterial bioluminescence," in *Bioluminescence and Chemiluminescence: Perspectives for the 21st Century*, A. Roda, M. Pazzagli, M. Kricka, and P. Stanley, Eds. London, U.K.: Wiley, 1999, pp. 520-523.
- [14] R. Davies, "Luminescence assays for kidney function assessment," Ph.D. dissertation, Dept. of Bioengineering, University of Utah, Salt Lake City, Utah, in preparation.
- [15] J.-Y. Eu, "Bioluminescent assays for galactose and galactose-1-phosphate: Application of immobilized enzymes and kinetic analysis," Ph.D. dissertation, Department of Material Science and Engineering, University of Utah, Salt Lake City, Utah, 2000.
- [16] D. Min, "Toward specific biosensors based bacterial bioluminescence," Ph.D. dissertation, Department of Material Science and Engineering, University of Utah, Salt Lake City, Utah, 1999.
- [17] D. Min and J. Andrade, "Preliminary study of the optimum conditions for a lactate sensor based on bacterial bioluminescence," in *Bioluminescence and Chemiluminescence: Molecular Reporting with Photons*, J. Hastings, L. Kricka, and P. Stanley, Eds. New York: Wiley, 1997, pp. 275-278.
- [18] C.Y. Wang, S. Hitz, J. Andrade, and R. Stewart, "Biotinylation of firefly luciferase in vivo: Purification and immobilization of bifunctional recombinant luciferase," in *Bioluminescence and Chemiluminescence: Molecular Reporting with Photons*, W. Hastings, L. Kricka, and P. Stanley, Eds. New York: Wiley, 1997, pp. 224-227.
- [19] C.Y. Wang, S. Hitz, J.D. Andrade, and R.J. Stewart, "Specific immobilization of firefly luciferase through a biotin carboxyl carrier protein domain," *Anal. Biochem.*, vol. 246, pp. 133-139, 1997.
- [20] D.J. Min, J.D. Andrade, and R.J. Stewart, "Specific immobilization of in vivo biotinylated bacterial luciferase and FMN:NAD(P)H oxidoreductase," *Anal. Biochem.*, vol. 270, pp. 133-139, 1999.
- [21] J.F. Carpenter, M.J. Pikal, B.S. Chang, and T.W. Randolph, "Rational design of stable lyophilized protein formulations: Some practical advice," *Pharm. Res.*, vol. 14, pp. 969-975, 1997.
- [22] R.H. Davies, R.A. Van Wagenen, and J.D. Andrade, "Stabilization of firefly luciferase with anti-oxidants: A preliminary study," presented at 11th Int. Symp. Bioluminescence and Chemiluminescence, Monterey, CA, 2000.
- [23] R.H. Davies, J.W. Corry, and J.D. Andrade, "Lactate assay based on bacterial bioluminescent: Enhancement, dry reagent development, and miniaturization," presented at the Proc. 11th Int. Symp. Bioluminescence & Chemiluminescence, Robinson College, Univ. Cambridge, Cambridge, U.K., 2002.
- [24] J. Brazzle, I. Papautsky, and A.B. Frazier, "Micromachined needle arrays for drug delivery or fluid extraction," *IEEE Eng. Med. Biol. Mag.*, vol. 18, pp. 53-58, 1999.
- [25] D. Duffy, "Rapid prototyping of microfluidic systems in poly(dimethylsiloxane)," *Anal. Chem.*, vol. 70, pp. 4974-4984, 1998.
- [26] B.H. Jo, L.M. Van Lerberghe, K.M. Motsegood, and D.J. Beebe, "Three-dimensional micro-channel fabrication in polydimethylsiloxane (PDMS) elastomer," *J. Microelectromech. Syst.*, vol. 9, pp. 76-81, 2000.
- [27] D.R. Reyes, D. Lissifidis, P.-A. Auroux, and A. Manz, "Micro total analysis systems. 1. Introduction, theory, and technology," *Anal. Chem. (ASAP Articles)*, vol. pp. A-N, 2002.
- [28] A. Rasmussen, M. Gaitan, L.E. Locascio, and M.E. Zaghoul, "Fabrication techniques to realize CMOS-compatible microfluidics in microchannels," *J. Microelectromech. Syst.*, vol. 10, pp. 286-267, 2001.
- [29] D.A. Bartholomeusz, J.D. Andrade, and A.B. Frazier, "Bioluminescent based chemchip for point-of-care diagnostics," presented at 1st Annu. Int. Conf. Microtechnologies in Medicine and Biology, Palais des Congres, Lyon, France, 2000.
- [30] W.G. Meathrel, H.M.S. Hand, and L.-H. Su, "The effects of hydrophilic adhesives on sample flow," *IVD Technol.*, pp. 56-66, July/Aug. 2001.
- [31] Y.D. Kim, C.B. Park, and D.S. Clark, "Stable sol-gel microstructured and microfluidic networks for protein patterning," *Biotechnol. Eng.*, vol. 73, pp. 331-337, 2001.
- [32] D.J. Kane and J. Lee, "Absolute calibration of luminometers with low-level light standards," *Bioluminescence and Chemiluminescence*, vol. 305, part C, in *Methods of Enzymology*, M.M. Ziegler and T.O. Baldwin, Eds. New York: Academic, 2000, pp. 87-96.
- [33] D.A. Bartholomeusz and J.D. Andrade, "Photodetector calibration method for reporting bioluminescence measurements in standardized units," presented at XIth Int. Symp. Bioluminescence and Chemiluminescence, Robinson College, University of Cambridge, Cambridge, U.K., 2002.
- [34] W. Vogt, D. Nagel, and H. Sator, *Cluster Analysis in Clinical Chemistry*. Chichester, U.K.: Wiley, 1987.
- [35] J. Andrade, "Proteins at interfaces," *Clinical Materials*, vol. 11, pp. 67-84, 1992.
- [36] F.B. Cerra, "Role of nutrition in the management of malnutrition and immune dysfunction of trauma," *J. Amer. Coll. Nutr.*, vol. 11, pp. 512-518, 1992.

STABILIZATION OF FIREFLY LUCIFERASE ACTIVITY AGAINST OXIDATION WITH ANTIOXIDANTS

R.H. DAVIES, R.A. VAN WAGENEN AND J. D. ANDRADE

*University of Utah, Department of Bioengineering, 2480 Merrill Engineering Building,
Salt Lake City, UT, 84112,
USA*

E-mail: rupert.davies@m.cc.utah.edu

1. INTRODUCTION

Biosensors must be stored at room temperature for extended time periods. Luciferase stability is essential for functional bioluminescent biosensors. Firefly luciferase activity at room temperature can be maintained by lyophilization. However, lyophilized firefly luciferase does lose activity with time. Additionally, the stability of firefly luciferase activity in aqueous solution is important for research and optimization. Some of the activity loss in aqueous and lyophilized states is probably due to oxidative reactions. The oxidative damage to proteins includes scission of the peptide backbone, formation of intra or inter-molecular crosslinks, and modification of several amino acids. This damage leads to changes in net charge, conformation, and/or hydrophobic nature of proteins, reducing enzymatic activity.

Oxidation caused by oxygen free radical species has been shown to significantly decrease the activity of firefly luciferase.¹ Although sulfhydryl groups are not absolutely essential for firefly luciferase activity,² the sequential recombinant elimination of sulfhydryl groups reduces firefly luciferase activity.³ Sulfhydryl groups are particularly susceptible to oxidation as well as other amino acid groups (Fig. 2). Although dithiothreitol (DTT) is generally used to protect sulfhydryl groups in enzymes, naturally occurring antioxidants such as vitamin C (ascorbic acid), vitamin E (α-tocopherol), and glutathione (GSH) have been shown to protect proteins against oxidation. Additionally, these naturally occurring antioxidants have been shown to work in concert in vivo forming an oxidation reduction pathway.⁴

2. METHODS AND MATERIALS

The inhibition of firefly luciferase activity by antioxidants was measured by injecting 50μl of an adenosine triphosphate (ATP) mixture (100μM ATP [Sigma] and 5mM magnesium sulfate [Sigma]) into 200μL of an antioxidant mixture including various concentrations (100mM, 10mM, 1mM, 0.1mM) of antioxidants

(DTT [sigma], GSH [Sigma], TroloxTM [Fluka Chemika], vitamin C [Fisher BioTech]), 0.1 mM D-luciferin (Biosynth AG), 40mM Sucrose (Pfanstiehl), 0.25mM Dextran T40 (Pharmacia), 1mg/ml of bovine serum albumin (BSA, Sigma), and 0.02 mg/ml of recombinant firefly luciferase.⁵ The light intensity of the bioluminescence was collected with a Turner TD 20/20 luminometer for 15 seconds. The same antioxidant mixture was lyophilized in two stages using a Virtis 12EL Lyophilizer. The lyophilized mixture was then reconstituted with 200µL of reagent grade water immediately, 1 week, 2 weeks, and 2 months after lyophilization. Storage conditions included room temperature (25 degrees Celsius), in the dark, and in brown glass vials. The firefly luciferase activity after the different time intervals was measure by injecting 50 µl of the same ATP mixture into the reconstituted antioxidant mixture and measuring the light intensity for 15 seconds.

The firefly luciferase activity in the biomimicry antioxidant experiment was measured by injecting an ATP mixture consisting of 10µM ATP, 500µL magnesium sulfate, and 0.1mM luciferin into an antioxidant cocktail, which had been storage at room temperature in micro centrifuge tubes for 40 hours. The antioxidant cocktail consisted of various antioxidants (vitamin C, Trolox, and GSH) at different concentrations (10mM, 1mM, and 0.1mM) in several combinations, 0.5 mg/ml BSA, and 52 µg/ml of firefly luciferase (Promega). The light intensity was measured for 15 seconds with a Turner TD 20/20 luminometer.

3. RESULTS AND DISCUSSION

Fig. 1 shows the inhibition of firefly luciferase activity by various antioxidants at different concentrations. Fig. 2 depicts the results of the biomimic of the naturally occurring oxidation reduction pathway. Fig. 3 depicts the decreased firefly activity with time for various antioxidants. Fig. 4 shows the remaining activity of lyophilized firefly luciferase after two months of storage.

Inhibition of firefly luciferase activity was only observed at concentrations exceeding 10mM, with the exception of Trolox (greater than 1mM). The combinations of Trolox, vitamin C, and GSH did not show stabilization of the firefly luciferase activity greater than GSH alone after aqueous storage of 40 hours. Lyophilized firefly luciferase activity was preserved most effectively with DTT and GSH.

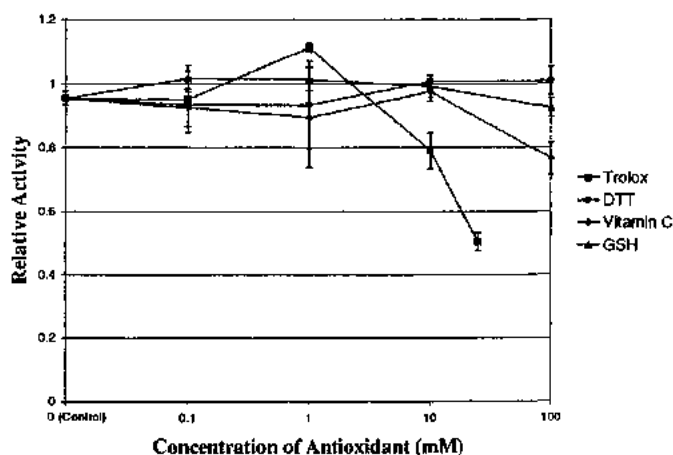


Fig. 1 Each point represents the average of three integrated light intensities collected for 15 seconds. The activity is relative to control firefly luciferase cocktail with no added antioxidant or sucrose before lyophilization. The error bars indicate one standard deviation.

Firefly Luciferase Activity with 1mM GSH

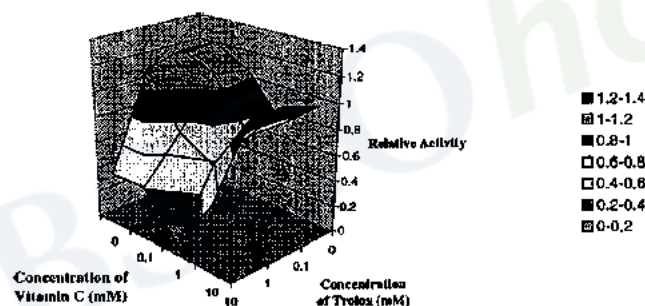


Fig. 2 Each intersection of lines represents a combination of three antioxidants at various concentrations. The activity value is based on the average of three integrated light intensities collected for 15 seconds. The activity is relative to control firefly luciferase cocktail with no added antioxidant after 40 hours of aqueous storage.

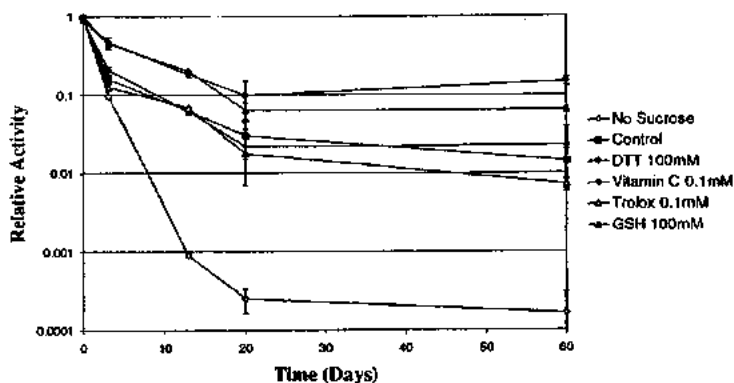


Fig. 3 Each point represents the average of three light intensities collected over 15 seconds. The activity is relative to control firefly luciferase cocktail with no added antioxidant or sucrose before lyophilization. The error bars indicate one standard deviation. Only the concentration that maintained the greatest activity for each antioxidant is shown.

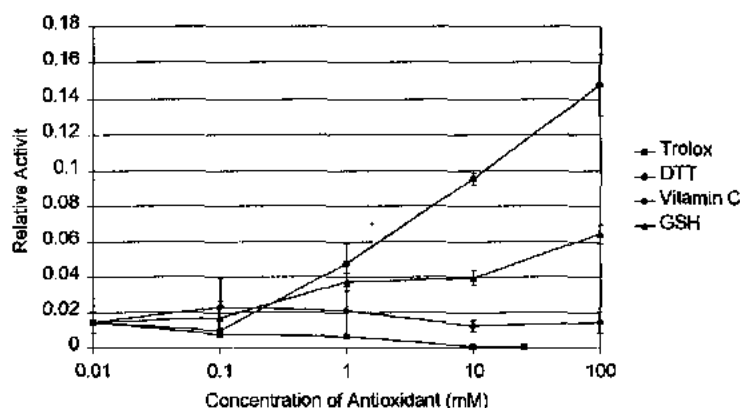


Fig. 4 Each point represents the average of three integrated light intensities collected for 15 seconds. The activity is relative to a control firefly luciferase cocktail with no added antioxidant or sucrose before lyophilization. The error bars indicate one standard deviation.

Acknowledgements

Special thanks to Protein Solutions, Inc. for laboratory space. This work has been partially supported by the Whitaker Foundation (a grant in the Cost Reducing Health Care Technologies Program – a joint program with the National Science Foundation) and NIH SBIR Phase I grant (1R43DK55426-1). Please note that Protein Solutions, Inc. has ceased operations.

References

1. Thompson A, Nigro J, Seliger HH. Efficient Singlet oxygen inactivation of firefly luciferase. *Biochem Biophys Res Commun* 1986; **140**: 888-894
2. Ohmiya Y, Tsuji FI. Mutagenesis of firefly luciferase shows that cysteine residues are not required for bioluminescence activity. *FEBS Lett* 1997; **404**:115-117
3. Kumita JR, Jain L, Safroneeva E, Wooley GA. A Cysteine-free firefly luciferase retains luminescence activity. *Biochem Biophys Res Commun* 2000; **267**: 394-397
4. Scott G. Antioxidants in science, technology, medicine and nutrition. Chichester: Albion Publishing 1997: 191-259
5. Ho C, Limberis L, Caldwell KD, Spewart RJ. A metal-chelating pluronic for immobilization of histidine-tagged Proteins at interfaces: Immobilization of firefly luciferase on polystyrene beads. *Langmuir* 1998; **14**: 3889-3894

Characterization of Vapor-deposited Silver Films Exhibiting Surface-enhanced Raman Scattering by Raman and X-ray Photoelectron Spectroscopy

L. V. DELPRIORE,* C. DOYLE,† and J. D. ANDRADE‡

Department of Bioengineering and Surface Analysis Laboratory, University of Utah, Salt Lake City, Utah 84112

Index Headings: Surface analysis; Raman spectroscopy; X-ray photoelectron spectroscopy; XPS; SERS; Silver films; Carbon films.

The observation of a 10^6 -fold increase in the Raman scattering cross section of pyridine adsorbed onto rough-

ened silver electrodes or onto thin silver films has focused interest on Raman spectroscopy as a tool for surface analysis. Since the original observation of surface-enhanced Raman scattering (SERS) of pyridine,¹⁻⁵ SERS has been observed for a variety of admolecules on silver including cyanide,⁶⁻⁹ thiocyanate,¹⁰ and carbon monoxide.¹¹ Many of these spectra exhibit prominent Raman peaks at 1380 and 1590 cm^{-1} , and weaker features at 2925 cm^{-1} . Howard *et al.*¹² have suggested that this background spectrum is necessary for SERS, yet its origin is uncertain, having been attributed to surface carbonates and graphitic carbon.^{6-9, 13, 14}

In the present study, we use x-ray photoelectron spectroscopy (XPS), Raman spectroscopy, and scanning electron microscopy (SEM) to characterize the contaminants and surface roughness of vapor-deposited silver films. XPS is established as a powerful surface analysis method, as emitted photoelectrons of characteristic kinetic energies are detected only from the outermost atomic layers.¹⁵ Hammond *et al.*¹⁶ have used XPS to study the controlled oxidation of silver, reporting the main peak positions for AgO, Ag₂O, and Ag₂O₃. Carlson¹⁷ also reported some core electron binding energy shifts of the major peaks corresponding to the different oxidation states of silver. The shifts of core peak positions due to carbon and oxygen bonding have also been reported^{17, 18} and are used in our analysis. XPS and Raman data have previously been used together to study bonding in silver complexes.¹⁹

SEM was used to determine the surface roughness of the vapor deposited silver films. In current SERS models roughening increases the Raman scattering in one or more of the following ways: (1) by allowing coupling of the external light to surface plasmons in the silver,²⁰ (2) by exciting collective electromagnetic resonances in small ($\sim \lambda/10$) silver particles,²¹ and (3) by enhancing the production of electron-hole pairs.²² Experimentally, the marked effect of surface roughness on SERS is well established. Electrochemical roughening leads to an increase of $\sim 10^6$ in the SERS from pyridine adsorbed on a silver electrode.²³ In an ultra-high vacuum study, Rowe *et al.*²⁴ have shown that a silver surface roughened on the order of 100 to 300 nm gives a 10^3 increase in SERS over smoother (~ 10 nm) or rougher (~ 2 to 5μ) surfaces. Although Furtak²⁵ has pointed out the difficulty of quantifying the enhancement factor, the demonstration of some surface enhancement is clear. It was thus important to characterize the roughness of our vapor deposited silver films before analysis.

In this note, we conclude that a vapor deposited silver film, with surface roughness < 10 nm, was covered by carbon and oxygen species on the order of several monolayers. Raman spectra can readily be obtained from this material. Since neither admolecule absorbs in the visible, the Raman scattering of these species appears to be surface enhanced.

Three samples were prepared by evaporating 50 ± 10 nm of 99.99% pure silver onto quartz chips at 2×10^{-6} Torr (at room temperature). The quartz chips were pre-

* Present address: Box 230, Strong Memorial Hospital, University of Rochester, Rochester, NY 14642.

† Present address: Sherbourne Farm Cottage, Shere Road, Albury, Near Guilford, Surrey, England.

‡ Author to whom correspondence should be addressed.

Received 22 February 1981; revision received 22 June 1981.

cleaned by immersion in an 80°C chromic acid bath followed by subsequent 5-min rinsing in deionized water, doubly-distilled water (three times) and 100% ethanol (three times), and dried in Freon vapor. XPS, Raman, and SEM measurements were obtained within 4 h of sample preparation.

Raman spectra of the film were obtained from front scattering in a 90° geometry, using 400 MW of the 476.5 or 514.5 nm argon-ion laser lines (Spectra Physics). The scattered light was focused on the entrance slit (~10 cm⁻¹) of a 1-m double monochromator (SPEX 1401). Spectra were obtained by scanning at 10 nm/min and recorded directly in wave-numbers (cm⁻¹). Spectra were obtained with a cooled RCA C31-34 photomultiplier tube and Ortec photon counting electronics.

The photoelectron spectra were obtained using a Hewlett-Packard 5950B ESCA spectrometer with monochromatic Al K α 12 (1487 eV) radiation at 800 W (power at the anode). The spectra were obtained by signal averaging 50 scans over a 20-eV binding energy range. Peak areas were obtained by computer-assisted background subtraction and integration.

The samples were examined for surface topography on a JEOL 35 scanning electron microscope at 25 kV for a resolution of surface topography of approximately 10 nm.

The Raman spectrum of the silver film shows strong peaks at approximately 1380 and 1590 cm⁻¹ (Fig. 1). Similar spectra obtained with 514.5 nm radiation confirmed the inelastic nature of the scattering. The strong peaks have previously been observed in the background of Raman scattering from various admolecules on silver. Otto⁶ first observed similar features from a cyanide monolayer chemically deposited onto a polished silver block, and attributed these to adsorbed surface carbonate. McQuellan *et al.*¹³ observed similar features in the surface Raman spectrum of a silver electrode at +0.3 V (SCE) in 0.1 M potassium formate and also attributed these to unspecified surface carboxy species. The peak at 1590 cm⁻¹ persisted at -0.9 V (SCE), and showed an anomalous shift to 1540 cm⁻¹ when the electrode was immersed in 0.1 M sodium carbonate. Mahoney *et al.*¹⁴ observed similar spectra from silver electrode surfaces at -0.2 V (SCE) in various electrolytes, and attributed this to surface graphitic carbon.

An XPS scan of binding energies from 0 to 1000 eV showed that only carbon, oxygen, and silver were detected in the surface volume of our silver films. Table I

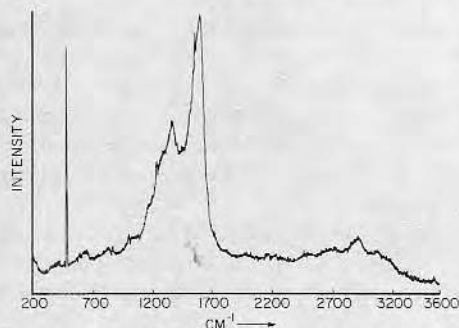


Fig. 1. Raman spectrum of the silver film using 400-MW laser excitation at 476.5 nm. The major feature is the so-called "cathedral peaks" at approximately 1380 and 1590 cm⁻¹. See text for discussion. Laser emission lines are present at 492 cm⁻¹ and 1456 cm⁻¹. Other laser emission lines were removed from the spectrum for clarity.

presents the binding energy shifts for the carbon constituent.

Fig. 2 presents the Ag 3d region of the XPS spectrum. Each of the Ag 3d peaks is split, indicating substantial surface oxidation. The feature approximately 4.3 eV higher in binding energy from the Ag metal 3d lines is a plasmon loss peak.²⁵ It can be seen from Fig. 3 (a high resolution scan of C-1s) that the major carbon (C-1s) line was at 284.1 eV with a significant component at 287.2 eV which was assigned to carbon-oxygen bonding. In addition, a small, higher energy feature was noted at +6.0 eV from the main peak. This could be due to either a carbonate-like carbon¹⁸ or to a $\pi \rightarrow \pi^*$ transition, which was demonstrated by Clark²⁶ for aromatic polymers. The feature at 287.2 eV (i.e., 3.1 eV shifted from the main peak) could be attributed either to ester-type, carbonyl-type, or quinone-like bonding. The literature indicates that the ester group gives a binding energy shift of approximately 4 eV,¹⁸ whereas quinone-like bonding is observed^{27, 28} at a shift of 2.5 eV. Although the observed feature was a little high in binding energy, it may be due to a quinone species, especially when it is considered in conjunction with the higher bonding energy C-1s peak which may well be a $\pi \rightarrow \pi^*$ satellite. Such a feature would point to a graphitic type carbon being present.^{27, 28}

The mean free path for silver (3d) electrons is approximately 1.5 nm in silver and more than 5 nm in carbon,²⁸ thus we are sampling a hierarchy of structures, including bulk elemental silver, silver oxide, and oxidized graphitic carbon overlayers.

XPS analysis showed that approximately 80% of the carbon present was of graphitic or alkyl type. Approximately 20% of the carbon is present in oxidized forms, possibly quinone-like. Oxygen was also present as silver oxide (possibly Ag₂O) or bonded to carbon.

The silver surface appeared smooth when examined under SEM at 10 nm resolution, yet we were able to obtain a Raman spectrum of adsorbed carbon.

Our Raman spectrum closely resembles that of gra-

TABLE I. X-ray photoelectron spectroscopy core binding energies for carbon (1s).

Binding energy (eV)	Δ BE (eV)	Type of bonding	% of total surface composition
284.1	0.0	Graphitic and/or alkyl	80
287.2	3.1	Quinone, ester, or related species	20
290.1	6.0	$\pi \rightarrow \pi^*$ and/or carbonate	...

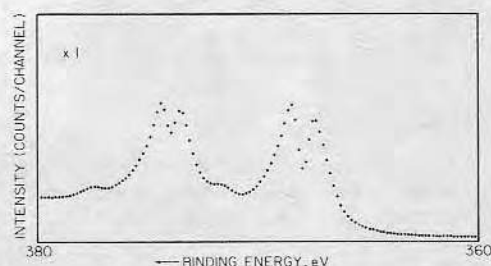


Fig. 2. High-resolution x-ray photoelectron spectrum of the silver 3d binding energy region. The shifts in the two 3d spin orbit peaks are evidence of silver oxide in the surface region on the silver metal. The two minor peaks at about 4.3 eV from the silver metal lines are due to plasmon excitations.

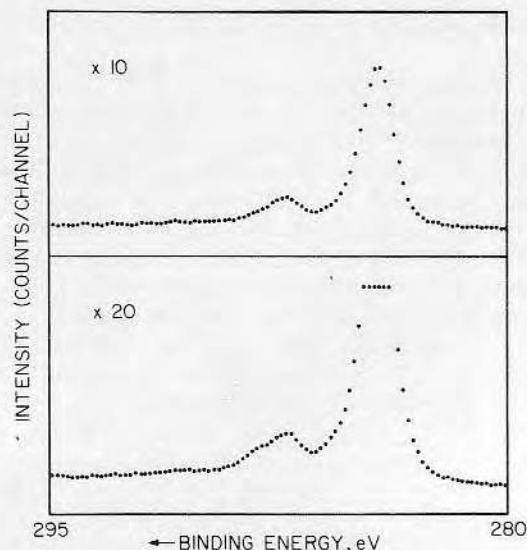


FIG. 3. High-resolution x-ray photoelectron spectrum of the C-1s region. Top spectrum shows the carbon alkyl line at 284.1 eV; a peak approximately 3 eV higher in binding energy is present; also note the features at 6 to 7 eV higher in binding energy (arrow), probably due to $\pi \rightarrow \pi^*$ C-1s satellites. This is shown in further detail in the bottom spectrum.

phitic carbon²⁹; we attribute the peaks at 1380 and 1590 cm^{-1} to this species. Graphitized carbon shows a G-line at approximately 1590 cm^{-1} , due to in-plane vibrations of the layers; a D-line at approximately 1360 cm^{-1} , associated with in-plane vibrations, resulting from structural imperfections; and features at 2700 to 2740 cm^{-1} which are a function of the population of zone boundaries. We note that our spectrum at 2700 cm^{-1} closely resembles that of graphitic carbon. However, we also observe a broad, weak feature at approximately 2925 cm^{-1} , perhaps associated with other surface contaminants.

Many authors previously reporting SERS from ad-molecules on silver electrodes, bulk silver in ultra-high vacuum, and vapor deposited silver films have observed two common features in the spectrum: (1) a background continuum from 0–4000 cm^{-1} , attributed to inelastic scattering from electron hole pairs^{22, 30}; and (2) prominent “cathedral peaks” at 1380 and 1590 cm^{-1} . Howard *et al.*¹² suggest that graphitic carbon overlayers are necessary for SERS by (1) increasing the surface concentration of adsorbed pyridine, and (2) inducing the formation of colored pyridine-carbon intercalation compounds with subsequent resonant enhancement. We note that numerous experimenters have vapor-deposited silver films on cold substrates (11 to 100 K). This would increase the amount of surface carbon due to cryoadsorption compared with our room temperature experiments, and increase the contribution of this species to the SERS.

The full role of surface carbon in SERS has yet to be fully elucidated.

ACKNOWLEDGMENTS

The work was funded by National Institutes of Health Grant HL 18519. We thank Dr. Fritz Luty for use of the Raman apparatus, Dr. F. Moatammed for use of the JEOL 35 scanning electron microscope, Dr. Lee Smith for preparation of the silver films, and Dr. Fran Adar of Instruments, S.A. for collaboration with related Raman studies which are not reported here.

- M. G. Albrecht and J. A. Creighton, *J. Am. Chem. Soc.* **99**, 5215 (1977).
- B. Pettinger and V. Wenning, *Chem. Phys. Lett.* **56**, 253 (1978).
- J. A. Creighton, M. G. Albrecht, R. E. Hester, and J. A. D. Matthew, *Chem. Phys. Lett.* **55**, 55 (1978).
- B. Pettinger, V. Wenning, and D. M. Kolb, *Ber. Bunsenges. Physik. Chem.* **82**, 1326 (1978).
- A. Otto, *Surf. Sci.* **75**, L392 (1978).
- T. E. Furtak, *Solid State Commun.* **28**, 903 (1978).
- J. P. Heritage, J. G. Bergman, A. Pinczuk, and J. D. Worlock, *Chem. Phys. Lett.* **67**, 229 (1979).
- J. G. Bergman, J. P. Heritage, A. Pinczuk, J. M. Worlock, and J. H. McFee, *Chem. Phys. Lett.* **68**, 412 (1979).
- R. P. Cooney, E. S. Reid, M. Fleischmann, and P. J. Hendra, *J. Chem. Soc. Faraday Trans.* **73**, 1691 (1977).
- T. H. Wood and M. V. Klein, *J. Vac. Sci. Technol.* **16**, 459 (1979).
- M. W. Howard, R. P. Cooney, and A. J. McQuillan, *J. Raman Spectrosc.* **9**, 273 (1980).
- A. J. McQuillan, P. J. Hendra, and M. Fleischmann, *J. Electroanal. Chem.* **65**, 933 (1975).
- M. R. Mahoney, M. W. Howard, and R. P. Cooney, *Chem. Phys. Lett.* **71**, 59 (1980).
- K. Slegbahn, C. Nordling, A. Fahlman, R. Nordberg, K. Hamon, J. Hedman, G. Johansson, T. Bergonark, S. E. Karlson, I. Lindgren, and B. Lindberg, *ESCA: Atomic, Molecular, and Solid State Structure Studies by Means of Electron Spectroscopy* (Almqvist and Wiksells, Stockholm, 1967), *Nova Acta Regiae Soc. Sci. Upsaliensis Ser. IV*, Vol. 20.
- J. S. Hammond, S. W. Gaarenstroom, and N. Winograd, *Anal. Chem.* **47**, 2193 (1975).
- T. A. Carlson, *Photoelectron and Auger Spectroscopy* (Plenum, New York, 1975), p. 365.
- H. R. Thomas, Ph.D. thesis, University of Durham, United Kingdom, 1977.
- P. J. Trolter, M. G. Mason, and L. J. Gerenser, *J. Phys. Chem.* **81**, 1325 (1977).
- E. Kretschmann, *Opt. Commun.* **5**, 331 (1972).
- D. S. Wang, H. Chew, and M. Kerker, *Appl. Opt.* **19**, 2256 (1980).
- E. Burstein, Y. J. Chen, C. Y. Chen, S. Lundqvist, and E. Tosatti, *Solid State Commun.* **29**, 567 (1979).
- D. L. Jeanmaire and R. P. van Duyne, *J. Electroanal. Chem.* **84**, 1 (1977).
- J. E. Rowe, C. V. Shank, D. A. Zwemer, and C. A. Murray, *Phys. Rev. Lett.* **44**, 1770 (1980).
- T. E. Furtak, Panel discussion, *Proc. VIIth Int. Conf. on Raman Spectroscopy*, August 1980.
- D. T. Clark, The investigation of polymer surface by means of ESCA, in *Polymer Surfaces*, D. T. Clark and W. J. Feast, Eds. (Wiley, New York, 1978).
- R. N. King, J. D. Andrade, A. D. Haubold, H. S. Shim, “Surface analysis of Si-alloyed and unalloyed LTI pyrolytic carbon, in *Characterization of Polymer Molecular Structure* . . . , ACS Symp. Series, D. Dwight *et al.*, Eds) (American Chemistry Society, 1981), in press.
- P. Cadman, G. Gossedge, and J. D. Scott, *J. Electron Spect. Relat. Phenom.* **13**, 1 (1978).
- R. Vidano and D. B. Fischbach, *J. Am. Ceram. Soc.* **61**, 13 (1978).
- C. Y. Chen, E. Burstein, and S. Lundqvist, *Solid State Commun.* **32**, 63 (1979).

1. M. Fleischmann, P. J. Hendra, and A. J. McQuillan, *Chem. Phys. Lett.* **26**, 163 (1974).

Adsorption of low density lipoproteins onto selected biomedical polymers

D. E. Dong, J. D. Andrade, and D. L. Coleman

Department of Pharmaceutics, University of Utah, Salt Lake City, Utah 84112

This study examines the interaction of human low density lipoprotein (LDL) with a select group of biomedical polymers. The adsorption characteristics of LDL on cured filler-free poly(dimethyl Siloxane) (C-PDMS), Biomer, Cardiomat 610, Kraton 1650, poly(hydroxyethyl methacrylate) (PHEMA) and glass are presented. Adsorption of LDL to charged hydrophilic glass control surfaces occurred rapidly, reaching plateau concentrations within one minute ($0.19 \pm 0.01 \text{ ug/cm}^2$). Adsorption of LDL to polymer surfaces appeared to be dependent upon both the polymer hydrophobicity (or apolar nature), and flexibility (or dynamic nature) at the interface. Increased surface concentrations were observed for Biomer ($0.32 \pm 0.01 \text{ ug/cm}^2$) as well as other polymers which exhibited both hydrophobic and elastomeric properties. Temperature changes between 25°C

and 37°C were found to significantly influence the surface concentration of LDL on Biomer ($0.16 \pm 0.01 \text{ ug/cm}^2$ at 25°C versus $0.32 \pm 0.01 \text{ ug/cm}^2$ at 37°C). A lipid core phase transition at 36°C was believed to be responsible for the temperature influence. Preliminary competitive adsorption studies of LDL with albumin (HSA) and serum on silicone surfaces suggests that LDL adsorption occurred rapidly and preferentially ($0.25 \pm 0.01 \text{ ug/cm}^2$ for LDL alone; $0.33 \pm 0.01 \text{ ug/cm}^2$ for LDL + HSA; $0.15 \pm 0.01 \text{ ug/cm}^2$ LDL + serum). Preliminary studies on the role of LDL in calcification were not conclusive. It can be concluded that LDL adsorption is dependent upon polymer hydrophobicity, flexibility and temperature. Competitive adsorption experiments suggests that LDL may have a substantial influence on protein adsorption.

INTRODUCTION

The effects of lipid and lipoprotein adsorption on the blood-materials interface are of interest in the compatibility of prostheses. Swelling, cracking and loss of mechanical performance of Silastic heart ball poppets were attributed to the adsorption and absorption of selected lipid and lipoprotein components.^{1,2} Similarly, sorption of lipids and lipoproteins may act as sites for the initiation of calcification,^{3,4} as sources of phospholipids for platelet activation,⁵⁻⁷ or may affect the overall mechanical performance of the material by accelerating oxidative degradation.⁸

The low density lipoprotein fraction was chosen for the evaluation of lipid-lipoprotein adsorption based on its high concentrations of cholesterol and cholesterol esters,⁹ and its roles in atherogenesis.¹⁰ There were also previous *in vitro* studies on silicone rubber suggesting that cholesterol components are actively absorbed by these materials.¹¹

There are few reported studies concerning the adsorption of LDL onto polymer materials (Table I). Most studies only report interactions of LDL with hydrophilic glass substrates.¹²⁻²⁰ The report by Dana¹² indicated that adsorption of LDL on glass surfaces reached saturation equilibrium with high affinity and temperature independence. The report by Lewis¹³ suggested the inhibitory role of LDL in the adhesion of thrombocytes (platelets) to glass surfaces. Other lipid fractions are also thought to activate platelets and increase adhesion.^{6-7,21} Brown,¹⁴ as a result of routine lipoprotein isolation procedures, found that LDL irreversibly bound to radio-frequency glow-discharged polystyrene (PS) surfaces. The removal of LDL from the treated PS surface was only possible after treatment with the enzyme trypsin, which is known to specifically cleave at the lysine and arginine residues. More recent studies by Bantjes²⁰ evaluated the competitive adsorption of LDL, high density lipoprotein (HDL), and fibrinogen from serially diluted plasma onto polyvinylchloride (PVC) and PS. Adsorption of LDL produced less inhibition of adsorption of other plasma proteins in comparison to HDL.

These studies have given us some indication of the behavior of LDL adsorption onto material surfaces. Studies are now necessary to determine lipid and lipoprotein adsorption characteristics to more relevant biomedical materials. The importance and role of lipids and lipoproteins in determining the overall biocompatibility and performance of a material is still unclear and also require further evaluation. The purpose of this study is to evaluate the adsorption behavior of LDL onto a selected group of biomedical materials, including filler-free poly(dimethyl siloxane), Biomer, Cardiomat 610, Kraton 1650, and poly(hydroxyethyl methacrylate).

MATERIALS AND METHODS

Materials processing

Biomer®, a poly(ether urethane urea), was a gift from Ethicon Inc., Somerville, New Jersey; Cardiomat® 610, a poly(ether urethane), was a gift from Kontron Cardiovascular Inc., Everett, Massachusetts; and Kraton® 1650, a triblock copolymer of styrene-ethylene-butylene-styrene (SEBS), was a gift from Shell Chemical Corp., Houston, Texas.

Biomer (10% w/v in dimethylacetamide, DMAC), Cardiomat 610 (15-18% w/v in 2:1 dioxane:tetrahydrofuran, THF), and Kraton 1650 (20% w/v in redistilled decahydronaphthalene) were cast into 0.01 cm thick sheets on a Mylar® substrate and solvent evaporated under a positive pressure nitrogen atmosphere at 60°C.

Filler-free poly(dimethyl siloxane) (PDMS) was a gift from Thoratec Labs, Berkeley, California. A 10% (w/v) solution of PDMS was prepared in THF. Samples were dip cast onto silica-filled Silastic® sheets (Dow Corning) that had been extracted in methylene chloride overnight. Samples were then cured at 80°C for 12 hrs in a humid nitrogen-filled environment followed by a 45 min steam autoclave at 80°C to insure a complete cure. Samples were

TABLE I
A Review of Current Literature on the Adsorption of Lipoproteins at Solid Interfaces

Protein	Surface	Results	Investigator	Year	Ref.
LDL	Hydrophilic glass	High affinity; saturability	Dana	1977	12
LDL	Polystyrene culture plates	High affinity; irreversible	Brown	1976	14
LDL	Hydrophilic glass	Inhibit pigeon thrombocyte adhesion	Lewis	1979	13
HDL	Silane-treated glass	Binds reversibly to apoA-I but irreversibly to apoA-II	Shen	1979	16
VLDL	Cellulose nitrate	Extreme high saturability irreversible binding	Holmquist	1982	15
Lipid mixture	Biomer	Cholesterol, cholesterol ester absorption	Lyman	1976	17
β and α -lipoprotein fractions	Biomer, PDMS, glass	No adsorption or absorption; decreased thrombus formation	Halbert	1969	18
Phospholipids	Glass, polystyrene	High affinity, disaturated phospholipid bound with greater affinity than monosaturated phospholipid	Gershfeld	1982	19
LDL and HDL	PVC and PS	Preferential adsorption HDL from plasma; low surface conc. LDL from plasma solution	Bantjes	1983	20
LDL and HDL	Glass and DDS-treated glass	Increased LDL adsorption to both surfaces in comparison to HDL using new method of TIRIF	Hlady	1986	49

minimally tacky, smooth and without defects as determined by the characterization protocol described below.

Hydroxyethyl methacrylate (HEMA) was a gift from Hydro Med Sciences, Inc., New Brunswick, New Jersey. The HEMA was cast against acid cleaned glass plates using azobis-(methyl isobutyrate) as the initiator. Polymerization was allowed to proceed for 12 hrs at 60°C.

Borosilicate glass (Gold Seal) was used for the control substrate. Glass was prepared by the cleaning process described by King.²²

Materials characterization

Light microscopy and scanning electron microscopy were used to examine the gross surface roughness and morphology of the cast polymers. All material surfaces except Biomer were smooth and free of gross or microscopic defects. Biomer surfaces were difficult to render free of defects due to the presence of unfilterable gel particles and the formation of microbubbles upon evaporation of the solvents even under controlled environmental conditions (Fig. 1).

The surface chemical composition was determined by the use of x-ray photoelectron spectroscopy (XPS). XPS was performed on each lot of cast

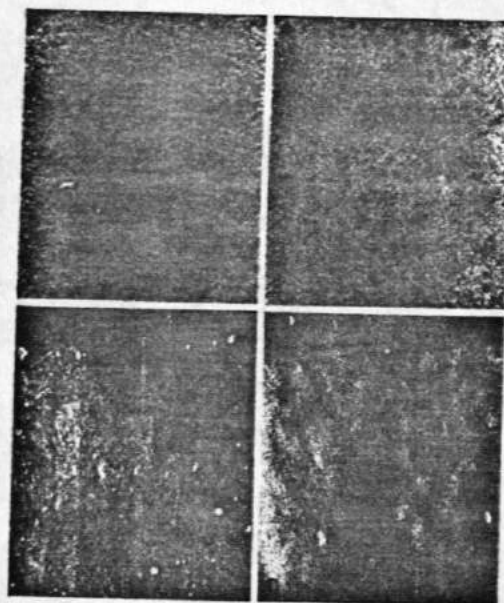


Figure 1. Surface morphology of (a) unfiltered Biomer via light microscopy at original magnification of 200 X; (b) 3- μ M Fluoropore filtered Biomer; light microscopy at original magnification of 200 X; (c) Cardiomat 610 scanning electron micrograph (SEM) at original magnification of 5400 X (d) Kraton 1650, SEM at original magnification of 2100 X. The surface roughness of Biomer samples was due to the presence of unfiltered gel particles and formation of microbubbles upon evaporation of solvent under controlled environmental conditions (see text).

samples. Both the Mylar facing surfaces and surfaces cast against a nitrogen atmosphere were analyzed (Table II). Both urethanes showed an increase in the ether carbon and decrease in the alkyl carbon for the surface cast against a Mylar substrate. This is expected, considering the polar surface composition of Mylar.

The Wilhelmy plate²³ method was used to determine the surface hydrophobicity and hydrophilicity under dynamic conditions. The receding water contact angle was used as an indication of the hydrophilicity of the polymer surface. The receding water contact angles showed PDMS and Kraton 1650 to be the most hydrophobic polymers. Biomer and Cardiomat 610 showed greater hydrophobicity than glass or PHEMA (Table III).

Low density lipoprotein isolation

Fresh human blood was used in all experiments. The blood was allowed to clot at room temperature for 1 hr and then was centrifuged at $1500 \times g$ for 30 minutes at 5°C to isolate serum. All solutions used in the procedure contained 0.01% Thimerosal (sodium ethyl mercurithiosalicylate) as a bactericide, 0.01% EDTA to chelate metal ions, 0.013%-amino caproic acid as a protease inhibitor, and 0.05% glutathione (reduced) as an antioxidant.²⁴ Isolation of LDL from whole serum followed the sequential ultracentrifugation protocol of Lindgren²⁵ at $105,000 \times g$ for 18 hrs at 16°C. Density adjustment was performed by the addition of NaCl and NaBr solutions. Low density lipoprotein was collected between the density of 1.006 g/mL and 1.063 g/mL. Washed LDL was passed over a column of Sephadex G50 in phosphate buffered saline (PBS) (0.15M NaCl, pH 7.4) at 4°C to remove NaBr.

Isolated LDL was characterized by polyacrylamide slab gel electrophoresis (PAGE),²⁶ immunodiffusion²⁷ and transmission electron microscopy (TEM).²⁸ Polyacrylamide gel electrophoresis of LDL was performed on 7.5% linear gels. No protein contaminants were detected. Uniformity of particle size by TEM and non-identity of LDL by immunoelectrophoresis against human serum albumin and other serum proteins also confirmed sample purity. Protein was determined by a modified Lowry procedure.²⁹ Lipid analysis for total cholesterol and triglyceride was determined by the use of the Worthington® enzymatic assay kits for serum lipids.^{30,31} Lipid analysis of whole serum cholesterol and triglyceride of blood donors fell within population sample norms of 138–294 mg/dL and 36–165 mg/dL, respectively.^{30,31}

Experimental protocol

LDL was tritium labeled by reductive methylation of the lysine residues by the procedure of Jentoff and Dearborn.^{32,33} The radio-labeled LDL was characterized as described above. Greater than 95% activity was associated with the LDL protein band as determined by polyacrylamide gel hydrolysis.³⁴ All polymer samples were cut into 16 mm diameter circular discs. Samples were

TABLE II
Elemental Surface Composition (%) of Polymers Studied for LDL Adsorption as Determined by ESCA

Polymer	n	$\pi - \pi^*$ C ₂₉₀	Urethane C ₂₈₈	Ether C ₂₈₅	Alkyl C ₂₈₄	O	N	Si
C-PDMS	2	—	—	—	50	23.6	—	26.3
Biomer	5	—	2.39 ± 1.04	26.34 ± 5.09	46.42 ± 3.51	18.12 ± 1.64	2.66 ± 0.79	4.46 ± 0.35
N ₂ Cast Surface	3	—	1.55 ± 0.27	33.42 ± 3.26	41.67 ± 5.63	17.17 ± 1.39	3.16 ± 1.00	1.00 ± 1.08
Mylar	3	—	1.56 ± 1.12	28.62 ± 6.73	47.20 ± 7.60	18.01 ± 0.08	1.77 ± 0.73	3.48 ± 0.64
Cardiomat 610	3	—	1.72 ± 0.43	33.78 ± 2.41	43.38 ± 1.93	18.16 ± 1.28	2.47 ± 0.33	0.71 ± 0.50
N ₂ Cast Surface	3	0.22 ± 0.03	—	—	85.90 ± 3.19	8.03 ± 1.57	—	0.64 ± 1.51
Mylar	3	0.22 ± 0.40	—	—	94.97 ± 1.96	1.56 ± 1.26	—	1.25 ± 1.08

TABLE III
Wilhelmy Plate Advancing and Receding Water Contact
Angles for Polymers After 24-Hour Hydration in PBS at 25°C

Polymer	Adv. Angle	Rec. Angle
Glass	<10	<10
C-PDMS-FF	110 ± 6	74 ± 8
Biomer	81 ± 7	42 ± 6
Cardiomat 610	84 ± 1	32 ± 2
Kraton 1650	103 ± 3	57 ± 5
PHEMA	100 ± 7	22 ± 3

extracted for 12 hrs in PBS to remove unreacted monomer and catalyst and then hydrated in PBS for 24 hrs prior to exposure to LDL solutions. Polymer samples were suspended in a PBS solution followed by the addition of a concentrated LDL solution. This procedure was followed to avoid the interaction of the polymer with a denatured lipoprotein layer at the air-liquid interface. Adsorption was allowed to proceed at 37°C for up to 2 hrs. A constant mild agitation at 125 rpm was applied by a shaker bath to minimize the presence of a denatured boundary layer at the interface. Following the appropriate time intervals, the protein solution was displaced by equal volumes of fresh PBS flushed through an inlet port and out an exit port, again minimizing the interaction of the polymer with the protein-air interface. Three 30-mL rinses of PBS at 5-min intervals were used to displace the protein solution and to remove loosely bound protein from the surface. The flow rate was 60 mL/min. The polymer samples were transferred to vials and 10 mL of scintillation cocktail (Aquasol II, New England Nuclear) was added. The samples were allowed to equilibrate for 24 hr at 4°C before sample activity was determined. All experiments were performed in triplicate.

A preliminary competitive adsorption study was performed with human serum albumin (HSA) and diluted whole serum. Albumin and LDL were combined in PBS to give a final solution concentration at 5 mg/mL and 0.4 mg/mL, respectively. Serum was diluted to give a final protein concentration at 10 mg/mL with a LDL concentration at 0.5 mg/mL.

Data analysis

The analysis of covariance,³⁵ the nonparametric Kruskal-Wallis analysis of variance,³⁶ and the Wilcoxon-Rank Sum Test for multiple sample comparison³⁶ were performed on the data where applicable. The "P" represents the probability that the observation is significant at the stated α -level of significance.

Experimental results

The influence of blood donor LDL variability was studied (Fig. 2). Examination of the data (Table IV) reveals significant overlap of the standard deviations, suggesting that the difference among the donors may not actually exist but may reflect the small sample size used in the statistical analysis. Therefore, donor variability was interpreted as not having a dominant effect on LDL adsorption in glass substrates.

Radio methylation was found to significantly influence the surface concentration of adsorbed LDL (Fig. 3). LDL labeled with ≥ 20 methyl groups/mol of protein resulted in a significantly lower surface concentration compared to LDL labeled with ≤ 2 methyl groups/mol of protein. Perhaps the methylation of the lysine residues results in a decreased electrostatic interaction with the negatively charged glass surface. It was determined that a high specific activity was necessary to obtain reliable statistics because of the counting geometry used and the low concentration of adsorbed protein. A medium degree of label (10–15 methyl groups/mol of protein) was chosen for the remainder of the study.

Adsorption studies performed as a function of temperature were found to show a significantly greater LDL surface concentration on Biomer and PDMS at 37°C compared to 25°C. No significant difference in surface concentrations were observed for glass controls between the two temperatures (Fig. 4). Subsequent studies were performed at 37°C.

The adsorption of LDL onto control glass substrate was found to be largely independent of both time and concentration (Figures 5, 6, and Table V). Adsorption was both rapid (<1 min) and resistant to displacement following three 30-mL PBS 5-min rinses at 37°C. Plateau surface concentrations were observed at the earliest time interval of 1 min.

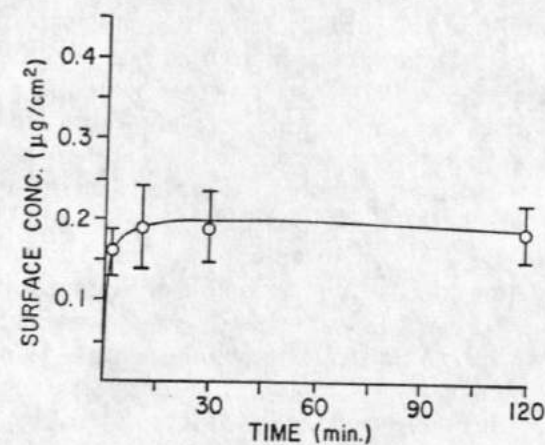


Figure 2. Average surface concentration ($\mu\text{g}/\text{cm}^2$) of ^3H -LDL (0.3 mg/mL) from four donors onto hydrophilic glass at 37°C. Degree of label = 7.3 ± 1.9 methyl groups/LDL molecule. The individual donor data are given in Table IV.

TABLE IV
Surface Concentrations ($\mu\text{g}/\text{cm}^2$) of Adsorbed ^3H -LDL (0.26 mg/mL) in PBS on Hydrophilic Glass at 37°C Using LDL of Four Different Donors^a

Donor	n ^b	Conc. (mg/mL)	1 min	10 min	30 min	120 min
1.	3	0.30	0.13 \pm 0.01	0.16 \pm 0.01	0.15 \pm 0.01	0.16 \pm 0.01
2.	3	0.18	0.16 \pm 0.01	0.21 \pm 0.01	0.22 \pm 0.02	0.21 \pm 0.02
3.	3	0.26	0.16 \pm 0.01	0.16 \pm 0.02	0.17 \pm 0.02	0.16 \pm 0.01
4.	3	0.29	0.19 \pm 0.01	0.23 \pm 0.04	0.21 \pm 0.01	0.21 \pm 0.02
\bar{X}	12	0.26	0.16 \pm 0.02	0.19 \pm 0.04	0.19 \pm 0.03	0.18 \pm 0.03

^aDegree label $\sim 7.3 \pm 2.9$ methyl group/LDL molecule.

^bThe n represents total number of samples in all experiments performed in triplicate

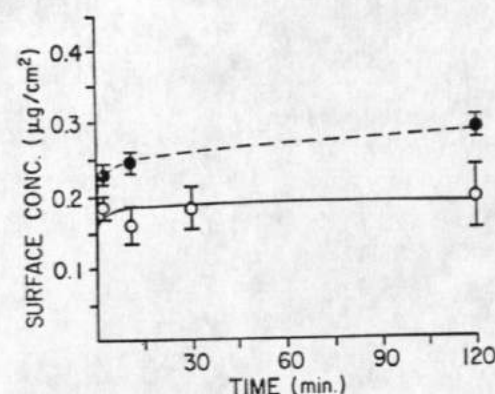


Figure 3. Effect of radiolabeling of LDL (0.3 mg/mL) on adsorption onto hydrophilic glass at 37°C. Degree of label: (○) high = 21.3 ± 2.7 methyl groups/LDL molecule (●) low = 2.3 ± 1.0 methyl groups/LDL molecules. All subsequent experiments were performed with a degree of label between 10–15 methyl groups/LDL molecule (see text).

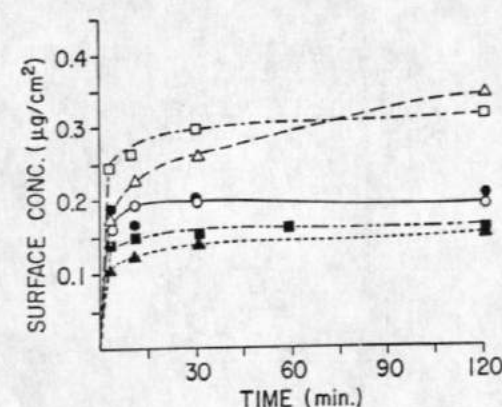


Figure 4. The effect of temperature on adsorption of ^3H -LDL onto hydrophilic glass (●, 0.3 mg/mL ^3H -LDL), C-PDMS (□, 0.4 mg/mL ^3H -LDL), Biomer (△, 0.5 mg/mL ^3H -LDL). Solution concentration standard deviations ranged between ± 0.01 and ± 0.04 mg/mL. Open symbols are 37°C; closed symbols are 25°C.

PDMS and Kraton 1650 adsorbed more LDL than hydrophilic glass. The kinetic profiles of both polymers showed evidence of concentration and time dependence (Figs. 5, 6, and Table V).

The adsorption of LDL to Biomer occurred relatively slowly, suggesting a stronger dependence upon both time and concentration (Figs. 5, 6, and Table V). These characteristics were also revealed in the isotherm plots. Although the adsorption kinetics of LDL onto Biomer were slow, prolonged exposure (120 min) resulted in significantly greater surface concentrations than the control glass substrates.

Cardiomat 610 and PHEMA both resulted in significantly lower surface concentrations than the glass controls (Figs. 7, 8, and Table V). The ad-

TABLE V
Surface Concentration ($\mu\text{g}/\text{cm}^2$) of LDL Adsorbed
onto Polymer Surfaces at 0.5 mg/mL at 37°C in PBS

Substrate	Time (min)			
	1	10	30	120
Glass	0.19 ± 0.01	0.17 ± 0.01	0.17 ± 0.01	0.18 ± 0.01
C-PDMS-FF	0.24 ± 0.02	0.26 ± 0.01	0.29 ± 0.01	0.30 ± 0.02
Biomer	0.16 ± 0.01	0.22 ± 0.03	0.25 ± 0.01	0.32 ± 0.01
Kraton 1650	0.30 ± 0.01	0.38 ± 0.02	0.41 ± 0.02	0.42 ± 0.01
Cardiomat 610	0.10 ± 0.01	0.06 ± 0.01	0.09 ± 0.03	0.17 ± 0.03
PHEMA	0.06 ± 0.01	0.09 ± 0.01	0.13 ± 0.01	0.15 ± 0.02

sorption kinetics for Cardiomat 610 were similar to Biomer, exhibiting a slow rate of adsorption and both a time and concentration dependence. The adsorption kinetics of PHEMA was also similar to glass, although the adsorption isotherm for PHEMA (Fig. 7) did not appear to reach an equilibrium plateau in contrast to the other materials in the study. Overall, adsorption of LDL appears to be greater on more hydrophobic polymers, as represented graphically in Figure 9.

Preliminary competitive adsorption studies onto PDMS indicate an inhibitory effect of serum upon adsorption of LDL and a positive influence of albumin on LDL adsorption (Fig. 10). Albumin was found to increase the surface concentration of LDL by 25% compared to LDL adsorption from pure LDL solution. In the presence of diluted serum, LDL was found to adsorb 50% the surface concentration found in adsorption from pure LDL solution.

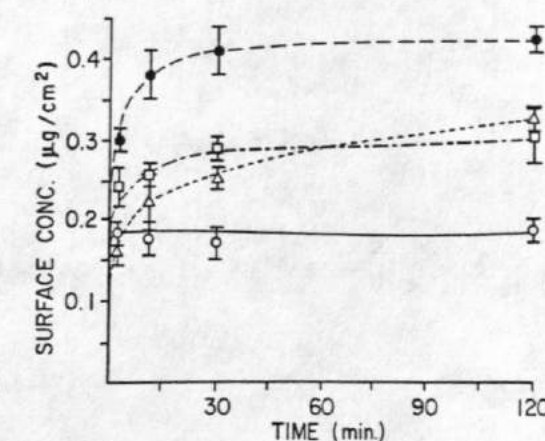


Figure 5. Adsorption kinetics of ^3H -LDL (0.5 mg/mL) onto hydrophilic glass (○), C-PDMS (□), Biomer (△) and Kraton 1650 (●) in PBS, 37°C for up to 120 min.

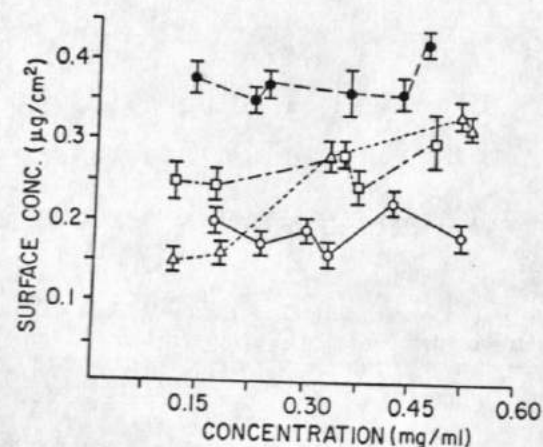


Figure 6. Adsorption isotherm of ^3H -LDL (0.5 mg/mL) onto hydrophilic glass (○), C-PDMS (□), Biomer (Δ) and Kraton 1650 (●) in PBS at 120 min., 37°C.

DISCUSSION

The structure of LDL is not completely known at this time although studies suggest that it exists as a spherical molecule similar in form to other lipoprotein complexes.^{37,38} The molecule is approximately 200–250 Å in diameter, consisting of a core lipid component of cholesterol ester (CE) and triglycerides (TG) and an outer shell of phospholipid, cholesterol and protein. The core lipid composite of CE and TG has also been shown to go through a reversible lipid phase transition (LPT) between the temperature of 20–40°C, with a peak transition at 36°C.^{39,40} The lipid core exists as a solid crystal below the LPT in a low energy state with minimal molecular motion or mobility. Within the range of the LPT and near the peak transition temperature, the core lipids melt to a liquid crystalline state and possess an increase in

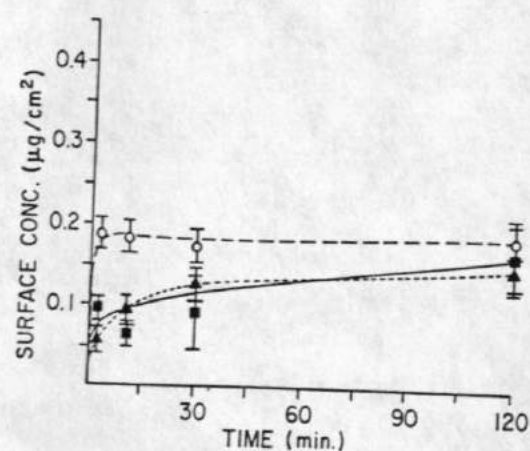


Figure 7. Adsorption kinetics of ^3H -LDL (0.5 mg/mL) onto hydrophilic glass (○), Cardiomat 610 (■), and PHEMA (▲) in PBS, 37°C for up to 120 min.

ADSORPTION OF LOW DENSITY LIPOPROTEINS

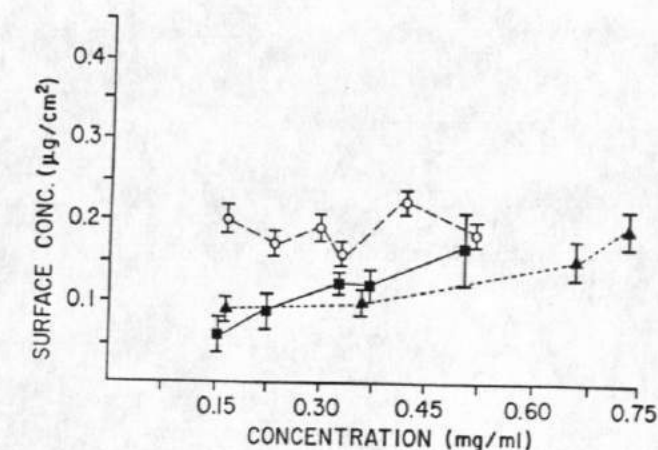


Figure 8. Adsorption isotherm of ^3H -LDL (0.5 mg/mL) onto hydrophilic glass (○), Cardiomat 610 (■) and PHEMA (▲) in PBS at 120 min, 37°C.

dynamic mobility. The increase in dynamics occurs not only for the core, but also for the entire LDL molecule, allowing exchange to occur between the core and surface lipids. This indirectly allows for the interaction of all components of the molecule with the environment. This is particularly important in a biological environment and may also be of importance in an artificially induced environment as well.^{41–43} The liquid–solid interface of LDL consists of both charged and hydrophobic domains.^{44,45} Approximately 40% of the total lipid composition and 100% of the protein component exists on the outer shell of the macromolecule.

Information concerning the molecular structure and dynamics of LDL can be used to formulate the following conclusions and hypothesis. Our data

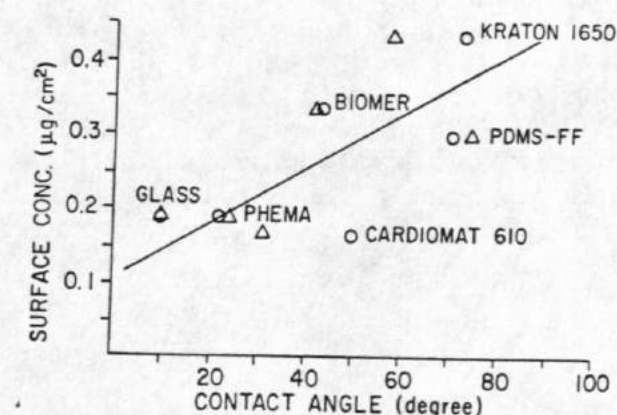


Figure 9. Correlation between the surface concentration at 120 min. adsorption ($\mu\text{g}/\text{cm}^2$) of adsorbed ^3H -LDL and the hydrophobicity of the polymers as determined by underwater captive bubble (○) and Wilhelmy plate receding (Δ) contact angle techniques. The hydrophobicity of the polymer appears to correlate with increased adsorption of LDL.

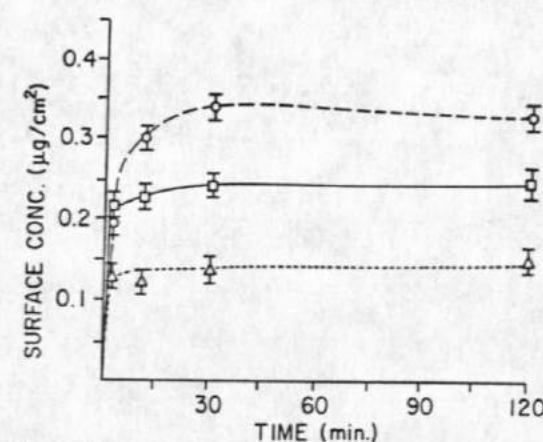


Figure 10. Competitive adsorption of ^3H -LDL on C-PDMS at 37°C. LDL alone (\square , 0.4 mg/mL), LDL with human serum albumin (Fraction V) (\circ , 0.4 mg/mL LDL and 5.2 mg/mL albumin in PBS) and LDL (Δ , 0.5 mg/mL LDL) with whole human serum (10 mg/mL total protein).

support a significantly greater surface concentration of LDL adsorbed at 37°C compared to 25°C on PDMS and Biomer. The increased surface concentration observed in these two polymers can be attributed to two synergistic effects: (1) the elastomeric nature of the polymers, since glass controls did not show a significant increase in surface concentration; and (2) the increased dynamics of LDL due to the LPT at the higher temperature.

The adsorption of LDL is increased on more hydrophobic and elastomeric polymers such as PDMS, Biomer and Kraton 1650. It is known from other studies that the adsorption of proteins to polymer surfaces is dependent upon the surface composition and bulk composition.⁴⁶ We hypothesize that the adsorption of LDL is dependent both on the surface (and bulk) composition as well as the elastomeric nature of the polymer. The importance of the two components in influencing protein adsorption is evident in the adsorption results of LDL on Biomer and Cardiomat 610. Although the two polymers are urethanes, their compositions differ in both the chain extender and the soft segment length, leading possibly to the difference observed in surface concentration. Biomer is composed of an ethylene diamine chain extender, with a soft segment of approximately 2000 molecular weight. The Wilhelmy plate receding contact angle measures $41.8 \pm 6.0^\circ$. Cardiomat 610 is composed of a butane diol chain extender and a soft segment of approximately 1000 molecular weight. Its contact angle ($31.5 \pm 1.8^\circ$) is somewhat more hydrophilic as one would expect with a more polar chain extender and smaller hydrophobic soft segment. Comparison of the data between other elastomeric polymers and non-elastomeric polymers in this study also support this hypothesis.

Although specific modes of interaction were not identified in these experiments, it is known that the adsorption of LDL onto glass occurs by electrostatic interactions.^{12,47,48} Other modes of interaction have not been as widely studied although the various hydrophobic lipids and hydrophilic protein components of LDL provide the capability for many different means of interaction. The varied composition of LDL and its dynamic nature also allows it to accommodate optimally to a surface. Recent studies by Hlady et al.⁴⁹ have examined the adsorption of HDL and LDL to hydrophilic glass and silane treated hydrophobic glass by the new method of total internal reflection intrinsic fluorescence.⁵⁰ Fluorescence characteristics of adsorbed protein can be used to gain information regarding the conformation of the protein on the surface and allow better understanding of lipoprotein surface interactions. More studies are required to determine the predominant factor in adsorption of LDL to surfaces.

The adsorption of LDL onto PDMS increased in the presence of albumin and significant adsorption was found in the presence of serum. Studies by Bantjes et al.²⁰ have examined the competitive adsorption of LDL and HDL with other serum proteins in solution mixtures. The adsorption of HDL from plasma occurred preferentially on PVC and PS surfaces. Adsorption of LDL resulted in lower surface concentrations in comparison to both HDL and pure protein solutions, but an equilibrium state was not achieved. Both adsorbed lipoproteins resulted in decreased adsorption of albumin, fibrinogen and immunoglobulin from plasma. The surface concentration of fibrinogen on PS surfaces in the presences of LDL was not reduced in comparison to the amount adsorbed from a pure protein solution. Bantjes et al.²⁰ did not study the influence of albumin on lipoprotein adsorption. Although we saw an increase in surface concentration of LDL in the presence of albumin, the interaction between albumin and LDL is still unclear. Both polymers in Bantjes et al. study are relatively rigid, polar and non-elastomeric in comparison to PDMS used in our study. This may possibly have lead to the unenhanced and lower surface concentrations seen in their results. We suggest that, in the presence of competing serum proteins LDL possesses a greater affinity for hydrophobic and elastomeric surfaces in comparison to other serum proteins. More studies are necessary to confirm this hypothesis.

In conclusion, the adsorption of LDL to specific polymer surfaces is influenced by temperature and by the hydrophobicity of the polymer surface. The possible implications from this study are numerous. The presence and role of LDL in atherosclerosis and calcification has been documented in numerous studies.⁵¹⁻⁵³ The effect of LDL adsorption in implanted prosthesis or hemodynamic devices (cardiac assist devices, artificial heart) may lead to similar biological conclusions. Studies showing lipid adsorption with changes in mechanical properties over time may now have an etiological basis.^{11,17} The presence of absorbed lipids may also act as a source of lipids in place of platelet lipids, initiating the coagulation cascade.^{6,7} It is therefore apparent that more attention should be focused on the role of lipids and lipoproteins in blood interactions with materials.

The work was partially supported by NIH Grant HL18519, HL27747 and HL07520. The assistance and advice of Drs. Donald Gregonis and Dana Wilson are gratefully acknowledged.

References

1. R. Carmen and S. C. Mutha, "Lipid absorption by silicone rubber heart valve poppets—in vitro and in vivo results," *J. Biomed. Mater. Res.*, **6**, 327-346 (1972).
2. H. P. Chin, E. C. Harrison, D. H. Blankenhorn, and J. Moacanin, "Lipids in silicone rubber valve prosthesis after human implantation," *Suppl J Circulation*, **53**, 151-155 (1971).
3. D. L. Coleman, "Mineralization of blood pump bladders," *Trans. Am. Soc. Artif. Int. Organs*, **27**, 708-715 (1980).
4. D. R. Owens and R. M. Zone, "A possible mechanism of surface calcification," *Trans. Am. Soc. Artif. Int. Organs*, **27**, 528-531 (1980).
5. M. Aviram, J. G. Brook, A. M. Lees, and R. S. Lees, "Low density lipoprotein binding to human platelets: Role of charge and of specific amino acids," *Biochem. Biophys. Res. Commun.*, **99**, 308-318 (1981).
6. E. Koller, F. Koller, and W. Doleschel, "Specific binding sites on human blood platelets for plasma lipoprotein," *Hoppe-Seyler's Z. Physiol. Chem.*, **363**, 395-405 (1982).
7. M. Aviram and J. G. Brook, "Platelet interaction with high and low density lipoproteins," *Atherosclerosis*, **46**, 259-268 (1983).
8. D. F. Williams, "The deterioration of materials in use," in *Implants in Surgery*, D. F. Williams and R. Roar, Eds., W. B. Saunders Co. Ltd., London, 1973, p. 737.
9. A. M. Scanu and C. Wisdom, "Serum lipoproteins: Structure and function," *Ann. Rev. Biochem.*, **41**, 703-729 (1972).
10. R. I. Levy, "Cholesterol, lipoproteins, apoproteins and heart disease: Present status and future prospects," *Clin. Chem.*, **27**, 653-662 (1982).
11. R. Carmen and P. Kahn, "In vitro testing of silicone rubber heart valve poppets for lipid absorption," *J. Biomed. Mater. Res.*, **2**, 457-464 (1968).
12. S. E. Dana, M. S. Brown, and J. L. Goldstein, "Specific, saturable, and high affinity binding of I^{125} -low density lipoprotein to glass beads," *Biochem. Biophys. Res. Commun.*, **74**, 1369-1376 (1977).
13. J. C. Lewis, R. G. Tayler, and L. L. Rudel, "Low density lipoprotein inhibition of avian thrombocyte adhesion to glass," *Thromb. Res.*, **13**, 543-549 (1978).
14. M. S. Brown, Y. K. Ho, and J. L. Goldstein, "The low density lipoprotein pathway in human fibroblasts: Relations between cell surface receptor binding and endocytosis of low density lipoprotein," *Ann. NY Acad. Sci.*, **276**, 244-257 (1970).
15. L. Holmquist, "Adsorption losses of human serum apolipoproteins C and E during manipulation of diluted solutions," *La Ricerea Clin. Lab.*, **12**, 163-167 (1982).
16. B. W. Shen, P. Lagocki, and A. M. Scanu, "Hydrophobic glass beads (HGB) as probes for the structure of high density lipoproteins I. Properties of A-I and A-II at the solid-water interface," *Circulation Suppl II*, **LII-55** (1979).
17. W. L. Hufferd and D. J. Lyman, "Materials testing and requirements for the ERDA nuclear powered artificial heart," NIH Annual Report on Contract E(11-1)-2147, Report #C002147-14, May 30, 1979.
18. S. P. Halbert, M. Anken, and A. E. Ushakoff, "Studies on the compatibility of various plastics with the proteins in human plasma," *Artificial Heart Program Conference*, Proceedings, Washington D.C., 1969, ed. R. J. Hegyeli, HE20. 3202: Ar7, pp. 223-231.
19. N. L. Gershfeld, "Selective phospholipid adsorption and atherosclerosis," *Science*, **204**, 506-508 (1979).
20. W. Broomhaar, E. Brinkman, D. J. Ellens, T. Beugeling, and A. Bantjes, "Preferential adsorption of high density lipoprotein from blood plasma onto biomaterial surfaces," *Biomaterials*, **5**, 269-273 (1984).
21. A. J. Marcus, "Platelet lipids," in *Hemostasis and Thrombosis*, R. W. Coleman, J. Hirsh, edited by V. J. Marder and E. W. Salzman, Lipincott, Philadelphia, 1982, pp. 472-485.
22. R. N. King, J. D. Andrade, S. M. Ma, D. E. Gregonis, and L. R. Brostrom, "Interfacial tensions at acrylic hydrogel-water interfaces," *J. Colloid Interface Sci.*, **103**, 62-75 (1985).
23. D. E. Gregonis, R. Hsu, D. E. Burger, L. M. Smith, and J. D. Andrade, "Wettability of polymers and hydrogels as determined by Wilhelmy plate technique," in *Solvent Property Relationship in Polymers*, R. B. Seymour and G. A. Stahl, Eds., Pergamon Press, New York, 1982, pp. 120-133.
24. D. M. Lee, A. J. Valenti, W. H. Kuo, and H. Maeda, "Properties of apolipoprotein B in urea and in aqueous buffers," *Biochem. Biophys. Acta.*, **666**, 133-146 (1981).
25. F. T. Lindgren, "Preparative ultracentrifugation laboratory procedures and suggestions for lipoprotein analysis," *Analysis of Lipids and Lipoproteins*, E. G. Perkins, Ed., American Oil Chemists Society, Champaign, IL, 1975, Chap. 13, pp. 204-223.
26. U. K. Laemmli, "Cleavage of structural proteins during the assembly of the head of bacteriophage T4," *Nature*, **227**, 680-685 (1970).
27. J. Clausen, "Immunochemical techniques for the identification and estimation of macromolecules," *Laboratory Techniques in Biochemistry and Molecular Biology*, Vol. 1, part 3, 2nd ed., T. S. Work and E. Work, Elsevier, New York, 1981.
28. G. M. Forte, A. V. Nichols, and R. M. Glaser, "Electron microscopy of human serum lipoproteins using negative staining," *Chem. Phys. Lipids*, **2**, 396-408 (1968).
29. M. K. Markwell, S. M. Haas, L. L. Bieber, and N. E. Tolbert, "A modification of the Lowry procedure to simplify protein determination in membrane and lipoprotein samples," *Anal. Biochem.*, **87**, 206-210 (1978).
30. C. C. Allain, L. S. Poon, C. S. G. Chan, W. Richmond, and P. C. Fu, "Enzymatic determination of total serum cholesterol," *Clin. Chem.*, **20**, 470-475 (1974).
31. G. Bucolo and H. David, "Quantitative determination of serum triglycerides by use of enzymes," *Clin. Chem.*, **19**, 476-482 (1973).
32. N. Jentoff and D. G. Dearborn, "Labeling of proteins by reductive methylation using sodium cyanoborohydride," *J. Biol. Chem.*, **254**, 4359-4365 (1979).
33. D. E. Dong, "Adsorption of low density lipoproteins to biomedical polymers," *Diss. Abst. Inter'l Sci. Eng.*, **44-10B**, 3089 (1983).
34. D. T. Mahin and R. T. Loffberg, "A simplified method of sample preparation for determination of [3 H], [14 C], [35 S] in blood or tissue by liquid scintillation," *Anal. Biochem.*, **16**, 500-509 (1966).
35. G. W. Snedecor and W. G. Cochran, *Statistical Methods*, 7th ed., Iowa State University Press, Ames, Iowa, 1980.
36. W. D. Daniels, *Applied Nonparameter Statistics*, 2nd ed., Houghton Mifflin, Boston, 1978.
37. B. W. Shen, A. M. Scanu, and F. J. Kezdy, "Structure of human serum lipoprotein inferred from compositional analysis," *Proc. Nat'l. Acad. Sci. USA*, **74**, 837-841 (1977).
38. L. P. Aggerbeck and A. Tardieu, "The investigation of serum lipoprotein structure by small-angle x-ray scattering," in *The Biochemistry of Athero-*

- sclerosis, Scanu, R. W. Wissler, and G. S. Getz, Eds., Marcel Dekker Inc., New York, 1979, pp. 51-74.
39. R. J. Deckelbaum, G. G. Shipley, and D. M. Small, "Structure and interaction of lipids in human plasma low density lipoprotein," *J. Biol. Chem.*, **252**, 744-754 (1977).
 40. P. Laggner, G. Degories, K. W. Muller, O. Glatter, G. Kostner, and A. Holasek, "Molecular packing and fluidity of lipids in human serum low density lipoproteins," *Hoppe-Seylers Z. Physiol. Chem.*, **358**, 771-778 (1977).
 41. F. P. Bell, "Lipoprotein lipid exchange in biological systems," *Low Density Lipoproteins*, C. E. Day and R. S. Levy, Ed., Plenum Press, New York, 1976, pp. 111-133.
 42. J. Ihig, J. L. Ellsworth, B. Chataing, and J. A. K. Harmony, "Plasma protein-facilitated coupled exchange of phosphatidylcholine and cholesterol ester in the absence of cholesterol esterification," *J. Biol. Chem.*, **257**, 4818-4827 (1982).
 43. S. Dayton and S. Hashimoto, "Recent advances in molecular pathology: A review. Cholesterol flux and metabolism in arterial tissue and atheromato," *Exp. Mol. Pathol.*, **13**, 253-268 (1970).
 44. K. H. Weisgraber, T. L. Inneraity, and R. W. Mahley, "Role of the lysine residue of plasma lipoproteins in high affinity binding to cell surface receptors on human fibroblasts," *J. Biol. Chem.*, **253**, 9053-9062 (1978).
 45. R. B. Gennis and A. Jonas, "Protein-lipid interactions," *Ann. Rev. Biophys. Bioeng.*, **6**, 195-238 (1977).
 46. E. W. Merrill and E. W. Salzman, "Properties of materials affecting the behavior of blood at their surfaces," in *Vascular Grafts*, P. N. Sawyer and M. J. Kaplitt, Ed., Appleton-Century Crafts, New York, 1976, pp. 119-129.
 47. R. W. Mahley, T. L. Inneraity, T. L. Pitas, R. E. Weisgraber, J. H. Brown, and E. Gross, "Inhibition of lipoprotein binding to cell surface receptors of fibroblasts following selective modification of arginyl residues in arginine-rich and B-apoproteins," *J. Biol. Chem.*, **253**, 9053-9062 (1978).
 48. M. S. Brown, T. F. Devel, S. K. Basu, and J. L. Goldstein, "Inhibition of binding of low-density lipoprotein to its cell surface receptor in human fibroblasts by positively charged protein," *J. Supra. Mol. Struct.*, **8**, 233-234 (1978).
 49. V. Hlady, J. Rickel, and J. D. Andrade, "Fluorescence of adsorbed protein layers II. Adsorption kinetics of human lipoproteins by total internal reflection intrinsic fluorescence," *J. Colloid Interface Sci.*, submitted.
 50. R. A. Van Wagenen, S. Rockhold, and J. D. Andrade, "Probing protein adsorption: Total internal reflection intrinsic fluorescence," *Biomaterials: Interfacial Phenomena and Application*, Advances in Chemistry Series 199, edited by N. A. Peppas and S. L. Cooper, American Chemical Society, Washington, D.C. 1982, pp. 351-370.
 51. D. Steinberg, "Lipoprotein and atherosclerosis. A look back and a look ahead," *Atherosclerosis*, **3**, 283-301 (1983).
 52. J. A. Hamilton and E. H. Cordes, "Lipid dynamics in human low density lipoproteins and human aortic tissue with fibrous plaque," *J. Biol. Chem.*, **254**, 5435-5441 (1979).
 53. E. B. Smith, "Relationship between lipids and atherosclerosis," in *Thrombosis and Haemostasis*, A. L. Bloom and D. P. Thomas, Eds., Churchill Livingstone, New York, 1981, pp. 554-574.

Received June 23, 1986

Accepted December, 1986

Adsorption of low density lipoproteins onto selected biomedical polymers

D. E. Dong, J. D. Andrade, and D. L. Coleman

Department of Pharmaceutics, University of Utah, Salt Lake City, Utah 84112

This study examines the interaction of human low density lipoprotein (LDL) with a select group of biomedical polymers. The adsorption characteristics of LDL on cured filler-free poly(dimethyl Siloxane) (C-PDMS), Biomer, Cardiomat 610, Kraton 1650, poly(hydroxyethyl methacrylate) (PHEMA) and glass are presented. Adsorption of LDL to charged hydrophilic glass control surfaces occurred rapidly, reaching plateau concentrations within one minute ($0.19 \pm 0.01 \text{ ug/cm}^2$). Adsorption of LDL to polymer surfaces appeared to be dependent upon both the polymer hydrophobicity (or apolar nature), and flexibility (or dynamic nature) at the interface. Increased surface concentrations were observed for Biomer ($0.32 \pm 0.01 \text{ ug/cm}^2$) as well as other polymers which exhibited both hydrophobic and elastomeric properties. Temperature changes between 25°C

and 37°C were found to significantly influence the surface concentration of LDL on Biomer ($0.16 \pm 0.01 \text{ ug/cm}^2$ at 25°C versus $0.32 \pm 0.01 \text{ ug/cm}^2$ at 37°C). A lipid core phase transition at 36°C was believed to be responsible for the temperature influence. Preliminary competitive adsorption studies of LDL with albumin (HSA) and serum on silicone surfaces suggests that LDL adsorption occurred rapidly and preferentially ($0.25 \pm 0.01 \text{ ug/cm}^2$ for LDL alone; $0.33 \pm 0.01 \text{ ug/cm}^2$ for LDL + HSA; $0.15 \pm 0.01 \text{ ug/cm}^2$ LDL + serum). Preliminary studies on the role of LDL in calcification were not conclusive. It can be concluded that LDL adsorption is dependent upon polymer hydrophobicity, flexibility and temperature. Competitive adsorption experiments suggests that LDL may have a substantial influence on protein adsorption.

INTRODUCTION

The effects of lipid and lipoprotein adsorption on the blood-materials interface are of interest in the compatibility of prostheses. Swelling, cracking and loss of mechanical performance of Silastic heart ball poppets were attributed to the adsorption and absorption of selected lipid and lipoprotein components.^{1,2} Similarly, sorption of lipids and lipoproteins may act as sites for the initiation of calcification,^{3,4} as sources of phospholipids for platelet activation,⁵⁻⁷ or may affect the overall mechanical performance of the material by accelerating oxidative degradation.⁸

The low density lipoprotein fraction was chosen for the evaluation of lipid-lipoprotein adsorption based on its high concentrations of cholesterol and cholesterol esters,⁹ and its roles in atherogenesis.¹⁰ There were also previous *in vitro* studies on silicone rubber suggesting that cholesterol components are actively absorbed by these materials.¹¹

There are few reported studies concerning the adsorption of LDL onto polymer materials (Table I). Most studies only report interactions of LDL with hydrophilic glass substrates.¹²⁻²⁰ The report by Dana¹² indicated that adsorption of LDL on glass surfaces reached saturation equilibrium with high affinity and temperature independence. The report by Lewis¹³ suggested the inhibitory role of LDL in the adhesion of thrombocytes (platelets) to glass surfaces. Other lipid fractions are also thought to activate platelets and increase adhesion.^{6-7,21} Brown,¹⁴ as a result of routine lipoprotein isolation procedures, found that LDL irreversibly bound to radio-frequency glow-discharged polystyrene (PS) surfaces. The removal of LDL from the treated PS surface was only possible after treatment with the enzyme trypsin, which is known to specifically cleave at the lysine and arginine residues. More recent studies by Bantjes²⁰ evaluated the competitive adsorption of LDL, high density lipoprotein (HDL), and fibrinogen from serially diluted plasma onto polyvinylchloride (PVC) and PS. Adsorption of LDL produced less inhibition of adsorption of other plasma proteins in comparison to HDL.

These studies have given us some indication of the behavior of LDL adsorption onto material surfaces. Studies are now necessary to determine lipid and lipoprotein adsorption characteristics to more relevant biomedical materials. The importance and role of lipids and lipoproteins in determining the overall biocompatibility and performance of a material is still unclear and also require further evaluation. The purpose of this study is to evaluate the adsorption behavior of LDL onto a selected group of biomedical materials, including filler-free poly(dimethyl siloxane), Biomer, Cardiomat 610, Kraton 1650, and poly(hydroxyethyl methacrylate).

MATERIALS AND METHODS

Materials processing

Biomer®, a poly(ether urethane urea), was a gift from Ethicon Inc., Somerville, New Jersey; Cardiomat® 610, a poly(ether urethane), was a gift from Kontron Cardiovascular Inc., Everett, Massachusetts; and Kraton® 1650, a triblock copolymer of styrene-ethylene-butylene-styrene (SEBS), was a gift from Shell Chemical Corp., Houston, Texas.

Biomer (10% *w/v* in dimethylacetamide, DMAC), Cardiomat 610 (15-18% *w/v* in 2:1 dioxane:tetrahydrofuran, THF), and Kraton 1650 (20% *w/v* in redistilled decahydronaphthalene) were cast into 0.01 cm thick sheets on a Mylar® substrate and solvent evaporated under a positive pressure nitrogen atmosphere at 60°C.

Filler-free poly(dimethyl siloxane) (PDMS) was a gift from Thoratec Labs, Berkeley, California. A 10% (*w/v*) solution of PDMS was prepared in THF. Samples were dip cast onto silica-filled Silastic® sheets (Dow Corning) that had been extracted in methylene chloride overnight. Samples were then cured at 80°C for 12 hrs in a humid nitrogen-filled environment followed by a 45 min steam autoclave at 80°C to insure a complete cure. Samples were

TABLE I
A Review of Current Literature on the Adsorption of Lipoproteins at Solid Interfaces

Protein	Surface	Results	Investigator	Year	Ref.
LDL	Hydrophilic glass	High affinity; saturability	Dana	1977	12
LDL	Polystyrene culture plates	High affinity; irreversible	Brown	1976	14
LDL	Hydrophilic glass	Inhibit pigeon thrombocyte adhesion	Lewis	1979	13
HDL	Silane-treated glass	Binds reversibly to apoA-I but irreversibly to apoA-II	Shen	1979	16
VLDL	Cellulose nitrate	Extreme high saturability	Holmquist	1982	15
Lipid mixture	Biomer	irreversible binding	Lyman	1976	17
β and α -lipo-protein fractions	Biomer, PDMS, glass	Cholesterol, cholesterol ester absorption	Halbert	1969	18
Phospholipids	Glass, polystyrene	No adsorption or absorption; decreased thrombus formation	Gershfeld	1982	19
LDL and HDL	PVC and PS	High affinity, disaturated phospholipid bound with greater affinity than monosaturated phospholipid	Bantjes	1983	20
LDL and HDL	Glass and DDS-treated glass	Preferential adsorption HDL from plasma; low surface conc. LDL from plasma solution	Hlady	1986	49
		Increased LDL adsorption to both surfaces in comparison to HDL using new method of TIRIF			

minimally tacky, smooth and without defects as determined by the characterization protocol described below.

Hydroxyethyl methacrylate (HEMA) was a gift from Hydro Med Sciences, Inc., New Brunswick, New Jersey. The HEMA was cast against acid cleaned glass plates using *azobis*-(methyl isobutyrate) as the initiator. Polymerization was allowed to proceed for 12 hrs at 60°C.

Borosilicate glass (Gold Seal) was used for the control substrate. Glass was prepared by the cleaning process described by King.²²

Materials characterization

Light microscopy and scanning electron microscopy were used to examine the gross surface roughness and morphology of the cast polymers. All material surfaces except Biomer were smooth and free of gross or microscopic defects. Biomer surfaces were difficult to render free of defects due to the presence of unfilterable gel particles and the formation of microbubbles upon evaporation of the solvents even under controlled environmental conditions (Fig. 1).

The surface chemical composition was determined by the use of x-ray photoelectron spectroscopy (XPS). XPS was performed on each lot of cast

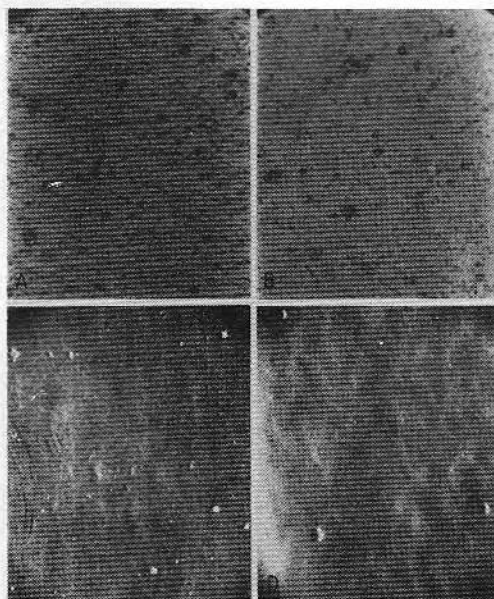


Figure 1. Surface morphology of (a) unfiltered Biomer via light microscopy at original magnification of 200 X; (b) 3- μ M Fluropore filtered Biomer; light microscopy at original magnification of 200 X; (c) Cardiomat 610 scanning electron micrograph (SEM) at original magnification of 5400 X (d) Kraton 1650, SEM at original magnification of 2100 X. The surface roughness of Biomer samples was due to the presence of unfiltered gel particles and formation of microbubbles upon evaporation of solvent under controlled environmental conditions (see text).

samples. Both the Mylar facing surfaces and surfaces cast against a nitrogen atmosphere were analyzed (Table II). Both urethanes showed an increase in the ether carbon and decrease in the alkyl carbon for the surface cast against a Mylar substrate. This is expected, considering the polar surface composition of Mylar.

The Wilhelmy plate²³ method was used to determine the surface hydrophobicity and hydrophilicity under dynamic conditions. The receding water contact angle was used as an indication of the hydrophilicity of the polymer surface. The receding water contact angles showed PDMS and Kraton 1650 to be the most hydrophobic polymers. Biomer and Cardiomat 610 showed greater hydrophobicity than glass or PHEMA (Table III).

Low density lipoprotein isolation

Fresh human blood was used in all experiments. The blood was allowed to clot at room temperature for 1 hr and then was centrifuged at $1500 \times g$ for 30 minutes at 5°C to isolate serum. All solutions used in the procedure contained 0.01% Thimerosal (sodium ethyl mercurithiosalicylate) as a bactericide, 0.01% EDTA to chelate metal ions, 0.013%—amino caproic acid as a protease inhibitor, and 0.05% glutathione (reduced) as an antioxidant.²⁴ Isolation of LDL from whole serum followed the sequential ultracentrifugation protocol of Lindgren²⁵ at $105,000 \times g$ for 18 hrs at 16°C. Density adjustment was performed by the addition of NaCl and NaBr solutions. Low density lipoprotein was collected between the density of 1.006 g/mL and 1.063 g/mL. Washed LDL was passed over a column of Sephadex G50 in phosphate buffered saline (PBS) (0.15M NaCl, pH 7.4) at 4°C to remove NaBr.

Isolated LDL was characterized by polyacrylamide slab gel electrophoresis (PAGE),²⁶ immunodiffusion²⁷ and transmission electron microscopy (TEM).²⁸ Polyacrylamide gel electrophoresis of LDL was performed on 7.5% linear gels. No protein contaminants were detected. Uniformity of particle size by TEM and non-identity of LDL by immunoelectrophoresis against human serum albumin and other serum proteins also confirmed sample purity. Protein was determined by a modified Lowry procedure.²⁹ Lipid analysis for total cholesterol and triglyceride was determined by the use of the Worthington® enzymatic assay kits for serum lipids.^{30,31} Lipid analysis of whole serum cholesterol and triglyceride of blood donors fell within population sample norms of 138–294 mg/dL and 36–165 mg/dL, respectively.^{30,31}

Experimental protocol

LDL was tritium labeled by reductive methylation of the lysine residues by the procedure of Jentoff and Dearborn.^{32,33} The radio-labeled LDL was characterized as described above. Greater than 95% activity was associated with the LDL protein band as determined by polyacrylamide gel hydrolysis.³⁴ All polymer samples were cut into 16 mm diameter circular discs. Samples were

TABLE II
Elemental Surface Composition (%) of Polymers Studied for LDL Adsorption as Determined by ESCA

Polymer	<i>n</i>	$\pi - \pi^*$ C ₂₉₀	Urethane C ₂₈₈	Ether C ₂₈₅	Alkyl C ₂₈₄	O	N	Si
C-PDMS	2	—	—	—	50	23.6	—	26.3
Biomor								
N ₂ Cast Surface	5	—	2.39 ± 1.04	26.34 ± 5.09	46.42 ± 3.51	18.12 ± 1.64	2.66 ± 0.79	4.46 ± 0.35
Mylar	3	—	1.55 ± 0.27	33.42 ± 3.26	41.67 ± 5.63	17.17 ± 1.39	3.16 ± 1.00	1.00 ± 1.08
Cardiomat 610								
N ₂ Cast Surface	3	—	1.56 ± 1.12	28.62 ± 6.73	47.20 ± 7.60	18.01 ± 0.08	1.77 ± 0.73	3.48 ± 0.64
Mylar			1.72 ± 0.43	33.78 ± 2.41	43.38 ± 1.93	18.16 ± 1.28	2.47 ± 0.33	0.71 ± 0.50
Kraton 1650								
N ₂ Cast Surface	3	0.22 ± 0.03	—	—	85.90 ± 3.19	8.03 ± 1.57	—	0.64 ± 1.51
Mylar	3	0.22 ± 0.40	—	—	94.97 ± 1.96	1.56 ± 1.26	—	1.25 ± 1.08

TABLE III
Wilhelmy Plate Advancing and Receding Water Contact
Angles for Polymers After 24-Hour Hydration in PBS at 25°C

Polymer	Adv. Angle	Rec. Angle
Glass	<10	<10
C-PDMS-FF	110 ± 6	74 ± 8
Biomer	81 ± 7	42 ± 6
Cardiomat 610	84 ± 1	32 ± 2
Kraton 1650	103 ± 3	57 ± 5
PHEMA	100 ± 7	22 ± 3

extracted for 12 hrs in PBS to remove unreacted monomer and catalyst and then hydrated in PBS for 24 hrs prior to exposure to LDL solutions. Polymer samples were suspended in a PBS solution followed by the addition of a concentrated LDL solution. This procedure was followed to avoid the interaction of the polymer with a denatured lipoprotein layer at the air-liquid interface. Adsorption was allowed to proceed at 37°C for up to 2 hrs. A constant mild agitation at 125 rpm was applied by a shaker bath to minimize the presence of a denatured boundary layer at the interface. Following the appropriate time intervals, the protein solution was displaced by equal volumes of fresh PBS flushed through an inlet port and out an exit port, again minimizing the interaction of the polymer with the protein-air interface. Three 30-mL rinses of PBS at 5-min intervals were used to displace the protein solution and to remove loosely bound protein from the surface. The flow rate was 60 mL/min. The polymer samples were transferred to vials and 10 mL of scintillation cocktail (Aquasol II, New England Nuclear) was added. The samples were allowed to equilibrate for 24 hr at 4°C before sample activity was determined. All experiments were performed in triplicate.

A preliminary competitive adsorption study was performed with human serum albumin (HSA) and diluted whole serum. Albumin and LDL were combined in PBS to give a final solution concentration at 5 mg/mL and 0.4 mg/mL, respectively. Serum was diluted to give a final protein concentration at 10 mg/mL with a LDL concentration at 0.5 mg/mL.

Data analysis

The analysis of covariance,³⁵ the nonparametric Kriskal-Wallis analysis of variance,³⁶ and the Wilcoxon-Rank Sum Test for multiple sample comparison³⁶ were performed on the data where applicable. The "P" represents the probability that the observation is significant at the stated α -level of significance.

Experimental results

The influence of blood donor LDL variability was studied (Fig. 2). Examination of the data (Table IV) reveals significant overlap of the standard deviations, suggesting that the difference among the donors may not actually exist but may reflect the small sample size used in the statistical analysis. Therefore, donor variability was interpreted as not having a dominant effect on LDL adsorption in glass substrates.

Radio methylation was found to significantly influence the surface concentration of adsorbed LDL (Fig. 3). LDL labeled with ≥ 20 methyl groups/mol of protein resulted in a significantly lower surface concentration compared to LDL labeled with ≤ 2 methyl groups/mol of protein. Perhaps the methylation of the lysine residues results in a decreased electrostatic interaction with the negatively charged glass surface. It was determined that a high specific activity was necessary to obtain reliable statistics because of the counting geometry used and the low concentration of adsorbed protein. A medium degree of label (10–15 methyl groups/mol of protein) was chosen for the remainder of the study.

Adsorption studies performed as a function of temperature were found to show a significantly greater LDL surface concentration on Biomer and PDMS at 37°C compared to 25°C. No significant difference in surface concentrations were observed for glass controls between the two temperatures (Fig. 4). Subsequent studies were performed at 37°C.

The adsorption of LDL onto control glass substrate was found to be largely independent of both time and concentration (Figures 5, 6, and Table V). Adsorption was both rapid (<1 min) and resistant to displacement following three 30-mL PBS 5-min rinses at 37°C. Plateau surface concentrations were observed at the earliest time interval of 1 min.

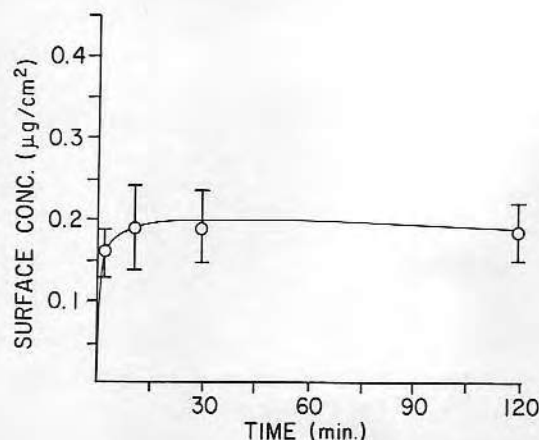


Figure 2. Average surface concentration ($\mu\text{g}/\text{cm}^2$) of ^3H -LDL (0.3 mg/mL) from four donors onto hydrophilic glass at 37°C. Degree of label = 7.3 ± 1.9 methyl groups/LDL molecule. The individual donor data are given in Table IV.

TABLE IV
Surface Concentrations ($\mu\text{g}/\text{cm}^2$) of Adsorbed ^3H -LDL (0.26 mg/ml) in
PBS on Hydrophilic Glass at 37°C Using LDL of Four Different Donors^a

Donor	<i>n</i> ^b	Conc. (mg/mL)	1 min	10 min	30 min	120 min
1.	3	0.30	0.13 ± 0.01	0.16 ± 0.01	0.15 ± 0.01	0.16 ± 0.01
2.	3	0.18	0.16 ± 0.01	0.21 ± 0.01	0.22 ± 0.02	0.21 ± 0.02
3.	3	0.26	0.16 ± 0.01	0.16 ± 0.02	0.17 ± 0.02	0.16 ± 0.01
4.	3	0.29	0.19 ± 0.01	0.23 ± 0.04	0.21 ± 0.01	0.21 ± 0.02
\bar{X}	12	0.26	0.16 ± 0.02	0.19 ± 0.04	0.19 ± 0.03	0.18 ± 0.03

^aDegree label $\sim 7.3 \pm 2.9$ methyl group/LDL molecule.

^bThe *n* represents total number of samples in all experiments performed in triplicate

TABLE IV
Surface Concentrations ($\mu\text{g}/\text{cm}^2$) of Adsorbed ^3H -LDL (0.26 mg/ml) in
PBS on Hydrophilic Glass at 37°C Using LDL of Four Different Donors^a

Donor	n^b	Conc. (mg/mL)	1 min	10 min	30 min	120 min
1.	3	0.30	0.13 ± 0.01	0.16 ± 0.01	0.15 ± 0.01	0.16 ± 0.01
2.	3	0.18	0.16 ± 0.01	0.21 ± 0.01	0.22 ± 0.02	0.21 ± 0.02
3.	3	0.26	0.16 ± 0.01	0.16 ± 0.02	0.17 ± 0.02	0.16 ± 0.01
4.	3	0.29	0.19 ± 0.01	0.23 ± 0.04	0.21 ± 0.01	0.21 ± 0.02
\bar{X}	12	0.26	0.16 ± 0.02	0.19 ± 0.04	0.19 ± 0.03	0.18 ± 0.03

^aDegree label $\sim 7.3 \pm 2.9$ methyl group/LDL molecule.

^bThe n represents total number of samples in all experiments performed in triplicate

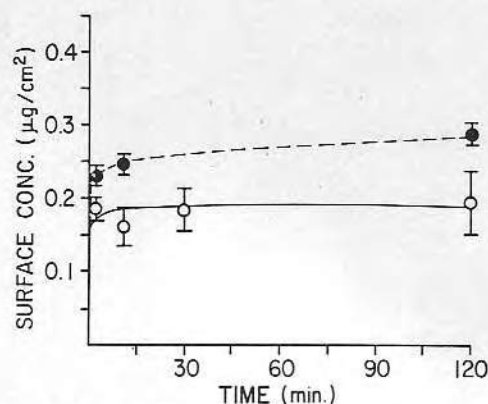


Figure 3. Effect of radiolabeling of LDL (0.3 mg/mL) on adsorption onto hydrophilic glass at 37°C. Degree of label: (○) high = 21.3 ± 2.7 methyl groups/LDL molecule (●) low = 2.3 ± 1.0 methyl groups/LDL molecules. All subsequent experiments were performed with a degree of label between 10–15 methyl groups/LDL molecule (see text).

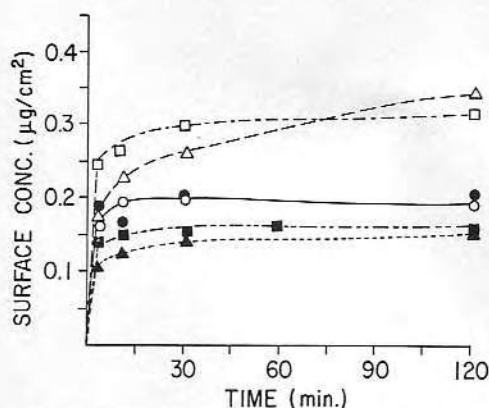


Figure 4. The effect of temperature on adsorption of ^3H -LDL onto hydrophilic glass (●, 0.3 mg/mL ^3H -LDL), C-PDMS (□, 0.4 mg/mL ^3H -LDL), Biomer (△, 0.5 mg/mL ^3H -LDL). Solution concentration standard deviations ranged between ± 0.01 and ± 0.04 mg/mL. Open symbols are 37°C; closed symbols are 25°C.

PDMS and Kraton 1650 adsorbed more LDL than hydrophilic glass. The kinetic profiles of both polymers showed evidence of concentration and time dependence (Figs. 5, 6, and Table V).

The adsorption of LDL to Biomer occurred relatively slowly, suggesting a stronger dependence upon both time and concentration (Figs. 5, 6, and Table V). These characteristics were also revealed in the isotherm plots. Although the adsorption kinetics of LDL onto Biomer were slow, prolonged exposure (120 min) resulted in significantly greater surface concentrations than the control glass substrates.

Cardiomat 610 and PHEMA both resulted in significantly lower surface concentrations than the glass controls (Figs. 7, 8, and Table V). The ad-

TABLE V
Surface Concentration ($\mu\text{g}/\text{cm}^2$) of LDL Adsorbed
onto Polymer Surfaces at 0.5 mg/mL at 37°C in PBS

Substrate	Time (min)			
	1	10	30	120
Glass	0.19 ± 0.01	0.17 ± 0.01	0.17 ± 0.01	0.18 ± 0.01
C-PDMS-FF	0.24 ± 0.02	0.26 ± 0.01	0.29 ± 0.01	0.30 ± 0.02
Biomer	0.16 ± 0.01	0.22 ± 0.03	0.25 ± 0.01	0.32 ± 0.01
Kraton 1650	0.30 ± 0.01	0.38 ± 0.02	0.41 ± 0.02	0.42 ± 0.01
Cardiomat 610	0.10 ± 0.01	0.06 ± 0.01	0.09 ± 0.03	0.17 ± 0.03
PHEMA	0.06 ± 0.01	0.09 ± 0.01	0.13 ± 0.01	0.15 ± 0.02

sorption kinetics for Cardiomat 610 were similar to Biomer, exhibiting a slow rate of adsorption and both a time and concentration dependence. The adsorption kinetics of PHEMA was also similar to glass, although the adsorption isotherm for PHEMA (Fig. 7) did not appear to reach an equilibrium plateau in contrast to the other materials in the study. Overall, adsorption of LDL appears to be greater on more hydrophobic polymers, as represented graphically in Figure 9.

Preliminary competitive adsorption studies onto PDMS indicate an inhibitory effect of serum upon adsorption of LDL and a positive influence of albumin on LDL adsorption (Fig. 10). Albumin was found to increase the surface concentration of LDL by 25% compared to LDL adsorption from pure LDL solution. In the presence of diluted serum, LDL was found to adsorb 50% the surface concentration found in adsorption from pure LDL solution.

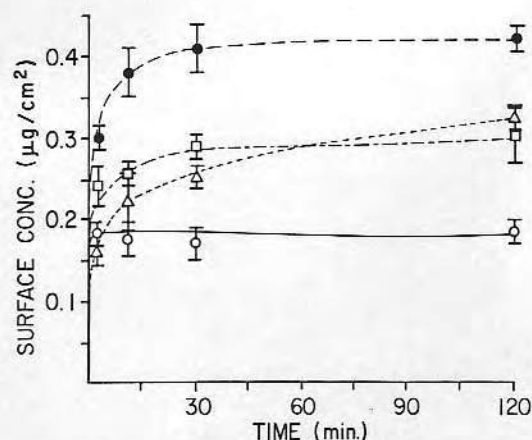


Figure 5. Adsorption kinetics of ^3H -LDL (0.5 mg/mL) onto hydrophilic glass (○), C-PDMS (□), Biomer (△) and Kraton 1650 (●) in PBS, 37°C for up to 120 min.

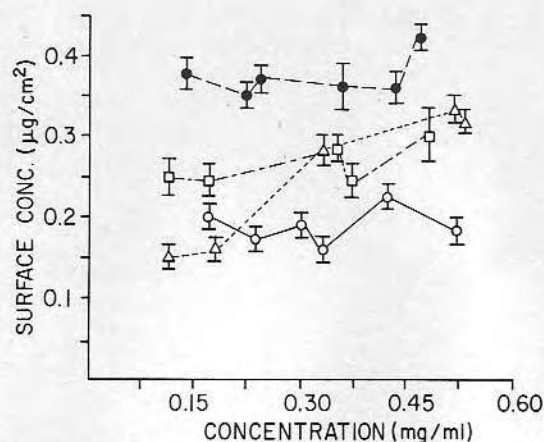


Figure 6. Adsorption isotherm of ^3H -LDL (0.5 mg/mL) onto hydrophilic glass (○), C-PDMS (□), Biomer (Δ) and Kraton 1650 (●) in PBS at 120 min., 37°C.

DISCUSSION

The structure of LDL is not completely known at this time although studies suggest that it exists as a spherical molecule similar in form to other lipoprotein complexes.^{37,38} The molecule is approximately 200–250 Å in diameter, consisting of a core lipid component of cholesterol ester (CE) and triglycerides (TG) and an outer shell of phospholipid, cholesterol and protein. The core lipid composite of CE and TG has also been shown to go through a reversible lipid phase transition (LPT) between the temperature of 20–40°C, with a peak transition at 36°C.^{39,40} The lipid core exists as a solid crystal below the LPT in a low energy state with minimal molecular motion or mobility. Within the range of the LPT and near the peak transition temperature, the core lipids melt to a liquid crystalline state and possess an increase in

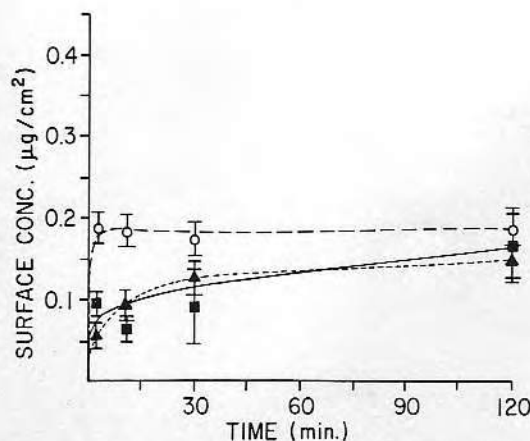


Figure 7. Adsorption kinetics of ^3H -LDL (0.5 mg/mL) onto hydrophilic glass (○), Cardiomat 610 (■), and PHEMA (▲) in PBS, 37°C for up to 120 min.

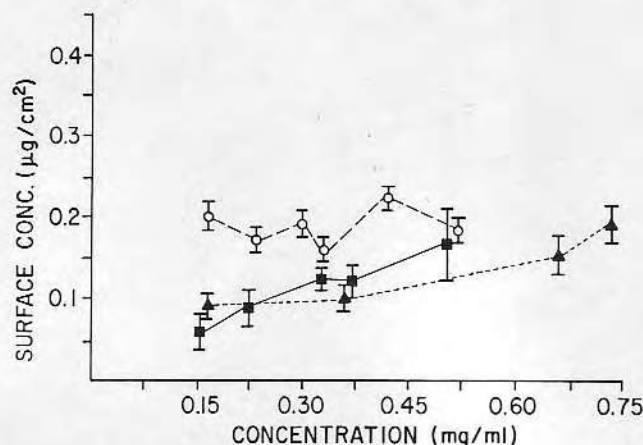


Figure 8. Adsorption isotherm of ^3H -LDL (0.5 mg/mL) onto hydrophilic glass (○), Cardiomat 610 (■) and PHEMA (▲) in PBS at 120 min, 37°C.

dynamic mobility. The increase in dynamics occurs not only for the core, but also for the entire LDL molecule, allowing exchange to occur between the core and surface lipids. This indirectly allows for the interaction of all components of the molecule with the environment. This is particularly important in a biological environment and may also be of importance in an artificially induced environment as well.⁴¹⁻⁴³ The liquid-solid interface of LDL consists of both charged and hydrophobic domains.^{44,45} Approximately 40% of the total lipid composition and 100% of the protein component exists on the outer shell of the macromolecule.

Information concerning the molecular structure and dynamics of LDL can be used to formulate the following conclusions and hypothesis. Our data

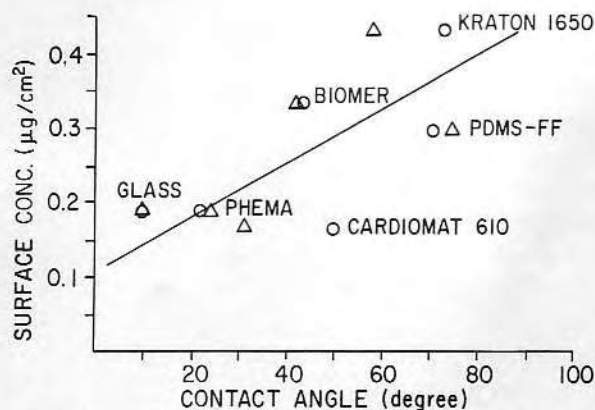


Figure 9. Correlation between the surface concentration at 120 min. adsorption ($\mu\text{g}/\text{cm}^2$) of adsorbed ^3H -LDL and the hydrophobicity of the polymers as determined by underwater captive bubble (○) and Wilhelmy plate receding (Δ) contact angle techniques. The hydrophobicity of the polymer appears to correlate with increased adsorption of LDL.

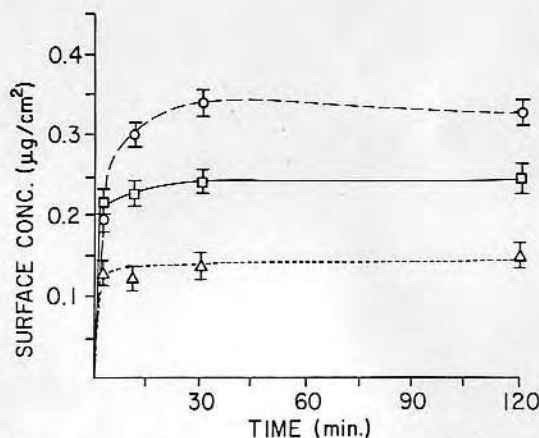


Figure 10. Competitive adsorption of ^3H -LDL on C-PDMS at 37°C . LDL alone (\square , 0.4 mg/mL), LDL with human serum albumin (Fraction V) (\circ , 0.4 mg/mL LDL and 5.2 mg/mL albumin in PBS) and LDL (\triangle , 0.5 mg/mL LDL) with whole human serum (10 mg/mL total protein).

support a significantly greater surface concentration of LDL adsorbed at 37°C compared to 25°C on PDMS and Biomer. The increased surface concentration observed in these two polymers can be attributed to two synergistic effects: (1) the elastomeric nature of the polymers, since glass controls did not show a significant increase in surface concentration; and (2) the increased dynamics of LDL due to the LPT at the higher temperature.

The adsorption of LDL is increased on more hydrophobic and elastomeric polymers such as PDMS, Biomer and Kraton 1650. It is known from other studies that the adsorption of proteins to polymer surfaces is dependent upon the surface composition and bulk composition.⁴⁶ We hypothesize that the adsorption of LDL is dependent both on the surface (and bulk) composition as well as the elastomeric nature of the polymer. The importance of the two components in influencing protein adsorption is evident in the adsorption results of LDL on Biomer and Cardiomat 610. Although the two polymers are urethanes, their compositions differ in both the chain extender and the soft segment length, lending possibly to the difference observed in surface concentration. Biomer is composed of an ethylene diamine chain extender, with a soft segment of approximately 2000 molecular weight. The Wilhelmy plate receding contact angle measures $41.8 \pm 6.0^\circ$. Cardiomat 610 is composed of a butane diol chain extender and a soft segment of approximately 1000 molecular weight. Its contact angle ($31.5 \pm 1.8^\circ$) is somewhat more hydrophilic as one would expect with a more polar chain extender and smaller hydrophobic soft segment. Comparison of the data between other elastomeric polymers and non-elastomeric polymers in this study also support this hypothesis.

Although specific modes of interaction were not identified in these experiments, it is known that the adsorption of LDL onto glass occurs by electrostatic interactions.^{12,47,48} Other modes of interaction have not been as widely studied although the various hydrophobic lipids and hydrophilic protein components of LDL provide the capability for many different means of interaction. The varied composition of LDL and its dynamic nature also allows it to accommodate optimally to a surface. Recent studies by Hlady et al.⁴⁹ have examined the adsorption of HDL and LDL to hydrophilic glass and silane treated hydrophobic glass by the new method of total internal reflection intrinsic fluorescence.⁵⁰ Fluorescence characteristics of adsorbed protein can be used to gain information regarding the conformation of the protein on the surface and allow better understanding of lipoprotein surface interactions. More studies are required to determine the predominant factor in adsorption of LDL to surfaces.

The adsorption of LDL onto PDMS increased in the presence of albumin and significant adsorption was found in the presence of serum. Studies by Bantjes et al.²⁰ have examined the competitive adsorption of LDL and HDL with other serum proteins in solution mixtures. The adsorption of HDL from plasma occurred preferentially on PVC and PS surfaces. Adsorption of LDL resulted in lower surface concentrations in comparison to both HDL and pure protein solutions, but an equilibrium state was not achieved. Both adsorbed lipoproteins resulted in decreased adsorption of albumin, fibrinogen and immunoglobulin from plasma. The surface concentration of fibrinogen on PS surfaces in the presences of LDL was not reduced in comparison to the amount adsorbed from a pure protein solution. Bantjes et al.²⁰ did not study the influence of albumin on lipoprotein adsorption. Although we saw an increase in surface concentration of LDL in the presence of albumin, the interaction between albumin and LDL is still unclear. Both polymers in Bantjes et al. study are relatively rigid, polar and non-elastomeric in comparison to PDMS used in our study. This may possibly have lead to the unenhanced and lower surface concentrations seen in their results. We suggest that, in the presence of competing serum proteins LDL possesses a greater affinity for hydrophobic and elastomeric surfaces in comparison to other serum proteins. More studies are necessary to confirm this hypothesis.

In conclusion, the adsorption of LDL to specific polymer surfaces is influenced by temperature and by the hydrophobicity of the polymer surface. The possible implications from this study are numerous. The presence and role of LDL in atherosclerosis and calcification has been documented in numerous studies.⁵¹⁻⁵³ The effect of LDL adsorption in implanted prosthesis or hemodynamic devices (cardiac assist devices, artificial heart) may lead to similar biological conclusions. Studies showing lipid adsorption with changes in mechanical properties over time may now have an etiological basis.^{11,17} The presence of absorbed lipids may also act as a source of lipids in place of platelet lipids, initiating the coagulation cascade.^{6,7} It is therefore apparent that more attention should be focused on the role of lipids and lipoproteins in blood interactions with materials.

The work was partially supported by NIH Grant HL18519, HL27747 and HL07520. The assistance and advice of Drs. Donald Gregonis and Dana Wilson are gratefully acknowledged.

References

1. R. Carmen and S. C. Mutha, "Lipid absorption by silicone rubber heart valve poppets—*in vitro* and *in vivo* results," *J. Biomed. Mater. Res.*, **6**, 327–346 (1972).
2. H. P. Chin, E. C. Harrison, D. H. Blankenhorn, and J. Moacanin, "Lipids in silicone rubber valve prosthesis after human implantation," *Suppl J Circulation*, **53**, 151–155 (1971).
3. D. L. Coleman, "Mineralization of blood pump bladders," *Trans. Am. Soc. Artif. Int. Organs*, **27**, 708–715 (1980).
4. D. R. Owens and R. M. Zone, "A possible mechanism of surface calcification," *Trans. Am. Soc. Artif. Int. Organs*, **27**, 528–531 (1980).
5. M. Aviram, J. G. Brook, A. M. Lees, and R. S. Lees, "Low density lipoprotein binding to human platelets: Role of charge and of specific amino acids," *Biochem. Biophys. Res. Commun.*, **99**, 308–318 (1981).
6. E. Koller, F. Koller, and W. Doleschel, "Specific binding sites on human blood platelets for plasma lipoprotein," *Hoppe-Seyler's Z. Physiol. Chem.*, **363**, 395–405 (1982).
7. M. Aviram and J. G. Brook, "Platelet interaction with high and low density lipoproteins," *Atherosclerosis*, **46**, 259–268 (1983).
8. D. F. Williams, "The deterioration of materials in use," in *Implants in Surgery*, D. F. Williams and R. Roar, Eds., W. B. Saunders Co. Ltd., London, 1973, p. 737.
9. A. M. Scanu and C. Wisdom, "Serum lipoproteins: Structure and function," *Ann. Rev. Biochem.*, **41**, 703–729 (1972).
10. R. I. Levy, "Cholesterol, lipoproteins, apoproteins and heart disease: Present status and future prospects," *Clin. Chem.*, **27**, 653–662 (1982).
11. R. Carmen and P. Kahn, "In vitro testing of silicone rubber heart valve poppets for lipid absorption," *J. Biomed. Mater. Res.*, **2**, 457–464 (1968).
12. S. E. Dana, M. S. Brown, and J. L. Goldstein, "Specific, saturable, and high affinity binding of I^{125} -low density lipoprotein to glass beads," *Biochem. Biophys. Res. Commun.*, **74**, 1369–1376 (1977).
13. J. C. Lewis, R. G. Tayler, and L. L. Rudel, "Low density lipoprotein inhibition of avian thrombocyte adhesion to glass," *Thromb. Res.*, **13**, 543–549 (1978).
14. M. S. Brown, Y. K. Ho, and J. L. Goldstein, "The low density lipoprotein pathway in human fibroblasts: Relations between cell surface receptor binding and endocytosis of low density lipoprotein," *Ann. NY Acad. Sci.*, **276**, 244–257 (1970).
15. L. Holmquist, "Adsorption losses of human serum apolipoproteins C and E during manipulation of diluted solutions," *La Ricerea Clin. Lab.*, **12**, 163–167 (1982).
16. B. W. Shen, P. Lagocki, and A. M. Scanu, "Hydrophobic glass beads (HGB) as probes for the structure of high density lipoproteins I. Properties of A-I and A-II at the solid-water interface," *Circulation Suppl II*, LII–55 (1979).
17. W. L. Hufferd and D. J. Lyman, "Materials testing and requirements for the ERDA nuclear powered artificial heart," NIH Annual Report on Contract E(11-1)-2147, Report #C002147-14, May 30, 1979.
18. S. P. Halbert, M. Anken, and A. E. Ushakoff, "Studies on the compatibility of various plastics with the proteins in human plasma," *Artificial Heart Program Conference, Proceedings*, Washington D.C., 1969, ed. R. J. Hegyeli, HE20. 3202: Ar7, pp. 223–231.

19. N. L. Gershfeld, "Selective phospholipid adsorption and atherosclerosis," *Science*, **204**, 506-508 (1979).
20. W. Breemhaar, E. Brinkman, D. J. Ellens, T. Beugeling, and A. Bantjes, "Preferential adsorption of high density lipoprotein from blood plasma onto biomaterial surfaces," *Biomaterials*, **5**, 269-273 (1984).
21. A. J. Marcus, "Platelet lipids," in *Hemostasis and Thrombosis*, R. W. Coleman, J. Hirsh, edited by V. J. Marder and E. W. Salzman, Lipincott, Philadelphia, 1982, pp. 472-485.
22. R. N. King, J. D. Andrade, S. M. Ma, D. E. Gregonis, and L. R. Brostrom, "Interfacial tensions at acrylic hydrogel-water interfaces," *J. Colloid Interface Sci.*, **103**, 62-75 (1985).
23. D. E. Gregonis, R. Hsu, D. E. Burger, L. M. Smith, and J. D. Andrade, "Wettability of polymers and hydrogels as determined by Wilhelmy plate technique," in *Solvent Property Relationship in Polymers*, R. B. Seymour and G. A. Stahl, Eds., Pergamon Press, New York, 1982, pp. 120-133.
24. D. M. Lee, A. J. Valenti, W. H. Kuo, and H. Maeda, "Properties of apolipoprotein B in urea and in aqueous buffers," *Biochem. Biophys. Acta.*, **666**, 133-146 (1981).
25. F. T. Lindgren, "Preparative ultracentrifugation laboratory procedures and suggestions for lipoprotein analysis," *Analysis of Lipids and Lipoproteins*, E. G. Perkins, Ed., American Oil Chemists Society, Champaign, IL, 1975, Chap. 13, pp. 204-223.
26. U. K. Laemmli, "Cleavage of structural proteins during the assembly of the head of bacteriophage T4," *Nature*, **227**, 680-685 (1970).
27. J. Clausen, "Immunochemical techniques for the identification and estimation of macromolecules," *Laboratory Techniques in Biochemistry and Molecular Biology*, Vol. 1, part 3, 2nd ed., T. S. Work and E. Work, Elsevier, New York, 1981.
28. G. M. Forte, A. V. Nichols, and R. M. Glaser, "Electron microscopy of human serum lipoproteins using negative staining," *Chem. Phys. Lipids*, **2**, 396-408 (1968).
29. M. K. Markwell, S. M. Haas, L. L. Bieber, and N. E. Tolbert, "A modification of the Lowry procedure to simplify protein determination in membrane and lipoprotein samples," *Anal. Biochem.*, **87**, 206-210 (1978).
30. C. C. Allain, L. S. Poon, C. S. G. Chan, W. Richmond, and P. C. Fu, "Enzymatic determination of total serum cholesterol," *Clin. Chem.*, **20**, 470-475 (1974).
31. G. Bucolo and H. David, "Quantitative determination of serum triglycerides by use of enzymes," *Clin. Chem.*, **19**, 476-482 (1973).
32. N. Jentoff and D. G. Dearborn, "Labeling of proteins by reductive methylation using sodium cyanoborohydride," *J. Biol. Chem.*, **254**, 4359-4365 (1979).
33. D. E. Dong, "Adsorption of low density lipoproteins to biomedical polymers," *Diss. Abst. Inter'l Sci. Eng.*, **44-10B**, 3089 (1983).
34. D. T. Mahin and R. T. Lofberg, "A simplified method of sample preparation for determination of [^3H], [^{14}C], [^{35}S] in blood or tissue by liquid scintillation," *Anal. Biochem.*, **16**, 500-509 (1966).
35. G. W. Snedecor and W. G. Cochran, *Statistical Methods*, 7th ed., Iowa State University Press, Ames, Iowa, 1980.
36. W. D. Daniels, *Applied Nonparameter Statistics*, 2nd ed., Houghton Mifflin, Boston, 1978.
37. B. W. Shen, A. M. Scanu, and F. J. Kezdy, "Structure of human serum lipoprotein inferred from compositional analysis," *Proc. Nat'l. Acad. Sci. USA*, **74**, 837-841 (1977).
38. L. P. Aggerbeck and A. Tardieu, "The investigation of serum lipoprotein structure by small-angle x-ray scattering," in *The Biochemistry of Athero-*

- sclerosis*, Scanu, R. W. Wissler, and G. S. Getz, Eds., Marcel Dekker Inc., New York, 1979, pp. 51-74.
39. R. J. Deckelbaum, G. G. Shipley, and D. M. Small, "Structure and interaction of lipids in human plasma low density lipoprotein," *J. Biol. Chem.*, **252**, 744-754 (1977).
 40. P. Laggner, G. Degories, K. W. Muller, O. Glatter, G. Kostner, and A. Holasek, "Molecular packing and fluidity of lipids in human serum low density lipoproteins," *Hoppe-Seyler's Z. Physiol. Chem.*, **358**, 771-778 (1977).
 41. F. P. Bell, "Lipoprotein lipid exchange in biological systems," *Low Density Lipoproteins*, C. E. Day and R. S. Levy, Ed., Plenum Press, New York, 1976, pp. 111-133.
 42. J. Ihig, J. L. Ellsworth, B. Chataing, and J. A. K. Harmony, "Plasma protein-facilitated coupled exchange of phosphatidylcholine and cholesterol ester in the absence of cholesterol esterification," *J. Biol. Chem.*, **257**, 4818-4827 (1982).
 43. S. Dayton and S. Hashimoto, "Recent advances in molecular pathology: A review. Cholesterol flux and metabolism in arterial tissue and atheromato," *Exp. Mol. Pathol.*, **13**, 253-268 (1970).
 44. K. H. Weisgraber, T. L. Innerarity, and R. W. Mahley, "Role of the lysine residue of plasma lipoproteins in high affinity binding to cell surface receptors on human fibroblasts," *J. Biol. Chem.*, **253**, 9053-9062 (1978).
 45. R. B. Gennis and A. Jonas, "Protein-lipid interactions," *Ann. Rev. Biophys. Bioeng.*, **6**, 195-238 (1977).
 46. E. W. Merrill and E. W. Salzman, "Properties of materials affecting the behavior of blood at their surfaces," in *Vascular Grafts*, P. N. Sawyer and M. J. Kaplitt, Ed., Appleton-Century Crafts, New York, 1976, pp. 119-129.
 47. R. W. Mahley, T. L. Innerarity, T. L. Pitas, R. E. Weisgraber, J. H. Brown, and E. Gross, "Inhibition of lipoprotein binding to cell surface receptors of fibroblasts following selective modification of arginyl residues in arginine-rich and B-apoproteins," *J. Biol. Chem.*, **253**, 9053-9062 (1978).
 48. M. S. Brown, T. F. Devel, S. K. Basu, and J. L. Goldstein, "Inhibition of binding of low-density lipoprotein to its cell surface receptor in human fibroblasts by positively charged protein," *J. Supra. Mol. Struct.*, **8**, 233-234 (1978).
 49. V. Hlady, J. Rickel, and J. D. Andrade, "Fluorescence of adsorbed protein layers II. Adsorption kinetics of human lipoproteins by total internal reflection intrinsic fluorescence," *J. Colloid Interface Sci.*, submitted.
 50. R. A. Van Wagenen, S. Rockhold, and J. D. Andrade, "Probing protein adsorption: Total internal reflection intrinsic fluorescence," *Biomaterials: Interfacial Phenomena and Application*, Advances in Chemistry Series 199, edited by N. A. Peppas and S. L. Cooper, American Chemical Society, Washington, D.C. 1982, pp. 351-370.
 51. D. Steinberg, "Lipoprotein and atherosclerosis. A look back and a look ahead," *Atherosclerosis*, **3**, 283-301 (1983).
 52. J. A. Hamilton and E. H. Cordes, "Lipid dynamics in human low density lipoproteins and human aortic tissue with fibrous plaque," *J. Biol. Chem.*, **254**, 5435-5441 (1979).
 53. E. B. Smith, "Relationship between lipids and atherosclerosis," in *Thrombosis and Haemostasis*, A. L. Bloom and D. P. Thomas, Eds., Churchill Livingstone, New York, 1981, pp. 554-574.

Received June 23, 1986

Accepted December, 1986

26. S. Nagaoka, Y. Mori, H. Takiuchi, K. Yokota, H. Tanzawa and S. Nishimura, Polymer Preprints **24** 67 (1983).
27. K. Yokota, A. Abe, S. Hosaka, Y. Sakai and H. Saito, Macromolecules **11** 95 (1978).
28. G. C. Levy, P. L. Rinaldi, J. J. Dechter, D. E. Axelson and L. Madelkern, J. Amer. Chem. Soc. **20** 119 (1980).
29. T. Cosgrove, T. L. Crowley, B. Vincent, K. G. Brnett and T. F. Tadros, Faraday Symposia of the Chemical Society **16** 101 (1981).
30. J. Schaefer, Macromolecules **6** 882 (1973).
31. R. K. Gilpin, Analytical Chem. **57** 1465-1474 (1985).
32. R. K. Gilpin and M. E. Gangoda, J. Chromat. Sci. **21**, 352-361 (1983).
33. J. F. M. Pennings and B. Bosman, Colloid Polym. Sci. **257** 720 (1979).

*J. D. Andrade, ed., Polymer Surface
Dynamics, Plenum Press, 1988*

MODELING OF THE WILHELMY CONTACT ANGLE METHOD WITH PRACTICAL SAMPLE GEOMETRIES

P. Dryden, J. H. Lee, J. M. Park, and J. D. Andrade

Bioengineering Department and Surface Analysis
Laboratory
College of Engineering, University of Utah
Salt Lake City, UT 84112.

INTRODUCTION

The Wilhelmy Plate procedure is a currently popular method of determining contact angles¹. Features contributing to its popularity are the ease of measurement and the convenient demonstration of both thermodynamic and kinetic hysteresis, making it a useful tool in the studies of surface dynamics. Surface homogeneity can also be tested as the meniscus traverses the length of the dipped portion of the sample. An extension of the technique to nonstandard geometries would allow measurements of contact angles on surfaces where direct visualization of the contact angle would be quite difficult. This is already being done with small diameter fibers, where the cross sectional area of the fiber remains constant. Extracting contact angle information from dipping experiments with samples of variable cross sectional area requires more elaborate calculations involving changes in meniscus shape, as explained below.

In this paper we endeavor to investigate the feasibility of calculating contact angles from force-displacement curves for some simple nonstandard geometries. They were chosen in a sequence of increasing complexity: 1) the solid cylinder, with constant cross section, 2) the flat disc, whose meniscus is approximately cylindrical, but which has a varying perimeter or cross section, and 3) the cone, which possesses radial symmetry and whose sides make a constant angle with the undisturbed liquid surface, but whose cross section varies with immersion depth. All samples were made from glass, chosen since it is perfectly wetting, with a zero contact angle. This approach was used to verify that experimental wetting curves match calculated data when all parameters are known. The inverse problem, that of determining contact angle from experimental data, was not attempted in this study.

METHODS AND MATERIALS

Experimental. The Wilhelmy balance has been described by Smith et al.² In the present case, the immersion depth axis was

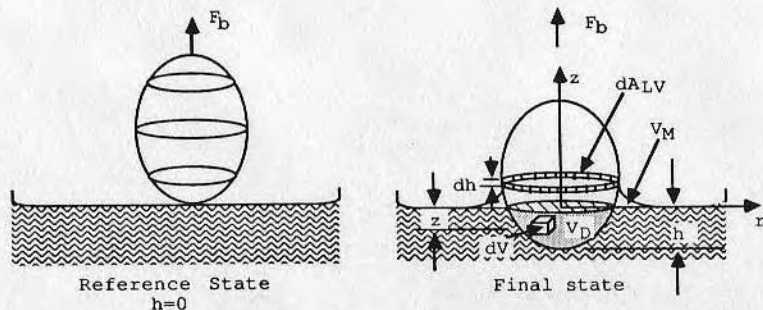


Figure 1. Notation used in developing equation 4, applicable to a general sample geometry. V_D is the region, exclusive of the meniscus, where the object has displaced liquid. V_M is the region in which liquid or vapor is present solely due to the formation of the meniscus. The band labelled dA_{LV} represents the area on the solid which would be wetted if immersion depth were to increase by dh .

also calibrated. Glass samples were cleaned with hot dichromate/sulfuric acid solutions and rinsed with doubly purified water. Dipping experiments were repeated several times with each sample and were reproducible to a high degree.

Glass rods of 0.60, 0.65, 1.45, and 2.0 mm diameters were measured against water to demonstrate that contact measurements are independent of diameter. Circular glass coverslips, 25 mm in diameter by 0.2 mm thick, were used for the disc experiments. The cone was hand-made from glass tubing and was somewhat rounded at the tip. Approximate dimensions of the cone were 6 mm in radius at the base and 30 mm in height. Adjustments in the calculations to compensate for the tip are discussed below.

Computational. Calculated force data were generated by a microcomputer. The data were plotted on an appropriate scale to match the force and position scales of the recorder output from the Wilhelmy balance.

A general approach to calculating forces was developed using concepts already in the literature.^{1,3} Given our sample at some arbitrary immersion depth h (see Figure 1), we assumed formation of a meniscus representing the equilibrium state at this immersion depth. Our first step was to calculate the difference in energy between this state and a reference state consisting of the same system in air, just before the sample touches the liquid ($h=0$, no meniscus). We assumed that the change in energy involves only work and no heat. Several types of work must be accounted for:

- 1) The sample is lowered in going from the reference to the final state. Energy of the system will decrease by mgh , where m = mass of the sample and g is the acceleration of gravity.
- 2) Liquid will be displaced by the sample as it is lowered. A volume equal to that displaced will be deposited on the liquid surface, so that, in effect, the displaced

liquid is moved to the liquid surface. For the small samples used in the Wilhelmy experiments, this displaced liquid will be of too small a volume to appreciably change the liquid level. For each incremental volume element dV located in the region V_D of Figure 1, work of $\rho_L z dV$ will be performed in displacing the water, where ρ_L is the density of the liquid, z is the height of the volume element relative to the liquid level, and V_D is the region occupied by the immersed portion of the sample in the final state. The total work is computed by summing over the whole volume, i.e.

$$W_D = \int_{V_D} \rho_L z dV.$$

- 3) Gravitational work may be required to lift elements of water in the meniscus if it is elevated, or may be expended if it is depressed. The same considerations as above will apply, so that the work to lift the meniscus

$$\text{is given by } W_M = \int_{V_M} \rho_L z dV, \text{ where } V_M \text{ is the region bounded}$$

by the level of the undisturbed fluid, by the meniscus surface, and by the sample surface, i.e., the volume of the meniscus.

- 4) Interfacial work will be done if there are changes in any interfacial areas between the reference and final states. This type of work is given by $\sum \gamma_i A_i$, where γ_i is the work required to create unit area of interface i , A_i is the interfacial area of interface i compared to the area of the same interface in the reference state, i referring to each of the liquid-vapor (LV), solid-liquid (SL), and solid-vapor (SV) interfaces.

- 5) Work is done by the balance since it exerts a force opposing the change in sample position from the reference state, where $h = 0$, to the final state at immersion

depth h . This work totals $\int_0^h F_b dh'$, where F_b is the force on the balance.

At equilibrium, energy is at a minimum. Therefore, in the final state, $dU/dh = 0$, where U is the energy at h . Since the sum of the above five terms represents U relative to the reference state described, the equilibrium condition expands to:

$$-mg + \frac{dW_D}{dh} + \frac{dW_M}{dh} + \sum \gamma_i \frac{dA_i}{dh} + F_b = 0. \quad (1)$$

It turns out that $\frac{dW_D}{dh}$ equals $\rho_L g V(h)$, where $V(h)$ represents the volume of the immersed portion of the sample, so that after rearrangement,

$$F_b = mg - \rho_L g V(h) - \frac{dW_M}{dh} - \gamma_{SV} \frac{dA_{SV}}{dh} - \gamma_{SL} \frac{dA_{SL}}{dh} - \gamma_{LV} \frac{dA_{LV}}{dh}. \quad (2)$$



Figure 2. Geometry and notation for disc experiment, perspective view in a) and profile in b)

Since $\frac{dA_{SL}}{dh} = -\frac{dA_{SV}}{dh}$, and invoking Young's equation, $\gamma_{SV} - \gamma_{SL} = \gamma_{LV}\cos\theta$,

$$F_b = mg - \rho_L g V(h) - \frac{dW_M}{dh} + \gamma_{LV}\cos\theta \frac{dA_{SL}}{dh} - \gamma_{LV} \frac{dA_{LV}}{dh}. \quad (3)$$

With our experimental apparatus only the force in excess of the sample weight is recorded. Therefore, in the balance of this paper we will consider F , defined as $F_b - mg$. Therefore, our general expression for the calculated force data is given by

$$F = -\rho_L g V(h) - \frac{dW_M}{dh} + \gamma_{LV}\cos\theta \frac{dA_{SL}}{dh} - \gamma_{LV} \frac{dA_{LV}}{dh}. \quad (4)$$

The terms, from left to right in the above equation, will be referred to as the buoyancy, meniscus gravitational, wall energy, and dilation terms, respectively.

In order to calculate the force curves specific to each geometry, each of the above terms must be expanded into shape-specific expressions. Each geometry will be considered in turn.

Solid cylinder. If the cylinder has a homogeneous surface, the meniscus should have the same shape regardless of immersion depth. As a consequence, $\frac{dW_M}{dh}$ and $\frac{dA_{LV}}{dh}$ will be zero. The immersed volume will be that of a cylinder of radius r and height h , i.e. $V(h) = \pi r^2 h$. The quantity $\frac{dA_{SL}}{dh}$ is constant and is equal in magnitude to the perimeter of the cylinder, $2\pi r$. The force equation for the cylinder therefore reduces to

$$F = 2\pi r \gamma_{LV}\cos\theta - \rho_L g \pi r^2 h. \quad (5)$$

Disc. Refer to Figure 2 for a depiction of the coordinate system and symbols used in the discussion. For this geometry the meniscus or three phase line will vary in length along the y

axis as the depth of immersion changes, but should change in profile (in the x direction, perpendicular to the disc surface) only near the edges.

In contrast to the solid cylinder or the glass plate, the dilation and meniscus gravitational terms will be nonzero. Both terms involve quantities determined by meniscus shape. These terms also involve derivatives. In order to evaluate these derivatives, we first developed analytical expressions for the quantities A_{LV} and W_M , then took the derivative of each with respect to h . The whole meniscus was approximated as a cylindrical surface, i.e. curved around axes in the y direction. Edge effects were ignored. Although the disc has two sides, the whole meniscus was treated as a single surface of length double that of the meniscus found on a single side of the disc.

Since the meniscus is semi-infinite, extending indefinitely away from the disc, liquid-vapor surface area has meaning only relative to the reference state, where the liquid is undisturbed. Any increase in liquid-vapor surface area relative to the flat liquid will be a consequence of meniscus curvature. The more strongly curved the meniscus, the longer will be the arc length of the meniscus profile (the curve $f(x)$ in Figure 2) compared to a flat meniscus (the x axis). The product of this increased profile length, which we will call λ , and the length of the meniscus in the y direction will give the increase in liquid-vapor surface area. While λ depends on contact angle, the length of the three phase line depends primarily on immersion depth. There is a slight dependence of the latter on wetting properties, however. To see this, consider a disc immersed to its midpoint, where $h = R$. If the contact angle were 90° , the meniscus length would be $4R$. For smaller contact angles, the meniscus would be displaced upward, and the meniscus length would decrease due to the curved edge of the disc. Meniscus length in the y direction, then, is twice the length of the chord formed on the disc by the three phase line. We used the symbol P to represent this length, since it is the analog to the perimeter in the flat plate, and the formula $P(\sigma) = 4\sqrt{2R\sigma - \sigma^2}$, evaluated at $\sigma = h + z^\circ$, for the meniscus length. The symbol z° represents the meniscus height at contact with the disc, and is the same as $f(x)$ evaluated at $x=0$ in Figure 2.

In order to determine z° and λ , the shape of the meniscus must be known. We used the results of Princen⁴, who integrated the Laplace equation to give the meniscus profile in parametric form, to calculate these two quantities. He used the parameter ϕ , defined by $dz/dx = -\tan\phi$. ($z(\phi)$ is used here in the sense of $f(x(\phi))$). His parametrizing equations are

$$z\sqrt{c} = 2\sin(\phi/2) \quad \text{and} \quad (6)$$

$$x\sqrt{c} = 0.532 - 2\cos(\phi/2) - \ln[\tan(\phi/4)]. \quad (7)$$

The constant 0.532 applies only to the zero contact angle case. The constant c includes the specific surface system properties and is defined as $\rho_L g / \gamma_{LV}$. Meniscus height at contact, z° , is easily evaluated from equation 6 by noting that ϕ at contact

with the disc will be $\pi/2-\theta$, where θ is the contact angle. To evaluate λ , the increase in profile length, we integrated

$$\lambda = \int_0^{\pi/2-\theta} \left\{ \sqrt{(dz/d\phi)^2 + (dx/d\phi)^2} - (dx/d\phi) \right\} d\phi.$$

$$= 2/\sqrt{c} [1 - \cos(\pi/4 - \theta/2)] \quad (8)$$

Increase of liquid-vapor surface area is given by $A_{LV} = \lambda P$, so that the meniscus dilation term for the disc is

$$-\gamma_{SL} \frac{dA_{SL}}{dh} = -\gamma_{SL} \lambda \frac{dP}{dh}. \quad (9)$$

To calculate the meniscus gravitational work term, we first computed W_M . Due to our assumption of a cylindrical meniscus, this quantity, like A_{LV} , is the product of meniscus length, P , and the work to lift unit length of meniscus, ω . The former depends on both h and the contact angle, while ω is independent of h . It was evaluated by taking a volume integral of $\rho_L g z$ over the volume of a unit length of meniscus, i.e. between the x axis and $f(x)$ of Figure 2, and over unit length in the y direction. The function $f(x)$ in the figure is the same as $z(\phi)$ (equation 6) from Princen. After integrating in the z and y directions, and changing variables from x to ϕ , the integral becomes

$$\omega = 2\rho_L g/c \int_0^{\pi/2-\theta} \sin^2(\phi/2) (\delta x/\delta \phi) d\phi \quad (10)$$

$$= 0.235\rho_L g c^{-3/2}, \text{ when } \theta = 0,$$

where $x(\phi)$ is the expression taken from Princen (equation 7). The meniscus gravitational term is therefore given by

$$-\frac{dW_M}{dh} = -\omega \frac{dP}{dh}. \quad (11)$$

Immersed volume of the disc was taken as the product of the area of the segment of a circle corresponding to the portion of the disc below the x - y plane and the thickness of the disc, t . Using this formula for $V(h)$, the buoyancy term for the disc becomes

$$-\rho_L g V(h) = -\rho_L g t [R^2 \arccos(1-h/R) - (R-h)\sqrt{2Rh-h^2}]. \quad (12)$$

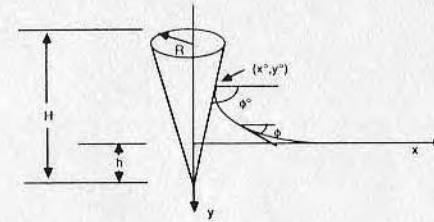


Figure 3. Coordinate system and notation for cone dipping experiment. Note that y axis points downward following the usage of Hu and Scriven.

The three phase line forms a chord across the circle which is the face of the disk. We took twice the area of the segment below this chord as an approximation of A_{SL} . The area of the edge was thus ignored. Therefore $\frac{dA_{SL}}{dh}$ becomes simply twice the length of this chord, and the wall energy term can be expressed as

$$\gamma_{LV} \cos \theta \frac{dA_{SL}}{dh} = 4\gamma_{LV} \cos \theta \sqrt{2R\sigma - \sigma^2}, \quad \sigma = h + z^\circ. \quad (13)$$

Force on the balance for the disc was obtained from equation 4 by substitution with the expressions developed above.

Cone. With the cone, as with the disc, all terms of equation 4 must be considered. The cone problem differs from the disc because the meniscus surface for the cone cannot be defined analytically as equations 6 and 7 do for the disc. To evaluate the terms from equation 4 we used numerical approximations of the meniscus surface and from these approximations, derived approximations for the quantities A_{LV} , W_M , and z° , all as functions of h . Because of the cylindrical symmetry of the cone, the meniscus surface can be described as a two dimensional profile, with the three dimensional surface generated as a revolution about the z axis. Refer to Figure 3 for the notation used.

Huh and Scriven⁵ have solved the problem of numerically approximating the axisymmetric meniscus surface. They give tabular values for a family of 24 such menisci, each being distinguished by the radial distance from the axis of symmetry of a point on the meniscus surface where the slope of the profile is 0.5° . Each of their 24 profiles are given as parametrized curves; their parameter ϕ is defined by $\tan \phi = dy/dx$, the slope of a vertically inverted profile (see Figure 3). Solutions to the depressed profile apply equally to an elevated profile formed by reflection about the base plane. Their x and y are dimensionless values corresponding to the

radial distance from the axis of symmetry and height above the undisturbed fluid level, respectively. Both are functions of ϕ and both are transformable to real dimensions by division with a constant, a , to be defined later. To calculate A_{LV} , W_M , and z° we took the following steps:

1. For each of the first 14 Huh and Scriven meniscus profiles, we interpolated between the tabular values using piecewise cubic polynomials determined from the values and slopes of the tabular endpoints of each piece. Closed form equations for the slopes $dy/d\phi$ and $dx/d\phi$ are given in the body of the Huh and Scriven⁵ paper.

2. We determined the surface area of the meniscus represented by each profile, using only that part of the profile applicable to our cone problem. The applicable part depends on the contact angle and taper of the cone, and is the portion of the profile parametrized from $\phi = 5^\circ$, which gives the furthest radial distance in the tabulation, to ϕ° , the value ϕ takes at contact with the cone. The meniscus surface was generated by revolving the applicable part of the profile about the vertical axis. We used the cubic polynomial pieces developed in step 1 to calculate the meniscus surface area by means of surface integrals. Romberg integration was used to compute the integrals. The area of a flat annulus extending from where the profile ended ($x(\phi')$, $\phi' = 5^\circ$) to some arbitrary but constant large x value (corresponding to the radius of the container of water) was added to the area obtained from the integral, so that A_{LV} consisted of two terms: area of the dilated portion of the meniscus plus the area of a flat portion of the liquid vapor interface. Equations used were:

$$\text{Area dilated} = 2\pi \int_{\phi=5^\circ}^{\phi^\circ} x(\phi) \sqrt{(dx/d\phi)^2 + (dy/d\phi)^2} d\phi \quad (14)$$

$$A_{LV} = \text{Area dilated} + \pi(x_{\text{large}}^2 - x^2(\phi=5^\circ)) \quad (15)$$

For the function $x(\phi)$ in equation 14 we used the interpolating polynomials developed in step 1.

3. We used the same three-dimensional surface and boundaries to determine the work against gravity in lifting the liquid of the meniscus above the undisturbed level by taking the integral of $\rho_L g y$ over the volume formed between the meniscus surface and the plane of the undisturbed fluid³. The three-dimensional integral reduces to a one-dimensional integral:

$$W_M = \pi \rho_L g \int x y^2 (dx/d\phi) d\phi \quad (16)$$

4. Knowing the radial (x°) and vertical (y°) coordinates of the circle where each meniscus contacts the cone, we computed the corresponding immersion depth (h) for each of the meniscus profiles from simple geometric considerations, i.e.:

$$(h+y^\circ)/x^\circ = H/R, \quad H, R \text{ as defined in fig. 3} \quad (17)$$

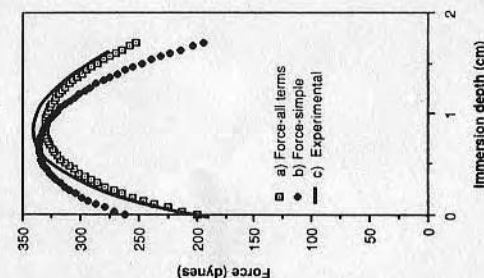


Figure 5. Comparison of experimental force curve c, with curve a, calculated using all terms, and b, using only wall energy and buoyancy terms.

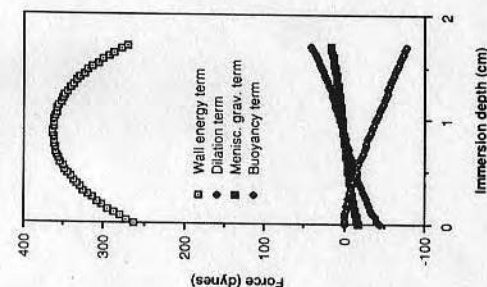


Figure 4. Contribution of each of the various terms in the force equation for the disc experiment. All but the volume terms are symmetrical about the depth of immersion equal to the midpoint less the meniscus height.

5. All of the above values were converted from the dimensionless ones of the Huh and Scriven tables to the glass/-water system by dividing immersion depth and z° by the constant a , area by the square of a , and work by the fourth power of a , where

$$a^2 = g\rho_L/\gamma_{LV} \quad (18)$$

6. The foregoing information was assembled into a 14 row table with each row containing h , A_{LV} , W_M , and z° for one meniscus profile from the Huh and Scriven paper. To determine dz°/dh , dA_{LV}/dh and dW_M/dh , we interpolated between the points in the table with cubic splines and used the derivatives of the cubic spline pieces as estimates of the derivatives. The latter two derivatives were used for the dilation and meniscus gravitational work terms.

7. To calculate dA_{SL}/dh , we took the derivative with respect to h of the formula for the area of a cone's curved surface, where the cone has height $h+z^\circ$ and base radius $k(h+z^\circ)$, k being the base radius to height ratio (R/H) of the sample cone. Thus for the wall energy term we used

$$\gamma_{LV}\cos\theta dA_{SL}/dh = 2\pi\gamma_{LV}\cos\theta k(h+z^\circ)(1+dz^\circ/dh)\sqrt{k^2+1}. \quad (19)$$

The volume of a cone of equal taper but height h was used to calculate the buoyancy term

$$-\rho_L g V(h) = -\rho_L g \pi (k^2) \left(\frac{h^3}{3}\right). \quad (20)$$

The above discussion applies to perfect cones. The glass cones used in experiments were rounded at the tip, rather than tapering into a fine point. The calculations were adjusted by using the frustum of a cone (i.e., a cone with the point sheared off) as a model. The only modifications required were to shift the functions by substituting $(h + \text{length truncated})$ for h in the above calculations and to correct the immersed volume by subtracting a constant amount corresponding to the volume of the missing part of the tip.

RESULTS

1. Cylinder. Calculated cosines of the contact angles of the variously sized glass cylinders averaged 1.012, with a standard deviation of 0.026. Some of the variation may be due to imperfections in the rods themselves, which were hand drawn from 2mm rod.

2) Disc. A plot of each of the terms used in calculating force on the balance is given in Figure 4. The force for a hydrophilic disc should increase with depth of immersion due to the increasing length of the three phase line until somewhere near the midpoint where this effect is overtaken by the monotonically increasing buoyancy term. Beyond the midpoint, the decreasing length of the three phase line and the buoyancy term combine to decrease the force. The dilation and gravitational terms associated with the meniscus have the effect of diminishing the force during the early stage of immersion when work must be expended to increase the meniscus in size; beyond the midpoint of the disc, these terms will increase the force felt by the balance as the meniscus shrinks in area and volume.

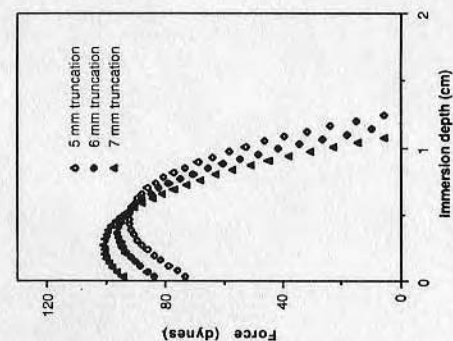


Figure 7. Effect of changing truncation length parameter on calculated force curve.

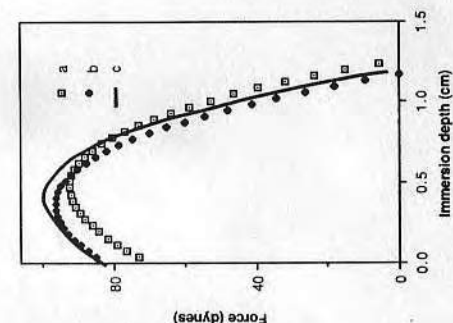


Figure 6. Calculated force compared with experimental for a glass cone. Parameters used in curve a are actual measured parameters, which were modified in curve b to achieve a better fit to the experimental data in curve c.

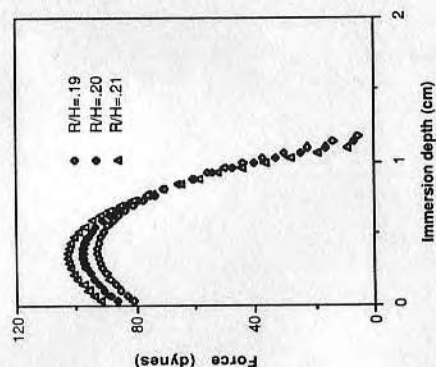


Figure 8. Effect of changing cone taper parameter on calculated force.

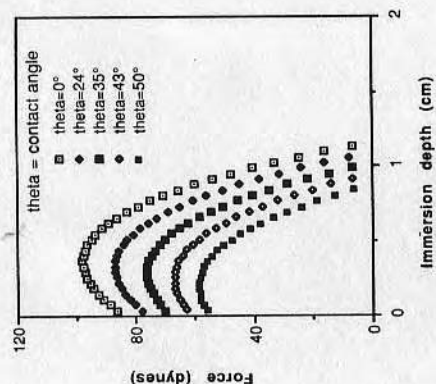


Figure 9. Calculated force curves for a series of contact angles.

The calculated force is compared to the experimental curve in Figure 5. Curves *a* and *b* represent calculated forces considering the meniscal shape contributions in *a* but not in *b*. Curve *a* gives the better match to the experimental data of curve *c*, indicating it is important to consider the extra work terms for this geometry. The small deviations between experimental and calculated forces may be due in part to the edge effects ignored in calculations.

3) Cone. An experimentally generated curve of force vs position for a dipping experiment with the cone is given in Figure 6. Two calculated curves are also overlain in the same figure. Curve *a* is based on a truncation length of 5 mm and a base radius/altitude ratio of 0.196, the measured values of these parameters. Curve *b* was obtained with 6 mm and 0.2 for the same parameters, and fits much more closely to the experimental data. Since the truncation length was difficult to accurately measure, 6 mm is not an unreasonable value. Also since our cone was rounded at the tip rather than truncated the model used for calculations was not strictly accurate. Nonetheless, such a large change in the force curve over small changes in geometric dimensions illustrates the dangers involved in using nonstandard geometries. To get some picture of the propagation of errors in the geometrical parameters, we have plotted calculated force curves for three truncation lengths in Figure 7, and for three base radius/altitude ratios in Figure 8. Changing truncation length values both changes the force maximum and shifts the curve along the immersion depth axis, while changing the degree of taper only changes the force maximum and the low immersion depth portions of the curves. The effect of decreasing contact angles is portrayed in Figure 9, where five curves of equally spaced values of the cosine of the contact angle are given. The curves are well separated, but so are the contact angles the curves represent.

Of the various terms contributing to the calculated force, only the wall energy and buoyancy terms appear to be significant for the cone geometry. Each term is plotted separately in Figure 10. The liquid surface area term actually consists of two opposing effects. As the radius of the contact circle increases, the area of the meniscus, i.e., disturbed surface, increases, but liquid vapor surface area is also destroyed as the cone displaces it. With increasing immersion depth the second factor dominates, and thus the liquid surface area term increases the force on the balance.

One might think that if only the wall energy and buoyancy terms are significant it would be reasonable to dispense with the interpolations of the Huh and Scriven tables. This would be true to some extent, but it would still be necessary to use them, or some other means, to determine the height of the meniscus at the contact point, so that the wall energy term could be evaluated at the height of the three phase line rather than at the immersion depth. To ignore that shift would introduce serious error into the calculation, as demonstrated in Figure 10 which compares the force curve calculated using only the buoyancy term and the wall energy term evaluated at the immersion depth with that using the fully developed equation.

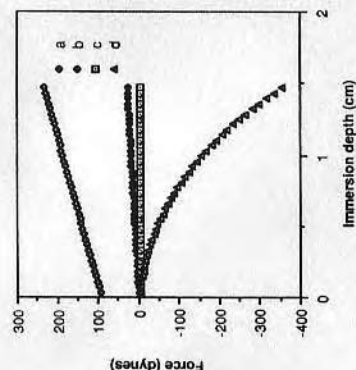


Figure 10. Relative contributions of each term contributing to calculated force for the cone experiment. Plotted from top to bottom are the a) wall energy, b) dilatation, c) meniscus gravitational, and d) buoyancy terms. Meniscus height at the contact circle is part of the solid vapor term, therefore interpolation of the Huh and Scriven tables were needed for it.

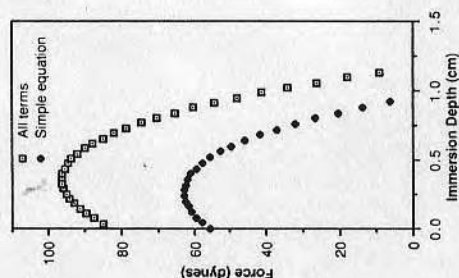


Figure 11. Comparison of the force curve for the cone calculated using all terms with one generated from a simple equation including only wall energy and buoyancy terms.

DISCUSSION

Reasonable success at predicting forces was experienced with all three geometries. Determination of the contact angle would involve inverting the force equations to solve for contact angle. Good sensitivity would require large changes in force for small changes in contact angle, therefore terms independent of contact angle are better kept small. The buoyancy term is usually as high or of higher order than the contact angle dependent terms and can cause problems if it becomes too large, as it must be subtracted out to isolate the contact angle dependent terms. Furthermore, small errors in dimension or in sample geometrical assumptions can cause rather large errors in the calculated volumes, as seen with the truncation length in the cone experiment. For these reasons, use of the Wilhelmy apparatus for other than prismatic objects should be undertaken with great care, and should be fully investigated with standards before being used with unknowns. Propagation of errors in the various parameters involved must also be studied.

The cone experiments suggest that, given precisely defined sample geometries for which the Laplace equation can be solved numerically, an approximate contact angle could be derived using an iterative least squares nonlinear model fitting algorithm. It would be possible to allow the program to adjust some parameters other than contact angle, especially when adjustment of these parameters affects a different feature of the calculated force curve than does contact angle. As an example, since we anticipated some error in measuring truncation length for our cone experiment, we could allow the model fitting program to adjust this parameter without great danger of confounding the two values. Examination of Figures 7 and 8 shows that an adjustment that decreases the force maximum will, for truncation length, shift its position towards higher immersion depth, but for contact angle, shift the maximum towards lower immersion depths. With some geometries, extracting contact angles might not be feasible, for example if the force curve were much more sensitive to the geometric parameters than to contact angle.

Putting such a program in place would involve a large investment in time for each geometry. The experimental data would need to be digitized for the curve-fitting program. Such a method of analysis would be most appropriate for repeated measurements on samples of identical geometry but possibly different wetting properties. Contact lenses might be an appropriate candidate for such a study since they have the requisite defined geometry and, being thin, would have a small buoyancy term if dipped sideways. Edge effects might pose a problem, especially with the smaller lenses. It might, therefore, be simpler to use meniscus height measurements when the lens is dipped convex side first into a liquid, deriving contact angle from meniscus height with the aid of the Huh and Scriven tables. In our experience, the Wilhelmy procedure produces highly reproducible results when used on identical samples, and is quite sensitive to surface contamination. It might then be valuable for quality control applications where contact angle measurements are not necessarily required, but where detection of variation in surface properties from sample to sample is of more importance.

ACKNOWLEDGEMENTS

We thank M. Reichert and P. Suci for a critical review and S. Garoff for stimulating discussions.

REFERENCES

1. R.E. Johnson, and R.H. Dettre, Wettability and contact angles, in: "Surface and Colloid Science, vol 2", Egon Matijevic, ed., Wiley-Interscience, New York (1969).
2. L. Smith, C. Doyle, D.E. Gregonis, and J.D. Andrade, Surface Oxidation of Cis-Trans Polybutadiene, J. Appl. Polym. Sci. 26:1269 (1982).
3. L.W. Schwartz and S. Garoff, Contact angle hysteresis and the shape of the three-phase line, J. Colloid and Interf. Sci. 106:422 (1985).
4. H.M. Princen, The equilibrium shape of interfaces, drops, and bubbles. Rigid and deformable particles at interfaces, in: "Surface and Colloid Science, vol 2", Egon Matijevic, ed., Wiley-Interscience, New York (1969).
5. C. Huh and L.E. Scriven, Shapes of axisymmetric fluid interfaces of unbounded extent, J. Colloid and Interf. Sci. 30:323 (1969).

Polyester Textile Bioadhesion to Muscle and Bone

HAROLD K. DUNN, ROBERT KING, JOSEPH D. ANDRADE, JR., and
KENNETH L. DE VRIES

College of Medicine and Engineering, University of Utah, Salt Lake City,
Utah 84112

Summary

Surgical repair of injuries to the flexor tendons of the hand does not give satisfactory clinical results. In an attempt to solve this clinical problem, basic studies have been done aimed at developing an artificial tendon. In this paper, the anatomy of the flexor tendons and the physiology of their wound healing is related to the clinical problems encountered in this type surgery. It is proposed that a satisfactory way to solve this clinical problem is development of a permanently implantable functional flexor tendon prosthesis. Dacron polyester fabric of four various weave configurations were implanted into the musculotendinous junction of rabbits and into the femurs of dogs for periods varying from 2 to 8 weeks. The strength of the ingrowth into these fabrics was mechanically measured and related to surface area and porosity of the implant. Histological studies of the ingrowth was made. It would appear, at the musculotendinous junction, the strength of the ingrowth into the implant is primarily dependent on the internal fabric porosity and not the surface morphology. The strength of the ingrowth from the bone into the implant exceeded the strength of the materials in all specimens.

INTRODUCTION AND BACKGROUND

An area of current biomaterials research at the University of Utah is aimed at development of a permanently implantable flexor tendon prosthesis for the hand. In order to understand the

3. Two vol% Rohm & Haas DMP-30 is then added to the solution in (2) and the entire solution containing the specimen allowed to cure in a warming oven at 60°C overnight.
4. The sample surface is then polished using standard metallographic techniques.
5. Sample surface-stained with Paragon frozen section multiple stain.
6. Sample surface is then observed using incident light microscope techniques.

References

1. McFarland, G. B.: Flexor Tendon Prosthesis, U.S. Patent #3, 613, 120, October 19, 1971.
2. Henze, C. W., and Mayer, L.: *Surg. Gynecol. Obstet.*, 21, 10 (1914).
3. Wheeldon, T.: *J. Bone Joint Surg.*, 21, 393 (1939).
4. Goenicdtian, S. A.: *Arch. Surg.*, 26, 181 (1949).
5. Koth, D. R., and Sewell, W. H.: *Surg. Gynecol. Obstet.*, 101, 615 (1955).
6. Ashley, F. L., et al.: *Plast. Reconstruct. Surg.*, 23, 526 (1959).
7. Nichols, H. M.: *Ann. Surg.*, 129, 223 (1949).
8. Gonzalez, R. I.: *Surgery*, 36, 181 (1949).
9. Gonzalez, R. J.: *Plast. Reconstruct. Surg.*, 23, 562 (1958).
10. Hochstrasser, A. E., et al.: *Rocky Mt. Med. J.*, 57, 30 (1960).
11. Ashley, F. L.: *The Bulletin*, Dow Corning Center, Vol. 4, July 1962.
12. Thatcher, H. H.: *S. Med. J.*, 32, 13 (1939).
13. Mayer, L., and Ransohoff, N.: *J. Bone Joint Surg.*, 18, 607 (1936).
14. Davis, L. and Aries, L. J.: *Surgery*, 2, 877 (1937).
15. Hanisch, C. M. and Kleiger, B.: *Bull. Hosp. Joint Dis.*, 9, 22 (1948).
16. Milgram, J. E.: *Bull. Hosp. Joint Dis.*, 21, 250 (1960).
17. Anzel, S. H. et al.: *Am. J. Surg.*, 101, 355 (1961).
18. Sarkin, T. L.: *British J. Plast. Surg.*, 44, 232 (1956).
19. Arkin, A. M., and Siffert, R. S.: *Am. J. Surg.*, 85, 795 (1953).
20. Grau, H. R.: *J. Plast. Reconstruct. Surg.*, 22, 562 (1958).
21. Sakata, Y.: *J. Japan Orthop. Ass.*, 36, 1021 (1962).
22. Williams, R. D.: *Sci. Forum*, 11, 39 (1960).
23. Carroll, R. E., et al.: Formulation of Tendon Sheaths by a Silicone Rod Implant, paper presented at the 18th Annual Meeting of the Am. Soc. for Surg. of the Hand, January 1963.
24. Hunter, J. M.: *Am. J. Surg.*, 109, 325 (1965).
25. Bader, D. F., et al.: *J. Plast. Reconstruct. Surg.*, 41, 157 (1968).
26. Wesolowski, J. A.: *Ann. N.Y. Acad. Sci.*, 146, 325 (1968).
27. Klawitter, J. J.: Workshop 1—Bio Evaluation of Hard Material Implants. Paper presented at Symposium-Workshop on Research Techniques in Biomaterials Evaluation, Clemson University, March 1971.
28. Leininger, R. I., et al.: *Trans. Am. Soc. Artif. Intern. Organs*, 10, 237 (1964).

significance of this work, a brief discussion of the anatomy, function, and clinical problems encountered in repair of flexor tendons will be given.

The body of a tendon is principally composed of dense collagen bundles, longitudinally oriented and parallel (Fig. 1). Fibroblasts surround these dense collagen bundles and are necessary for maintenance of their integrity. There is no evidence of vasculature in the collagen bundles, but they are surrounded by a delicate framework, the endotenon, and are further grouped by the epitenon consisting of a thin, closely adherent, fibroblastic layer containing small blood vessels surrounding the tendon body. The epitenon aids the gliding mechanism. A synovial sheath surrounds the tendon body and between it and the epitenon is a scant amount of lubricating synovial fluid. The synovial sheath is quite similar to the epitenon and serves the same function. It is most fully developed in the areas of maximum excursion of the tendon body and less well developed at each end of the tendon. Immediately surrounding the synovial sheath is the perisheath consisting of highly vascularized tissues whose function is supply of the necessary fluids for maintenance of the enclosed structures and as a basis for the repair mechanism in tendon injuries. In the hand and proximal portion of the digits, the perisheath soft tissue is specialized to act as a pulley mechanism preventing the flexor tendons from "bow stringing." This is the fibrous flexor sheath, which is a dense fibrous tissue connected to the underlying bone forming a strong osteofascial tunnel for passage of the tendon. The body of the tendon is connected at intervals to its synovial sheath and perisheath tissues by a mesotenon which is a delicate band of

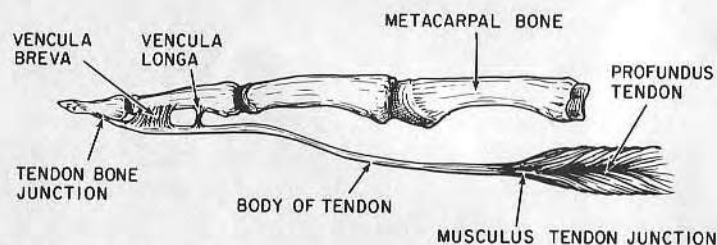


Fig. 1. Flexor tendon.

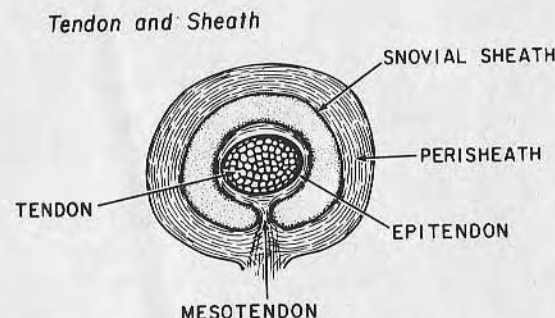


Fig. 2. Cross-section of flexor tendon.

vascular connective tissue appearing as a cleft in the synovial sheath extending out to the tendon proper (Fig. 2). Certain areas of the mesotenon are highly specialized structures being long and mobile, and are designated as vincula. The vincula are very delicate and when injured do not reconstitute themselves. They act to supply the tendon body with a blood and a nerve supply.

As important an area as the tendon body is its attachment to the muscle and bone. At the musculotendinous junction the collagenous fibers of the epimysium, which surrounds the entire muscle body, and the endomysium, which surrounds individual muscle fibers, blend indistinguishably into the collagen fibers of the tendon body.

At the tendon-bone junction the collagen bundles of the tendon body penetrate the cortex of the bone and extend well down into the medullary canal as Sharpey's fibers. They are diffused into the collagenous matrix of the osseous structure.

The tendon acts to transfer force from the motor units or muscle, to the member which it acts on, the bone. In the hand where a wide range of motion for the digits is necessary, the excursion of the tendon from full extension to full flexion varies from 4 to 8.5 cm. Any limitation of excursion in the musculotendinous unit results in impairment of function in the digit it serves.

Successful surgical repair and restoration of function of a flexor tendon, particularly after injury within the fibrous flexor sheath, is difficult to achieve. The physiological processes

necessary for healing invariably limit mobility of the tendon. The tendon itself is relatively avascular and possesses little capacity, if any, to provide a healing response. A damaged tendon primarily relies on infiltration of granulation tissue from the surrounding soft tissues of the perisheath structures to effect repair. While essential for adequate restoration of tendon continuity, this ingrowth provides the basis for rehabilitation problems following tendon surgery. As granulation tissue invades the damaged tendon-effecting repair, it forms dense fibrous connections or adhesions with the surrounding structures and tends to tether the tendon to its surroundings resulting in loss of excursion. Thus, while tendon continuity is successfully restored, loss of function results. In order to restore the function these adhesions must be stretched or broken to permit motion. To facilitate stretching these adhesions, surgeons remove external constraints or bandages about 3 weeks following repair of flexor tendons and begin motion of the hand. Unfortunately, this early motion frequently disrupts the surgical repair despite elaborate suturing techniques. Studies indicate that 3 weeks following repair, a direct tendon anastomosis possesses only 12% of the tensile strength of a normal tendon and that 4 months is usually necessary for normal tensile strength to develop (1).

Since the early 1900's many investigators have attempted to overcome the adhesion problem following surgery and repair. Early surgeons repaired lacerated tendons and kept the hand immobilized 6-8 weeks and then secondarily attempted to surgically cut or lyse the inevitable adhesions that formed. This approach failed for several reasons. Surgical lysis of adhesions results in a raw, bleeding area of tissue on the tendon and a similar area on the adjacent tendon sheath. These two areas rapidly try to heal together again and most frequently do. Further, after 4-6 weeks immobilization of a hand, adhesions form within the small joints of the fingers and the collateral ligaments of the joints contract resulting in marked limitation of motion in the digits unrelated to tendon adhesion. This limitation of motion can be permanent and irreversible by re-establishment of tendon function.

Later surgeons attempted to completely block formation of adhesions by introducing semipermeable or impermeable

membranes around their repairs (2-11). The role of these adhesions in early healing has been discussed and these "blocking devices" succeeded only in preventing healing. In many instances, the lack of biocompatibility of the blocking materials produced a greater tissue response than normally would have occurred had they not been used.

Direct surgical repair of lacerated flexor tendons in the area of the fibrous sheath of the hand resulted in such poor results that the area gained the title "no man's land" (Fig. 3). Many surgeons began advocating primary replacement of severed tendons in this area with an autogenous free tendon graft. Their rationale was that this resulted in a suture line at the distal phalanx where no motion occurs, hence adhesions cause no ill effects and another in the forearm where the soft tissues are pliable and adhesions don't limit excursion. Clinical results of this technique have not been as good as expected. Adhesions form between the free

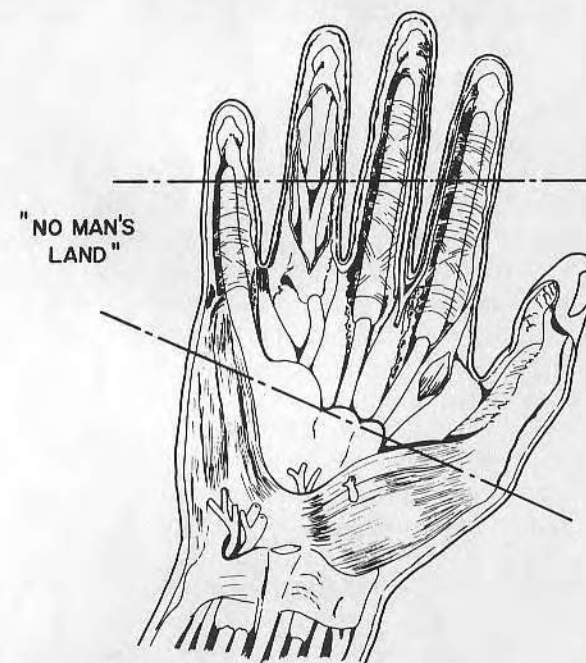


Fig. 3. No-man's land of the hand.

tendon graft and the surrounding synovial sheath. These are much worse if the sheath has been damaged but are inevitable even if it has not. To function, a free tendon graft must establish a blood supply and biologic viability. As pointed out previously, the graft is not an inert bundle of collagen but is a matrix of collagen that must have supporting fibroblasts. After surgical implantation the graft "seeks" support from surrounding tissues and, in essence, the healing response is evoked throughout its length.

Attempts to provide a better fibrous sheath for implantation have improved results of free tendon grafting (12-17). The principle of this technique is surgical placement of inert foreign material in the bed of a previously damaged tendon sheath. The foreign material stimulates formation of a shiny scar tissue membrane which is grossly similar to a tendon sheath. The free tendon graft is passed through this artificially induced sheath after a 6- to 8-week period of time. However, many of the materials utilized such as Teflon, Ivalon, and Celloidin were not sufficiently biologically inert and a significant foreign body reaction occurred. Other materials such as stainless steel obviously were too rigid allowing little passive motion, and stiffness developed in the small joints of the hand. Other researchers attempted to add active motion transference to their implants bypassing the traditional grafting technique. Most failed because of foreign body reactions, lack of structural integrity, or poor mechanical and functional design. The most well known materials used for this concept were nylon fiber and polyethylene tubing combinations (18), braided Tantalum wire (19), wire and silk covered polyethylene tubes (20), arterial tissue and nylon thread combinations (21), and Teflon rods (22).

Often a lack of knowledge concerning the mechanics of flexion and extension of the digits led to a poor choice and design of materials. In some cases the reinforcing materials of the prosthesis failed under tension, during flexion, or were not properly bonded to the matrix. Also the tube-cord concept offered a continual threat of deadspace collection of body fluids, blood, and bacteria, with resulting infection. The mechanical inefficiency of the prosthesis was further emphasized by its

tendency to produce excessive frictional wear and to kink on flexion.

More recent studies, however, have shown promise in the development of permanently implantable tendon prosthesis. The more notable of these contributions were made by Carroll (23), Hunter (24), and Bader (25).

Carroll successfully maintained passive motion of the hand while using a flexible silicone rod to aid formation of a flexor sheath. The main importance of this work was the fact that a material had finally been found which was essentially biocompatible and possessed the desired bending characteristics of a tendon. Carroll later attached the silicone rod to the proximal and distal ends of the excised tendon and provided active function for a period of nearly 5 months. Suture-line failure ultimately necessitated removal of the implant and subsequent use of a free tendon graft. Hunter continued the concept introduced by Carroll and developed the "Hunter tendon," a single-unit flexor tendon prosthesis. Essentially the Hunter tendon is an expanded version of Carroll's work generally consisting of a fiber reinforced silicone rubber rod incorporating either sutures, loops, mesh work, or tapes for attachment to either of the tendon stubs. The Hunter tendon has been used primarily as a passive implant designed to provide the initial functional benefit while forming a new tendon sheath. This increases the mobility and power of the entire tendon motor unit and softens the moving planes of the hand. When failure of the prosthesis has occurred it has been replaced with a free tendon graft.

Bader recently explored the problem of the loss of tendon pulleys often resulting after tendon injury. A necessary requirement for a successful free tendon graft or artificial tendon is its containment to the area of the original tendon. If this cannot be done, the body of the tendon tends to "bow string" when tension is placed on it decreasing force and excursion transmitted to the bone. Bader successfully circumvented the problem using prosthetic pulleys in the digits consisting of silastic rubber and polyester mesh. The significance was that he successfully anchored his prosthesis via tissue response rather

than mere mechanical fixation by suturing. Thus, the induced soft tissue proliferation present in all tendon reconstruction had been advantageously made of use and further indicated an alternate method for prosthetic attachment for the skeletal system other than suturing.

McFarland (1) has apparently combined the development of these earlier investigators into a flexor tendon prosthesis shown in Fig. 4 which he patented. To our knowledge, there has been no scientific publication of this work.

Our present research is aimed at developing a clinically acceptable prosthesis which directly attaches at the musculotendinous origin and bony insertion of the flexor digitorum pro-

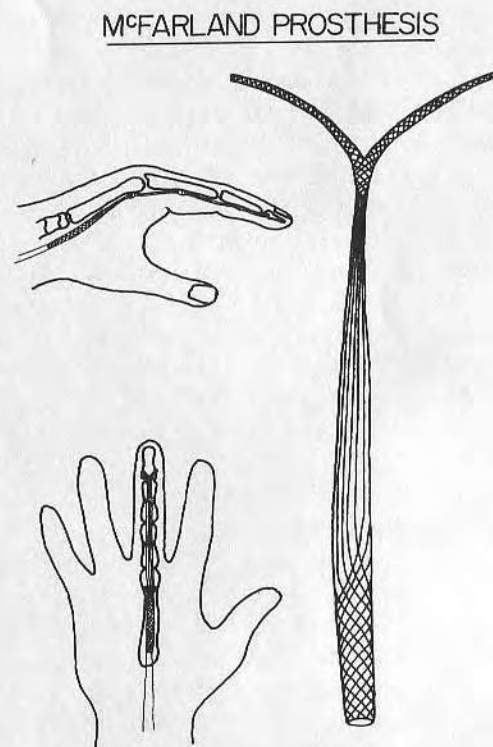


Fig. 4. Mc Farland prosthesis.

fundus tendon of the hand providing permanent function thus bypassing the previously discussed adhesion problems encountered in tendon surgery. The project can be broken down into three basic areas of interest: (1) the musculotendinous junction; (2) the tendon-bone junction; (3) the body of the tendon.

This paper reports the initial findings in the first two areas. Our attachment concepts for these two areas is essentially analogous employing a fabric which permits tissue ingrowth through the inherent fabric porosity to provide a firm mechanical interlock with the biological system. The choice of polymeric fabric material to provide a scaffolding for tissue ingrowth over other porous materials such as calcium aluminate ceramics or sintered metals is based on three important criteria: (1) the fabric has a pliability which more closely approximates the physiological resiliency of the muscle and tendon tissue than does the more rigid porous materials and is, therefore, more mechanically compatible with the biological system; (2) textile technology has reached the state-of-the-art in which the proposed prosthesis may be constructed in a continuous fiber process, uninterrupted from muscle origin to bone insertion, greatly enhancing long-term mechanical stability of the prosthesis, and (3) there is a nearly infinite selection of fabric structures such as weaves, knits, braids, velours, felts, etc., which can be fabricated to meet practically any biologically desirable properties.

However, for this particular application there is an inherent property of most fabrics with a relative open structure (thus a greater porosity) which precludes their use. Under tension loading most open fabrics have a tendency to elongate sacrificing their original geometry for a more closed structure. This presents two problems for an artificial flexor tendon. First, some of the muscle contraction is taken up in fabric extension resulting in reduced excursion of the tendon. Second, because the extensibility reduces the porous nature of the fabric any tissue ingrowth which has occurred will tend to be pinched and possibly even severed by the contracting fabric. This may lead to tissue necrosis and loss of fixation. Obviously the problem does not present itself in bone due to the more rigid nature of the bony

supporting matrix which does not permit extension and contraction of the implanted fabric.

We have initially been trying to determine the ultimate fabric geometry and porosity which will give maximum tissue ingrowth and mechanical fixation at the muscle and bone junctions. When these parameters have been determined the emphasis will be placed on reduction of fabric extension under dynamic loading while maintaining the desired fabric geometry. The following report summarizes our findings on four fabrics implanted in the muscle tissues of rabbits and bone tissues of dogs for periods of up to 8 weeks.

EXPERIMENTAL PROCEDURE

Fabric Identification

The materials used in the study were Dacron polyester fabrics, three of which were kindly supplied by the United States Catheter and Instrument Corporation (Glens Falls, New York) and identified as: 1. U.S.C.I.C. #6079 fabric matrix Dacron felt; 2. U.S.C.I.C. #6108 one-sided Dacron velour; 3. U.S.C.I.C. #KG-1125 two-sided Dacron velour; 4. a proprietary fabric, identified as DN-4 braided Dacron cord supplied by the Eimco Corporation, Filter Media Division, Salt Lake City, Utah.

Fabric Preparation

The design and preparation of the fabrics is as follows: 1. Using a template, each U.S.C.I.C. fabric was cut to the implant size and geometry shown in Figs. 5a and b. The small tapered end of each implant was then dipped to a height of 0.5 in. in a silicone rubber solution consistent of 80 vol.-% Dow-Corning # 92-009 dispersion coating and 20 vol.-% VM & P naptha. 2. The Eimco Dn-4 braided Dacron cord muscle implants were hand-fabricated into "artificial" weaves by first teasing the cord into 16 individual fiber strands which were tied together two at a time in a regular fashion producing two planes of fabric, 8 strands each,

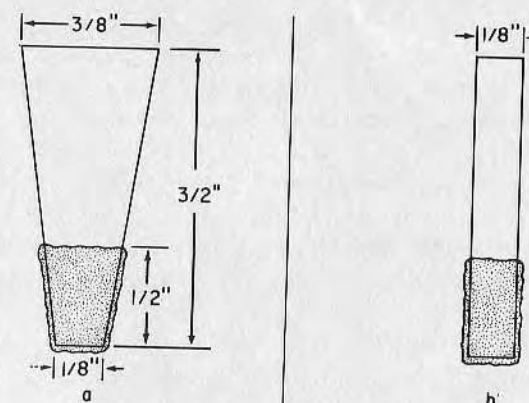


Fig. 5. Implant configuration of Dacron weaves and velours: 5-A. implantation at Musculo-Tendinous Junction; 5-B. implantation in bone.

as shown in Fig. 6a. The bone implants were again separated into 16 strands, teased and tied at the top and center as shown in Fig. 6b. In both cases, the tying material was commercial grade, cotton-coated Dacron polyester sewing thread. Prior to surgery, the implants were sterilized by steam autoclaving at 250°-270° for 15 min.

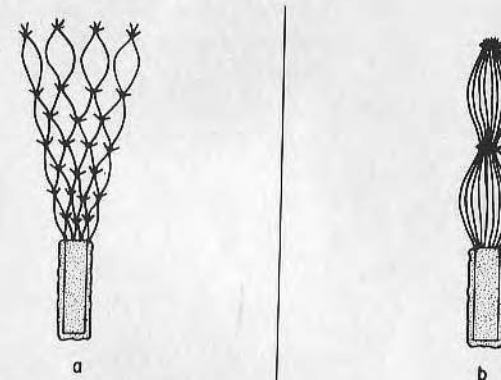


Fig. 6. Implant configuration of Dacron cord: 6-A. implantation at musculo-tendinous junction; 6-B. implantation in bone.

Fabric Characterization

Microstructures. SEM (Scanning Electron Microscope) photomicrographs of three fabric microstructures are shown in Figs. 7a-c.

Porosities. Porosities of the implants were measured in terms of the quantity of water flow through a unit area of fabric per unit time ($\text{ml H}_2\text{O}/\text{cm}^2/\text{min}$) at a pressure head of 120 mm Hg using the technique described by Wesolowski (26) in his investigations of fabrics for prosthetic arterial grafts.

Tensile tests. Tensile tests were performed on each of the four fabrics under two conditions: a. Dry-tested "as supplied" by the manufacturer, and b. Wet-tested after boiling for 6 hr in a 1.0 M phosphate buffered saline solution.

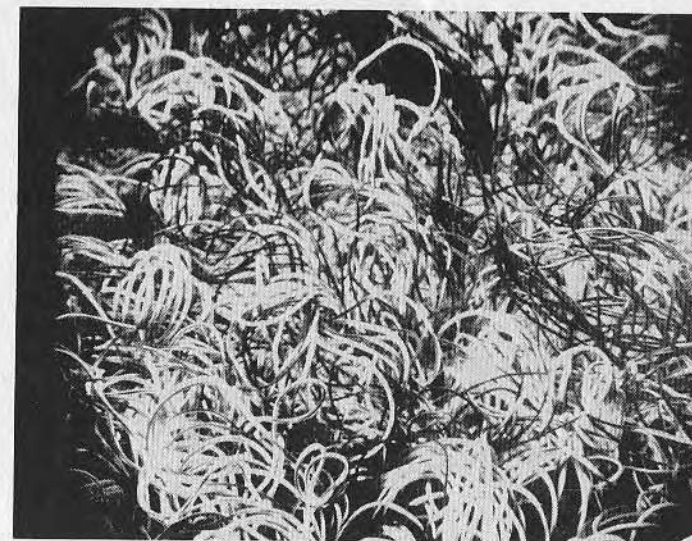
Testing was accomplished with a Model 1130 Instron, using a constant strain rate of 0.2 in/min. The fabric geometries tested were those of the muscle and bone implants of Figs. 5 and 6.

Surgical Technique

A total of 71 rabbits were used in the muscle fabric evaluation studies. A single fabric was placed at the musculotendinous junction of both hind limbs of the rabbit, one limb then being used for mechanical testing, one for histology. Three rabbits were used for each fabric at each of the 2-, 4-, 6-, and 8-week intervals of the time study for a total of 12 implants carried out on each fabric.

A total of 12 dogs were used in the bone-fabric evaluation studies. All four fabric materials were placed in each hind limb of a single dog, again one limb being used for histology and one limb for mechanical testing. Three dogs were used for each of the 2-, 4-, 6-, and 8-week intervals of the time study for a total of 12 implants carried out on each fabric.

Muscle implants Implants at the musculotendinous junction were carried out in adult New Zealand white rabbits. Anesthesia was induced with intravenous Pentobarbital and maintained by Penthrane inhalation. The hind leg was shaved and the skin prepped with tincture of iodine. The area was



(A)



(B)

Fig. 7 (continued)



(C)

Fig. 7. Scanning electron microscope photomicrograph of: 7-A. Dacron double velour; 7-B. Dacron felt; 7-C. Dacron single velour.

draped in a sterile manner and an incision made directly over the tendo Achille's extending well up on the muscle belly of the gastrocnemius and soleus muscles to about the insertion of the tendon in the os calcis. The muscle belly of the soleus was incised linearly parallel to the adjacent tibia. This incision was carried through the musculotendinous junction well down into the body of the tendon. The entire length of the incision was about 3 cm long and went completely across the muscle belly and tendon. This, in essence, split the musculotendinous junction but left the muscle and tendon intact. The implant material was then interposed between the split muscle and tendon and the edges of the muscle and tendon were brought together with interrupted 4-0 nylon sutures. Care was taken to be sure these sutures did not pass through the implant material. One end of the implant was left protruding from the body of the tendon to be used later in evaluating the strength of the implant muscle-tendon juncture. The skin wound was closed with a subcuticular

2-0 chromic suture. No special dressing or immobilization was applied to the leg and the rabbits were allowed to recover from the anesthesia and kept in standard cages and allowed unrestricted activity.

Bone implants. Implants in bone were carried out in large mongrel dogs. The dogs were anesthetized with intravenous Nembutal and their hind limbs were shaved, prepped with Tincture of Iodine and draped in a sterile manner. A longitudinal incision was made over the lateral aspect of the femur extending from the greater trochanter into the level of the knee. The underlying fascialata was incised and the femur approached through the lateral intermuscular septum. Hemostasis was secured by electrocautery and the lateral aspect of the femur was subperiosteally exposed. Four 0.25-in. drill holes were equally spaced in the shaft of the femur. The implants were then placed through these drill holes going all the way through the femur so that a portion of the implant extended from the femur on each side. The periosteum was then loosely closed over the ends of the implants and the fascialata was closed with interrupted 2-0 chromic sutures. The skin was closed with subcuticular wire suture. The dogs were allowed to recover from the anesthesia and no special dressing or cast was applied to the hind leg. These dogs were kept in a large dog cage and allowed full, unrestricted activity.

Controls. Four rabbits one for each time interval, were sham-operated for use as histology controls. The above surgical procedures were carried out, with the exception that no implants were placed in the split musculotendinous junction.

No histology controls were used in the bone-fabric evaluations. Mechanical testing controls for each fabric were surgically implanted as previously described and mechanically tested the following postoperative day.

In-Vivo Mechanical Testing

Equipment. Equipment used in the mechanical testing studies consisted of a Statham Universal Transducing Cell, Model UC3-Gold Cell (Honeywell, Inc., Denver, Colo.), with a

0-50 lb Statham Model UL4 Load Cell Accessory, Statham Analog Readout Meter, Model UR5, and a CEC Datagraph dual-channel recorder. The UC3 Transducer, UL4 readout meter and the CEC recorder were operated in series during testing, after precalibration to produce a full-scale millivolt readout corresponding to 0-16 lb on one recorder channel and 0-40 lb on the second recorder channel.

The 0- to 16-lb scale was used primarily for the muscle implant load characterization while the 0- to 40-lb scale was used for the bone implant load characterizations. The serrated parts of the grip system were fabricated from the actual tensile-grip jaws of a large commercial testing machine and provided an excellent method of attachment of the testing device to the implants. No evidence of grip slippage or fabric failure in the gripped area appeared during the 2-month evaluation study.

Procedure. The following procedures were used in the *in-vivo* mechanical evaluation of the fabric implants.

Muscle procedure. (1) After sacrificing the rabbit, the position of the implant was determined, and the end tab exposed through a small incision. The silicone-coated portion of the implant was freed of all encapsulating tissue and attached to the grip mechanism. (2) The limb containing the implant was firmly pinned to the plate of the testing assembly by passing two B&S #20 gauge steel wires through the corresponding holes in the plate by twist-wrapping them around several segments of the limb. (3) The grip mechanism was attached to the testing device which was retracted by manual rotation of the threaded assembly thus producing an extension and corresponding load on the implant, which was sensed by the cell and thus recorded.

Bone procedure. After sacrificing the dog, the femur section containing the four implants was removed distally and proximally to the implanted area with a bone saw. The removed section was then firmly fixed to the testing assembly plate as in (2) above, and tested as in (3) above. Several points should be noted regarding the testing procedure: It was determined that surgical exposure of an

implant end tab which was not silicone rubber-coated could produce wide variations in the amount of implant surface remaining exposed to the ingrown tissue, which would thus affect mechanical test results by introducing a nonuniform interface area. Thus, silicone rubber coating before implantation assured a uniform tissue ingrowth area upon surgical exposure of the end tab of the implant, and correspondingly less variance in the data obtained. It should also be noted that after sacrifice of the animal, 5 min was set as the maximum allowed time limit for completing mechanical testing of the muscle implants, and 20 min (5 min each) as the maximum allowed time limit for mechanical testing of all four bone implants. This procedure was considerably easier than working with an anesthetized animal, and it was felt that this short time limit after sacrifice produced very little test variance when compared to that produced in the living animal and thus could safely be referred to as an "in-vivo" mechanical evaluation.

Histology

After mechanical testing was completed on the sacrificed animals, the corresponding surrounding tissues and implants were surgically removed and, along with the mechanically tested implants were fixed in 10% formalin for use in histology studies. Two different histologic techniques were investigated, one using a conventional soft tissue paraffin method, and one using a modified hard tissue technique as developed by Klawitter (27). Both methods are detailed in Appendices I and II.

After dehydration, each implant was sectioned in half along the long axis. Then, for comparison, one half was prepared by the conventional soft tissue technique, one half by the modified hard tissue technique. The primary histological evaluations made on the implants were as follows: (1) Degree of tissue ingrowth; (2) type of tissue present; (3) cell types present; (4) fabric fiber integrity and appearance; and (5) correlation with mechanical data.

RESULTS

Fabric Characterizations

Porosity. Results of porosity measurements on the implanted fabrics are shown in Table I. The Weaveknit material listed in the table was used as a control fabric for comparison with the Wesolowski results.

Tensile strength tests. Table II lists the tensile test results on three materials in both of the described conditions. The two main purposes of the tensile tests were to (1) determine the ultimate strengths of the fabrics in both the muscle and bone

TABLE I
Fabric Porosity

Fabric	Porosity (ml H ₂ O/cm ²)/min 120 mm Hg
1. Weaveknit (Control)	4,000
2. U.S.C.I.C. #6079 Felt	3,783
3. U.S.C.I.C. #6108 Velour	4,145
4. U.S.C.I.C. #KG-1125 Velour	4,016
5. Braided Dacron Cord	32,889

TABLE II
Load to Failure

Fabric	Average load @ failure (lbs) as supplied PBS-6 hours	
U.S.C.I.C. #6079 Felt		
(a) muscle	16.7 (± 0.7)	23.2 (± 1.2)
(b) bone	19.2 (± 3.8)	14.7 (± 2.3)
U.S.C.I.C. #6108 Velour		
(a) muscle	12.8 (± 0.0)	11.3 (± 0.1)
(b) bone	13.0 (± 0.2)	13.1 (± 0.5)
U.S.C.I.C. #KG-1125 Velour		
(a) muscle	5.2 (± 0.0)	6.6 (± 0.6)
(b) bone	6.5 (± 0.5)	5.7 (± 0.5)

configurations, and (2) to determine the effect of environment on the materials in order to predict or justify loads for tensile failure during in-vivo mechanical testing. Results are based on two tests each for each fabric configuration and treatment.

In-Vivo Mechanical Testing

Muscle implants. The graphs shown in Figs. 8-11 indicate the average test results for the four muscle implant fabrics during the 2-month study. Results are based on averaging the load values obtained from three rabbits at each of the 2-, 4-, 6-, and 8-week intervals. A 12-week study is currently in progress.

Bone Implants

Table III lists the test results for the bone implants, based on the individual load values obtained from three dogs at each of the 2-, 4-, 6-, and 8-week intervals. Those data with an asterisk (*) indicate external tensile failures in the fabrics before they could be removed from the bone.

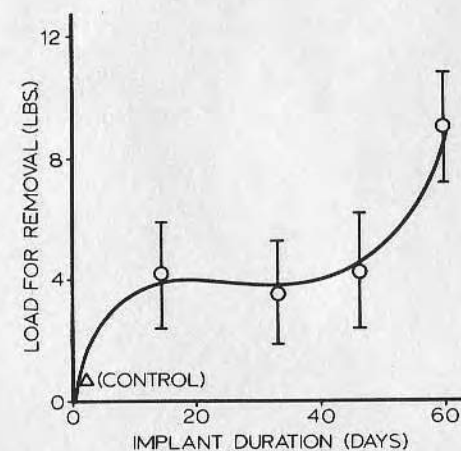


Fig. 8. Load to failure curve of single velour at musculo-tendinous junction.

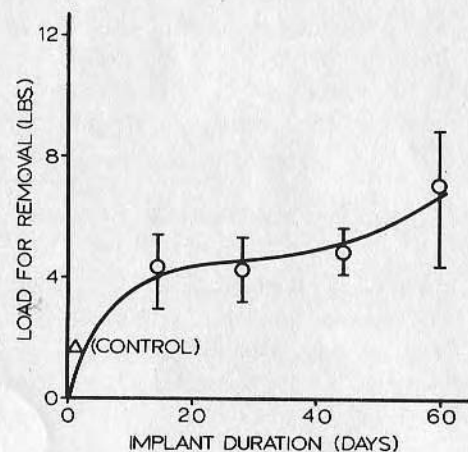


Fig. 9. Load to failure curve of double velour at musculo-tendinous junction.

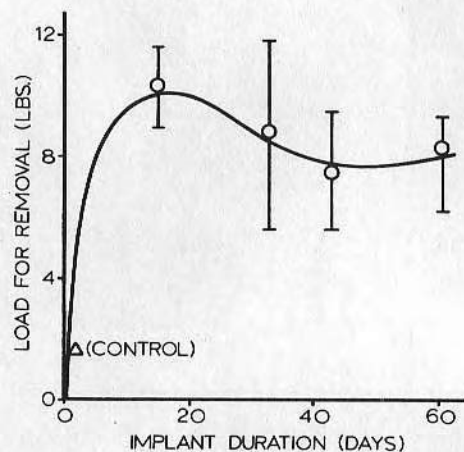


Fig. 10. Load to failure curve of felt at musculo-tendinous junction.

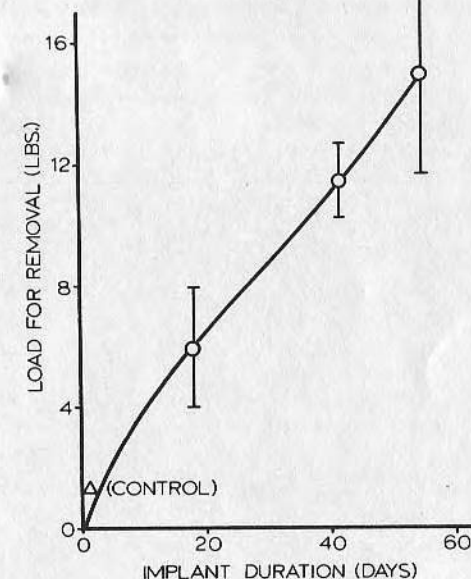


Fig. 11. Load to failure curve of braided cord at musculo-tendinous junction.

Histology

Representative histology sections for both the muscle and bone implant fabrics after four weeks implantation are shown in Figs. 12-14.

Animal Mortality

During the 3-month study, four rabbits died of pneumonia, and approximately 20% of the remainder developed infection in at least one limb. The source of infection is presumed to be primarily due to migration of the relatively stiff implant end tabs, which were often noted to present themselves at the skin surface. Future studies call for the fixation of the implant end tabs to their underlying tissues. No infections were noted in the

TABLE III

In-Vivo Mechanical Characterization of Bone Implants

Dog I. D. #	Time Implanted (Days)	Load for Pull-Out			
		#6079 Felt	Eimco Cord	#6108 Velour	#KG-1125 Velour
13	14	16.0*	18.8	8.8	8.8*
14	14	18.4	18.8	9.2	13.6*
21	14	8.0*	16.0	5.0	12.5*
18	28	22.5*	22.0*	22.0*	17.5*
15	42	22.0*	28.0	5.0*	8.0*
16	42	20.0*	26.0*	6.0*	13.0*
17	42	21.0*	23.0	5.8*	6.0*
10	56	9.0*	>28.0	4.5*	7.0*
11	56	11.0*	>25.0	**	**
12	56	14.0*	30.0*	**	**

* Fabric tensile failure outside bone.

** Implants severed during surgical exposure.



Fig. 12. Histologic section, H & E stain of Dacron felt in bone at 4 weeks.

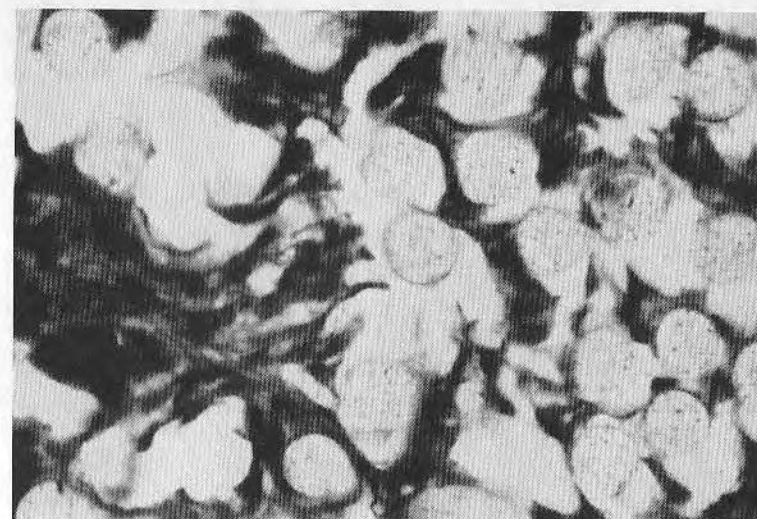


Fig. 13. Histological section of Dacron felt at musculo-tendinous junction at 4 weeks.



Fig. 14. Histological section of Dacron felt at musculo-tendinous junction at 4 weeks.

dog studies. One dog developed distemper 2 weeks postoperatively, and was immediately sacrificed for testing before the condition progressed. One dog died of an anesthesia overdose during surgery.

DISCUSSION

Fabric Characterization

Porosity. As seen in the data of Table I, little fabric porosity variation was noted in the U.S.C.I.C. implant materials regardless of overall fabric surface structure.

The most notable variation is that of the hand fabricated braided Dacron cord, which showed a porosity nearly 8 times greater than any of the three other materials evaluated.

Wesolowski (27) has concluded that a biological porosity of approximately 10,000 (ml H₂O/cm²)/min is ideal for producing a normal wound-healing response in the presence of a foreign material, and that the threshold value for long-term viable tissue ingrowth in the presence of a foreign material is near the 5,000 (ml H₂O/cm²)/min range. Thus, it may be assumed (as does Wesolowski), that the reported porosity values near 4,000 (ml H₂O/cm²)/min lie within this acceptable range. If this is true, then strictly from a porosity evaluation, the hand-fabricated Dacron cord, which possesses a porosity of greater than 32,000 (ml H₂O/cm²)/min, should show greater tissue ingrowth and biological acceptance when compared to the other materials. However, it should be noted that the Wesolowski findings are based on arterial tissue ingrowth and thus may show no correlation with muscle and bone tissue in growth.

Tensile strength tests. The results of Table II indicate that within experimental error there does not appear to be a significant change in fabric strength due to this specific in-vitro environment. However, with long-term implantation polyester does seem to show a gradual embrittlement, as indicated by Leininger (28) who reported an increase in stress at fracture from 18,300 to 18,400 psi and no change in per cent strain at fracture for Mylar over a period of 17-months implantation. This would indicate that our evaluation technique did not simulate a

long-term in-vivo evaluation, but possibly might be indicative of material changes within the relatively short 2-month period covered in this report.

Further studies in this area are currently being performed.

In-Vivo Mechanical Testing

Muscle implants. The significant outcome of the in-vivo mechanical testing is the fact that in the initial 2-month study, implant strength appears to primarily depend on the internal fabric porosities, and not on their various surface morphologies. This is clearly seen in Figs. 8 and 9, which represent the data for both the one- and two-sided U.S.C.I.C. Dacron velours.

The ratio of the total velour surface of the two-sided velour (U.S.C.I.C. #Kg-1125) compared to the one-sided velour (U.S.C.I.C. #6108) is about 2:1, respectively. Thus, if surface geometry is significant for ingrowth, the two-sided velour should show a measurable increase in implant strength over the 2-month period.

Comparison of Figs. 8 and 9 shows no difference between the two fabrics. Thus, it is felt that the contribution of surface structure to implant strength can be considered negligible for implantations of less than 2 months duration. The main criteria for implant adhesion and corresponding tissue ingrowth appears to be fabric porosity, with the greater porosity yielding the greater adhesion.

From the mechanical testing data for an implant geometry as used in this study, a fabric porosity of approximately 4000 (ml H₂O/cm²)/min results in a fabric pull-out strength of between 7 and 8 lbs in 8 weeks, whereas a fabric porosity of approximately 32,000 (ml H₂O/cm²)/min results in a fabric pull-out strength between 14 and 16 lbs in 8 weeks.

Histology

Histologic examination of specimens has not yet been completed. Review of representative sections of the basic implants show callus formation and incorporation of the fibers of

the Dacron felt as early as 4 weeks. There is very little foreign body reaction about the material in the bone (Fig. 14). This is in contrast to the specimen implanted in the musculotendinous junction. Here marked reaction is seen (Figs. 12 and 13). The individual Dacron fibers appear to be surrounded by fibro-blasts in a vascular matrix. No significant collagen fibers have been seen forming about the Dacron. Considerable technical difficulties have been encountered in sectioning specimens, however, no conclusions are being drawn from this portion of the study as yet.

The authors of this paper greatly appreciate the efforts of R. Wright, D. Malm, B. Holt, Dr. D. Loken, and R. Van Wagenen for their contributions to this research effort.

This project was made possible by a grant from the National Science Foundation.

APPENDIX I

Conventional Paraffin Soft-Tissue Technique

References

1. Removed implant and surrounding tissue are placed in a 10% formalin solution.
2. Sample rinsed with continuous flow of H₂O for 24 hr.
3. Sample placed in 70% ethyl alcohol (C₂H₅OH) for 24 hr (fresh solution every 12 hr).
4. Sample placed in 95% ethyl alcohol for 24 hr (fresh solution every 12 hr).
5. Sample placed in 100% ethyl alcohol for 24 hr (fresh solution every 12 hr).
6. Sample placed in 100% xylene for 24 hr (fresh solution every 12 hr).
7. Sample placed in 50% xylene-50% paraffin in warming oven at 50°-60°C for 24 hr (fresh solution every 12 hr).
8. Sample placed in 100% paraffin in warming oven at 50°-60°C for 48 hr.
9. Sample blocked, microtome sectioned, and transferred to microscope slide.
10. Sample stained with hematoxylin and eosin.

APPENDIX II

Modified Hard-Tissue Technique

References

1. Follow Procedures 1-5 in Appendix I.
2. Sample placed in solution consisting of 53 vol% Shell Epon 812 Epoxy, and 47% NMA (Nadic Methyl Anhydride), and vacuum-dessicated overnight.

3. Two vol% Rohm & Haas DMP-30 is then added to the solution in (2) and the entire solution containing the specimen allowed to cure in a warming oven at 60°C overnight.
4. The sample surface is then polished using standard metallographic techniques.
5. Sample surface-stained with Paragon frozen section multiple stain.
6. Sample surface is then observed using incident light microscope techniques.

References

1. McFarland, G. B.: Flexor Tendon Prosthesis, U.S. Patent #3, 613, 120, October 19, 1971.
2. Henze, C. W., and Mayer, L.: *Surg. Gynecol. Obstet.*, 21, 10 (1914).
3. Wheeldon, T.: *J. Bone Joint Surg.*, 21, 393 (1939).
4. Goeniedtian, S. A.: *Arch. Surg.*, 26, 181 (1949).
5. Koth, D. R., and Sewell, W. H.: *Surg. Gynecol. Obstet.*, 101, 615 (1955).
6. Ashley, F. L., et al.: *Plast. Reconstruct. Surg.*, 23, 526 (1959).
7. Nichols, H. M.: *Ann. Surg.*, 129, 223 (1949).
8. Gonzalez, R. I.: *Surgery*, 36, 181 (1949).
9. Gonzalez, R. J.: *Plast. Reconstruct. Surg.* 23, 562 (1958).
10. Hochstrasser, A. E., et al: *Rocky Mt. Med. J.*, 57, 30 (1960).
11. Ashley, F. L.: *The Bulletin*, Dow Corning Center, Vol. 4, July 1962.
12. Thatcher, H. H.: *S. Med. J.* 32, 13 (1939).
13. Mayer, L., and Ransohoff, N.: *J. Bone Joint Surg.*, 18, 607 (1936).
14. Davis, L. and Aries, L. J.: *Surgery*, 2, 877 (1937).
15. Hanisch, C. M. and Kleiger, B.: *Bull. Hosp. Joint Dis.*, 9, 22 (1948).
16. Milgram, J. E.: *Bull. Hosp. Joint Dis.*, 21, 250 (1960).
17. Anzel, S. H. et al.: *Am. J. Surg.*, 101, 355 (1961).
18. Sarkin, T. L.: *British J. Plast. Surg.*, 44, 232 (1956).
19. Arkin, A. M., and Siffert, R. S.: *Am. J. Surg.*, 85, 795 (1953).
20. Grau, H. R.: *J. Plast. Reconstruct. Surg.*, 22, 562 (1958).
21. Sakata, Y.: *J. Japan Orthop. Ass.*, 36, 1021 (1962).
22. Williams, R. D.: *Sci. Forum*, 11, 39 (1960).
23. Carroll, R. E., et al.: Formulation of Tendon Sheaths by a Silicone Rod Implant, paper presented at the 18th Annual Meeting of the Am. Soc. for Surg. of the Hand, January 1963.
24. Hunter, J. M.: *Am. J. Surg.*, 109, 325 (1965).
25. Bader, D. F., et al.: *J. Plast. Reconstruct. Surg.*, 41, 157 (1968).
26. Wesolowski, J. A.: *Ann. N.Y. Acad. Sci.*, 146, 325 (1968).
27. Klawitter, J. J.: Workshop 1—Bio Evaluation of Hard Material Implants. Paper presented at Symposium-Workshop on Research Techniques in Biomaterials Evaluation, Clemson University, March 1971.
28. Leininger, R. I., et al.: *Trans. Am. Soc. Artif. Intern. Organs*, 10, 237 (1964).



Homogeneous Bioluminescence Assay for Galactosuria: Interference and Kinetic Analysis

Ji-yang Eu,^{*1} Chung-yih Wang,[†] and Joseph Andrade[‡]

^{*}Department of Materials Science and Engineering and [‡]Department of Bioengineering, University of Utah, Salt Lake City, Utah 84112; and [†]Protein Solutions, Inc., Salt Lake City, Utah

Received December 18, 1998

Elevated galactose concentration in urine is an important clinical symptom of galactosemia and other metabolic disorders. A quantitative assay for galactose using firefly luciferase bioluminescence is presented. The assay couples the galactokinase and firefly luciferase reactions. A higher concentration of galactose present in the sample produces a faster decrease in ATP concentration, which is monitored by firefly luciferase bioluminescence. The kinetic assay is modeled and analyzed. The interference between the two reactions, the interference of certain sugars and other components in the urine, the specificity, and the optimal pH for galactokinase were studied. Calibration curves were constructed and compared with a conventional spectrophotometric assay for galactose. The bioluminescence assay is relatively fast and specific for galactose with a linear range from 1 to 20 mM galactose. The effect of other galactose metabolites (galactonate and galactitol) has also been studied. © 1999 Academic Press

Galactose is normally metabolized to glucose through the coordinated activities of three key enzymes in galactose metabolism: galactokinase, galactose-1-phosphate uridylyltransferase (GALT), and uridine diphosphate 4'-epimerase. Deficiency of any one of the three enzymes is diagnosed as galactosemia (1, 2). Galactosemia is an autosomal recessive inherited disorder which leads to no or lower activity of one of these key enzymes in galactose metabolism (1, 2). Three types of galactosemia have been identified: galactokinase deficiency (type I), galactose-1-phosphate uridylyltransferase deficiency (type II), and uridine diphos-

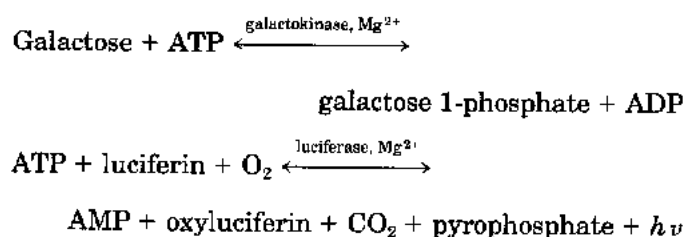
phate 4'-epimerase deficiency (type III). Type II galactosemia has the highest average incidence of 1:62,000 (2). Galactosemia generally leads to elevated galactose levels in biological fluids (3). Excretion of high concentration of galactose in urine (galactosuria) is an important clinical symptom of galactosemia. Galactosuria may also be the result of hepatitis, cirrhosis, carcinoma metastatic to liver, and hyperthyroidism (3). Newborns can be screened for galactosemia by measuring GALT activity and/or total galactose concentration (galactose + galactose 1-phosphate) in blood samples (4–6).

Several enzymatic assays have been developed for measuring galactose in urine. Most used is the galactose dehydrogenase-based assay, which converts urine galactose to nicotinamide dinucleotide (NADH); the concentration change of NADH is measured by spectrophotometry or fluorometry (7, 8). The assay is specific for galactose but requires a spectrophotometer or a fluorometer to detect the signal. The formation of NADH can also be measured by bacterial bioluminescence, an NADH-dependent process. Galactose concentration determination with bacterial bioluminescence has been reported by other workers (9, 10). Bacterial bioluminescence is more complicated than the firefly bioluminescence reaction. Galactose in urine has also been measured by galactose oxidase, which converts galactose to hydrogen peroxide (11). Hydrogen peroxide then reacts with peroxidase and a chromophore to produce a chromogenic end product. The oxidase-based galactose assay is less specific than the dehydrogenase-based assay since galactose oxidase utilizes lactose as a substrate to some extent. However, the oxidase-based assay produces a visually detectable color change which is beneficial for a dipstick-type assay (12). Quantitative determination of galactose using the oxidase-based assay requires a spectrophotometer or a colorimeter.

¹ To whom correspondence should be addressed at University of Utah, 50 S. Central Campus Dr., Rm. 2480, Salt Lake City, UT 84112-9202. Fax: (801) 583-4463. E-mail: Jiyang.Eu@m.cc.utah.edu.

The purpose of this article is to study the feasibility of using firefly luciferase bioluminescence to determine galactose in urine. Our preliminary study shows that the proposed assay may also determine galactose concentration in blood which might find use in galactosemia screening. Firefly luciferase bioluminescence emits a visible yellow-green light (562 nm) which can be detected by a luminometer, a charge-coupled device camera, photographic film, or even the unaided eye.

The proposed assay involves two biochemical reactions:



Firefly luciferase has been extensively used in determining ATP concentration (13). Firefly luciferase has unique reaction kinetics, due to product inhibition by oxyluciferin (14). When luciferin (a benzothiazole compound) and molecular oxygen are saturated, the bioluminescence time course shows a flash followed by a fast decay for ATP in the millimolar range. For micromolar concentrations of ATP (and below), the bioluminescence time course changes to almost constant light emission, suggesting that ATP consumption and product inhibition are less significant (15). For a "pseudo steady-state" light emission, the intensity is proportional to the concentration of ATP in the reaction mixture. When the two reactions are coupled together, a known micromolar concentration of ATP is included in the solution. ATP molecules competitively bind to both galactokinase and firefly luciferase. Since firefly luciferase consumes ATP in the micromolar range at a very slow rate, the depletion of ATP is mainly due to the phosphorylation of galactose by galactokinase. The bioluminescence time course basically "reflects" the concentration change of ATP in the solution. The rate of ATP consumption depends on the initial concentration of galactose present in the sample. A higher galactose concentration in the sample will lead to a faster depletion of ATP; thus, the firefly luciferase bioluminescence intensity decreases faster. A different concentration of galactose in the sample can thus be resolved by the light intensity decay.

MATERIALS AND METHODS

Chemicals

Galactokinase (from galactose adapted yeast), galactose 1-phosphate (dipotassium salt), D-galactose, D-glucose, D-fructose, lactose, sucrose, maltose, trehalose,

D-ribose, urea, uric acid, acetoacetic acid, β -hydroxybutyrate, adenosine 5'-triphosphate (disodium salt), bovine serum albumin (BSA),² galactitol, galactonate, and glycine-glycine buffer were purchased from Sigma (St. Louis, MO). Luciferin was obtained from Molecular Probes (Eugene, OR). $\text{MgSO}_4 \cdot 7\text{H}_2\text{O}$ was purchased from Mallinckrodt (Chesterfield, MO). Ascorbic acid and sodium chloride were purchased from Fisher Scientific (Fairlawn, NJ). Gly-gly buffers were prepared at two concentrations: 0.45 and 0.025 M. pH of the buffers was adjusted to 7.8 by adding 5 N NaOH. Firefly luciferase (*Photinus pyralis*) was produced recombinantly and preserved in 0.45 M gly-gly buffer. The protein concentration of firefly luciferase was measured with a Beckman 35 UV-VIS spectrophotometer at 280 nm. The luciferase carries a BCCP (biotin carboxyl carrier protein) domain (16). The extinction coefficient used to calculate protein concentration is $0.7 \text{ ml} \cdot \text{mg}^{-1} \text{ cm}^{-1}$.

Enzyme Activity Determination

Luciferase. Fifty microliters of 10 mM ATP in 0.45 M gly-gly buffer, 40 μl of 1 mg/ml BSA in 0.45 M gly-gly buffer, and 10 μl of 5 $\mu\text{g}/\text{ml}$ luciferase in 0.45 M gly-gly buffer were mixed in a $12 \times 50\text{-mm}$ disposable polypropylene test tube. Fifty microliters of 0.1 mM luciferin/10 mM $\text{MgSO}_4 \cdot 7\text{H}_2\text{O}$ in 0.025 M gly-gly buffer was added to the tube by an autoinjector. Bioluminescence was recorded by a Turner TD 20/20 luminometer for 10 s. The flash peak intensity divided by total amount of luciferase in the assay is used to represent the specific activity of the enzyme. The whole procedure was repeated three times with a fixed luciferase concentration. The averaged specific activity from three runs is $7.1 \pm 0.21 \times 10^8$ relative light units (RLU)/mg.

Galactokinase (17). D-Galactose (100 mM), 5.9 mM ATP, 16.2 mM phospho(enol) pyruvate (PEP), 800 mM KCl, 100 mM MgCl_2 , and 20 mM ethylenediaminetetraacetic acid (EDTA) were prepared in reagent grade water. β -Nicotinamide adenine dinucleotide (3.76 mM, β -NADH) was prepared in 160 mM potassium phosphate buffer. A pyruvate kinase/lactate dehydrogenase mixture was prepared in 1:1 volume ratio of glycerol and 0.45 M gly-gly buffer. The total activity of pyruvate kinase and lactate dehydrogenase was 500 and 200 U/ml, respectively. Then, 5.75 ml of 160 mM potassium phosphate buffer, 1.5 ml of ATP, 1.5 ml of PEP, 1.5 ml of KCl, 1.5 ml of MgCl_2 , 1.5 ml of EDTA, and 0.5 ml of β -NADH were mixed together as a reaction cocktail. The pH of reaction cocktail was adjusted to 7 at room temperature with 1 N HCl or 1 N NaOH if necessary.

² Abbreviations used: BSA, bovine serum albumin; BCCP, biotin carboxyl carrier protein; PEP, phospho(enol)pyruvate; RLU, relative light units; DTT, dithiothreitol; BAR, bioluminescence assay reagent.

Then 917 μ l of reaction cocktail was added to a quartz cuvette, followed by 17 μ l of pyruvate kinase/lactate dehydrogenase mixture, and 33 μ l of galactokinase solution. The reaction was started by adding 33 μ l of 100 mM galactose. Absorbance was measured with a Beckman-35 UV-VIS spectrophotometer at 340 nm. Absorbance was recorded immediately after the addition of galactose and every minute afterward up to 5 min. Background absorbance change can be measured by replacing galactokinase solution with buffer. The activity of galactose was calculated from the change of absorbance according to the equation

$$\text{Units/mg} = \frac{\Delta A_{340 \text{ nm}}/\text{min test} - \Delta A_{340 \text{ nm}}/\text{min blank}}{(6.22)(x \text{ mg/ml RM})},$$

where 6.22 is the millimolar extinction coefficient of β -NADH at 340 nm, RM refers to reaction mixture; x is the total amount of galactokinase in 1-ml reaction mixture.

Cross Interference from Galactokinase Reaction to Firefly Luciferase Reaction

Galactose 1-phosphate. Three different concentrations of galactose 1-phosphate were prepared in 0.025 M gly-gly buffer: 0.67, 3.35, and 6.7 mM. Fifty microliters of ATP (2, 4, 20, 40, and 200 μ M), 50 μ l of galactose 1-phosphate, 0.1 μ l of 0.5 μ g/ml luciferase in 0.45 M gly-gly buffer, and 49.9 μ l of 1 mg/ml BSA were mixed in a 12 \times 50 mm polypropylene test tube. Fifty microliters of 0.1 mM luciferin/10 mM $\text{MgSO}_4 \cdot 7\text{H}_2\text{O}$ in 0.025 M gly-gly was added by an autoinjector. Bioluminescence was recorded by a Turner TD 20/20 luminometer for 20 s.

Galactokinase. Ten microliters of various concentrations of galactokinase (20, 10, 1, 0.1, 0.01, 0.001 U/ml), 50 μ l of 40 mM ATP in 0.45 M gly-gly buffer, 30 μ l of 1 mg/ml BSA in 0.45 M gly-gly buffer, and 10 μ l of 2.5 μ g/ml firefly luciferase were mixed in a 12 \times 50-mm disposable test tube. Bioluminescence was initiated by adding 0.1 mM luciferin/10 mM $\text{MgSO}_4 \cdot 7\text{H}_2\text{O}$ mixture using an autoinjector. Bioluminescence was recorded with a Turner TD 20/20 luminometer for 20 s.

Galactose. Galactose standards were prepared in 0.025 M gly-gly buffer (50, 150, and 250 μ M). ATP solutions were prepared in 0.025 M gly-gly buffer (4, 6, 8, and 15 μ M). Fifty microliters of ATP solution, 50 μ l of galactose solution, 10 μ l of 6.3 μ g/ml firefly luciferase, and 40 μ l of 1 mg/mL BSA were mixed in a 12 \times 50-mm polypropylene test tube. Bioluminescence was initiated by adding 100 μ l of 0.1 mM luciferin/10 mM $\text{MgSO}_4 \cdot 7\text{H}_2\text{O}$ mixture. Bioluminescence was recorded for 20 s with a Turner TD-20/20 luminometer.

Cross-Interference from Firefly Luciferase Reaction to Galactokinase Reaction

Luciferase. Similarly to the galactokinase activity determination, different amounts of luciferase were added to the reaction cocktail. Then 917 μ l of reaction cocktail with luciferase was added to quartz cuvette. The reactions were started by adding 17 μ l of pyruvate kinase/lactate dehydrogenase mixture, 33 μ l of 0.4 U/ml galactokinase, and 33 μ l of 100 mM galactose. The final concentrations of luciferase in the assay were 810, 81, and 8.1 nM. Absorbance was recorded immediately after the reaction started and every minute afterward up to 3 min.

Luciferin. The same procedure used in investigating the effect of luciferase on galactokinase was applied to investigate the effect of luciferin. The final concentrations of luciferin were 25, 2.5, and 0.25 μ M.

Specificity of Galactokinase

Concentrations (10 mM) of D-galactose, D-glucose, D-fructose, lactose, maltose, sucrose, trehalose, and D-ribose were prepared in reagent grade water. In microtiter wells, 25 μ l of 0.8 mg/ml BSA/8 mM dithiothreitol (DTT) mixture, 20 μ l of 2 U/ml galactokinase, 25 μ l of 10 mM sugar solution, and 25 μ l of 0.45 M gly-gly buffer were mixed together. The galactokinase reaction was initiated by adding 25 μ l of 50 mM $\text{MgSO}_4 \cdot 7\text{H}_2\text{O}$ and 50 μ l of 1 mM ATP in 0.45 M gly-gly buffer. Two minutes later, the bioluminescence assay reagent was added to the microtiter well. The bioluminescence assay reagent (BAR) consisted of 10 μ l of 0.25 mg/ml firefly luciferase and 20 μ l of 2 mM luciferin. Bioluminescence was recorded by a Santa Barbara Instrument Group ST-6 CCD camera at 1, 8, and 28 min after the addition of the BAR. The integration time of the CCD camera was 20 s. Controls were performed by replacing sugar solutions with reagent grade water.

Interference from Sugars and Key Urine Components

Concentrations (10 mM) of glucose, fructose, lactose, maltose, sucrose, trehalose, and D-ribose, 0.4 M NaCl, 0.5 M urea, 5 mM uric acid, 7.4 mM acetoacetic acid, 2.84 mM ascorbic acid, and 0.58 mM hydroxybutyrate were prepared in reagent grade water. In microtiter wells, 20 μ l of 8 mg/ml BSA/8 mM DTT, 20 μ l of 2 U/ml galactokinase, 25 μ l of 10 mM galactose in 0.025 M gly-gly buffer were mixed. The galactokinase reaction was initiated by adding 25 μ l of 50 mM $\text{MgSO}_4 \cdot 7\text{H}_2\text{O}$ and 50 μ l of 1 mM ATP in 0.45 M gly-gly buffer. Two minutes later, the BAR was added to the microtiter well. Light was recorded by a SBIG ST-6 CCD camera at 1, 8, and 28 min after the addition of the BAR. The integration time of the CCD camera was 20 s. Controls were performed by replacing the interfering compo-

TABLE 1
Cross-Interference between Galactokinase Reaction and Luciferase Reaction

System	Interfering component	Concentration (μ M)	Change in I_{\max} (%)	Concentration (μ M)	Change in I_{\max} (%)	Concentration (μ M)	Change in I_{\max} (%)
Luciferase	D-Galactose	20	+4.1	60	-2	100	-0.4
	Galactokinase	2.2×10^{-5}	-5	2.2×10^{-4}	-7	2.2×10^{-3}	-7.6
	Galactose 1-phosphate	170	-5.1	850	-2.4	1700	+3.9
	Interfering component	Concentration (μ M)	Change in $\Delta A_{340\text{nm}}$ (%)	Concentration (μ M)	Change in $\Delta A_{340\text{nm}}$ (%)	Concentration (μ M)	Change in $\Delta A_{340\text{nm}}$ (%)
Galactokinase	Luciferase	0.008	+6	0.08	+0.5	0.8	-1
	Luciferin	0.25	-0.5	2.5	+4	25	-0.5

Note. The effect on enzyme activity is calculated by comparison to the control. Maximal bioluminescence intensity is proportional to the activity of firefly luciferase. The absorbance change (over 1 min) is proportional to the activity of galactokinase. For galactose 1-phosphate, only the data for 250 μ M ATP were listed. For galactose, only the data for 4 μ M ATP were listed. Other ATP concentrations showed similar results.

nents with reagent grade water. The whole procedure was performed again to study the interfering effects on luciferase by replacing galactokinase solution with 0.45 M gly-gly buffer.

Galactose Concentration Determination with Bioluminescence

Galactose standards (1, 2, 4, 6, 8, 10, 15, and 20 mM) were prepared in Syscon standard urine (lot No. C8102C, Santee, CA). Ten microliters of 40 μ M ATP in 0.45 M gly-gly buffer, 20 μ l of 4.5 μ g/ml firefly luciferase in 0.45 M gly-gly buffer, 2 μ l of 1 U/ml galactokinase in 1 mg/ml BSA, and 28 μ l of 1 mg/ml BSA were mixed in a 1.7-ml microcentrifuge tube. Ten microliters of galactose standard was added followed by the addition of 50 μ l of 0.1 mM luciferin/10 mM $\text{MgSO}_4 \cdot 7\text{H}_2\text{O}$ mixture in a 0.025 M gly-gly buffer with an autoinjector. Bioluminescence was recorded by a Turner TD 20/20 luminometer for 300 s.

Effect of Galactonate and Galactitol

Galactose standards (5 and 10 mM) were prepared in Syscon standard urine (lot No. C8102C). Each galactose standard was spiked with 2.5 mM galactonate/12.5 mM galactitol and 25 mM galactonate/125 mM galactitol. Galactose concentration was determined as described previously. Bioluminescence was recorded for 180 s.

RESULTS AND DISCUSSION

Cross-Interference between the Two Reactions

One of the most important considerations in coupled reactions is the possible cross-interference between the two reactions. Cross-interference must be minimized. The activity of firefly luciferase was determined in the

presence of the substrates from the galactokinase reaction, and vice versa. The results are summarized in Table 1.

For the firefly luciferase reaction, the alteration in enzyme activity was represented by normalizing the peak intensity to the control (no interfering components). For the galactokinase reaction, the effect was calculated by normalizing the absorbance change at 340 nm to the control, since the activity was determined using a spectrophotometer. From Table 1, all the results show less than 7.6% change in enzyme activities. This suggests that cross-interference is small when the two reactions are coupled. In addition to the components studied in Table 1, the adenosine 5'-diphosphate (ADP) product from the galactokinase reaction has been known to be a competitive inhibitor for ATP in the firefly luciferase reaction ($K_i = 2.5$ mM) (18). Since the initial ATP concentration in the assay was 3.3 μ M, ATP was the limiting substrate for both galactokinase and firefly luciferase. The final concentration of ADP in the assay should be less than 3.3 μ M, far below its inhibition constant. The ADP formed during the reaction should not significantly influence the activity of firefly luciferase. The results suggest that the reaction of galactokinase and firefly luciferase do not interfere with each other, assuring that a homogeneous assay for galactose is practical.

Specificity of Galactokinase and Effect of Key Urine Components and Sugars

The specificity of galactokinase was studied using the firefly luciferase bioluminescence assay. The concentration change of ATP in the galactokinase reaction can be monitored by bioluminescence in the presence of different sugars. The decrease of bioluminescence intensity can be interpreted as the activity of galactoki-

TABLE 2
Specificity of Galactokinase and the Effect of Sugars and Key Components in Urine

Components	Final concentration (mM)	Galactokinase activity at various pH (% of activity at pH 8.6) ^a	Specificity of galactokinase (% of intensity normalized to the control) ^a	Interference to galactokinase (% of intensity normalized to the control) ^b	Interference to firefly luciferase (% of intensity normalized to the control) ^b
pH 6.2	—	42.1	—	—	—
pH 7.0	—	62.7	—	—	—
pH 7.8	—	87	—	—	—
pH 8.6	—	100	—	—	—
ATP	0.25	—	100	—	100
D-Galactose	1.25	—	43.8	100	101
D-Glucose	1.25	—	101.6	103.3	100.6
D-Fructose	1.25	—	101.7	104.8	101
Lactose	1.25	—	103	107	100.7
Maltose	1.25	—	102.6	109.2	100.7
Sucrose	1.25	—	101.1	104	99.6
Trehalose	1.25	—	101.5	97	99.2
D-Ribose	1.25	—	98.3	101.2	97.2
NaCl	50	—	—	59	72.8
Urea	62.5	—	—	94.6	100.7
Uric acid	0.625	—	—	100.7	101.2
Acetoacetic acid	0.925	—	—	97	102.1
Hydroxy butyrate	0.073	—	—	107	101.4
Ascorbic acid	0.355	—	—	94.3	101.6

Note. All the numbers shown in the table are the percentage of bioluminescence intensity normalized to the control.

^a Galactokinase activity was calculated from the bioluminescence decrease during the first minute of the reaction and then normalized to the activity at pH 8.6.

^b The values were calculated using the bioluminescence intensity at 30 min after the galactokinase reaction. For the definition of the controls, please refer to Materials and Methods.

nase when normalized to the control (no added sugar). D-Galactose, D-glucose, D-fructose, lactose, sucrose, maltose, trehalose, and D-ribose were all used as substrates, individually, for galactokinase (Table 2, column 4).

All sugars showed negligible light intensity decrease or increase over a 30-min reaction time, except for galactose. Galactokinase using galactose as substrate retained only 43.8% of light intensity compared to the control, which suggests that yeast-adapted galactokinase is specific for galactose in the group of sugars we chose to study. The optimal pH for galactokinase activity was also studied using bioluminescence under conditions similar to those in the specificity studies. Galactokinase showed optimal activity at pH 8.6 (Table 2, column 3). However, the activity decreased only 13% from pH 8.6 to 7.8. An assay pH of 7.8 was chosen since this is the optimal pH for firefly luciferase (19). Our results for optimal pH and specificity of galactokinase agree with the work of Schell and Wilson (20).

In addition to the specificity of galactokinase, the effects of sugars and key components in the urine were also studied (Table 2, column 5). Key components in urine include sodium chloride, urea, uric acid, acetoacetic acid, hydroxybutyrate, and ascorbic acid; all were tested. All the components tested showed slight

decreases or increases except for 50 mM NaCl. In the presence of 50 mM NaCl, the intensity was 59% of the control (Table 2, column 5), suggesting that the activity of galactokinase is enhanced (more ATP is consumed, light intensity is lowered) and/or the activity of firefly luciferase is inhibited by NaCl.

The effects of sugars and key urine components were also studied for firefly luciferase (Table 2, column 6). NaCl (50 mM) showed an inhibitory effect on firefly luciferase (72.8% of bioluminescence intensity compared to the control), suggesting that the observed inhibitory effect of NaCl on bioluminescence intensity for galactokinase (Table 2, column 5) is mainly due to the inhibition of firefly luciferase. Cl^- has been reported as an inhibitor of firefly luciferase with an inhibition constant $K_i = 130$ mM (21, 22). The Cl^- concentration in healthy urine ranges from 110 to 250 mM (23). Altered Cl^- concentration in galactosemia patients has not been reported. Also, the defective galactose metabolism should not affect Cl^- concentration in urine. Our standard assay involves a dilution factor of 12; thus the actual Cl^- concentration ranges from 9.2 to 20.8 mM. A separate experiment showed that the activity of firefly luciferase is lowered by 6% as the concentration of chloride increased from 8 to 32 mM (data not shown). The result suggests that Cl^- has a

limited effect (less than 6% variation) in the actual assay. However, the pathological state of galactosemia does lead to the presence of other galactose metabolites in urine; the effect of these metabolites will be discussed later.

Galactose Concentration Determination with Bioluminescence Assay

Gulbinsky and Cleland studied the kinetics of *Escherichia coli* galactokinase in 1968 (24). Their studies showed that *E. coli* galactokinase follows random bi-bi kinetics, so a steady-state rate equation can be derived:

$$v = \frac{V_1 \left[AB - \frac{PQ}{K_{eq}} \right]}{K_{ia}K_b + K_bA + K_aB + AB + \frac{K_{ia}K_bP}{K_{ip}} + \frac{K_{ia}K_bQ}{K_{iq}} + \frac{K_{ia}K_bPQ}{K_{ip}K_{iq}} + \frac{K_{iq}K_bAP}{K_{ip}K_{ia}} + \frac{K_{ia}K_bBQ}{K_{iq}K_{ib}}}, \quad [1]$$

where, following traditional enzyme reaction nomenclature, A, B, P, and Q represent the concentrations of galactose, ATP, ADP, and galactose 1-phosphate, respectively. In Eq. [1], K_a and K_b are the Michaelis-Menten constants for galactose and ATP, respectively. V_1 is the maximal reaction velocity of the forward direction and K_{eq} is the equilibrium constant. K_{ia} and K_{ib} are the inhibition constants for galactose and ATP, respectively (please refer to the original article for the definition of the rest of the kinetic constants). At the beginning of the reaction, the concentration of the product of P and Q can be assumed to be close to zero, so the reverse reaction is actually negligible. K_a is an index for the affinity between galactose and the ATP-saturated galactokinase and K_{ia} represents the affinity between galactose and the free galactokinase, respectively. If we further assume that K_a is equal to K_{ia} (in Gulbinsky and Cleland's study, the values of K_a and K_{ia} were very similar under certain reaction conditions), then Eq. [1] can be simplified to:

$$v = \frac{V_1 AB}{K_a K_b + K_b A + K_a B + AB} = V_1 \left(\frac{A}{K_a + A} \right) \left(\frac{B}{K_b + B} \right) \quad [2]$$

The Michaelis-Menten kinetic constants for yeast galactokinase are $K_{m(ATP)} = 0.15$ mM (K_b) and $K_{m(galactose)} = 0.6$ mM (K_a), as originally reported by Schell and Wilson (19). The initial ATP concentration was 3.3 μ M in the proposed assay, much lower than the $K_{m(ATP)}$ for

yeast galactokinase ($B \ll K_b$), allowing Eq. [2] to be further simplified to:

$$v = -\frac{dB}{dt} = \frac{V_1 B}{K_b} \left(\frac{A}{K_a + A} \right). \quad [3]$$

The concentration of galactose (A) can be approximately given as the initial concentration of galactose (A_0), since the galactose concentration range we are interested in (millimolar) is in great excess compared to the concentrations of ATP and galactokinase. Equation [3] can now be solved for B:

$$B(t) = B_0 e^{-(V_1/K_b)(A_0/(K_a + A_0))t}, \quad [4]$$

where B_0 is the initial concentration of ATP. In the firefly luciferase reaction, the intensity time course switches from "flash-decay" kinetics to pseudo steady-state kinetics as the concentration of ATP decreases from millimolar to micromolar. In the pseudo steady-state emission (micromolar ATP) range, light intensity is proportional to the concentration of ATP. Equation [4] can thus be further modified to:

$$I = KB(t) = KB_0 e^{-(V_1/K_b)(A_0/(K_a + A_0))t} \\ = K[ATP]_0 e^{-(V_1/K_b)([gal]_0/(K_a + [gal]_0))t} \quad [5]$$

In Eq. [5], I represents the bioluminescence intensity and K is the proportionality constant between intensity and ATP concentration. The term of $K[ATP]_0$ is actually the initial bioluminescence intensity I_0 . Equation [5] predicts that the intensity-time course of the assay should follow an exponential decay, and the rate of decay is a function of the initial concentration of galactose. For very high concentrations of galactose (15–20 times higher than the K_m for galactose), the index of the exponential term in Eq. [5] will be constant since $[gal]_0$ is much greater than K_a ($[gal]_0 \gg K_a$). Thus the intensity decreases at the same rate for all high concentrations of galactose.

Figure 1 shows the light intensity profile for a homogeneous galactose assay from 0 to 300 s. The control experiment (Fig. 1, curve A, no added galactose) showed the typical pseudo steady-state kinetics of firefly luciferase with the expected slow decrease in light intensity. All the intensity time profiles reached a similar maximal intensity at about 3 s, suggesting that the delay in light emission is probably due to the mixing of the reactants. The decrease following the maximal light intensity agrees with exponential decay (fitted lines not shown, but R^2 for all the fitted curves are greater than 0.95, except for the control which ideally should be constant light emission). For higher concentrations of galactose in Fig. 1 (10, 15, and 20 mM), the

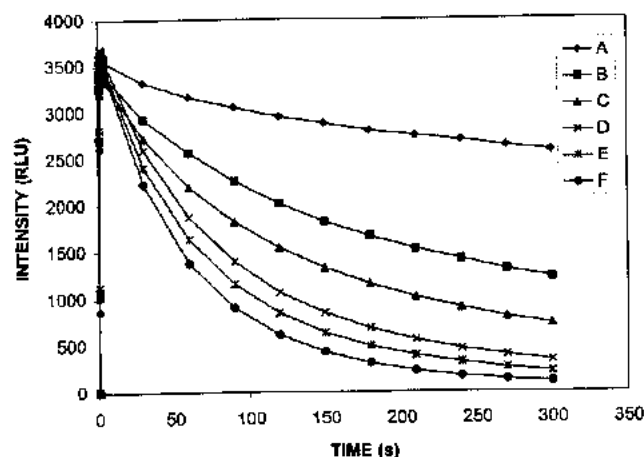


FIG. 1. Intensity time course in the presence of different concentrations of galactose: 0 (A), 2 (B), 4 (C), 10 (D), 15 (E), and 20 mM galactose (F). All galactose standards were prepared in Syscon standard urine.

decays are very similar due to the saturation of galactose, as described previously. In Eq. [5], if a certain observation time t_1 is chosen, then Eq. [5] can be further rearranged by taking natural logarithm:

$$\ln\left(\frac{I_0}{I_{t_1}}\right) = \left(\frac{V_1 t_1}{K_b}\right) \left(\frac{[\text{gal}]_0}{K_a + [\text{gal}]_0}\right) \quad [6]$$

By taking the reciprocal of both sides of Eq. [6], a linear relation between $1/\ln(I_0/I_{t_1})$ and $1/[\text{gal}]_0$ is derived:

$$\frac{1}{\ln(I_0/I_{t_1})} = \frac{K_b}{V_1 t_1} + \frac{K_b K_a}{V_1 t_1 [\text{gal}]_0}, \quad [7]$$

where the slope is $K_a K_b / V_1 t_1$ and the intercept is $K_b / V_1 t_1$. The plot of $1/(\ln(I_0/I_{t_1}))$ against $1/[\text{gal}]_0$ should produce a straight line (Fig. 2). Ideally, curve A in Fig. 1 (0 mM galactose) should remain a constant light output since there is no galactose present. However, there is about 10% light intensity decrease due to the firefly luciferase reaction for the first 60 s. This intensity decrease is compensated in Fig. 2 by adding the difference between I_{max} (0 mM galactose) and I_{60} (0 mM galactose) to the intensities at 60 s for other galactose-containing samples. It is reasonable to use the maximal light intensity (I_{max}) to approximate the initial light intensity (I_0) used in the mathematical analysis since different initial concentrations of galactose all reached similar maximal light intensity at roughly the same time due to mixing. In Fig. 2, the observation time was chosen to be 60 s ($t_1 = 60$ s) since most of the assumptions made in the derivation of Eq. [7] are valid at the beginning of the reaction.

Figure 2 shows a good linear fit ($R^2 = 0.99$) for urine containing 1 to 20 mM galactose. For normal newborns during the second to sixth day after birth, the galactose concentration in urine ranges from 0.02 to 6.27 mM with a mean of 1.13 mM, which is mostly covered by the linear range of the assay (7). For adults, the galactose concentration in urine ranges from 0 to 0.57 mM (25). To determine galactose concentration beyond the linear range, the sample needs to be diluted or concentrated. The lower detection limit (1 mM galactose) results from the slow consumption of ATP by galactokinase. At galactose concentration lower than 1 mM, the background ATP consumption by the firefly luciferase reaction becomes predominant. The higher detection limit (20 mM galactose) results from galactose saturation as described previously.

Standard urine was tested for ATPase activity and residual ATP concentration to assure the accuracy of the calibration curve in Fig. 2. Standard urine is essentially free of ATPase activity by measuring ATP concentration using firefly luciferase bioluminescence. Residual ATP concentration in the urine was 1.8 nM determined by firefly luciferase bioluminescence using internal ATP standards (26). Residual galactose in standard urine was 4.6 μM , determined by Biochemical Genetics Laboratory of Children's Hospital, Los Angeles, California. Since the galactose concentration in standard urine was spiked into the millimolar range, the residual galactose in standard urine is insignificant. The pH change due to the addition of stan-

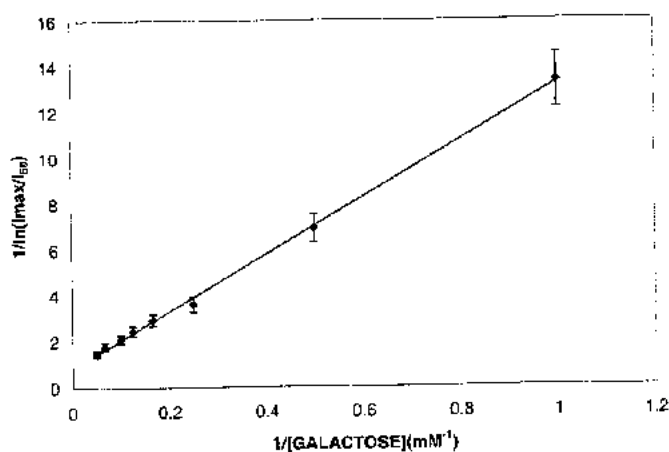


FIG. 2. The plot of $1/\ln(I_{\text{max}}/I_{60})$ versus $1/[\text{galactose}]_0$. The concentration of galactose standards used were 1, 2, 4, 6, 8, 10, 15, and 20 mM. Galactose standards were prepared in Syscon standard urine (level I). The intensity decrease due to the firefly luciferase reaction is compensated by adding the difference between I_{max} (curve A, 0 mM galactose) and I_{60} (curve A, 0 mM galactose) to intensities at 60 s of other galactose-containing standards. The data points shown here were the average of triplicates. The average coefficient of variation is 9% (indicated by the error bar). The fitted straight line has equation of $y = 12.44x + 0.8$ with $R^2 = 0.99$.

dard urine is negligible (from 7.8 to 7.67) since the assay has enough buffer capacity to maintain the pH.

The homogeneous bioluminescence assay was compared with the galactose dehydrogenase-based spectrophotometric assay (Fig. 3). The bioluminescence assay has a good agreement with the spectrophotometric assay using standards (1 to 8 mM galactose) prepared in Syscon standard urine.

The galactose dehydrogenase-based galactose assay is an end-point assay which requires an incubation period to convert the galactose present to NADH. The length of the incubation period also depends on the concentration of galactose present in the sample. For a high galactose sample, the assay generally needs at least 30 min to bring the reaction close to equilibrium. The kinetic bioluminescence assay requires a relatively short reaction time and provides similar accuracy over the physiological relevant concentration range.

Effect of Galactose and Galactonate

The pathological state of galactosemia triggers other metabolic pathways of galactose. Galactose can be further oxidized to galactonate by galactose oxidase or galactose dehydrogenase; also, it can be reduced to galactitol by an aldose reductase reaction (1). Both galactitol and galactonate are found in different tissues and urine collected from galactosemia patients. In urine, galactonate ranges from 0.18 to 10.6 mM and galactitol ranges from 0.51 to 118.7 mM (27). All the values are converted from millimole/mole creatinine by using an approximate urinary creatinine concentration

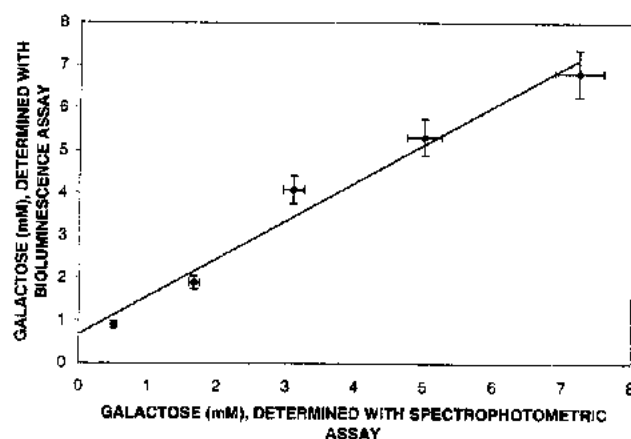


FIG. 3. Galactose concentration determination with both bioluminescence assay and the spectrophotometric assay. The values determined from both methods were the average of three measurements. The average coefficients of variation for the bioluminescence assay and spectrophotometric assay are 8% (vertical error bars) and 4.9% (horizontal error bars), respectively. The galactose concentrations used were 1, 2, 4, 6, and 8 mM. The fitted straight line has an equation of $y = 0.9x + 0.67$ with $R^2 = 0.97$.

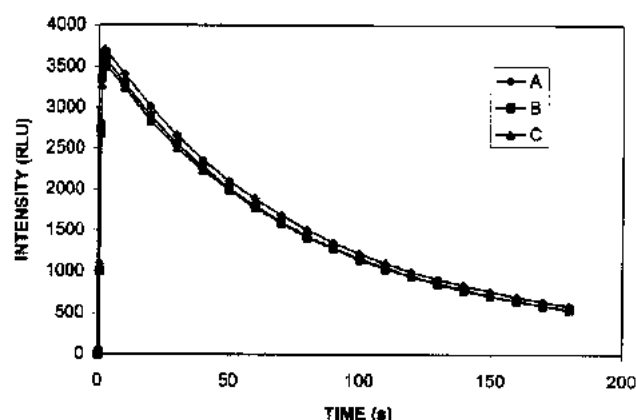


FIG. 4. Intensity time course at the presence of galactonate and galactitol: 0 mM galactonate/0 mM galactitol (A), 2.5 mM galactonate/12.5 mM galactitol (B), and 25 mM galactonate/125 mM galactitol (C). All the samples contained 10 mM galactose and were prepared in Syscon standard urine.

of 9 mM. The effect of galactonate and galactitol on the bioluminescence assay was studied with galactose containing standard urine spiked with galactonate and galactitol up to 25 and 125 mM, respectively. Figure 4 shows the intensity time course in the presence of galactonate and galactitol; all samples contained 10 mM galactose. All the curves in Fig. 4 are almost identical, which suggests that galactonate and galactitol have minimal effect on the assay up to 25 and 125 mM, respectively.

The galactose concentrations determined by using the standard curve in Fig. 2 are 9.28 ± 0.48 (curve A, 0 mM galactonate/0 mM galactitol), 10.37 ± 0.81 (curve B, 2.5 mM galactonate/12.5 mM galactitol), and 9.8 ± 0.73 mM (curve C, 25 mM galactonate/125 mM galactitol). All the values are the average of triplicates. The result demonstrates that the presence of galactonate and galactitol has minimal effect on the accuracy of the assay. Identical experiments were performed for standard urine with 5 mM galactose; a similar conclusion was derived.

ACKNOWLEDGMENTS

We thank Drs. R. Stewart and Dr. J. Lindsley for helpful discussions and laboratory space. This work is partially supported by the Whitaker Foundation, a University of Utah Graduate Research Fellowship, and Protein Solutions, Inc., Salt Lake City.

REFERENCES

1. Segal, S., and Berry, G. T. (1995) in *The Metabolic and Molecular Bases of Inherited Disease* (Scriver, C. R., Beaudet, A. L., Sly, W. S., and Valle, D., Eds.), pp. 967-1000, McGraw-Hill, New York.
2. Bientler, E. (1991) *Clin. Biochem.* **24**, 293-300.
3. Teitz, N. W. (1994) *Clinical Guide to Laboratory Tests*, Saunders, Philadelphia.

4. Webster, D., and Allen, D. (1994) in *Laboratory Methods for Neonatal Screening* (Terrell, B. L., Ed.), pp. 77–114, Am. Public Health Assoc., Washington, DC.
5. Dipenbrock, F., Heckler, R., Schickling, H., Engelhard, T., Bock, D., and Sander, J. (1992) *Clin. Biochem.* **25**, 37–39.
6. Misuma, H., Wada, H., Kawakami, M., Ninomiya, H., and Shohmori, T. (1981) *Clin. Chim. Acta* **111**, 27–32.
7. Dhalqvist, A., and Svenningsen, N. W. (1969) *J. Pediatr.* **75**(3), 454–462.
8. Orfanos, A. P., Jinks, D. C., and Guthrie, R. (1986) *Clin. Biochem.* **19**, 225–228.
9. Carlsson, H., Ljungerantz, P., Lindbladh, C., Persson, M., and Bulow, L. (1994) *Anal. Biochem.* **218**, 278–283.
10. Arthur, P. G., Kent, J. C., and Hartman, P. E. (1989) *Anal. Biochem.* **176**, 449–456.
11. Tengström, B. (1966) *Scand. J. Lab. Invest.* **18**:92, 104–113.
12. Dahlqvist, A. (1968) *Scand. J. Clin. Lab. Invest.* **22**:87, 87–93.
13. Brodin, S., and Wettermark, G. (1992) *Bioluminescence Analysis*, VCH, New York.
14. Lemasters, J. J., and Hackenbrock, C. R. (1977) *Biochemistry* **16**, No. 3, 445–447.
15. Wulff, K., Haar, H., and Michal, G. (1982) in *Luminescent Assays: Perspectives in Endocrinology and Clinical Chemistry* (Serio, M., and Pazzagli, M., Eds.), pp. 47–52, Raven Press, New York.
16. Wang, C. Y., Hitz, S., Andrade, J. D., and Stewart, R. J. (1997) *Anal. Biochem.* **246**, 133–139.
17. Henrich, M. R., and Howard, S. M. (1966) in *Methods in Enzymology* (Wood, W. A., Ed.), Vol. 9, pp. 407–412, Academic Press, New York.
18. Lee, R. T., Denberg, J. L., and McElroy, W. D. (1970) *Arch. Biochem. Biophys.* **141**, 38–52.
19. Webster, J. J., and Leach, F. R. (1980) *J. Appl. Biochem.* **2**, 469–479.
20. Schell, M. A., and Wilson, B. B. (1977) *J. Biol. Chem.* **252**, 1162–1166.
21. Denberg, J. L., and McElroy, W. D. (1970) *Arch. Biochem. Biophys.* **141**, 668–675.
22. Nichols, W. W., Curtis, G. D. W., and Johnston, H. H. (1981) in *Bioluminescence and Chemiluminescence: Basic Chemistry and Analytical Applications* (DeLuca, M. A., and McElroy, W. D., Eds.), pp. 485–490, Academic Press, New York.
23. Bishop, M. L., Duben-Engelkirk, J. L., and Fody, E. P. (1996) *Clinical Chemistry: Principles, Procedures, Correlations*, Lippincott, Philadelphia.
24. Gulbinsky, J. S., and Cleland, W. W. (1968) *Biochemistry* **7**, 566–575.
25. Hicks, J. M., and Young, D. S. (1997) *Directory of Rare Analyses*, AACC Press, Washington.
26. Lundin, A. (1997) in *A Practical Guide to Industrial Uses of ATP-Luminescence in Rapid Microbiology* (Stanley, P. E., Smither, R., and Simpson, W. J., Eds.), pp. 55–62, Cara Technology Limited, Lingfield.
27. Wehrli, S. L., Berry, G. T., Palmieri, M., Mazur, A., Elsas, L., III, and Segal, S. (1997) *Pediatr. Res.* **42**, No. 6, 855–861.

REFERENCES

1007 Page

- 1 J. H. Scofield, *J. Electron Spectrosc. Relat. Phenom.*, 8 (1976) 129.
- 2 R. F. Reilman, A. Msezane and S. T. Manson, *J. Electron Spectrosc. Relat. Phenom.*, 8 (1976) 389.
- 3 R. J. Baird, Ph.D. Dissertation, University of Hawaii, 1977 (Dissertation Order No. 77-23, 483).
- 4 W. B. Hermansfeldt, Electron trajectory program, SLAC Rep. 166, Natl. Tech. Inf. Serv., U.S. Department of Commerce, Springfield, VA 22151, 1973 (cited in ref. 3 above).
- 5 H. Weaver (Hewlett-Packard), private communication with R. J. Baird (cited in ref. 3 above).
- 6 M. P. Seah and W. A. Dench, *Surf. Interface Anal.*, 1 (1979) 2.
- 7 C. D. Wagner, L. E. Davis and W. M. Riggs, *Surf. Interface Anal.*, 2 (1980) 53.
- 8 D. R. Penn, *J. Electron Spectrosc. Relat. Phenom.*, 9 (1976) 29.
- 9 S. M. Hall, J. D. Andrade, S. M. Ma and R. N. King, *J. Electron Spectrosc. Relat. Phenom.*, 17 (1979) 181.
- 10 P. Cadman, S. Evans, G. Gossedge and J. M. Thomas, *J. Polym. Sci., Polym. Lett.*, 16 (1978) 461.
- 11 D. T. Clark, H. R. Thomas and D. Shuttleworth, *J. Polym. Sci., Polym. Lett.*, 16 (1978) 465.
- 12 B. Hupfer, H. Schupp, J. D. Andrade and H. Ringsdorf, *J. Electron Spectrosc. Relat. Phenom.*, 23 (1981) 103.
- 13 D. T. Clark, Y. C. T. Fok and G. G. Roberts, *J. Electron Spectrosc. Relat. Phenom.*, 22 (1981) 173.

Journal of Electron Spectroscopy and Related Phenomena, 28 (1983) 303-316
Elsevier Scientific Publishing Company, Amsterdam — Printed in The Netherlands

Data bank

CALCULATED CORE-LEVEL SENSITIVITY FACTORS FOR QUANTITATIVE XPS USING AN HP5950B SPECTROMETER

I. ELLIOTT, C. DOYLE and J. D. ANDRADE*

Surface Analysis Laboratory, Departments of Bioengineering and Materials Science and Engineering, University of Utah, Salt Lake City, UT 84112 (U.S.A.)

(First received 2 February 1982; in final form 20 August 1982)

Values of core-level sensitivity factors for a Hewlett-Packard HP5950B X-ray photoelectron spectrometer have been calculated using theoretical photoionization cross-sections, asymmetry parameters, and an instrument throughput function. These sensitivity factors, when combined with an appropriate mean-free-path function for the sample of interest, permit semiquantitative elemental analysis by XPS.

A simplified form of the basic expression for quantitative XPS is

$$N_{i,k} = I_0 \rho_i \sigma_{i,k} \lambda_{i,k} T_{i,k} \quad (1)$$

where $N_{i,k}$ is the experimentally determined peak intensity for the k th shell of an atom of type i in the sample, I_0 is the X-ray flux incident on the sample and is considered constant, ρ_i is the volume density of element i in the surface volume examined by XPS (this is the quantitative information normally desired in the experiment), and $\sigma_{i,k}$ is the differential photoionization cross-section given [2] by

$$\sigma_{i,k}(h\nu', \phi) = \sigma_{i,k}(h\nu) F_{i,k}(\beta, \phi) \quad (2)$$

where $\sigma_{i,k}(h\nu)$ is the Scofield total photoionization cross-section [1], which is a function of photon energy $h\nu$, and where the second term of eqn. 2 is given [2] by

$$F_{i,k}(\beta, \phi) = 1 + \beta/2[(3/2)\sin^2 \phi - 1] \quad (3)$$

where β is an angular asymmetry parameter — a characteristic of atomic orbital and atomic number — as calculated and discussed in detail by Reilman

* Author to whom correspondence should be addressed.

et al. [2], and ϕ is the angle between the X-ray photons and the emitted photoelectrons (73° in the Hewlett—Packard instrument).

$T_{i,k}$ is the instrument transmission or throughput function. The Hewlett—Packard instrument uses a preretardation lens analyzer which is kinetic-energy dependent. The main component of this transmission function is the solid angle of acceptance, which has been modeled by Baird [3] using an electron-optics computer program [4] and lens dimensions supplied by Weaver [5]. The Baird data were normalized so that the value of the transmission function at the binding energy of the C1s peak was 1.00. These data were fitted to several power functions; a seventh-degree polynomial (as a function of E_b) provided the best fit*.

Using the Scofield cross-sections [1], the asymmetry parameter β [2] and the instrument transmission function [3], the values in Table 1 were calculated and are presented as XPS core-level sensitivity factors for the Hewlett—Packard Al K α instrument, normalized to a C1s sensitivity factor of 1.00.

The top value in each entry of the Table is the approximate binding energy (eV), the next entry is the Scofield differential photoionization cross-section [1]. The next entry is the Scofield value multiplied by the asymmetry term (eqns. 2 and 3) normalized to a C1s value of 1.00. The bottom number incorporates the instrument throughput function — this is the overall elemental sensitivity factor normalized to a C1s value of 1.00.

It is important to point out that these sensitivity factors can be used only after taking into account the mean free path $\lambda_{i,k}$ in the sample. Several authors have discussed experimental and theoretical values of mean free paths [6 — 13]. Wagner et al. [7] have shown that most of the available experimental data can be fitted approximately as the power function $\lambda_{i,k} = C E_{kin}^m$, where C and m are functions of the solid material. They have shown that for kinetic energies greater than 300 eV, m is ~ 0.75 for inorganic solids and is in the range 0.7—1.0 for organic solids.

CONCLUSIONS

Given the data in Table 1, coupled with reasonable estimates of mean-free-path dependencies for the sample of interest, it is possible to obtain semiquantitative elemental analysis. The data provided in Table 1 can assist users of Hewlett—Packard instruments in doing semiquantitative XPS as long as some reasonable estimate of the mean-free-path dependencies is incorporated into the analysis. Of course, if the surfaces are not homogeneous in depth, a more complex analysis must be performed in order to account for the appropriate structure of the surface region.

ACKNOWLEDGMENTS

The authors acknowledge earlier discussions with Dr. M. Kelly at Surface Science Laboratories, Palo Alto, CA regarding the throughput function for the Hewlett—Packard instrument, and Dr. C. Fadley, University of Hawaii, for making us aware of the thesis of Baird [3].

* The polynomial is available from the authors on request.

Z	Element	1s _{1/2}	2s _{1/2}	2p _{1/2}	2p _{3/2}	3s _{1/2}	3p	3d
3	Li	55 0.06 0.06 0.05						
4	Be	111 0.19 0.19 0.18						
5	B	188 0.49 0.49 0.48						
6	C	284 1.00 1.00 1.00						
7	N	399 1.80 1.80 1.96						
8	O	532 2.93 2.93 3.49	24 0.14 0.14 0.17					
9	F	686 4.43 4.43 6.25	31 0.21 0.21 0.30					
10	Na	1072 8.52 8.52 31.35	63 0.42 0.42 0.39	31 0.19 0.16 0.15				
12	Mg		89 0.58 0.58 0.54	52 0.33 0.28 0.26				
13	Al		118 0.75 0.75 0.72	74 0.54 0.46 0.43	73			

Z	Element	1s _{1/2}	2s _{1/2}	2p _{1/2}	2p _{3/2}	3s _{1/2}	3p _{1/2}	3p _{3/2}
14	Si		149 0.96 0.96 0.93	100 0.82 0.71 0.67	99			
15	P		189 1.18 1.18 1.16	136 1.19 1.04 1.00	135	16 0.11 0.11 0.10		
16	S		229 1.43 1.43 1.42	165 1.68 1.49 1.44	164	16 1.46 1.46 1.35		
17	Cl		270 1.69 1.69 1.69	202 0.78 0.69 0.68	200	18 0.18 0.18 0.17		

(continued)

Z Element	1s _{1/2}	2s _{1/2}	2p _{1/2}	2p _{3/2}	3s _{1/2}	3p _{1/2}	3p _{3/2}
18 Ar	320 1.97 1.97 2.03	247 1.03 0.93 0.90	245 2.01 1.81 1.76	25 0.23 0.23 0.21	12 0.24 0.22 0.20		
19 K	377 2.27 2.27 2.45	297 1.35 1.22 1.23	294 2.62 2.38 2.40	34 0.29 0.29 0.27	18 0.36 0.32 0.30		
20 Ca	438 2.59 2.59 2.87	350 1.72 1.57 1.65	347 3.35 3.05 3.20	44 0.35 0.35 0.33	26 0.51 0.46 0.42		
21 Sc	500 2.91 2.91 3.35	407 2.17 1.99 2.19	402 4.21 3.86 4.25	54 0.41 0.41 0.38	32 0.65 0.59 0.54		
22 Ti	564 3.24 3.24 3.95	461 3.69 2.47 2.80	455 5.22 4.80 5.38	58 0.47 0.47 0.44	34 0.81 0.74 0.68		
23 V	628 3.57 3.57 4.71	520 3.29 3.04 3.56	513 6.37 5.89 6.89	66 0.54 0.54 0.50	38 1.00 0.91 0.84		
24 Cr	695 3.91 3.91 5.59	584 3.98 3.68 4.60	575 7.69 7.12 8.82	74 0.60 0.60 0.56	43 1.17 1.01 0.99		

Z Element	2s _{1/2}	2p _{1/2}	2p _{3/2}	3s _{1/2}	3p _{1/2}	3p _{3/2}	3d
25 Mn	769 4.23 4.23 6.68	650 4.74 4.39 5.97	641 9.17 8.50 11.39	84 0.67 0.67 0.63	49 1.42 1.31 1.22		
26 Fe	846 4.57 4.57 8.13	723 5.60 5.19 7.63	710 10.82 10.03 14.54	95 0.74 0.74 0.70	56 1.67 1.54 1.44		
27 Co	926 4.88 4.88 10.10	794 6.54 6.05 9.81	779 12.62 11.68 18.45	101 0.82 0.82 0.78	60 1.93 1.79 1.66		
28 Ni	1008 5.16 5.16 14.29	872 7.57 7.00 13.08	855 14.61 13.50 24.44	112 0.89 0.89 0.85	68 2.22 2.06 1.92		
29 Cu	1096 5.46 5.46 22.43	951 8.66 7.98 17.63	931 16.73 15.42 32.37	120 0.96 0.96 0.91	74 2.48 2.31 2.17		
30 Zn	1194 5.76 5.71 32.47	1044 9.80 9.00 29.53	1021 18.92 17.38 51.10	137 1.04 1.04 1.00	87 2.83 2.64 2.49		
31 Ga	1143 11.09 10.16 49.43	1116 21.40 19.60 86.84	158 1.13 1.13 1.10	107 1.10 1.03 0.98	103 2.11 1.98 1.88	18 1.08 0.93 0.86	

(continued)

Z Element	2s _{1/2}	2p _{1/2}	2p _{3/2}	3s _{1/2}	3p _{1/2}	3p _{3/2}	3d _{3/2}	3d _{5/2}	4s _{1/2}	4p _{both}	4d _{both}	5s _{1/2}
32 Ge		1249 12.52 11.43 75.10	1217 24.15 22.06 133.59	181 1.23 1.23 1.19	129 1.24 1.16 1.11	122 2.39 2.24 2.15	29 1.42 1.23 1.13					
Z Element	3s _{1/2}	3p _{1/2}	3p _{3/2}	3d _{3/2}	3d _{5/2}	4s _{1/2}	4p _{both}	4d _{both}	5s _{1/2}			
33 As	204 1.32 1.32 1.29	147 1.39 1.31 1.26	141 2.68 2.52 2.42	41 1.82 1.59 1.46								
34 Se	232 1.43 1.43 1.42	168 1.55 1.46 1.42	162 2.98 2.81 2.73	57 2.29 2.00 1.86								
35 Br	257 1.53 1.53 1.52	189 1.72 1.62 1.59	182 3.31 3.12 3.03	70 2.84 2.50 2.35	69 2.49 2.64 2.54	27 0.19 0.19 0.17						
36 Kr	289 1.64 1.64 1.64	223 1.89 1.78 1.76	214 3.65 3.43 3.36	89 3.48 3.06 2.88		24 0.21 0.21 0.21	11 0.48 0.45 0.41					
37 Rb	322 1.75 1.75 1.80	248 2.07 1.96 1.92	239 4.00 3.78 3.74	112 1.72 1.52 1.44	111 2.49 2.64 2.54	30 0.25 0.25 0.23	14 0.62 0.59 0.55					
38 Sr	358 1.86 1.86 1.97	280 2.25 2.13 2.13	269 4.37 4.13 4.13	135 2.06 1.82 1.75	133 2.99 2.64 2.54	38 0.29 0.29 0.27	20 0.78 0.74 0.68					
39 Y	395 1.98 1.98 2.16	313 2.44 2.31 2.36	301 4.75 4.50 4.55	160 2.44 2.16 2.10	158 3.54 3.13 3.01	46 0.33 0.33 0.31	26 0.91 0.86 0.79					
40 Zr	431 2.10 2.10 2.35	345 2.64 2.50 2.63	331 5.14 4.87 5.06	183 2.87 2.54 2.46	180 4.17 3.70 3.58	52 0.37 0.37 0.34	29 1.05 1.00 0.92					
41 Nb	469 2.22 2.22 2.51	379 2.84 2.69 2.91	363 5.53 5.24 5.55	208 3.35 2.97 2.91	205 4.86 4.31 4.18	58 0.40 0.40 0.37	34 1.17 1.11 1.04					
42 Mo	505 2.34 2.34 2.71	410 3.04 2.88 3.17	393 5.94 5.63 6.14	230 3.88 3.45 3.38	227 5.62 5.00 4.90	62 0.44 0.44 0.41	35 1.31 1.25 1.16					
43 Tc	544 2.45 2.45 2.94	445 3.23 3.06 3.43	425 6.36 6.03 6.63	257 4.46 3.97 3.93	263 6.47 5.76 5.70	68 0.48 0.48 0.45	39 1.45 1.38 1.28					
44 Ru	585 2.57 2.57 3.21	483 3.44 3.26 3.72	461 6.78 6.42 7.25	284 5.10 4.54 4.54	279 7.39 6.58 6.58	75 0.52 0.52 0.49	43 1.59 1.52 1.41					
45 Rh	627 2.70 2.70 3.56	521 3.64 3.45 4.04	496 7.21 6.83 7.85	312 5.80 5.17 5.27	307 8.39 7.48 7.63	81 0.56 0.56 0.53	48 1.75 1.67 1.55					

(continued)

TABLE 1 (continued)

Z Element	3s _{1/2}	3p _{1/2}	3p _{3/2}	3d _{3/2}	3d _{5/2}	4s _{1/2}	4p _{both}	4d _{both}	5s _{1/2}
46 Pd	670 2.81 2.81 3.91	559 3.83 3.63 4.43	531 7.63 7.22 8.52	340 6.56 5.85 6.08	335 9.48 8.45 8.79	86 0.60 0.60 0.56	51 1.88 1.80 1.67		
47 Ag	717 2.93 2.93 4.28	602 4.03 3.81 4.88	571 8.06 7.63 9.38	373 7.38 6.59 7.05	367 10.66 9.52 10.18	95 0.64 0.64 0.60	62 0.70 0.67 0.62	56 1.36 1.30 1.21	
48 Cd	770 3.04 3.04 4.74	651 4.22 3.99 5.43	617 8.50 8.03 10.44	411 8.27 7.38 8.12	404 11.95 10.67 11.63	108 0.69 0.69 0.66	67 2.25 2.15 2.02		

Z Element	3s _{1/2}	3p _{1/2}	3p _{3/2}	3d _{3/2}	3d _{5/2}	4s _{1/2}	4p _{1/2}	4p _{3/2}	4d _{both}	5s _{1/2}
49 In	826 3.16 3.16 5.40	702 4.40 4.15 5.98	664 8.93 8.43 11.63	451 9.22 8.22 9.21	443 13.32 11.88 13.18	122 0.74 0.74 0.71	77 2.45 2.35 2.21	16 2.28 2.05 1.89		
50 Sn	884 3.26 3.26 6.23	757 4.58 4.32 6.65	715 9.35 8.82 12.88	494 10.25 9.14 10.51	485 14.80 13.20 15.04	137 0.79 0.79 0.76	89 2.67 2.56 2.40	24 2.70 2.44 2.24		
51 Sb	944 3.36 3.36 7.29	812 4.76 4.48 7.48	766 9.77 9.20 14.26	537 11.35 10.10 12.02	528 16.39 14.59 17.22	152 0.85 0.85 0.81	99 2.88 2.76 2.59	32 3.14 2.84 2.61		

52 Te	1006 3.46 3.46 9.48	870 4.92 4.63 8.61	819 10.21 9.60 16.22	582 12.52 11.15 13.94	572 18.06 16.08 19.78	168 0.90 0.90 0.88	110 3.11 2.98 2.83	40 3.63 3.29 3.06	12 0.12 0.12 0.12	
53 I	1072 3.53 3.53 13.24	931 5.06 4.75 9.98	875 10.62 9.96 18.72	631 13.77 12.22 16.13	620 19.87 17.19 22.52	186 0.96 0.96 0.93	123 3.34 3.20 3.04	50 4.13 3.74 3.48	14 0.14 0.14 0.13	
54 Xe	1145 3.62 3.62 17.73	999 5.20 4.86 12.88	937 10.99 10.27 21.88	685 15.10 13.38 18.87	672 21.79 19.31 26.84	208 1.02 1.02 0.99	147 3.58 3.43 3.29	63 4.68 4.24 3.95	18 0.16 0.16 0.15	

Z Element	3s _{1/2}	3p _{1/2}	3p _{3/2}	3d _{3/2}	3d _{5/2}	4s _{1/2}	4p _{1/2}	4p _{3/2}	4d _{3/2}	4d _{5/2}	5s _{1/2}	5p _{1/2}	5p _{3/2}	5d _{3/2}	5d _{5/2}
55 Cs	1217 3.73 3.73 22.59	1065 5.29 4.92 17.61	998 11.38 10.58 27.93	740 16.46 14.54 21.81	726 23.76 20.99 31.07	231 1.08 1.08 1.06	172 1.27 1.22 1.18	162 2.56 2.46 2.39	79 2.15 1.95 1.84	77 3.10 2.81 2.65	23 0.18 0.18 0.17	13 0.17 0.16 0.15	12 0.33 0.32 0.29		
56 Ba		1137 5.42 5.00 23.84	1063 11.71 10.81 38.70	796 17.92 15.78 25.56	781 25.84 22.76 36.19	253 1.13 1.13 1.12	192 1.34 1.29 1.25	180 2.73 2.62 2.54	93 3.46 3.14 2.95	90 4.21 4.01 3.85	40 0.21 0.21 0.20	17 0.20 0.19 0.18	15 0.40 0.38 0.35		
57 La		1205 5.55 5.08 29.78	1124 12.11 11.09 50.56	849 19.50 17.10 30.61	832 28.12 24.65 42.64	271 1.19 1.19 1.18	206 1.42 1.36 1.32	192 2.91 2.79 2.71	99 6.52 5.93 5.57	99 9.99 9.53 9.17	33 0.23 0.23 0.22	15 0.69 0.66 0.61			

Z Element	4s _{1/2}	4p _{1/2}	4p _{3/2}	4d _{3/2}	4d _{5/2}	4f _{5/2}	4f _{7/2}	5s _{1/2}	5p _{1/2}	5p _{3/2}	5d _{3/2}	5d _{5/2}
-----------	-------------------	-------------------	-------------------	-------------------	-------------------	-------------------	-------------------	-------------------	-------------------	-------------------	-------------------	-------------------

72 Hf	538 1.76 1.76 2.09	437 2.06 1.97 2.19	380 4.88 4.66 5.03	224 6.13 5.54 5.43	214 8.84 7.99 7.83	19 3.32 2.89 2.66	18 4.20 3.66 3.37	65 0.34 0.34 0.32	38 0.32 0.31 0.29	31 0.70 0.67 0.62		
-------	-----------------------------	-----------------------------	-----------------------------	-----------------------------	-----------------------------	----------------------------	----------------------------	----------------------------	----------------------------	----------------------------	--	--

(continued)

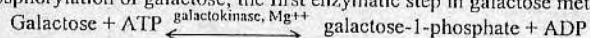
73 Ta	566	465	405	242	230	27	25	71	45	37		
	1.79	2.08	5.02	6.40	9.24	3.80	4.82	0.36	0.35	0.75		
	1.79	1.99	4.79	5.78	8.34	3.31	4.20	0.36	0.33	0.73		
	2.20	2.25	5.22	5.66	8.17	3.05	3.86	0.34	0.31	0.68		
74 W	595	492	426	259	246	37	34	77	47	37		
	1.81	2.10	5.16	6.68	9.65	4.32	5.48	0.38	0.37	0.81		
	1.81	2.00	4.92	6.02	8.70	3.76	4.77	0.38	0.35	0.78		
	2.30	2.30	5.46	5.96	8.52	3.50	4.44	0.36	0.33	0.73		
75 Re	625	518	445	274	260	47	45	83	46	35		
	1.84	2.12	5.30	6.95	10.06	4.88	6.20	0.40	0.39	0.87		
	1.84	2.02	5.05	6.25	9.05	4.25	5.39	0.40	0.37	0.84		
	2.43	2.36	5.66	6.25	8.96	3.95	4.98	0.38	0.35	0.78		
76 Os	655	547	469	290	273	52	50	84	58	46		
	1.86	2.13	5.45	7.23	10.48	5.48	6.96	0.42	0.41	0.93		
	1.86	2.03	5.19	6.50	9.42	4.77	6.05	0.42	0.39	0.89		
	2.53	2.44	5.86	6.50	9.42	4.44	5.63	0.40	0.37	0.83		
77 Ir	690	577	495	312	295	63	60	96	63	51		
	1.88	2.14	5.59	7.51	10.90	6.12	7.78	0.44	0.42	0.97		
	1.88	2.04	5.32	6.75	9.79	5.32	6.76	0.44	0.41	0.93		
	2.67	2.53	6.12	6.88	9.89	4.95	6.29	0.41	0.38	0.87		
78 Pt	724	608	519	331	314	74	70	102	66	51		
	1.90	2.14	5.74	7.73	11.32	6.81	8.65	0.46	0.44	1.04		
	1.90	2.03	5.46	6.93	10.15	5.92	7.52	0.46	0.43	1.00		
	2.81	2.62	6.39	7.21	10.36	5.56	7.07	0.44	0.40	0.93		
79 Au	759	644	546	352	334	87	83	108	72	54		
	1.92	2.14	5.89	8.06	11.74	7.54	9.58	0.48	0.46	1.10		
	1.92	2.03	5.59	7.23	10.53	6.55	8.32	0.48	0.44	1.06		
	2.96	2.74	6.71	7.66	10.95	6.16	7.82	0.46	0.42	0.98		
80 Hg	800	677	571	379	360	103	99	120	81	58		
	1.94	2.14	6.04	8.33	12.17	8.32	10.57	0.50	0.48	1.17		
	1.94	2.03	5.73	7.46	10.90	7.23	9.18	0.50	0.47	1.13		
	3.16	2.84	7.05	8.06	11.55	6.87	8.63	0.48	0.44	1.05		
81 Tl	846	722	609	407	386	122	118	137	100	76	16	13
	1.95	2.13	6.19	8.60	12.60	9.14	11.62	0.52	0.51	1.25	0.99	1.39
	1.95	2.02	5.86	7.69	11.27	7.93	10.09	0.52	0.49	1.20	0.90	1.27
	3.47	2.97	7.56	8.38	12.17	7.53	9.59	0.50	0.46	1.13	0.83	1.17
82 Pb	894	764	645	435	413	143	138	148	105	86	22	20
	1.96	2.12	6.33	8.87	13.02	10.01	12.73	0.54	0.53	1.33	1.11	1.58
	1.96	2.01	5.99	7.92	11.63	8.68	11.04	0.54	0.51	1.28	1.01	1.44
	3.82	3.12	8.09	8.79	12.79	8.33	10.60	0.52	0.48	1.20	0.93	1.33
83 Bi	939	806	679	464	440	163	158	160	117	93	27	25
	1.96	2.10	6.48	9.14	13.44	10.93	13.90	0.56	0.55	1.41	1.24	1.76
	1.96	1.98	6.12	8.14	11.97	9.47	12.04	0.56	0.52	1.36	1.13	1.61
	4.19	3.27	8.87	9.19	13.28	9.19	11.68	0.54	0.50	1.28	1.04	1.48
84 Po	995	851	705	500	473	184	177	132	104	81	31	
	1.97	2.07	6.62	9.40	13.87	27.04	0.58	0.57	0.57	1.50	3.31	
	1.97	1.95	6.24	8.36	12.33	23.41	0.58	0.54	0.54	1.44	3.02	
	5.14	3.49	9.05	9.61	13.93	22.71	0.57	0.52	0.52	1.37	2.78	
85 At	1042	886	740	533	507	210	195	148	115	40		
	1.96	2.04	6.77	9.65	14.29	29.36	0.60	0.58	0.58	1.58	3.63	
	1.96	1.92	6.37	8.55	12.66	25.38	0.60	0.56	0.56	1.52	3.31	
	6.37	3.69	9.56	10.18	14.69	24.87	0.59	0.54	0.54	1.44	3.08	
86 Rn	1097	929	768	567	541	238	214	164	127	48		
	1.95	2.00	6.92	9.90	14.70	31.81	0.62	0.60	0.60	1.67	3.95	
	1.95	1.88	6.49	8.75	12.99	27.46	0.62	0.58	0.58	1.61	3.60	
	8.04	3.93	10.12	10.76	15.58	26.91	0.61	0.56	0.56	1.53	3.35	

BIOLUMINESCENCE ASSAY FOR GALACTOKINASE ACTIVITY

Ji-yang Eu¹ and Joseph. D. Andrade²¹Dept. of Materials Science and Engineering and ²Dept. of Bioengineering
University of Utah, 50S. Central Campus Dr., Rm. 2480, Salt Lake City, UT 84112, USA

Introduction

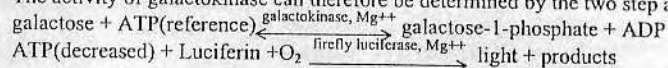
Galactose is present in the form of the disaccharide lactose, the principal carbohydrate of mammalian milk. Hydrolysis of lactose by β -galactosidase (E.C.3.2.1.23) in the intestinal microvilli results in the release of galactose and glucose. Galactokinase (E.C.2.7.1.6) catalyzes the phosphorylation of galactose; the first enzymatic step in galactose metabolism:



A significantly decreased galactokinase activity will result in accumulation of galactose and other toxic galactose derivatives- a metabolic disorder known as Type I galactosemia (1). The reaction of galactokinase (from *E. coli*) follows the random bi-bi mechanism (2), meaning that the two substrates randomly and independently bind to the two different active sites on the enzymes. The reaction is reversible, but the equilibrium favors the formation of galactose-1-phosphate and ADP (3). Since the reaction of galactokinase requires ATP as a substrate, the activity of galactokinase can be determined by measurement of the consumption of ATP.

Firefly luciferase has been extensively used to determine the concentration of ATP (4). The maximum light intensity produced by the firefly luciferase reaction is proportional to ATP concentration up to 1 $\mu\text{mol/L}$ when luciferin and molecular oxygen are saturated (5). In our experience, the linearity is maintained up to 8 $\mu\text{mol/L}$ ATP.

The activity of galactokinase can therefore be determined by the two step assay:



The actual concentration of reference ATP before and after the galactokinase reaction can be determined from an external ATP/luciferase bioluminescence standard curve. The difference between the ATP concentrations measured before and after exposure to the sample represents the galactokinase activity in the sample. A spectrophotometric method to determine the galactokinase activity is used for comparison (6).

Materials and Methods

Galactokinase (from galactose adapted yeast), galactose, ATP (disodium salt), glycine-glycine buffer, and bovine serum albumin (BSA) were purchased from Sigma (St. Louis, Missouri, USA). Luciferin was purchased from Molecular Probes (Eugene, Oregon, USA). $\text{MgSO}_4 \cdot 7\text{H}_2\text{O}$ was purchased from Mallinckrodt (Chesterfield, Missouri, USA). Gly-gly buffers were prepared in two concentrations: 0.025 mol/L and 0.45 mol/L in reagent grade water. The pH was adjusted to 7.8 for both buffers by adding 5N NaOH or NaOH pellets. 10 mmol/L ATP/ 50 mmol/L MgSO_4 solution was prepared in 0.45 mol/L gly-gly buffer; 0.1 mmol/L luciferin was prepared in 0.025 mol/L gly-gly buffer. 1 mg/mL BSA was prepared in 0.45 mol/L gly-gly buffer. Galactokinase was freshly reconstituted with reagent grade water. The stock solution of galactokinase (20 U/mL) was further diluted to 0.25, 0.5, 0.75, 1, 1.25, 1.75, and 2 U/mL. 10 mmol/L galactose was prepared in 0.025 mol/L gly-gly buffer. Recombinant firefly luciferase was purchased from Promega (Madison, Wisconsin, USA). The concentration of firefly luciferase was 13.33 mg/mL with a specific activity of 2.56×10^{10} light units/mg protein according to the supplier. Firefly

maintained linearity up to 2.5 U/mL galactokinase (by bioluminescence assay) with a slope of 1.48. The deviation from the ideal slope of unity indicates that the activity determined by the bioluminescence assay is higher than the activity determined by the spectrophotometric method. The discrepancy may be the result of the different pH values for the two assays. The bioluminescence assay was performed at pH 7.8 and spectrophotometric assay was performed at pH 7. In a separate experiment, yeast adapted galactokinase showed optimal activity at pH 8.0. Galactokinase from *E. coli*, pig liver, and human red blood cells also has a optimal pH range between 7.7 to 8 (10).

Conclusion

Bioluminescence based galactokinase activity assay showed a linear relationship between flash light intensity and galactokinase activity. The activity measured by the bioluminescence assay is higher compared to the values determined by the spectrophotometric method due to the different pH environment. The chemistry involved in the bioluminescence assay is relatively simple (two enzymatic steps compared to 3 enzymatic steps). To perform a spectrophotometric assay, the minimal requirement is 4 substrates and 2 enzymes. For a bioluminescence-based assay, only two substrates and one enzyme is needed. The procedure for a bioluminescence-based assay is simpler and faster than the spectrophotometric method since the chemistry is less complicated. However, the bioluminescence assay requires a luminometer which is not readily available in most analytical laboratories. Bioluminescence assay provides quantitative results for galactokinase up to 2.5 U/mL. The linear range covers the physiological activity of galactokinase in human red blood cells. The proposed assay could be an alternative way to measure galactokinase activity in red blood cells for the diagnosis of galactokinase deficient galactosemia (1).

Acknowledgements

Portions of this work were supported by Protein Solutions, Inc. via an NIH Phase I SBIR Grant and by the Whitaker Foundation program in Cost Reducing Health Care Technologies- a joint program with the National Science Foundation.

References

- Segal S, Berry GT. Disorders of Galactose Metabolism. In: Scriver CR et al, editors. The Metabolic and Molecular Bases of Inherited Diseases. McGraw-Hill Inc, 1995:967-1000.
- Gulbinsky JS, Cleland WW. Kinetic studies of *Escherichia coli* galactokinase. *Biochemistry* 1968;7:566-75.
- Atkinson MR, Burton RM, Morton RK. Equilibrium Constants of Phosphoryl Transfer from Adenosine triphosphate to galactose in the presence of galactokinase. *Biochem J* 1961;78:813-20.
- Brolin S, Wettermark G. Bioluminescence Analysis. New York: VCH, 1992.
- Lundin A. Techniques Related to Accuracy of Luminometric ATP measurements. In: Stanley PE, Smither R, Simpson WJ editors. A Practical Guide to Industrial Use of ATP-Luminescence in Rapid Microbiology. Lingfield: Cara Technology Limited, 1997:55-62.
- Heinrich MR, Howard SM. Galactokinase. In: Wood WA, editor. Methods in Enzymology Volume IX. New York: Academic Press, 1966:407-12.
- Lee RT, Denburg JL, McElroy WD. Substrate binding of firefly luciferase: II ATP binding site. *Arch Biochem Biophys* 1970; 14:38-52.
- Eu J. Ph.D. Dissertation. University of Utah, 2000, in preparation.
- Schell MA, Wilson BD. Purification and properties of galactokinase from *Saccharomyces Cerevisia*. *J Biol Chem* 1977;252:1162-6.
- Blume G, Beutler E. Purification and properties of galactokinase from human red cells. *J Biol Chem* 1971;246:6507-10.

luciferase was further diluted to 6.3 µg/mL with 1 mg/mL BSA. Galactokinase reaction assay was prepared in a 1.7 mL microcentrifuge tube containing the following reagents: 400 µL of 1 mg/mL BSA, 500 µL of 10 mmol/L galactose, 80 µL of 10 mmol/L ATP/ 50 mmol/L MgSO₄. The bioluminescence assay was prepared in 12x50 mm polypropylene test tubes by adding 10 µL of 6.3 µg/mL firefly luciferase and 40 µL of 1 mg/mL BSA. 20 µL of various concentrations of galactokinase standards was added to the galactokinase reaction assay to initiate the reaction. After 13 min incubation, 10 µL of the reaction mixture was drawn and further diluted by a factor of 100 with 0.025 mol/L gly-gly buffer. 100 µL of the diluted reaction mixture was then transferred to the test tube containing the bioluminescence assay. 100 µL of 0.1 mmol/L luciferin/10 mmol/L MgSO₄ was added via the auto injector; bioluminescence was recorded for 20 sec with a Turner Designs TD 20/20 luminometer. The external ATP standard curve was constructed by replacing the 100 µL diluted galactokinase reaction mixture with 2, 4, 6, and 8 µmol/L ATP standard solutions. The spectrophotometric assay procedure is described in reference 6.

Results and Discussion

Potential cross interferences from the galactokinase reaction components were tested. Galactose, galactokinase, and galactose-1-phosphate showed little effect on the peak intensity of bioluminescence. The variations on the peak intensity are less 7.6% (data not shown). The only component of the galactokinase reaction which was not studied is adenosine-5'-diphosphate (ADP). ADP is a competitive inhibitor for ATP in the firefly luciferase reaction with $K_i = 2.5 \times 10^{-3}$ mol/L (7). Since ATP is the limiting substrate for galactokinase, after the dilution by a factor of 100, the maximal concentration of ADP that may appear in the bioluminescence reaction is only 2.4 µmol/L even though the reaction of galactokinase is 100% complete. At this concentration, the effect of ADP on the bioluminescence assay should be negligible. The results indicate that the conditions used in the galactokinase assay will not significantly influence the accuracy of ATP concentration determination by the firefly luciferase reaction.

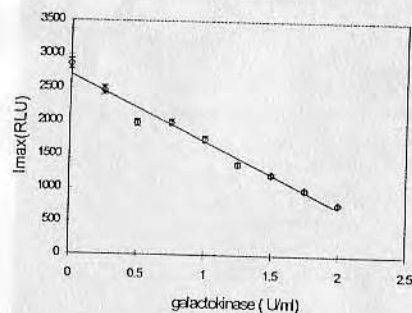


Fig. 1 Flash intensity (I_{max}) vs. galactokinase activity. The data points shown here are the average of three experiments. The coefficients of variation are smaller than 2.8% for all data points. The equation of the fitted straight line is $y = -993x + 2708$ with $R^2 = 0.98$. The galactokinase activity was provided by the supplier.

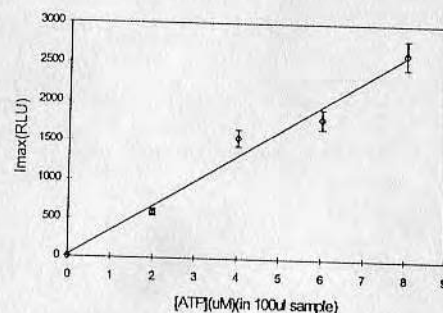


Fig. 2. ATP standard curve. The data points shown here are the average of three experiments with coefficient of variation smaller than 7%. The equation of the fitted straight line is $y = 323x + 23$ with $R^2 = 0.98$.

Fig. 1 is the plot of peak intensity versus the activity of galactokinase 13 min after the initiation of the galactokinase reaction. The optimal reaction time (13 min) was determined from other experiments (8). The K_m (galactose adapted yeast galactokinase) for ATP and galactose are 0.15 mmol/L and 0.6 mmol/L, respectively (9). The assay conditions chosen (0.8 mmol/L ATP and 5 mmol/L galactose) saturate the enzyme for each substrate, reducing to a pseudo zero-order reaction:

$$v = -d[ATP]/dt = K[E], \text{ --- [1]}$$

where $[E]_t$ denotes the total concentration of galactokinase, and K is the kinetic constant. After integrating and rearranging equation [1], the following relation between depleted ATP and galactokinase concentration can be derived:

$$[ATP] = [ATP]_0 - K[E]_t \text{ --- [2]}$$

$[ATP]_0$ is the initial ATP concentration, and t is the incubation time for the galactokinase reaction. Since the flash intensity of firefly luciferase is proportional to the ATP concentration for ATP up to 1 µmol/L when luciferin and oxygen are saturated, the peak intensity has a linear relationship with galactokinase activity but with a negative slope:

$$I_{max} = K_1[ATP] = K_1[ATP]_0 - K_1K[E]_t \text{ --- [3]}$$

In equation [3], I_{max} is the maximal intensity and K_1 is the proportionality constant between intensity and ATP concentration. Fig. 1 shows a straight line with a negative slope for total galactokinase activity up to 2 U/mL. The purpose of the dilution step is to keep the residual ATP concentration within the linear range of the bioluminescence assay. The activity of galactokinase can thus be calculated by the consumption of ATP. The corresponding ATP concentration for a certain light intensity is obtained from an external ATP standard curve (Fig. 2).

The ATP consumption by the galactokinase can be calculated from the difference in bioluminescence intensity between the control (no added galactokinase) and the sample using an external ATP standard curve (Fig. 2). One unit of activity of galactokinase determined by the bioluminescence assay is defined as 1 µmole ATP converted to ADP per minute at pH 7.8, 25°C. The activity of galactokinase determined by the bioluminescence assay is plotted against the activity measured spectrophotometrically in Fig. 3.

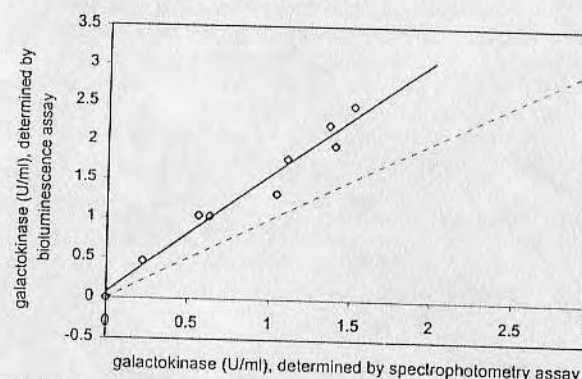


Fig. 3 Galactokinase activity determined from two different methods. The activity determined by bioluminescence was calculated based on the average intensity of three measurements. The equation of the fitted straight line is $y = 1.48x + 0.07$ with $R^2 = 0.96$. The dashed line has an equation of $y = x$.

All the data points on Fig. 3 should be located on the dashed line (slope=1) if the two assays agree with each other perfectly. The galactokinase activity determined by both methods



An illustration from the book *Il Fayforo o vero la Pietra Bolognese* by Marc' Antonio Cellio (1680), depicting the "Bolognian Stone", the first object of scientific study of the luminescence phenomenon.

We are grateful to Dr. Mario Baraldini for supplying the front cover design, which shows the city of Bologna, Italy.



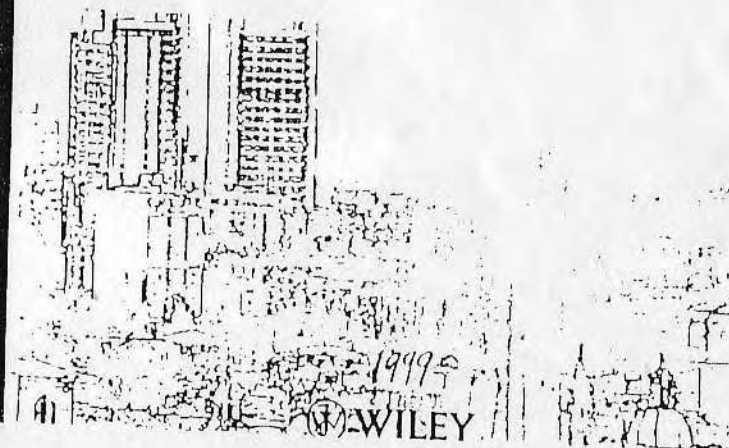
BIOLUMINESCENCE AND CHEMILUMINESCENCE

Perspectives for the 21st Century

Proceedings of 10th
International Symposium 1998

Edited by

A. Roda, M. Pazzagli, L. J. Kricka and P. E. Stanley



WILEY

Properties of firefly luciferase immobilized through a biotin carboxyl carrier protein domain

Jiyang Eu¹ and Joseph Andrade^{2*}

¹Department of Materials Science and Engineering, University of Utah, Salt Lake City, UT, USA

²Department of Bioengineering, University of Utah, Salt Lake City, UT, USA

Received 11 April 2000; revised 21 July 2000; accepted 28 July 2000

ABSTRACT: A fusion protein, consisting of biotin carboxyl carrier protein (BCCP) domain from *Escherichia coli* and firefly luciferase (FL) from *Photinus pyralis*, was immobilized through the biotin–avidin interaction on 6% cross-linked agarose beads. Several properties of the immobilized BCCP–FL were studied. Immobilized and free enzymes showed no significant difference in thermal stability; both retained at least 91% activity after incubation at 4°C and 25°C for 22 h. Incubation at 37°C for 22 h caused significant activity loss. K_M and k_{cat} values were determined for both free and immobilized enzymes. K_M values were similar between free and immobilized enzymes; however, k_{cat} of immobilized BCCP–FL was one-third of the k_{cat} of the free enzyme. 294 $\mu\text{mol/L}$ Co-enzyme A (CoA) and 44 mmol/L dithiothreitol (DTT) enhanced the total bioluminescence output. Triton X-100, Tween 20, PEG 8,000, PVP 40,000 and PVP 360,000 did not enhance the bioluminescence reaction of immobilized BCCP–FL. Copyright © 2001 John Wiley & Sons, Ltd.

KEYWORDS: immobilization; firefly luciferase; biotin carboxyl carrier protein (BCCP); co-enzyme A (CoA); dithiothreitol (DTT)

INTRODUCTION

Firefly luciferase (FL) is extensively used in the measurement of adenosine 5'-triphosphate (ATP) with a sensitivity of 10^{-13} mol/L (1, 2). The enzyme produces yellow-green light (562 nm) in the presence of ATP, luciferin (a benzothiazole compound), Mg^{++} and O_2 with a quantum efficiency of 0.88. It is also widely used as a genetic reporter (3).

Early immobilization methods of FL generally involved direct amino acid modification. Lee *et al.* covalently linked firefly luciferase to alkylamine glass beads but lost over 99% of activity (4). Ugarova *et al.* immobilized Russian FL (*Luciola mingrelica*) on cyanogen bromide-activated carriers and retained 20–30% activity (5). Weinhausen *et al.* observed 44–84% activity with *Photinus pyralis* luciferase on cyanogen bromide-activated Sepharose (6). Other solid supports, such as collagen strips, epoxy methacrylate polymer and nylon tubes, were also reported (7–9). Filippova *et al.* immobilized *L. mingrelica* luciferase on lipidated membrane and retained 100% activity because no covalent linkage was involved (10).

*Correspondence to: J. Andrade, University of Utah, 50 S. Central Campus Dr. Rm. 2480, Salt Lake City, UT 84112-9202, USA. E-mail: joe.andrade@m.cc.utah.edu

Contract/grant sponsor: Whitaker Foundation/National Science Foundation, USA.

Contract/grant sponsor: Protein Solutions Inc., Salt Lake City, UT, USA.

Immobilization can also be achieved by introducing extra residues, such as a polyhistidine tag or a BCCP domain. BCCP is a subunit of acetyl-CoA carboxylase, which is post-translationally modified with a biotin molecule on one of the lysine residues. A thermostable mutant (retained >70% activity after 60 min at 50°C) of *L. lateralis* (a Japanese firefly) luciferase was fused with either biotin acceptor peptide No. 84 or BCCP by Tatsumi *et al.* with biotinylation level greater than 95% (11). The fusion protein between *Escherichia coli* BCCP and *Photinus pyralis* FL (BCCP–FL) was first reported by Wang *et al.* with a biotinylation level between 55–58% (2). Biotin binds to avidin with $K_d = 10^{-15}$ mol/L (12). A poly-histidine tag binds to Ni^{++} with $K_d = 10^{-13}$ mol/L (13). Proteins fused with BCCP or poly-histidine tag can therefore be immobilized to avidin or Ni^{++} surfaces without direct chemical modification of the enzyme. Ho *et al.* reported that histidine-tagged FL retained 93% of activity after immobilization on metal-chelating pluronic beads in the presence of Ni^{++} (13). In the absence of Ni^{++} , the pluronic beads retained less than 1% bioluminescence activity.

We studied the immobilization kinetics, thermal stability and kinetic properties of immobilized BCCP–FL. In order to increase the sensitivity of immobilized enzyme towards ATP, the effects of potential enhancers, including CoA, DTT, Triton X-100, Tween 20, PEG 8,000, PVP 40,000 and PVP 360,000, were also investigated (14–16).

MATERIALS AND METHODS

Immobilization kinetics of BCCP-FL

200 μ L ImmunoPure immobilized avidin (on 6% cross-linked agarose beads, Pierce) was loaded in a 1.2 mL column (Biorad). The beads were washed with 3×1 mL gly-gly buffer (0.45 mol/L, pH 7.8) and transferred to a microcentrifuge tube by washing with 3×500 μ L gly-gly buffer. Buffer was removed until 200 μ L slurry was left after centrifugation. 250 μ L BCCP-FL (0.46, 0.68 and 0.91 mg/mL specific activity = 7.6×10^9 RLU/mg) was incubated with the beads. BCCP-FL concentration was determined by UV absorbance at 280 nm ($\epsilon = 0.7$ (mg/mL) $^{-1}$ cm $^{-1}$). The preparation and characterization of BCCP-FL have been reported elsewhere (2, 17). After 0, 3, 30, 60 and 90 min incubation, 20 μ L supernatant was collected and mixed with 800 μ L 1:5 dilution Bradford assay (Biorad) for 10 min. The absorbance at 595 nm was determined in a disposable cuvette and the residual FL concentration was calculated from a calibration curve (not shown). The amount of immobilized BCCP-FL was determined from solution depletion. The bioluminescence activity was determined by mixing 50 μ L 10 mmol/L ATP (Sigma) in gly-gly buffer (0.45 mol/L, pH 7.8) with 20 μ L BCCP-FL-immobilized slurry in a 12 \times 50 mm disposable test tube. The reaction was started by the addition of 50 μ L of 0.1 mmol/L luciferin (Molecular Probes)/ 50 mmol/L MgSO $_4$ ·7H $_2$ O in gly-gly buffer (25 mmol/L, pH 7.8) through an autoinjector. Bioluminescence was recorded with a Turner Designs TD 20/20 luminometer for 30 s. Commercial FL (Lot No. 114756, Promega) was used to study non-specific binding.

Thermal stability of immobilized BCCP-FL

750 μ L ImmunoPure immobilized avidin was loaded in a 1.2 mL column. The beads were washed with 3×1 mL gly-gly buffer and transferred to a microcentrifuge tube by washing with 3×500 μ L gly-gly buffer. Buffer was removed until 750 μ L slurry was left after centrifugation. 750 μ L 0.91 mg/mL BCCP-FL was incubated with the beads for 30 min. The unbound protein was drained and the beads were washed with 3×1 mL gly-gly buffer. The beads were transferred to a microcentrifuge tube by washing with 3×500 μ L gly-gly buffer. Buffer was removed until 750 μ L slurry was left after centrifugation. The enzyme-immobilized beads were incubated at 4, 25, 37 and 45°C, at each temperature for 0, 1, 3, 9 and 22 h. 20 μ L BCCP-FL-immobilized slurry was used to determine bioluminescence activity, as previously described.

Kinetic constants of BCCP-FL

To determine K_M (luciferin), 10 μ L BCCP-FL-immobilized slurry described in the previous section was mixed with 50 μ L luciferin (10, 20, 50, 100, 250 and 500 μ mol/L in 25 mmol/L gly-gly buffer). The reaction was initiated by the addition of 50 μ L 2 mmol/L ATP/10 mmol/L MgSO $_4$ ·7H $_2$ O in 0.45 mol/L gly-gly buffer. Bioluminescence was recorded for 30 s. To determine K_M (ATP), 10 μ L immobilized BCCP-FL slurry was mixed with 50 μ L ATP (20, 50, 100, 250, 500 and 1000 μ mol/L in 0.45 mol/L gly-gly buffer). The reaction was initiated by the addition of 50 μ L 0.8 mmol/L luciferin/ 10 mmol/L MgSO $_4$ ·7H $_2$ O in gly-gly buffer (25 mmol/L, pH 7.8).

Effect of CoA, DTT, surfactants and polymers on immobilized BCCP-FL

20 μ L BCCP-FL-immobilized slurry, 50 μ L 10 mmol/L ATP (or 10 μ mol/L) in gly-gly buffer (0.45 mol/L, pH 7.8), and 50 μ L CoA (or DTT or surfactants or polymers) were mixed in a 12 \times 50 mm disposable test tube. The reaction was initiated by the addition of 50 μ L 0.1 mmol/L luciferin/ 50 mmol/L MgSO $_4$ ·7H $_2$ O. Bioluminescence was recorded for 180 s. CoA (0.01, 0.1, 1, 2, 5 and 10 mmol/L, Sigma), DTT (150, 500 and 1000 mmol/L, Sigma), Triton X-100 (0.041, 0.41 and 4.1 mmol/L, Sigma), Tween 20 (0.008, 0.08 and 0.8 mmol/L Sigma), PEG 8000 (2.5, 25 and 250 mg/mL Sigma), PVP 40,000 (0.5, 5 and 50 mg/mL Sigma), and PVP 360,000 (0.5, 5 and 50 mg/mL Sigma) were prepared in gly-gly buffer (25 mmol/L, pH 7.8).

RESULTS AND DISCUSSION

Immobilization kinetics of BCCP-FL

115, 170 and 228 μ g BCCP-FL were used for immobilization on avidin-coated agarose beads. The diameter of the beads was in the range 45–165 μ m, with an exclusion limit of 4×10^6 Da. 1–2 mg avidin (62 kDa) was coated per mL gel, according to the supplier. The amount of BCCP-FL immobilized as a function of incubation time for three different initial enzyme concentrations is shown in Fig. 1a. 27.7 ± 0.6 , 41.3 ± 0.6 , and 47.6 ± 0.6 μ g was immobilized from 115, 170 and 228 μ g BCCP-FL, respectively. The bioluminescence activity (peak intensity, I_{max}) as a function of incubation time is shown in Fig. 1b. Maximal binding was reached with 30 min incubation (Figs 1a,b). The binding is rapid compared to traditional methods, such as cyanogen bromide-activated surfaces (hours). Commercial FL (no BCCP) showed less than 0.1% bioluminescence activity, suggesting that the binding of BCCP-FL was highly specific.

The final gly-gly concentration (0.27 mol/L) resulted

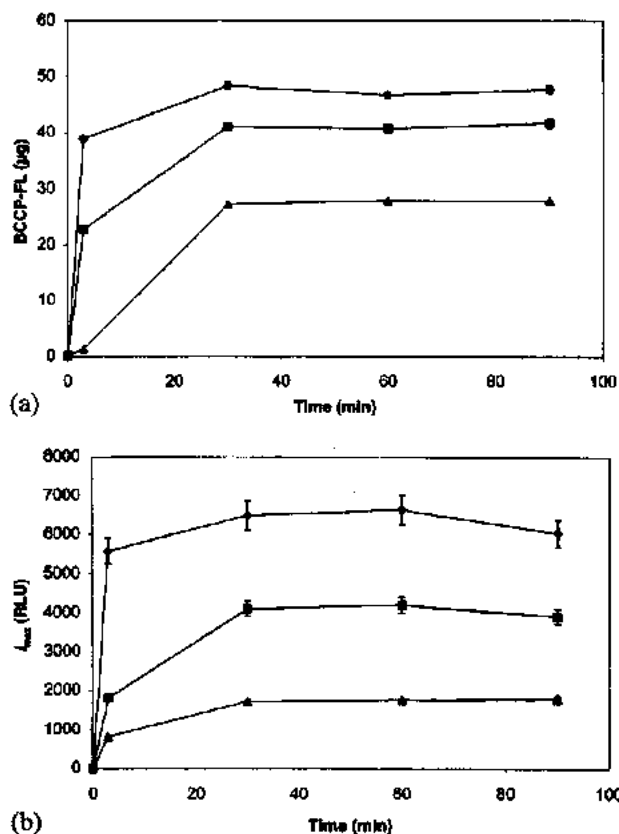


Figure 1. (a) Amount of immobilized BCCP-FL as a function of incubation time for three different initial concentrations. The data points are the average of three replicates. 115 µg (▲, c.v. = 1.1%), 170 µg (■, c.v. = 1.8%) and 228 µg (◆, c.v. = 1.3%). (b) Bioluminescence activity of immobilized BCCP-FL as a function of incubation time for three different initial concentrations. The data points are the average of three replicates. 115 µg (▲, c.v. = 5.7%), 170 µg (■, c.v. = 4.8%) and 228 µg (◆, c.v. = 2.5%). RLU, relative light unit.

in a 19% decrease in bioluminescence activity compared to the commonly used 0.025 mol/L (18, 19). The pH values of 10 mmol/L ATP solution prepared in 0.025 and 0.45 mol/L gly-gly buffer were 5.3 and 7.8, respectively. The final pH values of the assay were 7.8, regardless of the buffer concentration used. 0.025 mol/L gly-gly has enough buffer capacity to maintain the pH at 7.8. However, higher buffer capacity ensures an optimal pH at high ATP concentration if assay composition should change.

Thermal stability of immobilized BCCP-FL

The thermal stability of immobilized and free BCCP-FL was examined at four different temperatures: 4, 25, 37 and 45°C (Fig. 2). Both free and immobilized BCCP-FL retained at least 91 ± 11.8% of their original activity after 22 h incubation at 4°C and 25°C. 37°C caused significant loss of activity; 55.9 ± 1% and 48.1 ± 0.2% of activity remained after 22 h for free and immobilized enzymes,

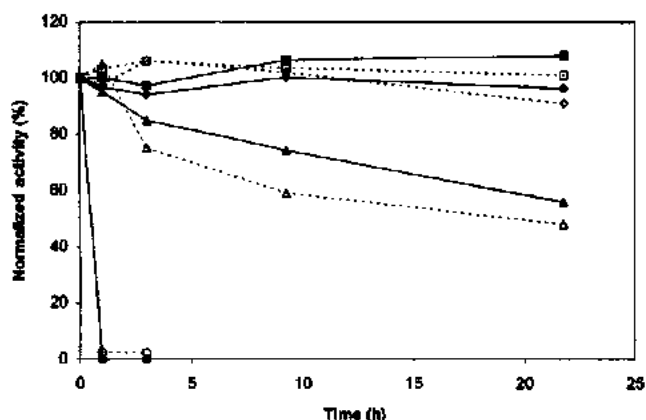


Figure 2. Normalized bioluminescence activity as a function of incubation time at different temperatures. Activities were normalized to $t = 0$ h; 4°C (diamonds), 25°C (squares), 37°C (triangles) and 45°C (circles). Solid labels and lines represent free BCCP-FL. Empty labels and dashed lines represent immobilized BCCP-FL. The data points are the average of three replicates (c.v. range, 3.2–5.8%).

respectively. Free and immobilized BCCP-FL retained less than $4.6 \pm 0.9\%$ of activity after 30 min incubation at 45°C. This observation agrees with the denaturation temperature (43°C) of BCCP-FL (20). No significant difference in thermal stability was observed between free and immobilized BCCP-FL. The thermal stability of commercial FL was also found to be similar to BCCP-FL, which agrees with previous results reported by Wang *et al.* and Tatsumi *et al.* (2, 11).

Kinetic constants of BCCP-FL

The generally accepted $K_M(\text{ATP})$ and $K_M(\text{luciferin})$ for *Photinus pyralis* FL are in the ranges 25–250 and 2–10 µmol/L, respectively (7, 8, 21–24).

Table 1 shows the K_M and k_{cat} values for both immobilized and free BCCP-luciferase calculated using Leonora software (25). Carrea *et al.* showed decreased $K_M(\text{ATP})$ (51–22 µmol/L) and increased $K_M(\text{luciferin})$ (2.4–28 µmol/L) for FL immobilized on nylon (7). A similar change was found on epoxy methacrylate polymer (8). K_M values for collagen-bound FL (24 and 11 µmol/L for ATP and luciferin, respectively) showed no difference from the free enzyme under mechanical stirring (26). Contrary to Carrea's results, the immobilized BCCP-FL has a decreased $K_M(\text{luciferin})$ and an increased $K_M(\text{ATP})$. The measured K_M values of the immobilized enzyme are of the same order of magnitude as the free enzyme; the affinity of the immobilized enzyme towards its substrates is similar to the free form. $K_M(\text{luciferin})$ and $K_M(\text{ATP})$ for commercial FL determined under the same conditions (34.7 ± 2.9 and 145.9 ± 20.5 µmol/L, respectively) were also similar to free BCCP-FL.

The k_{cat} determined from immobilized BCCP-FL was

Table 1. K_M and k_{cat} values for both free and immobilized BCCP-FL. The values were calculated using Leonora software

I	Fixed ATP (0.91 mmol/L)		Fixed luciferin (0.36 mmol/L)	
	Immobilized	Free	Immobilized	Free
$K_M(\text{luciferin})$ ($\mu\text{mol/L}$)	12.5 \pm 1.2	22.5 \pm 0.5	NA	NA
$K_M(\text{ATP})$ ($\mu\text{mol/L}$)	NA	NA	177.3 \pm 38.8	148.6 \pm 1.4
k_{cat} RLU ($\mu\text{g/mL}$) ⁻¹	215.6 \pm 10.4	613.3 \pm 7.4	633 \pm 98.1	1812.8 \pm 6.3

NA, not available.

35% of that of the free enzyme. The activity recovery of immobilized BCCP-FL (35%, k_{cat} (immobilized BCCP-FL)/ k_{cat} (free BCCP-FL)) is comparable to that of FL immobilized on cyanogen-bromide activated surfaces (5, 6).

BCCP-FL (71 kDa compared to the exclusion limit of 4×10^6 Da) can be immobilized inside the agarose beads. Bille *et al.* studied the diffusional constraints imposed by the solid matrix on immobilized yeast alcohol dehydrogenase and found that the kinetic properties of the immobilized enzyme are solid matrix-dependent (27). Concentration gradients of substrates are likely to be developed along the radius of the bead (high at the surface, low at the centre) due to diffusion limits imposed by the solid matrix. Enzymes immobilized inside the beads may become substrate-limited, which leads to lowered k_{cat} . The activity recovery should be improved if BCCP-FL is immobilized on the surface.

Effect of CoA on immobilized BCCP-FL

The effect of CoA (2.9, 29.4, 294, 600, 1500 and 3000 $\mu\text{mol/L}$) on immobilized BCCP-FL was studied. Two different concentrations of ATP were used: 2.9 $\mu\text{mol/L}$ and 2.9 mmol/L. 2.9 mmol/L ATP generally produces a flash-decay bioluminescence output, caused by a strong product inhibition. Oxyluciferin is a strong inhibitor for firefly luciferase, with $K_i = 0.23 \mu\text{mol/L}$ (21, 28). By contrast, 2.9 $\mu\text{mol/L}$ ATP produces a pseudo-steady-state bioluminescence which has little product inhibition. CoA is believed to enhance the FL bioluminescence by facilitating the release of oxyluciferin (15, 29). Arith *et al.* suggested that the formation of oxyluciferin-CoA leads to the release of the inhibitory product (15). Ford *et al.* showed that at least two different mechanisms (sites) must exist, since both the sulphhydryl and the adenine moieties of CoA are active (30). Wood compared enzymes that catalyse similar reactions to FL (4-coumarate: CoA ligase and long chain acyl-CoA synthetase), revealing an overall structural similarity (29, 31). The structural similarity suggested the possibility of a CoA binding site on FL. Gandelman *et al.* showed that the release rate of oxyluciferin was increased four times in the presence of CoA (32). However, no definitive mechanism for CoA enhancement has been reported to date.

The effect of CoA at two different levels of ATP is

shown in Fig. 3a (2.9 mmol/L) and b (2.9 $\mu\text{mol/L}$). In Fig. 3a, 2.9 $\mu\text{mol/L}$ CoA has no effect (superimposed with the 0 $\mu\text{mol/L}$ CoA control) and 29.4 $\mu\text{mol/L}$ CoA has only a marginal effect in enhancing bioluminescence. However, the rapid decay after flash was significantly reduced in the presence of 294 $\mu\text{mol/L}$ CoA. 294 $\mu\text{mol/L}$ of CoA increased the peak intensity (I_{max}) and the integrated intensity (I_{int} , integrated from 0 to 180 s) by 18.3% and 73.4%, respectively. The enhancement CoA saturates above 294 $\mu\text{mol/L}$, since higher CoA concentrations (600, 1500 and 3000 $\mu\text{mol/L}$; only 600 $\mu\text{mol/L}$ is shown) showed little improvement. Stronger enhancement was observed on free FL when CoA was combined with DTT (30, 31). The lowered CoA enhancement effect observed on the immobilized BCCP-FL may also be due to the diffusion constraint described previously.

On the contrary, all three levels of CoA showed no effect or inhibition at 2.9 $\mu\text{mol/L}$ ATP. This observation agrees with Ford *et al.* (30). CoA is only effective at high ATP levels, since the activity of firefly luciferase is rapidly inhibited by oxyluciferin.

The reusability of immobilized BCCP firefly luciferase was studied by 'regenerating' the enzyme with CoA. For each cycle, all reactants were washed away and the BCCP-FL immobilized beads were incubated with 0.1 and 1 mmol/L CoA for 5 min after a 60 s bioluminescence reaction. Fig. 4 shows the I_{max} (proportional to activity) for four cycles in the presence of CoA. The control (no CoA used in the regeneration) lost almost all the activity after four cycles. The regeneration with CoA showed little effect. All I_{max} values in Fig. 4 decayed exponentially ($R^2 > 0.95$). Later attempts using 5 mmol/L ATP/50 mmol/L $\text{MgSO}_4 \cdot 7\text{H}_2\text{O}$ or 0.5 mmol/L luciferin/50 mmol/L $\text{MgSO}_4 \cdot 7\text{H}_2\text{O}$ with CoA showed no difference. The results agree with the mechanism proposed by Wood, in which CoA reacts with luciferin-adenylate to form luciferin-CoA (29). Used luciferase cannot be regenerated, since the major product that remains on the active site is oxyluciferin.

Effect of DTT on immobilized BCCP-FL

DTT is often used in excess to help maintain the sulphhydryl group of CoA in the reduced form. The effect of DTT on immobilized BCCP-FL was studied at 2.9 mmol/L and 2.9 $\mu\text{mol/L}$ ATP (Fig. 5a, b, respec-

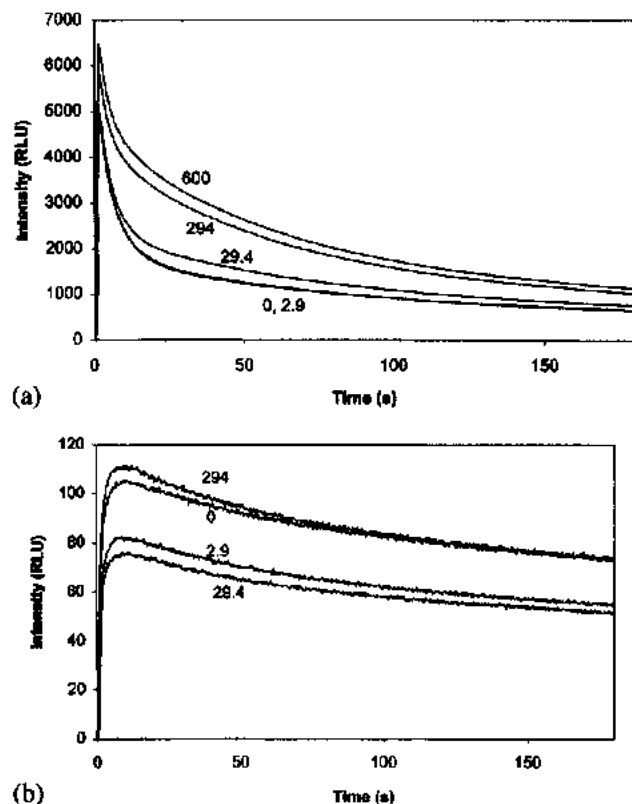


Figure 3. (a) Effect of CoA (0, 2.9, 29.4, 294 and 600 $\mu\text{mol/L}$) on immobilized BCCP-FL at 2.9 mmol/L ATP. The curves are the average of three replicates. 0 and 2.9 $\mu\text{mol/L}$ curves are superimposed. (b) Effect of CoA (0, 2.9, 29.4 and 294 $\mu\text{mol/L}$) on immobilized BCCP-FL at 2.9 $\mu\text{mol/L}$ ATP. The curves are the average of three replicates.

tively). In Fig. 5a, I_{max} decreases as the DTT concentration increases. The kinetics transform from flash-decay to a constant light intensity as the DTT concentration increases. 44 mmol/L DTT showed a 41.6% enhancement in I_{avg} at 2.9 mmol/L ATP. The decrease of both I_{max} and the decay rate may be due to a similar inhibitory effect from inorganic salts, reported by DeLuca *et al.* (18). However, Ford *et al.* reported that the presence of 2 and 3.3 mmol/L DTT increased I_{max} and slowed the decay rate significantly (30). DTT showed only inhibitory effect at micromolar levels of ATP (Fig. 5b) on immobilized BCCP-FL. Wood also observed the enhancement effect of DTT but the effect became inhibitory when the concentration exceeded 5 mmol/L (33).

Effect of surfactants and polymers on immobilized BCCP-FL

Kricka and DeLuca found that certain non-ionic surfactants (Triton X-100, Tween 20) and polymers (PEG 8000, PVP 40,000) enhance the bioluminescence output by several-fold (16). However, cationic and anionic surfactants completely inhibit the reaction. The

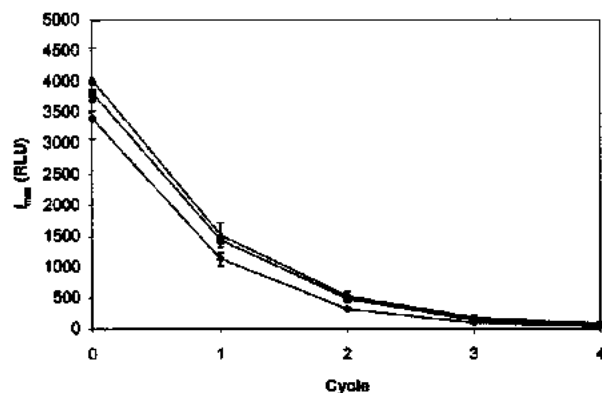


Figure 4. I_{max} as a function of regeneration cycle. In each cycle, reactants were washed away and the immobilized BCCP-FL was incubated with 0.1 or 1 mmol/L CoA for 5 min. The data points are the average of three replicates. 0 $\mu\text{mol/L}$ CoA (\blacklozenge , c.v. = 9.9%), 0.1 mmol/L CoA (\blacksquare , c.v. = 3.7%) and 1 mmol/L CoA (\blacktriangle , c.v. = 12.8%).

stimulation effect appears abruptly above a critical surfactant concentration that approximates to the critical micelle concentration (CMC). The mechanism of enhancement may involve micelles. Simpson and Ham-

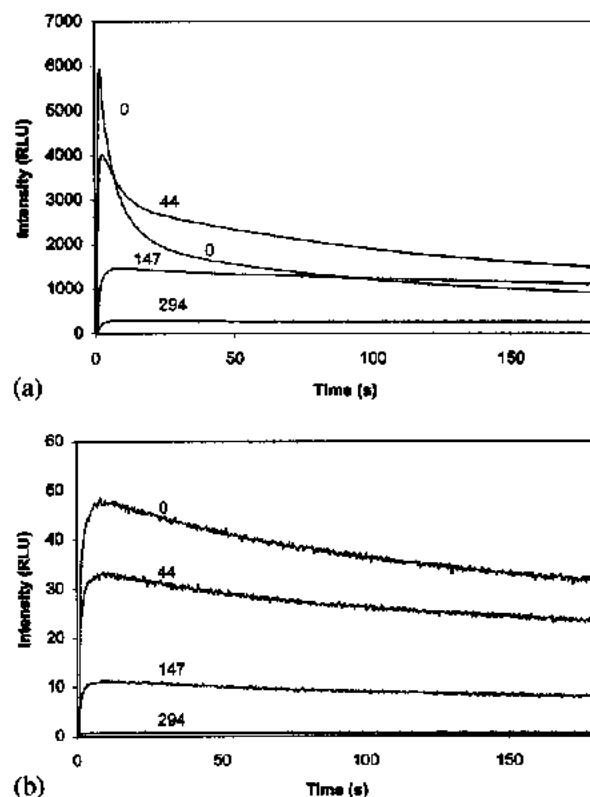


Figure 5. (a) Effect of DTT (0, 44, 147 and 294 mmol/L) on immobilized BCCP-FL at 2.9 mmol/L ATP. The curves are the average of three replicates. (b) Effect of DTT (0.44, 147 and 294 $\mu\text{mol/L}$) on immobilized BCCP-FL at 2.9 $\mu\text{mol/L}$ ATP. The curves are the average of three replicates.

Table 2. Effects of surfactants and polymers on immobilized BCCP-FL. Values were averaged from three replicates and normalized to the controls

	2.9 mmol/L ATP		2.9 μ mol/L ATP	
	I_{\max}	I_{lit}	I_{\max}	I_{lit}
Surfactants				
Triton X-100 (mmol/L)				
0	100 \pm 9.6	100 \pm 7.3	100 \pm 4.5	100 \pm 4.1
0.012	68 \pm 17.1	78 \pm 9.1	78.4 \pm 13.7	76.3 \pm 14
0.12	57.8 \pm 2	79.5 \pm 3.2	65.6 \pm 2.5	65.5 \pm 2.1
1.2	71.6 \pm 2.1	99.8 \pm 3.5	56.6 \pm 2.3	57.7 \pm 2.3
Tween 20 (mmol/L)				
0	100 \pm 9.6	100 \pm 7.3	100 \pm 4.5	100 \pm 4.1
0.0024	62.7 \pm 10.2	63 \pm 23.2	95 \pm 0.8	89.6 \pm 0.8
0.024	42.6 \pm 3.7	61.5 \pm 5.4	73.8 \pm 8	66.9 \pm 7.6
0.24	17.5 \pm 1.7	39.1 \pm 2	46.5 \pm 2.1	41.7 \pm 1.8
Polymers				
PEG 8000 (mg/mL)				
0	100 \pm 11.6	100 \pm 9.1	100 \pm 3.1	100 \pm 3.4
0.7	112.3 \pm 3.7	106.9 \pm 4.9	91.6 \pm 10.2	87.1 \pm 9.5
7.4	94.1 \pm 1.8	96.8 \pm 2.2	91.5 \pm 5.9	88.2 \pm 5
73.5	41.3 \pm 4.9	80.2 \pm 9.9	44.7 \pm 10.2	45.5 \pm 10.7
PVP 40,000 (mg/mL)				
0	100 \pm 9.6	100 \pm 7.3	100 \pm 4.5	100 \pm 4.1
0.147	59.8 \pm 9	60.9 \pm 8.7	50.6 \pm 0.5	46.1 \pm 0.4
1.47	50.3 \pm 8.7	54.7 \pm 9.9	43.9 \pm 2.2	40.5 \pm 2.1
14.7	35.8 \pm 3.6	52.1 \pm 5.2	5.6 \pm 1.5	26.1 \pm 1.6
PVP 360,000 (mg/mL)				
0	100 \pm 11.6	100 \pm 9.1	100 \pm 3.1	100 \pm 3.4
0.147	109 \pm 8.8	104.9 \pm 7.2	103.4 \pm 4.9	96.4 \pm 4
1.47	93.4 \pm 1.9	97.5 \pm 3.1	108 \pm 10.8	101 \pm 9.9
14.7	49.2 \pm 2.2	70.7 \pm 14.1	64.3 \pm 6.4	64.7 \pm 6.1

I_{\max} (peak intensity); I_{lit} (integrated intensity, 0 to 180 s).

mond investigated the effect of surfactants and polymers on commercially prepared FL; they found that only Tween 20 showed 30% stimulation of bioluminescence among the four surfactants or polymers mentioned previously (14). Contrary to Kricka and DeLuca's observation, they showed that the cationic surfactants enhance bioluminescence, as high as 94%. The effects of the previously mentioned surfactants and polymers on immobilized BCCP-FL are summarized in Table 2. The CMC values for Triton X-100 and Tween 20 (converted from 60 mg/L using an average MW of 1225) are 0.24 and 0.05 mmol/L, respectively (34). For both ATP levels, the surfactants and polymers showed inhibition or marginal enhancement. Even 1.2 mmol/L Triton X-100 and 0.24 mmol/L Tween 20 ($5 \times$ CMC) showed no effect. The immobilization of BCCP-FL on a solid surface may reduce the formation of micelles in the vicinity of the enzyme.

Acknowledgements

We thank Dr R. Stewart for helpful discussion and laboratory space. This work was supported by the

Whitaker Foundation (a grant in the Cost Reducing Health Care Technologies Program—a joint program with the National Science Foundation) and by Protein Solutions, Inc. (Salt Lake City, UT).

REFERENCES

- Brolin S, Wettermark G. *Bioluminescence Analysis*. VCH: New York, 1992.
- Wang C, Hitz S, Andrade JD, Stewart RJ. Specific immobilization of firefly luciferase through a biotin carboxyl carrier protein domain. *Anal. Biochem.* 1997; **246**: 133–139.
- Wood KV. Recent advances and prospects for use of beetle luciferases as genetic reporters. In *Bioluminescence and Chemiluminescence: Current Status*, Stanley PE, Kricka LJ (eds). Wiley: New York, 1991; 543–546.
- Lee Y, Jablonski I, DeLuca M. Immobilization of firefly luciferase on glass rods: properties of the immobilized enzyme. *Anal. Biochem.* 1977; **80**: 496–501.
- Ugarova NN, Brovko LY, Kost NV. Immobilization of luciferase from firefly *Luciola mingrelica*-catalytic properties and stability of the immobilized enzyme. *Enzyme Microb. Technol.* 1982; **4**: 224–228.
- Wienhausen GK, Kricka LJ, Hinkley JE, DeLuca M. Properties of bacterial luciferase/NADH:FMN oxidoreductase and firefly luciferase immobilized onto Sepharose. *App. Biochem. Biotech.* 1982; **7**: 463–473.
- Carrea G, Bovara R, Mazzola G, Girotti S, Roda A, Ghini S. Bioluminescent continuous-flow assay of adenosine 5'-triphos-

- phate using firefly luciferase immobilized on nylon tubes. *Anal. Chem.* 1986; **58**: 331–333.
8. Carrea G, Bovara R, Girotti S, Ferri E, Ghini S, Roda A. Continuous-flow bioluminescent determination of ATP in platelets using firefly luciferase immobilized on epoxy methacrylate. *J. Biolumin. Chemilumin.* 1989; **3**: 7–11.
 9. Blum LJ, Coulet PR, Gautheron DC. Collagen strip with immobilized luciferase for ATP bioluminescence determination. *Biotech. Bioeng.* 1985; **27**: 232–237.
 10. Filippova NY, Dukhovich AF, Ugarova NN. New approaches to the preparation and application of firefly luciferase. *J. Biolumin. Chemilumin.* 1989; **4**: 419–422.
 11. Tatsumi H, Fukuda S, Kikuchi M, Koyama Y. Construction of biotinylated firefly luciferases using biotin acceptor peptides. *Anal. Biochem.* 1996; **243**: 176–180.
 12. Savage MD, Mattson G, Desai S, Nielander GW, Morgensen S, Conklin EJ. *Avidin-Biotin Chemistry: A Handbook*. Pierce Chemical Company: Rockford, IL, 1992.
 13. Ho C, Limberis L, Caldwell KD, Stewart RJ. A metal-chelating pluronic for immobilization of histidine-tagged proteins at interfaces: immobilization of firefly luciferase on polystyrene beads. *Langmuir* 1998; **14**: 3889–3894.
 14. Simpson WJ, Hammond JR. The effect of detergents on firefly luciferase reactions. *J. Biolumin. Chemilumin.* 1991; **6**: 97–106.
 15. Arith RL, Rhodes WC, McElroy WD. The function of coenzyme A in luminescence. *Biochim. Biophys. Acta* 1958; **27**: 519–532.
 16. Kricka LJ, DeLuca M. Effect of solvents on the catalytic activity of firefly luciferase. *Arch. Biochem. Biophys.* 1982; **217**: 674–681.
 17. Eu J, Wang C, Andrade J. Homogeneous bioluminescence assay for galactosuria: interference and kinetic analysis. *Anal. Biochem.* 1999; **271**: 168–176.
 18. DeLuca M, Wannlund J, McElroy WD. Factors affecting the kinetics of light emission from crude and purified firefly luciferase. *Anal. Biochem.* 1979; **95**: 194–198.
 19. Denberg JL, McElroy WD. Anion inhibition of firefly luciferase. *Arch. Biochem. Biophys.* 1970; **141**: 668–675.
 20. Wang C. PhD Thesis, University of Utah, Salt Lake City, 1997.
 21. Denberg JL, Lee RT, McElroy WD. Substrate-binding properties of firefly luciferase I. Luciferin-binding site. *Arch. Biochem. Biophys.* 1969; **134**: 381–394.
 22. Lee RT, Denberg JL, McElroy WD. Substrate-binding properties of firefly luciferase II. ATP-binding site. *Arch. Biochem. Biophys.* 1970; **141**: 38–52.
 23. Lambert N, Idahl L-A. Regulatory effects of ATP and luciferin on firefly luciferase activity. *Biochem. J.* 1995; **305**: 929–933.
 24. Roda A, Grigolo B, Girotti S, Ghini S, Carrea G, Bovara R. Properties and analytical performance of immobilized recombinant firefly luciferase. In Stanley PE, Kricka LJ (eds). *Bioluminescence and Chemiluminescence: Current Status*. Wiley: New York, 1991; 487–489.
 25. Cornish-Bowden A. *Analysis of Enzyme Kinetic Data*. Oxford University Press: New York, 1995.
 26. Blum LJ, Coulet PR. Atypical kinetics of immobilized firefly luciferase. *Biotech. Bioeng.* 1986; **28**: 1154–1158.
 27. Bille V, Plainchamp D, Lavielle S, Chassaing G, Remacle J. Effect of the microenvironment on the kinetic properties of immobilized enzymes. *Eur. J. Biochem.* 1989; **180**: 41–47.
 28. Goto T, Kubota I, Suzuki N, Kishi Y. Aspects of the mechanism of bioluminescence. In Cormier MJ, Hercules DM, Lee J (eds) *Chemiluminescence and Bioluminescence*. Plenum: New York, 1973; 325–335.
 29. Wood KV. The evolutionary history of beetle luciferases. In *Modern Enzymology: Problems and Trends*, Kurganov BI, Kochetkov SN, Tishkov VI (eds), Nova Science: New York, 1994; 497–506.
 30. Ford SR, Buck LM, Leach FR. Does the sulfhydryl or the adenine moiety of CoA enhance firefly luciferase activity? *Biochim. Biophys. Acta* 1995; **1252**: 180–184.
 31. Wood KV. The origin of beetle luciferases. In Stanley PE, Kricka LJ (eds). *Bioluminescence and Chemiluminescence: Current Status*. Wiley: New York, 1991; 11–14.
 32. Gandelman OA, Brovko LY, Polenova TE, Ugarova NN. Non-steady state kinetics in bioluminescent firefly luciferase system. In *Bioluminescence and Chemiluminescence*, Szalay AA, Kricka LJ, Stanley PE (eds). Wiley: New York, 1993; 79–83.
 33. Wood KV. Promega Corporation: US Patent 5,650,289, 1997.
 34. Helenius A, Simons K. Solubilization of membranes by detergents. *Biochim. Biophys. Acta* 1975; **415**: 29–79.